AN ALL-SOLID-STATE OPTICAL PARAMETRIC OSCILLATOR FOR THE INFRARED

Jonathan A.C. Terry

A Thesis Submitted for the Degree of PhD
at the
University of St Andrews

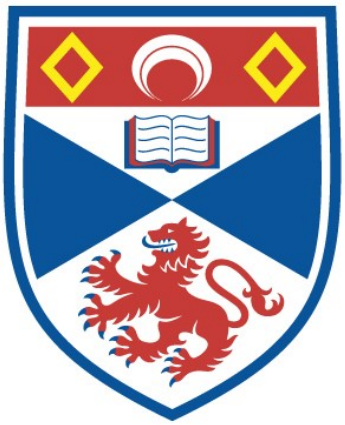

1994

Full metadata for this item is available in
St Andrews Research Repository
at:
http://research-repository.st-andrews.ac.uk/

Please use this identifier to cite or link to this item:
http://hdl.handle.net/10023/15032

This item is protected by original copyright

An all-solid-state optical parametric oscillator for the Infrared

A thesis submitted by

Jonathan A. C. Terry

to the University of St. Andrews

in application for the degree of

Doctor of Philosophy

September 1993

ProQuest Number: 10166818

All rights reserved

INFORMATION TO ALL USERS
The quality of this reproduction is dependent upon the quality of the copy submitted.

In the unlikely event that the author did not send a complete manuscript
and there are missing pages, these will be noted. Also, if material had to be removed,
a note will indicate the deletion.

ProQuest 10166818

Published by ProQuest LLC (2017). Copyright of the Dissertation is held by the Author.

All rights reserved.
This work is protected against unauthorized copying under Title 17, United States Code
Microform Edition © ProQuest LLC.

ProQuest LLC.
789 East Eisenhower Parkway
P.O. Box 1346
Ann Arbor, MI 48106 – 1346

TL B464

Declarations

I Jonathan A. C. Terry hereby certify that this thesis has been composed by myself, that it is a record of my own work, and that it has not been accepted in partial or complete fulfilment of any other degree of professional qualification. I was admitted to the Faculty of Science of the University of St. Andrews under Ordinance General No 12 as a candidate for the degree of Ph.D on 1st October 1989.

In submitting this thesis to the University of St. Andrews I understand that I am giving permission for it to be made available for use in accordance with the regulations of the University Library for the time being in force, subject to any copyright vested in the work not being affected thereby. I also understand that the title and abstract will be published, and that a copy of the work may be made and supplied to any bona fide library or research worker.

J.A.C.Terry
Sept 1993

I hereby certify that the candidate has fulfilled the conditions of the Resolution and Regulations appropriate to the Degree of Ph.D.

M.H.Dunn
Research Supervisor
Sept 1993

Abstract

A low threshold, efficient optical parametric oscillator (OPO) based on the material Potassium Titanyl Phosphate (KTP) and pumped by a diode-laser-pumped, Q-switched Nd:YLF laser has been demonstrated and investigated. This all-solid-state device was operated in a non-critical phase match (NCPM) geometry converting the 1 μm pump light to output wavelengths of 1.54 and 3.28 μm, and has potential as an 'eyesafe' laser source with scaling to higher powers. A major contributing factor to the success of this work was the extension of the steady state theory of the singly resonant OPO to include the build-up time effects that are dominant in the pulsed regime.

A number of diode pumped lasers were constructed, allowing a comparison to be made between side- and end-pumping geometries, and also between the materials Nd:YAG and Nd:YLF. The end-pumping geometry in conjunction with the higher absorption and longer upper state lifetime in Nd:YLF made it the design of choice for the case of low pump pulse energies (~ 12 mJ at 797 nm). Anamorphic expansion of the laser mode in the plane parallel to the diode laser junction was employed to achieve TEM_{00} operation of this laser. Subsequent Q-switching with a polariser and $LiNbO_3$ Pockels cell combination produced 2.2 mJ at 1.047 μm in an 18 ns pulse. Investigation of the dynamic loss of the Q-switch (which is due to the elasto-optic effect) allowed improvement of laser performance.

The established model for a pulsed singly resonant OPO which describes the case for a plane-plane resonator was inappropriate in this work and so the steady state focused beam theory was extended to include time dependence. Fair agreement was found between the computer model and the experimental results, where the effects of pump and signal focusing, and output coupling were investigated.

The high conversion efficiency of 30% for converting the 1 μm pump light to the eyesafe wavelength of 1.54 μm is superior to the present alternative source of the Er:glass laser. Pump energy thresholds of less than 0.5 mJ were obtained, along with internal conversions approaching 50 %. An empirical relation describing pump depletion was derived which showed good agreement with experiment.

A high resolution investigation of the spectral properties of the OPO identified the roles of resonant reflection and doubly resonant behaviour on the mode structure of the output. The former suggests a way in which single mode operation could be achieved without the use of additional intracavity elements, or a seeding source.

Acknowledgements

First, and foremost, I would like to thank my research supervisor, Professor Malcolm Dunn, for it was his enthusiasm and encouragement that facilitated the completion of this work. I would also like to thank my joint supervisor, Professor Wilson Sibbett, for obtaining the funding for both the research project itself and also my studentship. I therefore also wish to acknowledge said financial support from the Science and Engineering Research Council and the DRA (Fort Halstead), who jointly funded the project and myself through a CASE studentship.

Early collaboration on the construction of one of the lasers built in this work with Callum Norrie, and also help from Bruce Sinclair, is acknowledged, as is later help and collaboration, again with construction of a pump laser, with Cameron Rae. Still with regards to the work side of things, many thanks are expressed to the technical staff of the mechanical and electrical workshops, too numerous to mention, but in particular to Jimmy Lindsay for his helpful suggestions about redesign of mechanical components (!).

Many friendships were made at St. Andrews, and I thank the boys at 172 (Neil, Gordon and Jason) and also Angus, Sarah, Gordon, Malcolm and Christian for making my time at St. Andrews the most enjoyable period of my life, as far as I can remember.

Finally, I thank my parents who have supported me in everything I have ever done.

List of publications

Y.Cui, M.H.Dunn, C.J.Norrie, W.Sibbett, B.D.Sinclair, Y.Tang and J.A.C.Terry
"All-solid-state optical parametric oscillators tunable in the visible spectral region"
paper CTuR1, in Conference on Lasers and Electro-Optics 1992, vol. 12 OSA Technical Digest Series (Optical Society of America, Washington, DC 1992), p198

Y.Cui, M.H.Dunn, C.J.Norrie, W.Sibbett, B.D.Sinclair, Y.Tang and J.A.C.Terry
"All-solid-state optical parametric oscillator for the visible"
Opt. Lett. **17** (1992) 646

C.F.Rae, J.A.C.Terry, B.D.Sinclair, M.H.Dunn and W.Sibbett
"Single frequency, end-pumped Nd:YLF laser excited by a 12 mJ diode-laser array"
Opt. Lett. **17** (1992) 1673

J.A.C.Terry, C.F.Rae and M.H.Dunn
"Low threshold operation of an all solid state KTP OPO"
paper 133, in Technical Digest of 11th UK National Quantum Electronics Conference 1993, Belfast

J.A.C.Terry, Y.Cui, Y.Tang, W.Sibbett and M.H.Dunn
"Low threshold operation of an all solid state KTP OPO"
submitted to J. Opt. Soc. Am. B

Contents

Chapter 1 : Introduction

1.1	Why are tunable, coherent light sources required ?	1
1.2	How can tunable light be obtained ?	2
1.3	The OPO : a brief history	3
1.4	This work	7
1.5	References	9

Chaper 2 : Theory of Parametric Interactions

2.1	Introduction	12
2.2	The non-linear susceptibility	12
2.3	The coupled amplitude equations	15
2.4	Parametric amplification	17
2.5	Phase matching and acceptance parameters	20
	2.5.1 Phase matching	20
	2.5.2 Angular acceptance	22
	2.5.3 Poynting vector walk-off	23
	2.5.4 Spectral acceptance	24
2.6	Focused gaussian beams	24
2.7	Parametric oscillation	30
	2.7.1 Spontaneous parametric emission	30
	2.7.2 CW or steady-state parametric oscillation threshold	31
	2.7.3 Double resonance and the cluster effect	32
2.8	Parametric oscillation threshold for a pulsed pump	34
2.9	Conversion efficiencies	41
2.10	Summary	42
2.11	References	43

Chapter 3 : Non-linear Optical Materials

3.1	Introduction	45
3.2	Considerations for material selection	45
	3.2.1 Crystal symmetry and non-linear coefficients	46
	3.2.2 Tuning range	47
	3.2.3 Calculation of d_{eff} for the principal planes	50
	3.2.4 General considerations	52

3.2.5 Figures of Merit 53
3.3 Materials for use in the near infrared 55
3.4 Selection of material for OPO 57
3.5 Potassium Titanyl Phosphate (KTP) 59
3.5.1 Crystal symmetry and non-linearity 59
3.5.2 Transmission 60
3.5.3 Birefringence and dispersion 61
3.5.4 Thermal behaviour 64
3.5.5 Tuning 64
3.5.6 Optical damage threshold 66
3.6 Summary 67
3.7 References 68

Chapter 4 : The Pump Laser

4.1 Introduction 72
4.2 Laser diode pump sources 72
4.3 Laser diode pumped solid state lasers 74
4.4 Laser ions and solid-state hosts 76
4.4.1 Solid-state laser ions 76
4.4.2 Nd:YAG 77
4.4.3 Nd:YLF 78
4.5 Electro-optic Q-switching 78
4.5.1 General theory of Q-switching 79
4.5.2 Electro-optic Q-switcing 79
4.6 Side-pumped Nd:YAG lasers 82
4.6.1 Nd:YAG laser side-pumped by a single diode laser array 82
4.6.2 Double side-pumped Nd:YAG laser 85
4.7 End-pumped Nd lasers 89
4.7.1 Introduction 89
4.7.2 End-pumped Nd:YAG laser 90
4.7.3 End-pumped Nd:YLF laser 94
4.8 Comparison of side- and end-pumping and Nd:YAG and YLF 98
4.9 Summary 100
4.10 References 101

Chapter 5 : KTP OPO

5.1 Introduction 104
5.2 Design considerations 104
5.2.1 Gain 104
5.2.2 Loss 105

5.3 Early experiments 106
5.4 Zero-power mirrors 108
5.4.1 Mirror design 108
5.4.2 Mirrors obtained 110
5.5 KTP crystals 111
5.6 Experimental set-up and measurements 112
5.6.1 Pump lasers 112
5.6.2 OPO configuration 113
5.6.3 Experiments 114
5.7 Results for threshold, efficiency and transverse modes 117
5.7.1 Optical damage 117
5.7.2 OPO threshold 118
5.7.3 Efficiency 123
5.7.4 Transverse mode 129
5.8 Spectral Properties 130
5.8.1 Output wavelength 132
5.8.2 Spectral structure 134
5.9 Summary 137
5.20 References 139

Chapter 6 : Conclusions 140

Appendices

Appendix A : Non-linear Materials

A.1 Introduction A1
A.2 Lithium Niobate ($LiNbO_3$) and MgO:$LiNbO_3$ A1
A.3 Barium Sodium Niobate ($Ba_2NaNb_5O_{15}$, BSN, BNN) A3
A.4 Potassium Niobate ($KNbO_3$, KN) A5
A.5 Lithium Iodate ($LiIO_3$) A7
A.6 Proustite (Ag_3AsS_3) A9
A.7 References A12

Appendix B : Computer programs

B.1 Program to evaluate h_s from Guha, Wu and Falk B1
B.2 Program to evaluate pulsed thresholds B4

CHAPTER 1

Introduction

1.1 Why are tunable, coherent light sources required ?

Spectroscopy has for a long time been one of the most powerful analytical tools available for probing matter and gaining information about the world in which we live. By examining the absorption and emission properties of atoms and molecules, we can attempt to experimentally verify theories of atomic structure. As different species have resonances at different frequencies, a light source is required which provides access to the range of wavelengths of interest. This can be achieved with appropriate arc lamps and filtering of the effective black-body radiation, but these sources are only capable of producing a limited amount of power per unit wavelength per unit area per steradian. In order to provide higher resolution in the spectroscopic measurements a source of greater intensity is required. This boost was given originally when Schawlow and Townes [1] proposed the extension of maser techniques, by which intense, coherent radiation is produced in the microwave region of the spectrum, to the infrared and visible regions. The first 'optical maser', or laser, was successfully demonstrated in 1960 [2] by Maiman when a ruby rod was optically pumped by the emission from a flashlamp to produce an intense, coherent pulse of light with a wavelength of 694.3 nm. This starting point led to the diverse and world wide exploitation of laser technology that is available today.

Spectroscopy is only one of the uses to which light, particularly laser light, is put. Other uses, which may in effect involve spectroscopic techniques, include examination of combustion diagnostics, remote sensing, photochemistry, semiconductor studies, optical pumping, laser marking and welding systems, laser radar, communications (both in fibres and space), medicine including ophthalmology, dentistry and laser surgery [3-9]. The list is almost endless and is being extended continuously. However, most of the applications mentioned require, as well as a minimum amount of power, either a specific wavelength or a range of wavelengths. As laser emission tends to be due to an electronic transition in the outer shell of some atomic or molecular system, the emission tends to be of single frequency and at a specific wavelength which may not be suitable for the application in mind. It is therefore desirable to be able to produce the high intensity emission from lasers over a range of wavelengths. Some techniques which allow generation of frequency shifted or tunable output are discussed in the next section.

1.2 How can tunable light be obtained ?

Techniques for achieving the high intensity and coherence properties available from lasers in a tunable source can be split into two main areas ; the tunability is provided : 1) by the laser itself, or 2) by some non-linear optical technique which maintains, and even relies on, the coherence of the original laser.

If the levels between which the laser transition occurs are almost continuous manifolds due to broadening of vibrational and rotational sublevels by interaction with the host then absorption and emission spectra can be very wide (10s to 100s of nm). One of the traditional ways to obtain a tunable output is the use of an organic dye dissolved in a suitable solvent [9]. A large number of such dyes are available over the range 300 - 1200 nm, with tunability from each dye restricted to a few 100s of nm or less. The short upper state lifetime (~ ns) precludes energy storage and effectively limits the use of dyes to the cw and short pulse regimes where pulses of a few 10s of femtoseconds have been generated, e.g.[10]. Dyes have a number of disadvantages. As well as the limited spectral coverage mentioned above, exposure to the intense light fields involved results in degradation of the dye and so the dye must be replaced on a regular basis. This requires the operator to be exposed to messy, harmful chemicals.

An alternative technique for obtaining tunable output is that of the colour centre laser. If an alkali-halide crystal is treated in a certain way (e.g. electron bombardment) then the resulting removal of electrons or atoms from the lattice results in the creation of defect centres. These defect, or colour, centres act like a particle in a box with lower transition energies (i.e. longer wavelengths) than the dyes mentioned above. The wide bandwidths of these systems are suitable for ultrashort pulse generation, especially around the technologically important wavelength of 1.55 μm [11]. A major disadvantage of these systems is that they generally have to operated in dewars at cryogenic temperatures.

Recently there has been substantial interest in the use of so called 'vibronic lasers' which are created by the doping of a transition metal ion into a suitable crystal host. The strong coupling of the outer shell 3d electrons with the crystal field results in broadening of the vibrational levels to produce a wide bandwidth of absorption and emission [12], which in the case of the $Ti^{3+}:Al_2O_3$ (Ti:sapphire) laser stretches from around 650 nm up to 1100 nm [13]. This laser system has been used to produce the shortest pulses obtained directly from a laser at approx. 12 fs. Two other vibronic lasers of current interest consist of Cr doped in either $LiCaAlF_6$ or $LiSrAlF_6$ [14]. The tunability of these lasers is not as great as that obtained with the Ti:sapphire system mentioned above, at around 700 - 900 nm, but the absorption at 650 nm is accessible for diode pumping which may result in more activity with these lasers as the diode laser technology improves. These solid-state lasers have the advantages over dyes and colour

centres that they are robust, can operate at room temperature and do not chemically degrade.

However, although we have seen from the examples above (there are others) that tunable output can be obtained directly from lasers, the region of the spectrum that can be covered by any individual source is limited, and more importantly, is fixed in a particular region of the spectrum. In order to be able to obtain laser light in regions of the spectrum where no lasing transition exists we turn to some of the techniques of non-linear optics.

A number of non-linear techniques are available which allow frequency shifting of an input laser beam, e.g. stimulated Raman scattering, harmonic generation, sum and difference frequency mixing, and optical parametric amplification and oscillation. In Raman scattering, the input pump field is shifted by a discrete amount which is equal to the energy difference between two vibrational levels. This technique can be made to be efficient, in fact a conversion efficiency of 80 % has been reported [15]. Harmonic generation increases the frequency by an amount depending on which harmonic is generated. Equally sum and difference frequency generation can also alter the frequency of the pump laser. Any of these processes can be made more efficient by resonant enhancement, but in order to obtain a tunable output one of the input beams is generally required to be tunable. This does allow regions of the spectrum to be accessed which may not normally have been available, but perhaps at the expense of complexity.

Optical parametric amplification (or generation) and oscillation allow a tunable output where only one input frequency is required. In parametric generation, an intense pump beam is incident on a non-linear crystal and different frequencies, as determined by phase-matching considerations, build up from parametric noise. The resulting cone of generated wavelengths can be spatially filtered to produce a desired output. However, if the gain is not sufficient, only a small amount of power will be produced in the parametrically generated waves. By placing the non-linear crystal in a resonant cavity, an optical parametric oscillator can result where resonance of one or both of the generated waves enhances their growth and allows more control of their spatial and spectral properties. The optical parametric oscillator is the main topic of this thesis and in the next section we introduce some of its properties along with a brief history and some more recent results.

1.3 The OPO : a brief history

In an OPO, one can think of an incident high frequency photon (pump) being split into two lower frequency photons (referred to here as signal and idler), where the conversion is mediated by the non-linear susceptibility of the non-linear crystal involved. This situation is show schematically in fig. 1.1, and is described in more

detail in chapter 2.

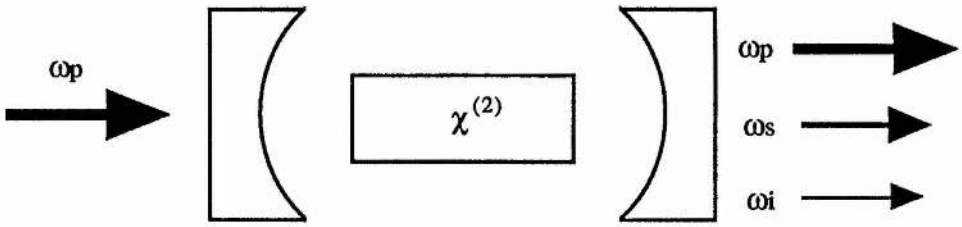

fig. 1.1 Schematic of an OPO

When the pump is incident on the crystal it couples with the vacuum fluctuations at the signal and idler frequencies (sometimes referred to as parametric noise) and transfers power to these fields. The pump can interact with any two frequencies which satisfy the energy conservation relation given by

$$\omega_p = \omega_s + \omega_i \tag{1.3.1}$$

However, only the fields which also satisfy the momentum conservation relation given

$$k_p = k_s + k_i \tag{1.3.2}$$

will receive an appreciable amount of gain. As the wavevector is affected by the refractive indices, by controlling the refractive indices we can control the frequencies which will see maximum gain and hence tune the output wavelengths. As most of the crystals which are used 2nd order non-linear experiments are also anisotropic, the refractive indices can be controlled by a number of means, usually by adjusting the angle of propagation into the crystal, or the crystal temperature.

Resonating the signal and/or idler enhances these fields in the cavity and increases the conversion from the pump field. We now present a brief history of the OPO, with more emphasis on recent work of note.

Optical parametric gain was first observed by Wang and Racette [16] back in 1965, closely followed by the first demonstration of an OPO by Giordmaine and Miller [17]. The success of this first device was aided by earlier work on second harmonic generation where the concept of phase matching [18] was recognised, and the importance of focusing [19], double refraction [20], and resonant cavities [21] were all investigated. The early devices used mainly $LiNbO_3$ or KDP, and the theoretical basis developed swiftly. Summaries of the early theoretical work and devices can be found in a number of review articles [22,23,24]. An excellent summary of early devices can be found in ref [25] and for this reason, and brevity, a review of the work of that period is not presented here.

Although the theoretical predictions were very promising, until recently the poor optical quality and low optical damage thresholds of non-linear crystals have resulted in OPOs not living up to their high expectations. The recent revival in OPOs has been fuelled by new and improved materials (e.g. $MgO:LiNbO_3$, $AgGaSe_2$, Ba_2BO_4 and LiB_3O_5)[26-29] and crystal growth techniques. The other major factor in OPO development has been the development of new pump sources, such as excimer [30] and laser diode pumped solid-state lasers [31]. These improvements have led to new horizons and applications for the new breed of OPOs, such as laser ranging, airborne communications, lidar, and spectroscopy, which were not open to the relatively unstable, inefficient OPOs of the past.

A short review of some more recent work is now presented. This introduces the context within which the work presented in this thesis can be set.

Most of the early work on OPOs concerned the use of pulsed IR lasers with tunable output in the near IR. Today, with suitable choice of non-linear material and pump laser, virtually any wavelength in the range near UV to 4.5 μm is available, with likely extension out to 10 μm and beyond. Pulsed lasers are still used in a fair proportion of situations, but output is now available in the ps and fs temporal regimes, as is true cw output. Due to the photon pair generation of the signal and idler outputs, OPOs are also being pursued as sources of squeezed light. As can be seen from the quick summary above, a large amount of effort is presently been put into development of OPOs and so the short review to follow is only intended to present some of the highlights and give a flavour of the variety and range of work being undertaken.

The renaissance of the OPO has, in the main, been materials led. In the time scale of ns pulsed OPOs, a major advance was the attainment of high quality crystals of the organic material urea. A continuous tuning range of 0.5-1.23 μm when pumping with the third harmonic of a Nd:YAG laser was achieved by Tang and co-workers [32], while when pumping with a XeCl excimer laser at 308 nm, Ebrahimzadeh et al demonstrated a peak efficiency of 65 % for 90° phase matching [33]. Despite the high single shot damage limit, urea suffered from long term damage problems and was superseded by β- BaB_2O_4 (BBO), one of a host of borate crystals developed by Chen and co-workers at the Fujian Institute for Materials Research, China [34]. When pumped with the 4th harmonic of a Nd:YAG laser at 266 nm, a BBO OPO was made to tune over the range 0.3-2.5 μm, though this required the use of more than one set of mirrors [35], while with a single set of mirrors tuning from 415 nm to 2.5 μm was achieved when pumping with the Nd:YAG third harmonic. The second of the borates to emerge from Chen's group at Fujian was LiB_3O_5 (LBO). This crystal has a smaller non-linearity and birefringence than BBO, but has a higher damage threshold, shorter UV transparency and can exhibit non-critical phase matching. Tuning has been obtained

throughout the range 372 nm to 1.8 μm when pumped with a XeCl excimer laser [36], making use of type II and non-critical phase matching. Pumping with the 3rd and 4th harmonics of a Nd:YAG laser have allowed tuning over the range 540 nm to 1.03 μm for 355 nm pumping [37] and low threshold, non-critically phase matched output at 314 nm and 1.74 μm for 266 nm pumping [38].

$KTiOPO_4$ (KTP) has been another material which has found wide spread applications. It is the material of choice for doubling 1 μm radiation and has been used in a number of OPO set ups. It also has excellent potential as a converter of 1 μm light to the eyesafe region of 1.54 μm in an all-solid-state configuration, as demonstrated in this work, and elsewhere, researchers at Fibertek achieved an impressive 64 % pump depletion [39]. Unfortunately, its IR transmission does not extend to 4.5 μm as originally thought, but an isomorph of KTP, $KTiOAsO_4$ (KTA) [40], which has a transmission out to 5 μm is currently under investigation for use in OPOs to provide tunable light in the technologically important region of 3-5 μm. Other materials offer the promise of tunability further out into the IR. $AgGaSe_2$ has produced tunable output continuously over the range 2.5-12 μm [41]. Similar performance is also available with $AgGaS_2$ [42]. Parametric superradiance in $ZnGeP_2$ and GaSe has produced output in the ranges 4-10 and 3.5-18 μm respectively when pumped with a 2.94 μm Er:YAG laser [43].

The broad linewidth of the output obtained from OPOs can be a problem in some applications. This area has been tackled by a number of groups with single longitudinal mode outputs obtained by intra-cavity methods either by using grazing incidence gratings [44] or by insertion of etalons [45]. Injection seeding is another useful technique, where a system which uses the output of one single frequency OPO to seed a higher power OPO is now available as a commercial product [46].

Although OPOs pumped by ns pulsed lasers were the most common form of OPO in the early experiments and are still a focus of current research, the temporal regime has been extended somewhat in recent years. OPOs pumped by modelocked lasers have the advantage that the high peak pump powers available can produce high gains while at the same time the damage thresholds of non-linear crystals are higher for these short pulses. Synchronous pumping of a KTP OPO with 70 ps pulses was demonstrated [47] and a reported tuning range of 0.6-4 μm was achieved when pumping with the 2nd harmonic of a mode-locked Nd:YLF laser [48]. Notable performance has been achieved with mode-locked diode pumped laser sources where 79 % pump depletion has been achieved with a singly resonant device utilising KTP [49], while temperature tuned LBO has been made to tune over the range 0.65-2.65 μm [50].

The use of short pulses was taken one step further with the advent of femtosecond lasers. A number of femtosecond OPO systems have been demonstrated recently, and

research in this area is currently a 'hot topic'. Of particular note is the pioneering work of the groups led by van Driel and Tang with both externally pumped and intracavity operation demonstrated, and even intracavity doubling of the OPO output [51-53]. To date, only KTP has been used in these systems, but other materials are sure to follow.

In the opposite time extreme work has progressed on cw OPOs. These lasers have developed from the unstable, intermittent operation of the early experiments to the achievement of true cw operation. Byer's work using the second harmonic of a monolithic MISER diode-pumped Nd:YAG laser achieved low thresholds with doubly resonant monolithic MgO:$LiNbO_3$ OPOs [54], and the same group has recently announced the achievement of cw singly resonant operation using KTP. Single resonance is ensured by the use of an intracavity prism, with an output power of 1.07 W at the non-resonant idler for 3.2 W incident [55].

Another area of research which is currently being actively pursued is the use of OPOs in quantum optical and squeezing experiments. Operating at degeneracy produces a beam of highly correlated subharmonic photons which are quantum noise limited and allow experiments to be carried out which were previously impossible [56,57].

1.4 This work

The brief summary above of the work that has been carried out on OPOs demonstrates the diversity that the OPO is now capable of. Early optimism was dampened due to material shortfalls, but the advances that have taken place in pump lasers and particularly in materials has brought the OPO to its current prominence as a practical source of tunable, coherent radiation.

The aim of the work described in this thesis was to achieve operation of an OPO using the high quality beams that are available from diode pumped solid-state lasers. In particular, the low threshold operation of a singly resonant OPO based on KTP pumped by the low energy output from a diode pumped Nd:YLF laser demonstrated the achievement of that aim. Sub 0.5 mJ thresholds were obtained with internal efficiency close to 50 %, with a conversion efficiency to the signal at 1.54 μm as high as 30 %. This efficiency of generation of this 'eyesafe' wavelength is superior to that of the usual source of this wavelength, i.e. the Er:glass laser.

The layout of the thesis is as follows. Chapter 2 introduces the theory behind parametric interactions and proceeds to the development of a new computer model for the calculation of pulsed threshold energies for singly resonant OPOs with focusing of the pump and signal, and with allowance being made for pulse build-up time effects. Chapter 3 introduces and summaries the properties of the non-linear crystals which were considered in this work (these features are also discussed in Appendix A). The

rough procedure by which a material, KTP, was chosen is presented followed by a comparative study of the optical properties of KTP. The properties of some of the other materials considered are presented in Appendix A. Chapter 4 describes the advantages of using laser diodes as pump sources for solid-state lasers, and goes on to describe the lasers built in this work, and their characterisation. Chapter 5 is the main experimental chapter, which describes the steps undergone to obtain operation of the OPO, followed by description of its threshold, efficiency, spatial and spectral properties. The conclusions of this work are presented in chapter 6, which discusses the achievements of this work and prospects for the future. Appendix B lists two of the main computer programs developed for the modelling.

1.5 References

[1] A. L. Schawlow and C. H. Townes, 'Infrared and optical masers', Phys. Rev. **112** (1958) 1940

[2] T. H. Maiman, 'Stimulated optical radiation in ruby', Nature **187** (1960) 493

[3] D. Brüggemann, J. Hertzberg, B. Wies, Y. Waschke, R. Noll, K.-F. Knoche and G. Herziger, 'Test of an optical parametric oscillator (OPO) as a compact and fast tunable Stokes source in coherent anti-Stokes Raman Spectroscopy (CARS)', Appl. Phys. B **55** (1992) 378

[4] M. J. Kavaya, S. W. Henderson and C. P. Hale, 'Solid-state progress supports coherent laser radar technology', Laser Focus World, Aug 89, 83

[5] E. Desurvive, 'Erbium-doped fiber amplifiers for new generations of optical communication systems', Opt. Phot. News, Jan 91, 6

[6] M. D. Kyzer, A. S. Aly, J. M. Davidson, L. Reinisch, R. H. Ossoff, 'Sub ablation effects of the KTP laser on wound healing', Lasers in Surgery and Medicine **13** (1993) 62

[7] J. R. Lesh and M. D. Rayman, 'Deep-space missions look to laser communications', Laser Focus and Electro-optics, Oct 88, 81

[8] B. Dance, 'Nd:YAG lasers mark ICs and packages', Laser Focus World, June 89, 44

[9] P. P. Sorokin, 'Organic lasers', Sci. Am. **220** (1969) 30

[10] J. A. Vladmanis, R. L. Fork and J. P. Gordon, 'Generation of optical pulses as short as 27 femtoseconds directly from a laser balancing self-phase modulation, group-velocity dispersion, saturable absorption and saturable gain', Opt. Lett. **10** (1985) 131

[11] G. T. Kennedy, R. S. Grant and W.Sibbett, 'Self-mode-locking of a NaCl:OH^- colour-centre laser', Proc. 11th Nat. Qu. Elec. Conf., Belfast Aug 93, paper 106

[12] B. Henderson and G. F. Imbusch, *Optical Spectroscopy of Inorganic Solids,* Oxford University Press, New York, 1989

[13] P. F. Moulton, 'Ti:sapphire lasers : Out of the lab and back in again', Opt. Phot. News, Aug 90, 20

[14] L. L. Chase and S. A. Payne, 'New tunable solid-state lasers', Opt. Phot. News, Aug 90, 16

[15] P. Frey and F. Padère, 'High-efficiency, narrow-linewdith Raman amplification and spectral compression', Opt. Lett. **5** (1980) 374

[16] C.C.Wang and G.W.Racette, 'Measurement of parametric gain accompanying optical difference generation', Appl. Phys. Lett. **6** (1965) 169

[17] J.A.Giordmaine and R.C.Miller, 'Tunable coherent parametric oscillation in $LiNbO_3$ at optical frequencies', Phys. Rev. Lett. **14** (1965) 973

[18] D.A.Kleinman, 'Theory of second harmonic generation of light', Phys. Rev. **128** (1962) 1761

[19] D.A.Kleinman, A.Ashkin and G.D.Boyd, 'Second harmonic generation of light by focussed laser beams' Phys. Rev. **145** (1966) 338

[20] G.D.Boyd, A.Ashkin, J.M.Dziedzic and D.A.Kleinman, 'Second harmonic generation of light with double refraction', Phys. Rev. **137** (1965) A1305

[21] A.Ashkin, G.D.Boyd and J.M.Dziedzic, 'Resonant optical second harmonic generation and mixing', IEEE J. Qu. Elec. **QE-2** (1966) 109

[22] S.E.Harris, 'Tunable optical parametric oscillators', Proc. IEEE **57** (1969) 2096

[23] R.G.Smith 'Optical Parametric Oscillators', in *Lasers : A series of advances,* A.K.Levine and A.J.DeMaria, Eds, Marcel Dekker, New York 1976

[24] R.L.Byer, 'Optical parametric oscillators', in *Quantum Electronics : A treatise vol1 part B*, H.Rabin and C.L.Tang, Eds, Academic Press 1973

[25] M.Ebrahimzadeh, 'Optical parametric oscillators pumped by excimer lasers', Ph.D. Thesis 1989, U. St.Andrews, unpublished

[26] N.P.Barnes, K.E.Murray, J.R.Heitenen and R.A.Ianinni, 'Low threshold, stable, $AgGaSe_2$ optical parametric oscillator' ,CLEO 90, paper CWE5

[27] D.A.Bryan, R.Gerson and H.E.Tomaschke, 'Increased optical damage resistance in lithium niobate', Appl. Phys. Lett. **44** (1984) 847

[28] D.Eimerl, L.Davis, S.Velsko, E.K.Graham and A.Zalkin, 'Optical, mechanical and thermal properties of barium borate', J. Appl. Phys. **62** (1987) 1968

[29] C.Chen, Y.Wu, A.Jiang, B.Wu, G.You, R.Li and S.Liu, 'New nonlinear-optical crystal : LiB_3O_5', J. Opt. Soc. Am. B **6** (1989) 616

[30] M.Ebrahimzadeh, M.H.Dunn and F.Akerboom, 'Highly efficient visible urea optical parametric oscillator pumped by a XeCl laser', Opt. Lett. **14** (1989) 560 ;

[31] C.D.Nabors, R.C.Eckardt, W.J.Kozlovsky and R.L.Byer, 'Monolithic $MgO:LiNbO_3$ optical parametric oscillator pumped by a frequency doubled diode laser pumped Nd:YAG laser', CLEO 88, paper FK2

[32] See, for example, L.K.Cheng, M.J.Rosker and C.L.Tang in *Tunable Lasers*, L.F.Mollennauer and J.C.White, Eds.,Berlin, Germany:Springer-Verlag, 1987

[33] A.J.Henderson, M.Ebrahimzadeh and M.H.Dunn, 'Characterization of urea optical parametric oscillators pumped by excimer lasers', J. Opt. Soc. Am. B **7** (1990) 1402

[34] C.Chen, B.Wu, A.Jiang and G.You, 'A new-type ultraviolet SHG crystal β-BaB_2O_4', Sci. Sin. Ser. B **28** (1985) 235

[35] L.K.Cheng, W.R.Bosenberg and C.L.Tang, 'Broadly tuneable optical parametric oscillation in β-BaB_2O_4', Appl. Phys. Lett. **53** (1988) 175

[36] M.Ebrahimzadeh, G.Robertson, M.Dunn and A.Henderson, 'Optical parametric oscillation from LiB_3O_5 optical parametric oscillators', CLEO '90, post deadline paper CPDP 26, Anaheim, CA, May 1990

[37] Z.Xu, D.Deng, Y.Wang, B.Wu and C.Chen, 'Optical parametric oscillation from LiB_3O_5 pumped at 355 nm', presented at CLEO '90, Anaheim, CA, May 1990

[38] Y.Tang, Y.Cui and M.H.Dunn, 'Lithium triborate optical parametric oscillator pumped at 266 nm', Opt. Lett. **17** (1992) 192

[39] L.R.Marshall, Alex Kaz and R.L.Burnham, 'Eyesafe laser with 2 % electrical efficiency', CWQ2 presented at CLEO '92, Anaheim, CA, May 1992

[40] J.D.Bierlein, H.Vanherzeele and A.A.Ballman, 'Linear and nonlinear optical properties of flux-grown $KTiOAsO_4$', Appl. Phys. Lett. **54** (1989) 783

[41] G.J.Quarles, C.L.Marquardt and L.Esterowitz, '2 μm pumped $AgGaSe_2$ with continuous tuning 2.49-12.05 μm', paper ELT7.1 presented at LEOS '90, Boston, Mass., 1990

[42] H.J.Bakker, J.T.M.Kennis, H.J.Kop and A.Lagendijk, 'Generation of intense picosecond pulses tunable between 1.2 and 8.7 μm', Opt. Comm. **86** (1991) 59

[43] K.L.Vodopyanov, L.A.Kulevskii, V.G.Voevodin, A.I.Gribenyukov, K.R.Allakhverdiev and T.A.Kerimov, 'High efficiency middle IR parametric superradiance in $ZnGeP_2$ and GaSe crystals pumped by an erbium laser', Opt. Comm. **83** (1991) 322

[44] W.R.Bosenberg and D.R.Guyer, 'Single-frequency optical parametric oscillator', Appl. Phys. Lett. **61** (1992) 387

[45] G.Robertson, A.Henderson and M.H.Dunn, 'Efficient, single-axial mode oscillation of a beta

barium borate optical parametric oscillator pumped by an excimer laser', Appl. Phys. Lett. **62** (1993) 123

[46] The MOPO 700 series from Spectra-Physics, Mountain View, CA

[47] L.J.Bromley, A.Guy and D.C.Hanna, 'Synchronously pumped optical parametric oscillation in KTP', Opt. Comm. **70** (1989) 350

[48] H.Vanherzeele, 'Picosecond laser system continuously tunable in the 0.6-4 μm range', App. Opt. **29** (1990) 2246

[49] M.J.McCarthy and D.C.Hanna, 'Continuous-wave mode-locked singly resonant optical parametric oscillator synchronously pumped by a laser-diode-pumped Nd:YLF laser', Opt. Lett. **17** (1992) 402

[50] M.Ebrahimzadeh, G.J.Hall and A.I.Ferguson, 'Broadly tunable, all-state, visible and infrared picosecond optical parametric oscillator', Opt. Lett. **18** (1993) 278

[51] E.S.Wachman, D.C.Edelstein and C.L.Tang, 'Continuous wave mode-locked and dispersion-compensated femtosecond optical parametric oscillator', Opt. Lett. **15** (1990) 136

[52] G.Mak, Q.Fu and H.M.van Driel, 'Externally pumped high repetition rate femtosecond infrared optical parametric oscillator', Appl. Phys. Lett. **60** (1992) 542

[53] R.J.Ellison and C.L.Tang, 'High-power, high-repetition-rate femtosecond pulses tunable in the visible', Opt. Lett. **18** (1993) 438

[54] C.D.Nabors, R.C.Eckardt, W.J.Kozlovsky and R.L.Byer, 'Efficient, single-axial-mode operation of a monolithic MgO:$LiNbO_3$ optical parametric oscillator', Opt. Lett. **14** (1989) 1134

[55] S.T.Yang, R.C.Eckardt, R.L.Byer, 'Continuous-wave singly resonant optical parametric oscillator pumped by a single-frequency doubled Nd:YAG laser', Opt. Lett. **18** (1993) 971

[56] L.-A.Wu, M.Xiao and H.J.Kimble, 'Squeezed states of light from an optical parametric oscillator', J. Opt. Soc. Am. B **1465** (1987) 1465

[57] J.G.Rarity, P.R.Tapster, J.A.Levenson, J.C.Garreau, I.Abram, J.Mertz, T.Debuisschert, A.Heidmann, C.Fabre and E.Ciacobino, 'Quantum correlated twin beams', Appl. Phys. B **55** (1992) 250

CHAPTER 2

Theory of Parametric Interactions

2.1 Introduction

Shortly after the demonstration by Franken et al [1] that the intense fields available from laser sources were of sufficient intensity to produce the second harmonic of the incident radiation, a number of authors [2-5] proposed the extension of the technique of parametric generation, which was already established in the microwave region [6], to the optical region. The first experimental observation of parametric gain [7] was followed closely by the first demonstration of an optical parametric oscillator (OPO) [8]. The period following this saw intensive experimental and especially theoretical work. Summaries of this early work can be found in a number of review articles [9-12].

This chapter both introduces and extends the background theory which is relevant to the operation of a pulsed optical parametric oscillator (OPO). The chapter consists of three aspects of the theory. Firstly, the basic theory of OPOs is introduced, in a tutorial manner, with regard to parametric amplification and the concepts of phase matching and acceptance parameters (spatial and spectral). The effect of interactions between focused, gaussian waves is introduced at an early stage as that is the regime of the work involved here. The difference between single and double resonance is emphasised with regard to steady state threshold calculations and spectral properties. Secondly, an in-depth review is presented concerning the earlier model for a pulsed singly resonant oscillator (SRO) due to Brosnan and Byer [13]. This model is only directly applicable to unfocused beams and so the theory of a SRO involving focused beams, as developed by Guha et al [14], is introduced and extended. A computer programme was written which reproduced the results of Guha as they applied in this instance. Thirdly, the theory was further extended by a computer model which was written to include build-up time effects so that the steady state theory of Guha could be used to predict OPO performance in the pulsed regime. The theoretical results produced here are compared, in chapter 5, with the experimental results.

Firstly a concise definition of the non-linear susceptibility will be given as there are different conventions adopted in the literature relating to this.

2.2 The non-linear susceptibility

When an electromagnetic wave propagates through a dielectric material it induces a polarisation. For most electromagnetic waves, where the electric field is considerably

smaller than the intra-atomic field, the response of the induced polarisation will be linear in the electric field, and can be expressed as

$$\mathbf{P} = \varepsilon_0 \chi \mathbf{E} \tag{2.2.1}$$

where ε_0 is the permittivity of free space, and χ is termed the electrical susceptibility. The electrical susceptibility is a frequency dependent, complex quantity, of which the real part is related to the refractive index, and the imaginary part is related to the absorption properties of the material, and is only significant close to an atomic resonance. This is referred to as the regime of *linear optics*. However, when the electromagnetic wave in question has an electric field strength comparable to the intra-atomic field, the response to the field can no longer be described by the linear relation of (2.2.1). We therefore expand the induced polarisation in powers of **E**, using a perturbative approach [5]. The relation between electric field and polarisation can now be expressed as

$$\mathbf{P} = \varepsilon_0 \left(\chi^{(1)} \mathbf{E} + \chi^{(2)} \mathbf{E}^2 + \chi^{(3)} \mathbf{E}^3 + \ldots \right) \tag{2.2.2}$$

where $\chi^{(1)}$, $\chi^{(2)}$, $\chi^{(3)}$, etc. are referred to as the first-, second-, third-, etc. order susceptibility and are in fact, despite the scalar notation, second, third, fourth, etc. order tensors. We adopt the scalar notation as it simplifies the notation, although we always bear in mind their tensor properties (this will be resolved more satisfactorily later).Thus we naturally refer to the regime where the response of the polarisation to the field is no longer linear as *non-linear optics*. As we are interested in this non-linear response of the media, it will prove useful to split the polarisation into linear and non-linear parts. We define this as

$$\mathbf{P} = \varepsilon_0 \chi^{(1)} \mathbf{E} + \mathbf{P}^{\mathrm{NL}} \tag{2.2.3}$$

The non-linear effects due to the quadratic and cubic response of the polarisation have been widely studied. The quadratic effect which involves the mixing of three frequencies gives rise to, amongst others, second harmonic generation, sum and difference frequency mixing, and optical rectification. The cubic term gives rise to third harmonic generation, Raman scattering, the Kerr effect, phase conjugation, and others. In the work described here, we are dealing with materials which possess a substantial second order non-linear susceptibility and we can therefore afford to neglect the higher order terms which will be considerably weaker.

As there appear to be a few slightly differing conventions adopted in the literature, for complete clarity the convention that has been adopted here is now presented. This follows the original proposals of Armstrong et al [5] as extended by Boyd and Kleinman [15], with the inclusion of the factor ε_0 such that the units of $\chi^{(2)}$ are mV^{-1}.

The second order non-linear polarisation is therefore defined here as, in tensor notation,

$$\mathbf{P}^{NL}(\omega_3) = \varepsilon_0 \chi^{(2)}(-\omega_3, \omega_2, \omega_1) : \mathbf{E}(\omega_1)\mathbf{E}(\omega_2) \tag{2.2.4}$$

The frequency dependence of the non-linear susceptibility is also included, about which more will be said shortly. Only materials which are non-centrosymmetric can possess a second order non-linearity and therefore the susceptibility is best described by a tensor (third order for $\chi^{(2)}$). This tensor is seen to obey the symmetry properties of its crystalline structure [16], and also some additional symmetries. The fact that $\chi^{(2)}$ satisfies permutation symmetry [5] means that the non-linear susceptibility is the same regardless of the three frequency mixing process. Additionally, if all three frequencies which are involved in the mixing are within the transmission bandwidth of the crystal, then according to Kleinman's conjecture [17], $\chi^{(2)}$ is real, independent of frequency and invariant to any permutation of the indices ijk.

As the non-linearity is almost invariably determined by second harmonic generation (SHG) experiments, it is convenient to express the equations in terms of non-linear coefficients, d_{ijk}, instead of $\chi^{(2)}$. As these d coefficients obey the same crystal symmetry as the piezoelectric coefficients, it is also convenient to use the condensed notation [16] that is applied to the piezoelectric coefficients. This condensed notation takes the form

$$d_{ijk} = d_{il(j,k)}$$

where

$$l(1,1) = 1\ ,\ l(2,2) = 2\ ,\ l(3,3) = 3\ ,\ l(2,3) = 4\ ,\ l(1,3) = 5\ ,\ l(1,2) = 6$$

The non-linear polarisation equations in terms of the d tensor for three frequency interactions are now given by [11]

$$\mathbf{P}(\omega_1) = \varepsilon_0 2d : \mathbf{E}^*(\omega_2)\mathbf{E}(\omega_3) \tag{2.2.5a}$$

$$\mathbf{P}(\omega_2) = \varepsilon_0 2d : \mathbf{E}^*(\omega_1)\mathbf{E}(\omega_3) \tag{2.2.5b}$$

$$\mathbf{P}(\omega_3) = \varepsilon_0 2d : \mathbf{E}(\omega_1)\mathbf{E}(\omega_2) \tag{2.2.5c}$$

where the notation implies a vector sum over the axial components. We can simplify matters still further by calculating a coefficient d_{eff} which is the net response of the non-linearity, taking into account the relations between the E field polarisation vectors and the symmetry of the d tensor. An example of how this is done is given in chapter 3. The use of d_{eff} allows use of scalar notation, which was non-rigorously introduced earlier for ease of notation.

An additional point of note here is with regard to the dispersion of the non-linear coefficients. It was noted by R.C.Miller [18] that although the non-linear coefficients measured for materials were seen to vary by over two orders of magnitude, multiplication of these coefficients by the linear susceptibilities of the three frequencies involved resulted in a coefficient, δ, which, within a factor of two, was seen to agree for all materials. This empirical rule is known as Miller's rule or Miller's delta. This rule has helped in the search for new materials in that it basically states that materials with high linear susceptibilities should also possess high non-linear susceptibilities. The rule also allows for calculation of the non-linear coefficient which is applicable when the frequencies that are involved differ from the frequencies involved at which the coefficients were reported. This additional factor can be expressed as [19]

$$M_{ij} = \frac{\left(n_i^2(\lambda_3)-1\right)\left(n_j^2(\lambda_2)-1\right)\left(n_k^2(\lambda_1)-1\right)}{\left(n_i^2(\Lambda_3)-1\right)\left(n_j^2(\Lambda_2)-1\right)\left(n_k^2(\Lambda_1)-1\right)} \tag{2.2.6}$$

where $n_{i,j,k}$ are the refractive indices, $\lambda_{1,2,3}$ are the wavelengths of interest, $\Lambda_{1,2,3}$ are the reference wavelengths, and the contracted index 1 is related to j and k as mentioned above. When working in the visible and near-IR, Miller's delta scales the non-linear coefficients with wavelength by an amount comparable to the measurement accuracy of the coefficients themselves, 5-20 %, and may therefore be considered almost an optional parameter. This tends to then agree with the Kleinman conjecture that the dispersion of the non-linearity in a region of transparency is negligible. However, Miller's delta has also been seen to give good agreement when scaling the non-linear coefficients to IR wavelengths, even near high absorptions, where Kleinman's conjecture doesn't hold.

2.3 The coupled amplitude equations

Now that the non-linear polarisation has been defined, we can describe how this allows for transfer of energy between waves of different frequency. Using equation 2.2.3 in the Maxwell wave equation gives

$$\nabla^2\mathbf{E} = \mu_0\sigma\frac{\partial\mathbf{E}}{\partial t} + \mu_0\varepsilon\frac{\partial^2\mathbf{E}}{\partial t^2} + \mu_0\frac{\partial^2\mathbf{P}^{NL}}{\partial t^2} \tag{2.3.1}$$

where the first term on the right side allows for absorption, and the other two are the source terms for wave propagation, which shows clearly that the non-linear polarisation acts as a source term in the wave equation. This is the general solution to the problem of waves propagating in a material with a quadratic non-linearity. To proceed further we must consider specific cases, and appropriate approximations.

In the rest of this section we will present the coupled amplitude equations which

demonstrate how energy can be transferred between waves. These only apply to the case of infinite extent, plane waves, however, most of the interesting properties of parametric amplification can be obtained from this formalism. In a later section, we show how the case of focused, gaussian waves, which is of interest in this work, can be dealt with by using a Green's function approach.

The coupled amplitude equations for plane waves, which give the dependence on propagation distance through the non-linear crystal of the amplitudes of the interacting waves, have been derived and considered extensively in many publications [20,21] and as such no derivation is reproduced here. The quadratic nature of the non-linearity allows for interaction between any three frequencies which satisfy the energy relation

$$\omega_3 = \omega_2 + \omega_1 \tag{2.3.2}$$

For the case of parametric generation, the interaction is such that energy is transferred from a strong pump wave at ω_3, to two other waves of lower frequency ω_1 and ω_2, which satisfy the energy relation above. We will see shortly that another constraint determines which pair of waves from the infinite set of pairs which satisfy (2.3.2) will in fact be generated.

It is appropriate at this point to spell out the convention for naming of the waves ω_1 and ω_2. In this work, we refer to ω_1 as the signal wave and ω_2 as the idler, where the relation is $\omega_1 > \omega_2$. This appears to be a generally accepted convention, but not a universally accepted one, so it is appropriate to define the convention adopted to avoid ambiguity.

We can therefore consider an electric field which has components at the three frequencies introduced above, and is assumed to be propagating in the z-direction. The plane wave assumption allows for the derivatives with respect to x and y to be set equal to zero. If we also apply the 'slowly varying envelope assumption' (i.e. $k\,\partial E/\partial z >> \partial^2 E/\partial z^2$) and sort out the resulting terms into their frequency components, the equations of interest are therefore

$$\frac{dE_s}{dz} + \alpha_s E_s = i\kappa_s E_p E_i^* \exp(i\Delta kz) \tag{2.3.3a}$$

$$\frac{dE_i}{dz} + \alpha_i E_i = i\kappa_i E_p E_s^* \exp(i\Delta kz) \tag{2.3.3b}$$

$$\frac{dE_p}{dz} = i\kappa_p E_s E_i \exp(-i\Delta kz) \tag{2.3.3c}$$

where $\alpha_{s,i} = \tfrac{1}{2}\mu_0 \sigma_{s,i} c$ are the field absorption coefficients, $\kappa_{s,i,p} = \left(\omega_{s,i,p} d_{eff} / n_{s,i,p} c\right)$ are the coupling coefficients, and where

$$\Delta k = k_p - (k_s + k_i) \tag{2.3.4}$$

is the phase mismatch term. We assume negligible absorption of the pump.

The phase mismatch term is of prime importance and the effect that it has on parametric generation will be discussed in detail shortly. An omission from the above equations is the initial relative phasing of the waves, $\Delta\phi = \phi_3 - \phi_2 - \phi_1$. In fact, this relative phasing determines which non-linear process ensues. For the case of a phase matched interaction, i.e. $\Delta k = 0$, maximum conversion from pump to signal and idler will occur if $\Delta\phi = -\pi/2$ [22]. Equally if the relative phase term is $\Delta\phi = \pi/2$ then the direction of energy flow will be reversed, and energy will flow from signal and idler to pump. For an intermediate value of $\Delta\phi$ power flows simultaneously in both directions and the net flow is determined by the wave magnitudes. If only two components are incident on the crystal, e.g. pump and signal, then the idler will automatically be generated with the correct phase to result in maximum power transfer to itself and correspondingly the signal. If all three waves are present, but with non-optimum phase, the signal and idler will decay until one of them is totally depleted and can take on the optimum phase which allows growth again. Equally, if at any point the pump were to become completely depleted, then it would start to be generated with the phase that transferred power back to itself from the signal and idler. This situation is referred to as back conversion.

2.4 Parametric Amplification

The coupled amplitude equations presented above describe the interaction between three waves. Exact solutions to these equations have been derived [5] which involve Jacobian elliptic functions and are therefore cumbersome and do not in themselves produce insight into what are the important parameters for the interaction. A commonly used approximation which allows solution of the amplitude equations is to assume that the pump beam is not substantially depleted by conversion to signal and idler waves. This 'undepleted pump' approximation reduces the three coupled equations to two (i.e. 2.3.3a and b), allowing solution with appropriate boundary conditions, and is valid for situations where conversion to signal and idler is small. The equations are therefore perfectly valid at threshold where pump depletion is negligible.

The resulting two amplitude equations have been solved for the general case of input waves at both signal and idler (as well as pump, of course), where the commonly used simplifying assumption of equal signal and idler absorption has not been made [23]. By using the substitution

$$A_{s,i}(z) = (n_{s,i}/\omega_{s,i})E_{s,i}(z) \tag{2.4.1}$$

the coupled equations for signal and idler which describe the case of a parametric amplifier with input at both signal and idler can now be written as

$$\frac{dA_s(z)}{dz} = -\frac{\alpha_s}{2}A_s(z) - i\gamma A_i^*(z)\exp(-i\Delta kz) \tag{2.4.2a}$$

$$\frac{dA_i^*(z)}{dz} = -\frac{\alpha_i}{2}A_i^*(z) + i\gamma A_s(z)\exp(i\Delta kz) \tag{2.4.2b}$$

where $\alpha_{s,i}$ is now the signal/idler power absorption coefficient and γ, the gain coefficient, is given by

$$\gamma = \sqrt{\kappa I_p} \tag{2.4.3}$$

where $\kappa = \dfrac{2\omega_s\omega_i d_{eff}^2}{n_s n_i n_p \varepsilon_0 c^3}$ is the non-linear interaction coefficient, and $I_p = \frac{1}{2}n_p c\varepsilon_0\left|E_p^2\right|$ is the pump intensity. Further manipulation of these equations allows a general form of solution to be achieved [23]. As the work described in this thesis deals mainly with singly resonant oscillators (SROs), rather than consider the general solution we adopt the limiting case where only one wave, which we take to be the signal, is present at the input to the amplifier. The resulting amplification of the signal is then given by

$$\frac{I_s(z)}{I_{s0}} = \frac{\exp(-\bar{\alpha}z)}{2}\left\{\left[1+\frac{(\Delta\alpha/2)^2+(\Delta k)^2}{|2b|^2}\right]\cosh(\beta z)+\left[1-\frac{(\Delta\alpha/2)+(\Delta k)^2}{|2b|^2}\right]\cos(\delta z)\right.$$
$$\left.+\frac{2}{|2b^2|}\left[(\beta\Delta\alpha/2+\delta\Delta k)\sinh(\beta z)+(\delta\Delta\alpha/2-\beta\Delta k)\sin(\delta z)\right]\right\} \tag{2.4.4}$$

where

$$|2b|^2 = \left[\left((2\gamma)^2+(\Delta\alpha/2)^2-(\Delta k)^2\right)^2+(\Delta k)^2(\Delta\alpha)^2\right]^{1/2},$$

$$\beta = \left[\left((2\gamma)^2+(\Delta\alpha/2)^2-(\Delta k)^2\right)^2+(\Delta k)^2(\Delta\alpha)^2\right]^{1/4}$$
$$\text{x}\ \cos\left[\tfrac{1}{2}\arg\left((2\gamma)^2+(\Delta\alpha/2)^2-(\Delta k)^2+i\Delta k\Delta\alpha\right)\right],$$

$$\delta = \left[\left((2\gamma)^2+(\Delta\alpha/2)^2-(\Delta k)^2\right)^2+(\Delta k)^2(\Delta\alpha)^2\right]^{1/4}$$
$$\text{x}\ \sin\left[\tfrac{1}{2}\arg\left((2\gamma)^2+(\Delta\alpha/2)^2-(\Delta k)^2+i\Delta k\Delta\alpha\right)\right],$$

$$\bar{\alpha} = \tfrac{1}{2}(\alpha_s+\alpha_i),\ \Delta\alpha = \alpha_i - \alpha_s$$

Equation 2.4.4 is therefore the solution to the problem of parametric amplification in the limits of infinite extent plane waves, negligible pump depletion, unequal signal and idler absorption, and input at only one of the parametrically generated waves (the signal here). We will show later how this equation, once modified, can be used in calculating the threshold energy for a SRO when the pump is only weakly focused.

Due to the number of terms involved in eqn 2.4.4 it does not grant an immediate insight into what the important parameters are in a parametric interaction. By limiting ourselves to the case of equal signal and idler absorption a solution for the gain at signal can be derived which allows a number of important ideas to be ascertained.

Again assuming that only the signal is incident on the parametric amplifier, the signal gain is then given by [11]

$$G_s(l_c) = \gamma^2 l_c^2 \frac{\sinh^2 g l_c}{(g l_c)^2} \tag{2.4.5}$$

where l_c is the crystal length, and g is the gain coefficient allowing for a phase mismatch, which is given by

$$g = \left(\gamma^2 - \left(\frac{\Delta k}{2} \right)^2 \right)^{1/2} \tag{2.4.6}$$

In the above expression for gain the effect of absorption is not included, as, with equal absorptions, they can be removed from the expression and will have the usual exponential form. This demonstrates clearly that the phase mismatch term reduces the gain that is available, and that the maximum gain, for the plane wave case, occurs for $\Delta k = 0$. As the gain decreases with phase mismatch we can therefore define a gain bandwidth within which the gain is half of that of the peak. The shape of the gain curve also depends on the magnitude of the peak gain (see Harris [9]) but to a good approximation we can define the FWHM gain bandwidth by

$$|\Delta k| = \frac{\pi}{l_c} \tag{2.4.7}$$

Note that although the calculations so far have been for the gain experienced by the signal wave, application of the Manley-Rowe relations [24] allows calculation of the idler. Every time a pump photon is 'split' to create a signal and idler pair, one photon is added to each of the signal and idler beams. The splitting ratio in terms of energy or power is simply the ratio of the signal and idler frequencies, i.e. the signal wave increase in energy is ω_s/ω_i that of the idler.

In summary, we have seen that the frequency pair which sees maximum gain is that

which satisfies the phase matching condition given by the requirement

$$k_p = k_s + k_i \tag{2.4.8}$$

and that we can define a gain bandwidth for the interaction. The next section describes how phase matching is achieved, and the effect the gain bandwidth has both in terms of the output properties of a parametric amplifier and in placing restraints on the pump.

2.5 Phase matching and acceptance parameters

2.5.1 Phase matching

Phase matching is the term used to describe processes by which the momentum or phase mismatch term, Δk, can be made equal to zero. The name *phase* matching arises because in this way the free electromagnetic waves propagate with the same *phase* velocity as the non-linear polarisation waves which give rise to them. This is necessary to allow the waves to grow continuously. A number of ways of achieving phase matching have been achieved, of which the most common is the use of the birefringence of the material.

As given previously in section 2.4. the phase match relation is defined as

$$k_p = k_s + k_i \tag{2.4.8}$$

Using the relation $k_i = 2\pi n_i/\lambda_i$, where n_i are the refractive indices and λ_i are the free space wavelengths (i =p,s,i), we can re-express the phase matching condition in the more useful form of

$$\frac{n_p}{\lambda_p} = \frac{n_s}{\lambda_s} + \frac{n_i}{\lambda_i} \tag{2.5.1.1}$$

In normally dispersive materials, the refractive index decreases with increasing wavelength, and the condition given by eqn 2.4.8 cannot generally be met. However, in

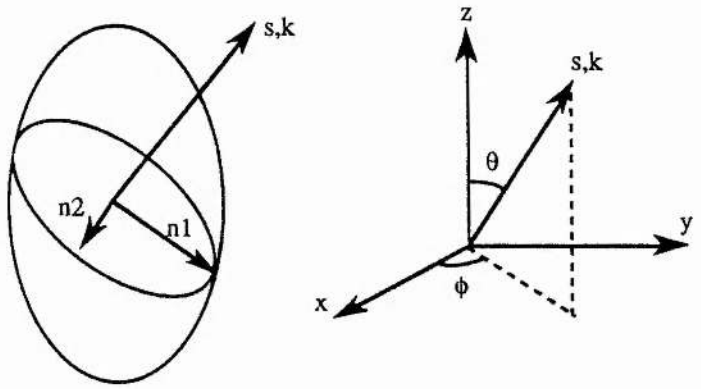

fig. 2.1 Optical indicatrix, and axial convention for describing refractive indices.

anisotropic crystals, which most materials used in second order non-linear experiments are, the refractive index depends additionally on the direction of propagation with respect to the dielectric axes and on the polarisation of the wave [25]. This behaviour is shown schematically in fig. 2.1 which shows an example of the optical indicatrix, or index ellipsoid, and the axial convention for describing it.

Theory shows that two waves, with orthogonal polarisations, can propagate independently in the crystal. These waves must satisfy the Fresnel equation which determines the dependence of refractive index with propagation direction, and can be written as [26]

$$\frac{\sin^2\theta\cos^2\phi}{n_{\omega,i}^{-2}-n_{x,\omega}^{-2}}+\frac{\sin^2\theta\sin^2\phi}{n_{\omega,i}^{-2}-n_{y,\omega}^{-2}}+\frac{\cos^2\theta}{n_{\omega,i}^{-2}-n_{z,\omega}^{-2}}=0 \qquad (2.5.1.2)$$

The two orthogonal polarisations experience different refractive indices, except in the case where the direction of propagation is along an optic axis. Thus by propagating through the crystal at a specific angle with a specific polarisation we can control the refractive index, and hence the k values, and in certain circumstances we can satisfy eqn 2.4.8, the phase matching condition. Because eqn 2.4.8 is a vector relation, it is possible to achieve phase matching for waves which are either collinearly or noncollinearly propagating.

Angular phase matching, as described above, is not the only means by which phase matching can be achieved. The refractive indices can also be changed by controlling the temperature of the crystal, though the dependence on temperature is stronger in some crystals than in others. If adjustment of the temperature allows phase matching to be achieved for propagation along one of the principal axes of the optical indicatrix, then this has advantages in terms of angular and spectral properties which will shortly be described.

Another technique which has seen success is the use of guided wave and periodic structures. As the phase velocity of a guided wave can differ significantly from that of the same wave in the bulk medium, it is possible to find combinations of modes in which the phase matching conditions are satisfied. Phase matching can also be achieved by introducing a periodicity into the structure (notably for guided waves) that modifies either the propagation constants, or the sign or magnitude of the non-linearity. A reversal of the sign of the non-linearity with a periodicity equal to an odd integer multiple of the coherence length (defined by $\Delta kz = \pi$) is referred to as quasi-phase matching and was in fact one of the original techniques suggested by Armstrong et al [5]. Ignoring the difficulty of producing these structures, they have the advantage that they allow phase matching where it was otherwise unobtainable, and they also allow the use of large non-linearities which may also not have been accessible with phase

matching by birefringent techniques.

2.5.2 Angular acceptance

As mentioned previously, the gain that can be obtained depends on the intensity of the interacting beams. Thus it is obviously advantageous to have as high an intensity as possible in the crystal to maximise the gain. The limit to this being that at some point the crystal will start to damage [27]. If the pump source is of limited energy then it is likely that to approach the damage threshold, the beam will have to be focused. Focusing of the beam inherently means that different parts of the beam will propagate through the crystal at different angles, and it will therefore become impossible to satisfy the phase match condition for the whole beam simultaneously. It is therefore appropriate to define a degree of focusing that can be utilised before the deviation away from phase matching negates the effect of the focusing. This is commonly referred to as the angular acceptance of the crystal, and it is defined to be the angular deviation from perfect phase matching at which the magnitude of the mismatch is no greater than π/l [28].

Generally the direction through the crystal at which phase matching occurs is specified by two angles, θ, the angle between the k vector and the z-axis and, ϕ, the angle between the projection of the k vector in the xy plane and the x-axis. This means that an acceptance angle can be defined with respect to both these planes. The derivation applies to both. If we expand the k-vector, to second order, about one of the phase matching angles, say θ, this can be represented by

$$k_i = k_{i0} + \frac{\partial k_i}{\partial \theta}\delta\theta + \tfrac{1}{2}\frac{\partial^2 k_i}{\partial \theta^2}\delta\theta^2 \qquad (2.5.2.1)$$

Inserting this in eqn. 2.3.4 and applying the condition that the centre wavelengths are matched, $k_{p0} - k_{i0} - k_{s0} = 0$, we get

$$\Delta k = 2\pi\left(\frac{1}{\lambda_p}\frac{\partial k_p}{\partial \theta} - \frac{1}{\lambda_i}\frac{\partial k_i}{\partial \theta}\right)\delta\theta + \pi\left(\frac{1}{\lambda_p}\frac{\partial^2 k_p}{\partial \theta^2} - \frac{1}{\lambda_i}\frac{\partial^2 k_i}{\partial \theta^2} - \frac{1}{\lambda_s}\frac{\partial^2 k_s}{\partial \theta^2}\right)\delta\theta^2 \qquad (2.5.2.2)$$

where the derivatives are evaluated at θ.

For phase match angles greater than 5°, expansion to first order is sufficiently accurate [29]. If propagation is close to one of the principle dielectric axes of the crystal, i.e. θ = 0 or 90°, then the first term vanishes and the remaining second order term means that the effect of the angle on the phase mismatch is much reduced. This results in an increase in the acceptance angle of the crystal for this direction, which, because of the relaxation of alignment sensitivity, is termed 'non-critical phase matching' (NCPM). In the case where the first term dominates, the tighter alignment sensitivity leads to

'critical phase matching'.

If the condition on the maximum magnitude of the allowable angular phase mismatch, $\Delta k = \pi/l$, is applied then an acceptance angle can be calculated from the resulting linear (critical) or quadratic (non-critical) equation in $\delta\theta$, which is normally quoted in mrad.cm for critical and mrad.cm$^{\frac{1}{2}}$ for NCPM.

2.5.3 Poynting vector walk-off

Critical phase matching does have a major disadvantage. In order to achieve phase matching, at least one of the waves must be of extra-ordinary or e- polarisation [25]. Because of the angular dependence of the refractive index, as described earlier, e-waves propagate with elliptical rather than spherical wavefronts. This results in the direction of energy flow, referred to as the Poynting vector, differing from the direction of the wave front normals. This means that although an e- and an o-wave may start off in the same direction, the e-wave will follow the Poynting vector and 'walk off' from the direction of the o-wave. This effect is seen to have a dramatic effect on amplification and oscillation thresholds as it results in a decoupling of the waves.

This effect is closely related to angular acceptance in that focusing of the interacting beams beyond a certain point reduces the coupling between the beams despite the fact that higher intensities are available due to the effects of focusing. In the case of angular acceptance, larger spot sizes, and hence less divergent beams, results in less phase mismatch across the wavefront. Larger spot sizes also reduce the effects of walk-off as for a given amount of walk-off, specified by the walk-off angle ρ, the fraction of the beams still overlapping after a distance, l_c, will be larger for larger spot sizes. This is perhaps more easily explained with the use of a diagram, see fig. 2.2, in which the rule of thumb of $w = \rho l_c$, as a minimum spot size is illustrated.

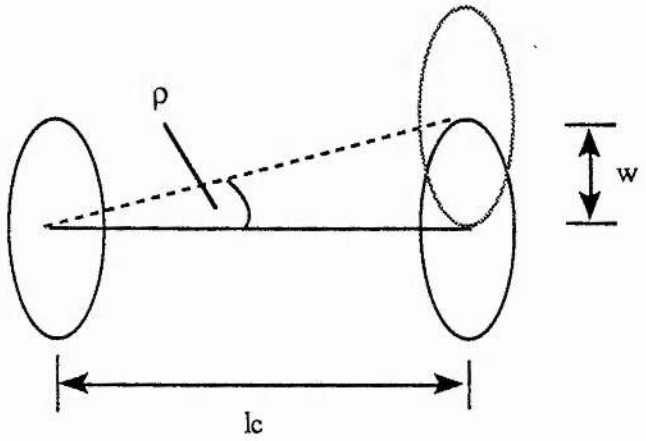

fig. 2.2 Effect of walk off on the interaction of two beams

The detrimental effects of walk-off can be eliminated by utilising a non-critical phase

match geometry where all wavefronts approximate to circular and the wavevector and poynting vector are collinear for all three waves (assuming collinear phase matching).

2.5.4 Spectral Acceptance

Obviously the phase mismatch condition can only be satisfied exactly for one set of pump, signal and idler wavelengths. It is of interest to know by how much these can vary before the gain is reduced by the resulting phase mismatch. This is completely analogous to the calculation of angular acceptance previously carried out. An equation similar to eqn 5.2.2.2 can be derived where the k-vector is expanded in terms of $\delta\omega$ or $\delta\lambda$. The pump spectral acceptance is calculated by holding the signal and idler frequencies fixed, and equally the bandwidth of signal and idler can be calculated by holding the other two frequencies constant, remembering that the additional relation $\delta\omega_s = -\delta\omega_i$ is required for energy conservation. The actual expression for the signal bandwidth for the case of o-oe phase matching in KTP is given in section 5.8.1.

2.6 Focused gaussian beams

Till now we have only considered the case of parametric interaction between infinite, uniform, plane waves. The equations relating to this brought out some of the salient points with regard to parametric amplification and were useful in that context. However, the laser beams that are used in practice are of finite spatial extent, have a non-uniform transverse structure and are usually focused to some degree. It is therefore necessary here to introduce the modifications and changes to the theory that allow us to assess the interaction which actually occurs in practice.

The electric field of an incident TEM_{00} pump beam can be given by

$$E_p = \frac{E_{p0}}{(1+i\tau_p)} \exp ik_p z \exp\left\{-\frac{(x^2+y^2)}{w_{p0}^2(1+i\tau_p)}\right\} \qquad (2.6.1)$$

where

$$|E_{p0}|^2 = \frac{16P_p}{n_p c w_{p0}^2}\ ,\ \tau_p = 2(z-l/2)/b_p\ ,\ b_p = w_{p0}^2 k_p$$

where P_p is the pump power, w_{p0} is the 1/e waist radius, b_p is the confocal parameter and the spot is focused at the centre of the crystal.

The effects of focused gaussian beams on the parametric interaction have been calculated by Boyd and Ashkin [30] for the case of near field focusing, i.e. $b>l_c$, and for the case of arbitrarily tight focusing by Boyd and Kleinman [15]. These analyses apply to the case of a DRO where both generated waves take the form of eqn 2.6.1 above. As

the work here involves a SRO, we present only some of the important points from these analyses and refer an interested reader to the original papers.

The interaction of two waves with gaussian transverse properties results in a polarisation wave with a gaussian transverse spatial extent described by

$$\frac{1}{\overline{w}_s^2} = \frac{1}{w_i^2} + \frac{1}{w_p^2} \tag{2.6.2}$$

where $\overline{w}_s$ is the signal polarisation radius with identical equations for idler and pump polarisations obtained by permutation of the indices. A coupling coefficient [31] can be calculated which allows for the coupling between electric field and driving polarisation. These coupling coefficients take the form

$$g_j = 2\frac{\overline{w}_j^2}{\overline{w}_j^2 + w_j^2} \tag{2.6.3}$$

and should be included in the coupled amplitude equations. Boyd and Ashkin [30] showed that maximisation of coupling, for fixed w_i and w_s, requires

$$\frac{1}{w_p^2} = \frac{1}{w_s^2} + \frac{1}{w_i^2} \tag{2.6.4}$$

In their near field analysis, they ignore walk off and so maximisation of the gain requires w_i and w_s as small as possible, which, when restricted to the constraint of a near field analysis, corresponds to the case of confocal focusing, giving the maximum parametric gain as

$$G = \Gamma^2 l_c^2 = \frac{4\omega_o^2\left(1-\delta^2\right)\left|d_{eff}^2\right|l_c^2}{n_p n_s n_i \varepsilon_0 c^3} \frac{P_p}{\pi\left(w_s^2 + w_i^2\right)} \tag{2.6.5}$$

where ω_0 is the degenerate frequency, δ is the frequency deviation from degeneracy and the other terms have their usual meaning.

The case of arbitrarily tight focusing allowing for poynting vector walk off and diffraction was considered by Boyd and Kleinman [15]. Because of the more complicated z dependence of the electric field, this problem is not analytically solvable and can only be solved by numerical techniques. The power gain experienced by an incident gaussian mode may be found by evaluating a volume integral of the form $\int \mathbf{E}^* . \mathbf{P} dv$. The effective single pass gain so derived differs from the above expression (2.6.5) for the confocal case only by a reduction factor $\overline{h}_m(B,\xi)$ where, $\xi = l_c/b$ is the focusing parameter, and B is the double refraction parameter given by

$$B = \frac{\rho}{2}\left(\frac{2\pi l_c n_0}{\lambda_0}\right)^{1/2}\left(\frac{n_p}{n_0}\right)^{1/2} \tag{2.6.6}$$

The reduction factor is a complicated function and its variation with focusing is reproduced from Boyd and Kleinman in fig. 2.3.

It is seen that an optimum focusing can be defined depending on the walk off, and that for large walk off, the reduction factor is less sensitive to the degree of focusing. The maximum value of $\bar{h}_m(B,\xi)$ is 1.07, and this occurs for the case of B = 0, i.e. no walk off, at an optimum focusing of $\xi = 2.84$. It can be seen from fig.2.3 that although the optimum focusing is considerably tighter than the confocal case, the increase in gain obtained is not great, approximately 20%.

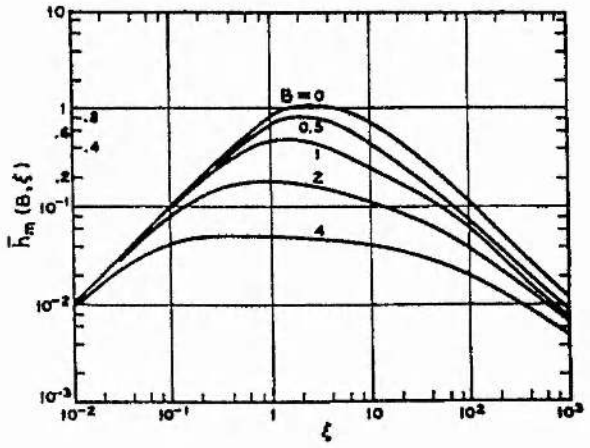

fig. 2.3 $\bar{h}_m(B,\xi)$ as a function of focusing parameter ξ, for different values of walk off parameter B

The gaussian beam analysis so far has assumed that both the signal and idler (and pump) can be described by a well defined radial variation. This is not necessarily correct in the case of a SRO. If only one of the beams, say the signal, is resonated then the other beam, the idler, will not be constrained to follow the modes of the resonator and will propagate freely with the radial variation of its driving polarisation. A general solution to this problem is first presented for arbitrary focusing, followed by the limiting case of weak focusing.

The calculation of the gain in a SRO when the resonated wave (taken to be the signal) is a mode of a stable, spherical mirror cavity and where the pump beam is mode matched to the cavity was performed by Asby [32] using a coupling coefficient approach, and also by Guha, Wu and Falk [14] using a Green's function approach. We refer to this case as involving the cold-cavity determined spot size. We find the analysis of Guha more amenable to inclusion of time dependence which will be included later to allow for pumping with a pulsed laser.

The Guha analysis calculates the steady state threshold of a SRO using a Green's function approach, allowing for diffraction, walk-off and focusing. It follows a similar approach to that of Boyd and Kleinman for the DRO [15], but does not make the assumption that the confocal parameters of all the waves are the same, and carries out a Green's function derivation as opposed to the heuristic ray-path approach adopted by Boyd and Kleinman, which was justified elsewhere [33].

The power gain in the signal is [14]

$$\Delta P_s = -\frac{1}{2}\omega_s \operatorname{Im}\int E_s^* \mathcal{P}_s dxdydz \tag{2.6.7}$$

In the derivation produced here, we differ slightly from Guha in that the non-linear interaction is type II o-oe and allowance is made for the pump focus being displaced from the centre of the crystal. The incident pump wave and TEM_{00} resonated signal wave can then be written as eqn 2.6.1 with the change for the pump

$$\tau_p = 2\left(z - f_p l\right)/b_p \tag{2.6.8}$$

Allowance is made for the pump wave being focused away from the centre via the variable f_p, such that $f_p = 0$ puts the focus at the input face and $f_p = 1$ puts it at the exit face.

The idler wave is not resonated and takes its form from the driving polarisation due to the interaction of the pump and signal fields. Following the convention of Boyd and Kleinman [15], the non-linear polarisation at the idler frequency is given as

$$\mathcal{P}_i = 2d_{eff}E_p E_s^* \tag{2.6.9}$$

Using this polarisation as a source term in the Maxwell wave equation gives the idler electric field as

$$E_i(r) = \frac{2\pi i\omega_i}{c}\int \mathcal{P}_i(r')G_e(r,r')dr' \tag{2.6.10}$$

where the external Green's function for an e-wave idler is given by

$$G_e(r,r') = \frac{\omega_i}{2\pi ic}\exp\left(-\frac{\alpha_i}{2}(z-z')\right)\frac{\exp\left(ik_i(z-z')\right)}{z-z'}\exp\left\{ik_i\frac{\left(\left(x-\rho_i(l-z')\right)-x'\right)^2+(y-y')^2}{2(z-z')}\right\}$$

and α_i and ρ_i are the absorption coefficient and walk-off angle respectively.

The signal polarisation can now be obtained from

$$\mathcal{P}_s = 2d_{eff}E_p E_i^* \tag{2.6.11}$$

using (2.6.10) and (2.6.1). Substituting the signal polarisation from (2.6.11) and signal field from (2.6.1) into (2.6.7), integration over the cavity with the low gain assumption that P_p, P_s and P_i are all constant during a single pass, gives the power generated in the signal mode as

$$\Delta P_s = K_3 P_s P_p h_s \tag{2.6.12}$$

where

$$K_3 = \frac{128\omega_s\omega_i\left(2d_{eff}\right)^2\pi^2 l}{n_s n_i n_p c^3}\frac{k_s k_p}{k_s + k_p}$$

$$h_s = \frac{1}{4}\frac{(1+k)}{\xi_p + k\xi_s}\mathrm{Re}(I_1)$$

$$I_1 = \int_0^{l_s}\int_0^{z_2} dz_1 dz_2 \frac{\exp\left((-\alpha_i/2 + i\Delta kl)(z_1 - z_2)\right)\exp\left(\rho_i^2 f_{wi}\right)}{\beta}$$

$$\beta = \frac{-i}{4}(z_1 - z_2)\left(\frac{1}{\xi_5} + \frac{1}{\xi_6}\right) + z_1 z_2 + \frac{1}{4\xi_5\xi_6} - \frac{1}{4}\frac{\xi_p\xi_s}{\xi_6}\left\{(z_1 - z_2)\frac{g_1}{i} - g_2 + (z_1 + z_2)g_3\right\}$$

$$g_1 = k'^2 - k'\left(2f_p + 1\right) + 2f_p \quad , \quad g_2 = \frac{2f_p}{\xi_5} + \left(\frac{\xi_s - 2f_p\xi_p}{\xi_p\xi_s}\right)k'$$

$$g_3 = \frac{1 + 2f_p}{\xi_5} + \frac{k'\left(\xi_s - \xi_p\right)}{\xi_s\xi_p} - \frac{\xi_s - 2f_p\xi_p}{\xi_s\xi_p}$$

$$k' = \frac{k - 2f_p}{k - 1} \quad , \quad f_{wi} = (z - z')^2\left(\frac{\left(a_3^*\right)^2}{ib_1} + a_3^*\right)$$

with the remaining terms as defined in Guha.

In this case the single pass gain is an additive term rather than a multiplicative term, and so the gain definition is

$$P_s(l) = P_s(0) + \Delta P_s = GP_s \tag{2.6.13}$$

where

$$G = 1 + \gamma \quad , \quad \gamma = \frac{\Delta P_s}{P_s} = K_3 P_p h_s \tag{2.6.14}$$

The parameter h_s in (2.6.14) encompasses all spatial effects, and is the optimisable parameter. The units involved in K_3 as defined in the original paper are cgs and esu. The definition of K_3 in the units adopted here is

$$K_3 = \frac{2.383x10^{-3} d_{eff}^2 l}{\lambda_s \lambda_i n_i \left(n_s \lambda_p + n_p \lambda_s\right)} \tag{2.6.15}$$

where d_{eff} is in pm/V, l is in cm, $\lambda_{p,s,i}$ are in μm, and power is in watts.

The work of Guha et al, from here on referred to simply as Guha for brevity, showed that the assumption of Boyd and Kleinman that the optimum situation occurred with all beams having equal confocal parameters did not apply in the general case. It was found, however, that for optimum focusing with no walk off, i.e. $\xi = l_c / b = 2.84$, the case of equal pump and signal confocal parameters is optimum. However, for less tight focusing of the pump (which is normally the case in practice), the signal should be focused tighter than the pump. This will be shown more clearly in the next section where some modelling of pulsed thresholds is presented. This modelling relied on computer calculations of the parameter h_s as given above. The program used in these calculations is given in Appendix B and was developed in this department by Tang Yan.

A simpler approach which is valid in many experimental set ups was developed by Brosnan and Byer [13] and applies to the case where all the interacting waves are weakly focused or effectively collimated. This approach assumes an undepleted pump and uses the first two of the coupled amplitude eqns, i.e. 2.3.3a and b. As the idler wave will not be resonated its polarisation assumes the shape of its driving polarisation, that is $\overline{w}_i = w_i$. The signal polarisation radius may therefore be written as

$$\frac{1}{\overline{w}_s^2} = \frac{1}{w_s^2} + \frac{2}{w_p^2} \tag{2.6.16}$$

A coupling coefficient has to be derived which allows for how this polarisation will couple into the signal cavity mode. The signal coupling coefficient is as eqn 2.6.3 with the polarisation given by 2.6.16, and the coupling coefficient for the idler is unity as it follows its driving polarisation. To allow for walk off, an effective crystal length can be derived which depends on the type of phase matching. In the case to be considered here of type II o-oe with resonant signal e-wave the effective length, l_{eff}, is

$$l_{eff} = l_w erf\left(\frac{\sqrt{\pi}}{2}\frac{l_c}{l_w}\right) \tag{2.6.17}$$

where l_w is the walk off length defined as

$$l_w = \frac{\sqrt{\pi}}{2}\frac{w_s}{\rho}\sqrt{\frac{w_p^2 + w_s^2}{w_s^2 + w_p^2/2}} \tag{2.6.18}$$

Allowing for unequal signal and idler absorption requires the use of the expression for the signal gain as given in eqn 2.4.4 where the effective crystal length is used and the

gain coefficient is now

$$\gamma = \sqrt{g_s \kappa I_p} \tag{2.6.19}$$

where g_s is the signal coupling coefficient and κ and I_p are as defined previously in section 2.4.

Now that the gain equations have been defined we can go on to consider the effect of placing the parametric amplifier in a resonant cavity, i.e. we now consider the optical parametric oscillator.

2.7 Parametric Oscillation

In this section we will discuss the effect of placing the previously discussed parametric amplifier in a resonant cavity. So far we have discussed the gain of a weak signal beam due to the interaction with a strong pump beam. In an oscillator the only input beam is the pump and generation of the signal and idler beams is facilitated by spontaneous parametric emission. Derivations of steady state thresholds are presented to demonstrate the difference between single and double resonance. The requirements that double resonance plays on the stability of the pump frequency and the cavity will be discussed. Calculation of thresholds for a pulsed pump laser are more complicated and presented here is a comparison between the model of Brosnan and Byer [13] and that developed in this work which incorporates time dependence into the calculations of Guha et al [14]. We also discuss the efficiencies that can be expected from these devices.

2.7.1 Spontaneous parametric emission

When a pumped non-linear optical material, i.e. a parametric amplifier, is placed within an optical resonator that possesses a high Q for either the signal or idler, (singly resonant oscillator, SRO) or both (doubly resonant oscillator, DRO) then the resultant device is called an Optical Parametric Oscillator (OPO).

We have seen in the previous sections that under the appropriate conditions of energy conservation, eqn 2.3.2, and momentum conservation, eqn 2.4.8, that if either a signal or idler beam, or both, is present they will experience amplification. (It is only necessary for the beams to lie within the gain bandwidth given by eqn 2.5.2.2 in order to experience some degree of gain.) If the gain received from the parametric interaction is large enough to overcome the cavity losses, both coupling and parasitic, then oscillation will occur. However, before amplification can occur we must have a few signal and/or idler photons present at the crystal to start with. These initial photons are provided by a process variously referred to as spontaneous parametric emission, parametric fluorescence, parametric luminescence and parametric noise [9].

When light from a pump laser is incident on a non-linear crystal, there is a probability that the pump photons will spontaneously split into signal and idler photons. This can be shown quantum mechanically [34,35] to be equivalent to the now accepted view [36] that the process is due to the interaction of the vacuum field fluctuations, equivalent to half a photon per mode, with the pump photons via the non-linear polarisation. This spontaneous parametric emission then provides a source of noise from which the signal and idler beams grow. It is interesting to note the similarities here between an OPO and a laser. Both consist of a gain medium enclosed by a resonator, where, in an OPO, the gain is created by the non-linear polarisation, and in a laser, the gain is provided by a population inversion, (usually![37]). Both also grow from noise, where, in an OPO, the noise is spontaneous parametric emission, whereas, in a laser, the noise is the spontaneous emission from the upper laser level. Spontaneous parametric emission can also be used for determining non-linear coefficients and measuring phase matching curves, where it has a number of advantages over the conventional technique of SHG [36].

2.7.2 CW or steady-state parametric oscillation threshold

The threshold pump power of the oscillator can de defined as the requirement that the single pass gain be sufficient to offset the cavity loss. As the signal and idler interact with the pump in only one direction (unless the pump beam is double passed or even resonated) the gain is only single pass. If we define a_1 and a_2 as the round trip electric field loss at the signal and idler frequencies respectively then the amplitude requirement for threshold is that the magnitude of each wave is the same after a round trip as it was before the round trip. (We also require the phase relation between the waves to be maintained, that is, the sum of the signal and idler phases is constant when referenced to the phase of the pump for stable single mode pair operation [38]). The relation between the magnitudes requires

$$E_j(z=0)=\left(1-a_j\right).G.E(z=0)=\left(1-a_j\right)E_j\left(z=l_c\right) \qquad (2.7.2.1)$$

where j corresponds to signal and idler, and G is the single pass gain. For demonstration purposes, we use here the solution to the coupled amplitude equations for infinite, uniform, plane waves under the assumption of an undepleted pump. The requirements on threshold assuming both signal and idler are resonated are [11]

$$\frac{1}{1-a_s}E_s(0)=E_s(0)\cosh\Gamma l_c+i\left(\frac{\kappa_s}{\Gamma}\right)E_pE_i^*(0)\sinh\Gamma l_c \qquad (2.7.2.2a)$$

$$\frac{1}{1-a_i}E_i(0)=E_i(0)\cosh\Gamma l_c+i\left(\frac{\kappa_i}{\Gamma}\right)E_pE_s^*(0)\sinh\Gamma l_c \qquad (2.7.2.2b)$$

Taking the complex conjugate of eqn 2.7.2.2b and solving the simultaneous equations

gives

$$\cosh \Gamma l_c = 1 + \frac{a_s a_i}{2 - a_s - a_i} \tag{2.7.2.3}$$

which for low losses at both waves, i.e. a DRO, reduces to

$$\Gamma^2 l_c^2 = a_s a_i \tag{2.7.2.4}$$

For low loss at only one wave and no feedback at the other $a_i = 1$, i.e. a SRO, we get

$$\Gamma^2 l_c^2 = 2a_s \tag{2.7.2.5}$$

We see from the above that the DRO threshold differs from that of the SRO by a factor $a_i/2$. Thus, if the resonator has a high Q for the resonated waves, i.e. low losses, then the DRO threshold may be two orders of magnitude less than that of the equivalent SRO. This assumes that both the signal and idler are resonated simultaneously in the DRO case, which requires a single frequency pump and a stabilised OPO cavity, about which more will be said in the next section. While the first cw DRO OPO was demonstrated as early as 1968 using $Ba_2NaNb_5O_{15}$ pumped at 532 nm [39], the large increase in threshold imposed by single resonance has only recently [40] allowed operation of a cw SRO.

2.7.3 Double resonance and the cluster effect

The previous section showed how a lower threshold is obtained by resonating both the signal and idler waves. However, this lower threshold is accompanied by the requirement of a stable, single frequency pump source and also places strict constraints on the stability of the OPO cavity.

The presence of a dispersive medium in the cavity, i.e. the non-linear crystal, means that the axial mode spacings at the signal and idler frequencies are different. Therefore, not every signal cavity resonance will have a corresponding idler resonance such that the two resonance frequencies satisfy the energy conservation condition (2.3.2). If fact, in general, there will be no pair of frequencies where an exact coincidence of resonances occur, though frequency pairs where the matching of resonances are close will occur, and are referred to as 'cluster frequencies'. General consideration of the operating point of a DRO as well as the concept of cluster spacing was first given by Giordmaine and Miller [41]. Fig.2.4 is a reproduction of a diagram from Eckardt et al [42] which expresses particularly well the ideas originally forwarded by Giordmaine and Miller.

The difference between signal and idler mode spacings, $\delta\omega_1$ and $\delta\omega_2$ respectively, is exaggerated in fig.2.4 for the purpose of illustration. The scales are obtained by considering the mode spectrum for both signal and idler cavity modes, and then

imaging the idler mode spectrum through the degeneracy point so that frequency increases from left to right for the signal, but from right to left for the idler. In this way, by placing the idler scale under the signal scale, signal and idler modes which satisfy energy conservation will coincide vertically. In general there will be some frequency mismatch $\Delta\omega$, which is the frequency shift required of signal or idler to produce exact coincidence. The blow up of a close coincidence, or cluster, shows how the frequency mismatch $\Delta\omega$ can be represented by signal, $\Delta\omega_1$, and idler, $\Delta\omega_2$, components which are the respective frequency displacements from the centres of the signal and idler cavity resonances to the frequencies most favourable for parametric oscillation.

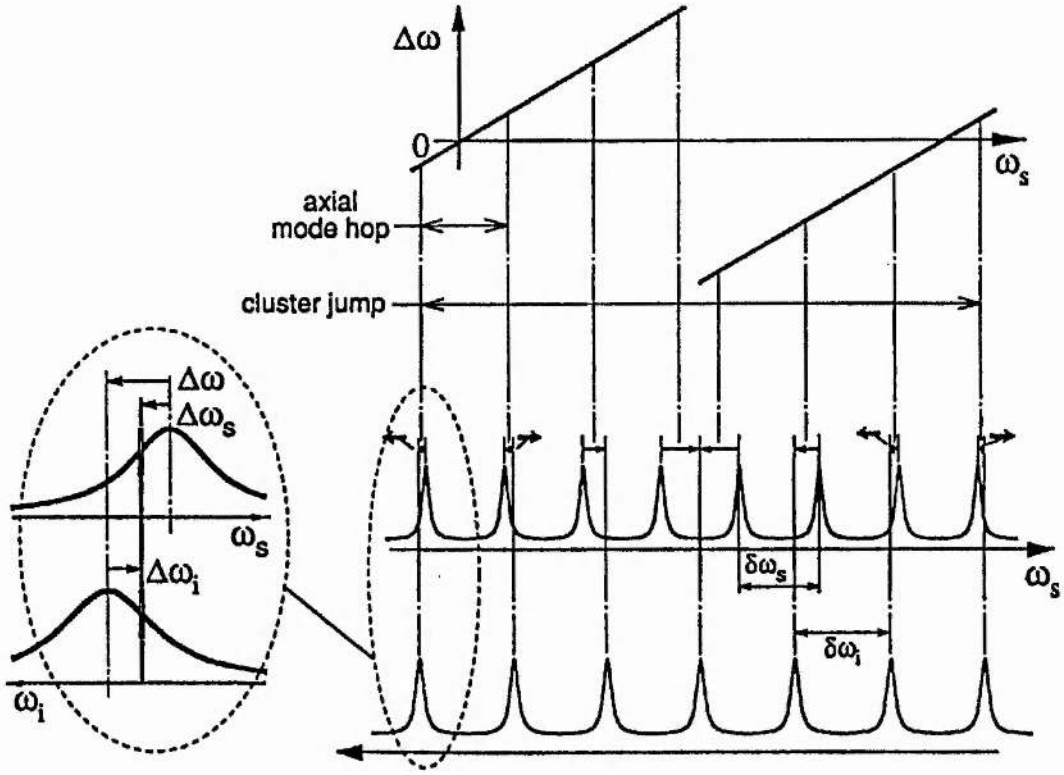

fig. 2.4 This diagram shows the relationship between signal and idler resonances, with frequency increasing from left to right for the signal, and right to left for the idler. Two modes which satisfy energy conservation are located vertically to each other. The blow up shows in more detail how there will generally be some frequency mismatch $\Delta\omega$.

As a tuning variable changes, e.g. pump frequency or cavity length, the signal-idler mode pair which best satisfies energy conservation may change, and subsequently, because of a lower threshold, the DRO will then tend to oscillate on the new, more favourable mode pair. This type of discontinuous frequency change is referred to as a mode hop. Phase matching also affects the operating point of the DRO. If a tuning variable changes sufficiently, then the operating point, which corresponds to the mode pair which best satisfies phase matching, energy conservation and mode overlap, may find a lower threshold a full cluster spacing away, and will hop to these modes. The

signal and idler frequencies progress along a single cluster curve until the operating conditions of the next cluster curve are more favourable, at which point it will cluster hop. An additional factor to be considered is the fact that because an OPO has an appreciable gain bandwidth, as given by $|\Delta k| = \pi/l_c$, then it is possible that there may be more than one cluster frequency within the gain bandwidth and the DRO may operate multi-longitudinal mode. Some further aspects of this are discussed later under spectral properties.

The effect that these resonance mismatches have on threshold depends on a number of factors, e.g. finesse and the degree of overlap, and was investigated by Falk [43]. This analysis was followed and extended in a recent paper by Eckardt et al [42], from which fig.2.4 is taken. These analyses show that in order to obtain the low thresholds that are offered by double resonance, the tuning parameters, i.e. pump wavelength and OPO cavity length, must be controlled accurately in order to obtain a stable, both frequency and amplitude, output. It is because of these stringent demands that the higher thresholds needed for single resonance are often seen as less of a problem than the stability requirements of DROs.

2.8 Parametric oscillation threshold for a pulsed pump

Up till now, we have only considered oscillation under the steady state conditions of a cw laser as the pump source. Although, as mentioned recently, the threshold for DROs can be two orders of magnitude less than the equivalent SRO, the frequency instabilities of the pump lasers have caused erratic operation of DROs. This is one of the reasons why, due to the high powers required to achieve threshold for a SRO, the most common pump sources have been Q-switched lasers with pulse lengths typically in the range 10 ns to 1μs. Additionally, the SRO has some favourable spectral properties, as will be discussed later. Although a Q-switched laser may have a very high peak power, and be many times the previously derived cw threshold it does not necessarily produce a good conversion efficiency. One of the criteria for a good pulsed pump source is that the OPO remains above threshold long enough for the signal and idler to build up, from noise, to a level comparable to the pump. It is therefore necessary to modify the approach taken so far so as to encompass time dependence.

The rise time for achieving oscillation can be given in terms of the number of round trips necessary to allow the signal and idler waves to be amplified to a certain level. In this way, the peak power, which determines the excess gain over losses, the pump pulse length and the cavity length and round trip time are all important parameters. The rise times for both DROs and SROs were calculated by numerical techniques by Pearson et al [44]. To be more exact, the work of Pearson et al predicted the number of times above cw or steady state threshold the oscillator had to be pumped in order to achieve an appreciable output under pulsed pumping, where the important parameters were

pump pulse length and OPO cavity length. This approach does not give immediate insight into the important parameters for a pulsed OPO. The approach which will now be presented presents a more easily digested account of the threshold of pulsed SRO OPOs.

In the rest of this section we detail two slightly different approaches to the calculation of pulsed threshold. As the aim of this work was to develop an OPO pumped by a low power diode-pumped solid-state laser it was important to be able to predict and optimise thresholds to a reasonable degree of accuracy. Because of this a fair amount of time was devoted to the modelling of the build-up to threshold.

An established model which had been published in the literature was that due to Brosnan and Byer [13]. (For ease of notation, from here on the abbreviation BB will be used to refer to the Brosnan and Byer work.) Their model applies specifically to the case where the OPO resonator is formed by two plane mirrors and the pump beam focusing is sufficiently weak such that the pump is effectively collimated within the OPO cavity.

In their Appendix A, BB show that the effect of the interaction of pump and idler waves with gaussian profiles is to produce a gaussian signal polarisation. The effect of this is that a stable signal mode can exist in the normally unstable plane-plane resonator due to the narrowing effect of the gain polarisation balancing out the spreading due to diffraction. A self consistent field approach produces a signal spot size which is determined by the pump spot size and diffraction. This formalism can easily be adapted to the case of spherical mirrors by modifying the round trip matrix to allow for the focusing effect of the mirrors. We refer to this case as the gain guided or self-consistent field spot size. This spot size should be valid during build up to threshold, but at higher pump powers when pump depletion sets in, the signal will expand due to the flattened gain profile. In the case of spherical mirrors, the mode should expand out towards that expected for the cold cavity. However, since an implicit assumption in this treatment is that the pump beam is a collimated, plane wave it is not to be expected that use of this model for the case of a focused pump beam, mode-matched to a spherical mirror cavity will produce accurate results.

As the signal is resonated, its driving polarisation must be expanded out in terms of cavity modes, and only the component that couples into the TEM_{00} mode is of relevance here. BB assume that the signal and idler have equal absorptions and that the interaction is phase matched, arriving at an expression for the signal gain as

$$G = \frac{E_s(l_c)}{E_s(0)} = \exp(-2\alpha l_c)\cosh^2 \Gamma l_{eff} \qquad (2.8.1)$$

where α is the signal/idler absorption and the other parameters are as detailed in section 2.6, eqns 2.17-2.19. As will be discussed in chapter 3, for the wavelengths of interest in this work the signal and idler absorptions are not equal. We have therefore used the fuller expression for the signal gain, as developed by Zahler and Ben-Aryeh [23] and given in eqn 2.4.4 with the value for the gain coefficient, γ, as given in eqn 2.6.19. We follow the procedure of BB by directly introducing the time dependence to the gain coefficient. Before introducing the exact way in which we calculate threshold in this work, we present the analysis of BB which, especially in their approximate model, brings out some important aspects which are not so evident in the modelling used here.

If we assume a gaussian time profile to the pump pulse, then we can also associate a time profile to the gain coefficient, γ, given by

$$\gamma = \gamma_0 \exp -(t/\tau)^2 \tag{2.8.2}$$

where τ is the $1/e$ intensity halfwidth of the pump pulse. Referring to eqn 2.8.1 it can be seen that the instantaneous gain seen by the signal, assumed to be constant during a single cavity round trip, gives the relation between the power before and after a cavity round trip as

$$P_m = P_{m-1}\left\{R_1 \exp(-4\alpha l_c)\cosh^2\left[\gamma_0 \exp -(t/\tau)^2 l_{eff}\right]\right\} \tag{2.8.3}$$

This equation can be iterated numerically until a defined threshold is reached.

BB reduced this to a simpler model for optimising the parameters that effect threshold. By introducing a time independent gain profile of width $\bar{\tau}$ and magnitude $\bar{\gamma}$ and making various simplifying assumptions, not reproduced here for brevity, they arrived at an equation for threshold of the form

$$\bar{\gamma}_{eff} = l_{opt}/c\bar{\tau}\ln(P_n/P_0) + 2\alpha l_c + \ln\left(1/\sqrt{R_1}\right) + \ln 2 \tag{2.8.4}$$

where l_{opt} is the optical cavity length. The eqn above has the interpretation of gain equals loss, where it is seen that the build up to threshold, as given by the first term on the right hand side of the equation, acts as a loss mechanism. That is, if the pump power is not sufficiently above the cw threshold that the signal and idler can build up from noise during the pulse duration, then the loss introduced by the build up time prevents oscillation.

We now present our approach to the iterative calculation of threshold. The same time dependence arguments can be applied whether the form of the non-linear gain is that due to BB or Guha.

The equations presented so far describe the steady state power gains expected for a

specified pump power or intensity and focusing arrangement. Due to the time dependence of the pump, these equations must be integrated over the temporal duration of the pump pulse to account for build-up effects. This integration is performed numerically by iterating temporally throughout the pump pulse in time steps of the cavity round trip time. For ease of computation, it is convenient to consider photon numbers as opposed to powers. Power is energy/time, which in this case is $Nh\upsilon/\tau_c$, where N is the number of photons in the cavity and τ_c is the cavity decay time. Therefore the power gain, G, also applies to photon numbers. If we define threshold as the case where 20 μJ, a detectable level of photons (which also corresponds experimentally here to the situation that the OPO would be 'on' for all pump pulses) at the signal wavelength are emitted from the cavity, then the numerical integration of photons emitted during the pump pulse must contain $20\mu J/h\upsilon$ photons. Taking $\lambda_s = 1.5$ μm, gives the threshold condition as $N_t \approx 10^{14}$ photons emitted during the pump pulse.

The generated signal wave is amplified as it makes *m* cavity transits from an initial parametric noise, which is set here as one photon in the signal cavity mode. The equations that are required are therefore ones which relate the signal photon number at the start of the $m+1_{th}$ round trip to that of the m_{th} round trip, and the number of photons that are emitted in the m_{th} round trip (through both mirrors). It is easily shown that for a single pass pump the required equations are

$$N_{m+1} = \left(R_1 R_2 (1-R_c)^4 \exp(-2\alpha_s l)\right) G(t) N_m \tag{2.8.5}$$

$$N_e = N_{m+1}\left\{\frac{1+R_2\left((1-R_1)(1-R_c)^2\exp(-\alpha_s l)-1\right)}{R_1 R_2 (1-R_c)^3 \exp(-\alpha_s l)}\right\} \tag{2.8.6}$$

where $R_{1,2}$ are the mirror reflectivities, R_c is the reflection loss per crystal face and G(t) is the time dependent gain calculated using either the BB or Guha approach with the appropriate time dependence of the pump intensity. It is sufficient to assume a gaussian time profile for the pump as it was found that calculations using the actual time profile of a Q-switched pulse produce a slightly lower estimate of threshold, but not substantially so. Therefore, assuming a pump pulse with the time profile

$$P_p = P_{p0} \exp -\left(t/\tau_p\right)^2 \tag{2.8.7}$$

where τ_p is the 1/e intensity halfwidth, iteration over the interval $-2\tau_p < t < 2\tau_p$ covers the pump between the 2% points.

Double passing of the pump can be allowed for in either of the BB or Guha situations by multiplying the gain coefficient G by a second gain factor G_{dp}, where G_{dp} allows for the percentage of the pump that is double passed. In addition, for the Guha case, a new

value of h_s must be calculated to allow for the pump not being focused in the centre of the crystal for the backward trip. However, for weak focusing this is only slightly different from that for the forward pass. In the BB case, the signal absorption is included in the gain coefficient and should therefore only be applied additionally for the backward pass when the pump is single passed, and for the case of a double passed pumped, all signal absorption is allowed for in the gain calculations.

Comparison between calculated thresholds and experimentally measured thresholds is made in chapter 5. A discussion of the difference between the models, and the difference between theory and measurement is also presented. To finish of this section we present some curves which show the effect that various parameters are expected to have on threshold. Experimentally, the only parameters investigated were variation of pump and signal confocal parameters, and variation of output coupling. Unfortunately, as will be mentioned in chapter 5, the parasitic loss was found to vary throughout the measurements and so the expected trend in the threshold variations is not so evident.

The following graphs were calculated by incorporating the Guha model for non-linear gain into our approach to the iterative calculation, as discussed above. They apply to the case of type II o-oe NCPM in KTP, with propagation along the a-axis, a pump wavelength of 1.047 μm, and signal and idler pair of 1.54 and 3.3 μm. Unless otherwise stated, the additional parameters valid for the calculations were as follows : FWHM pump pulse duration 20 ns, zero crystal absorption at pump and signal, crystal absorption at idler 0.45 cm^{-1}, crystal length 20 mm, zero reflection loss per crystal face, 20 % output coupling, crystal face-mirror separation 1 mm. In addition where signal and pump spot sizes are given, it is assumed that the mirror radius of curvature is varied such that a given spot size is maintained irrespective of cavity length.

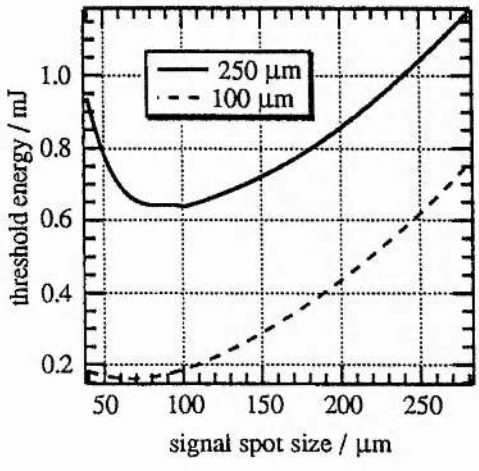

fig.2.6 Variation of threshold energy with signal spot size for the pump spot sizes of 100 and 250 μm

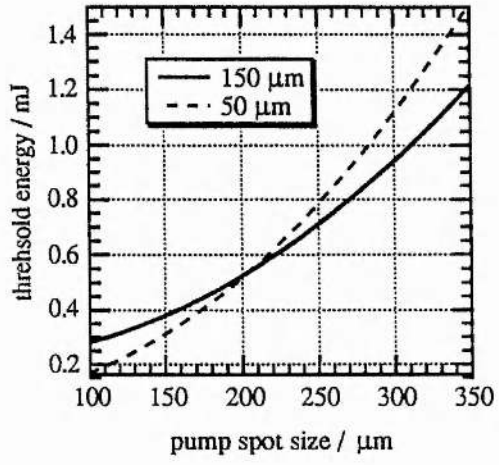

fig. 2.7 Variation of threshold energy with pump spot size for the signal spot sizes of 50 and 150 μm

It can be seen from fig. 2.6 that for the pump sizes considered here, i.e. 100 and 250 μm, there is an optimum signal spot size which is less than the pump spot size. It is then seen from fig. 2.7 that for the signal spot sizes considered, a lower threshold can be reached by further reduction of the pump spot size. This case, however, is unlikely to be reached for pulsed pumping due to the onset of crystal damage.

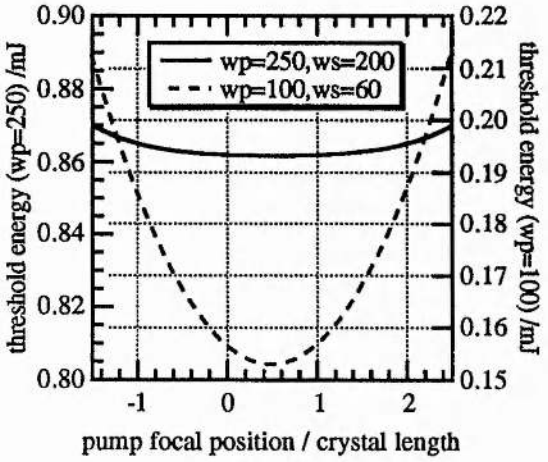

fig. 2.8 Variation of threshold energy with pump focal position for the pump and signal spot sizes indicated. Note different scales

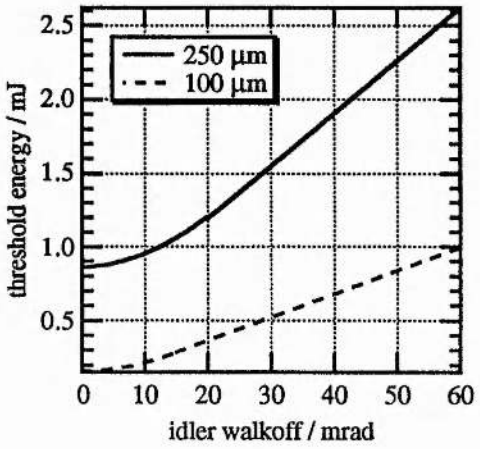

fig. 2.9 Variation of threshold energy with idler walkoff for pump spot sizes of 100 and 250 μm

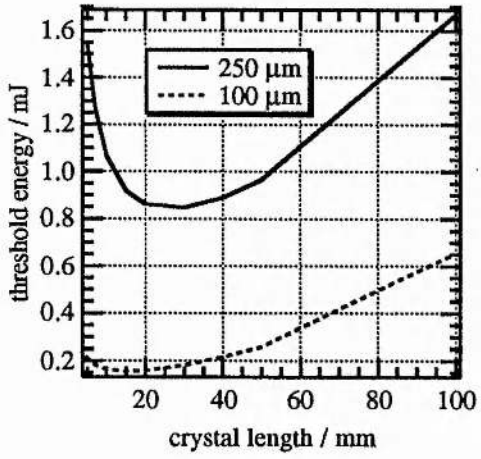

fig.2.10 Variation of threshold energy with crystal length for pump spot sizes of 100 and 250 μm

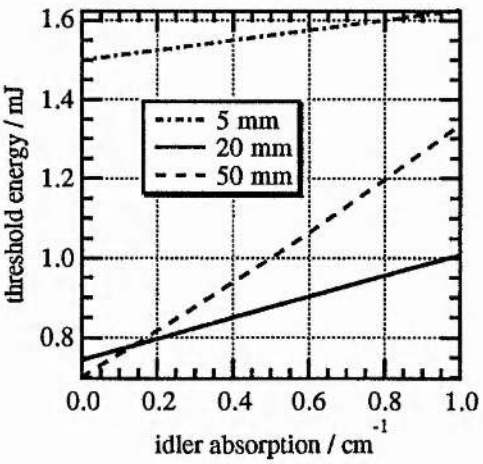

fig. 2.11 Variation of threshold energy with idler absorption, for crystal lengths of 5, 20 and 50 mm

Fig. 2.8 shows that until the pump spot size gets quite small the effect of the pump focus being shifted away from the centre of the crystal is not-critical (note the different scales used). After a slow initial rise, fig. 2.9 shows that increasing idler walkoff produces a linear increase in the threshold energy. The experimental studies described in this work are for NCPM, so walkoff is not a problem. However fig.2.9 shows the

detrimental effect that a large walkoff would have. Fig. 2.10 shows that there is an optimum crystal length that depends to some extent on the degree of pump focusing.

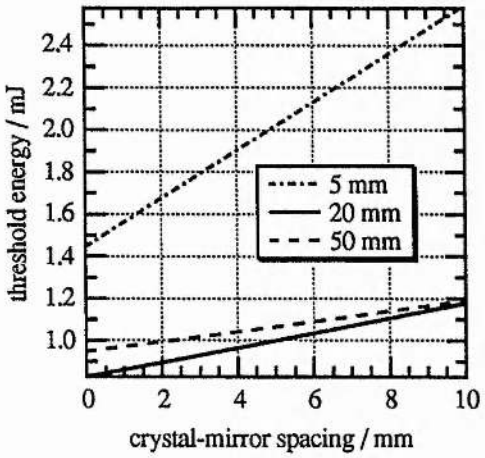

fig. 2.12 Variation of threshold energy with spacing between crystal face and mirror, for crystal lengths of 5, 20 and 50 mm

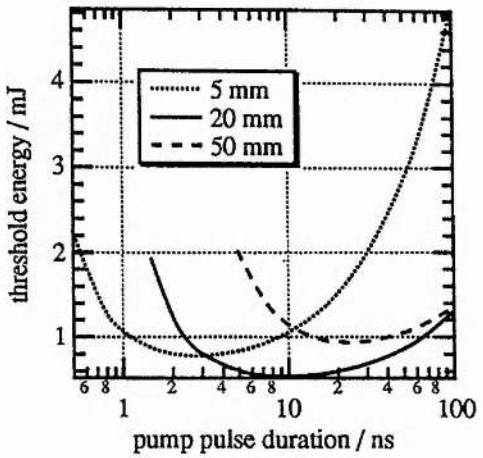

fig. 2.13 Variation of threshold energy with pump pulselength, for crystal lengths of 5, 20 and 50 mm

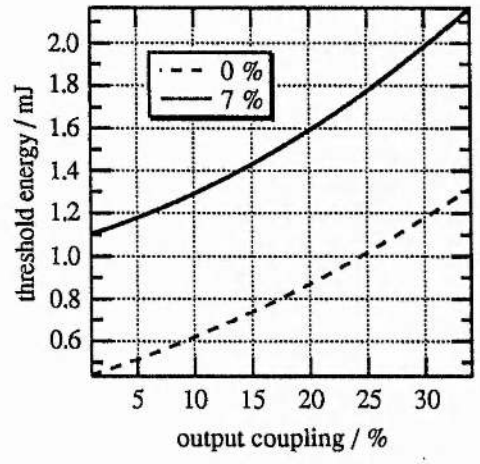

fig.2.14 Variation of threshold energy with output coupling, for loss per crystal face of 0 and 7 %, where signal absorption can be included in loss per face

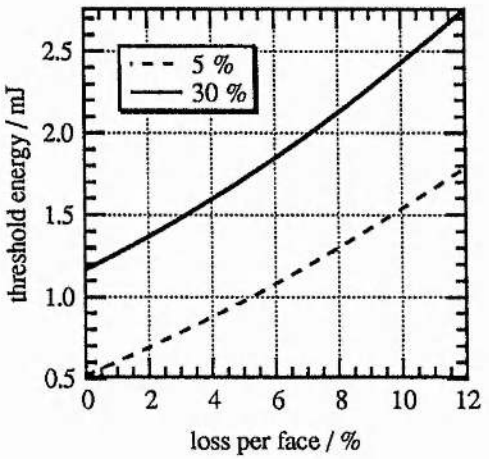

fig. 2.15 Variation of threshold energy with signal loss per crystal face, for output couplings of 5 and 30 %

We seen further on in fig. 2.13 that the pulse length also has a major effect on the optimum crystal length. This is mainly governed by the fact that although a larger non-linear gain can be obtained with a longer crystal, the reduced number of cavity transits the signal would experience during the pump pulse increases the threshold. This is seen directly in fig. 2.12 where the effect of increasing the crystal mirror spacing, i.e. lengthening the cavity, linearly increases the threshold energy.

Parasitic loss and output coupling, both being cavity losses, increase the threshold

energy, see figs.2.14 and 15. However the additional loss of increasing the output coupling also increase the external efficiency and may in fact be beneficial over all. It is clearly seen that the parasitic loss should be kept to a minimum. The threshold for the case of 1 % output coupling and 7 % loss per crystal face (Fresnel reflection for an uncoated KTP crystal at the wavelengths considered), which would have a very low external efficiency, is identical to the case of nearly 30 % output coupling with zero parasitic loss and a correspondingly higher external efficiency.

The results of the theoretical analyses discussed here will be compared with the experimental studies of the type II NCPM in KTP in chapter 5.

2.9 Conversion efficiencies

The first calculations on OPO efficiency were by Siegman [45], even before the demonstration of the first working device. These calculations predicted the limiting of the pump exiting the cavity to the threshold gain level, in a similar manner that the gain saturates in a laser. This was also the first realisation of what are called power dependent reflections of the pump, which are due to the signal and idler interacting on the return journey through the non-linear crystal and converting back into the pump frequency via sum frequency generation. These power dependent reflections only occur for DROs and limit the maximum conversion efficiency to 50%. If these phenomena can be removed, which is the case for a ring cavity where the signal and idler are not phase matched on the return journey and don't reproduce the pump, then the theoretical conversion efficiency, under the appropriate conditions, can reach 100%. The theoretical maximum efficiency for a SRO is also 100%. These comments apply to the case of uniform, plane waves.

The conversion efficiency for a DRO with power dependent reflections under the conditions of steady state operation is [11]

$$\eta = \frac{P_s + P_i}{P_{p0}} = \frac{2}{N}\left(\sqrt{N} - 1\right) \tag{2.9.1}$$

where N is the number of times steady state threshold of the pump. It can be seen that the maximum efficiency is 50 %, and occurs for N=4. By eliminating the power dependent back reflections, e.g. by using a ring resonator, the efficiency is increased to 100 % for N=4.

The conversion efficiency for a SRO in steady state can reach 100 %, and is governed by the implicit relation

$$\sin c^2 \beta l_c = 1/N \tag{2.9.2}$$

where β is a gain parameter given by $\beta = \kappa_i \kappa_p |E_s|^2$. For Δk=0, the SRO reaches 100 % efficiency for pumping $(\pi/2)^2$ times threshold. As mentioned above, this theory only applies to the case of uniform, plane waves.

When the transverse nature of the pump is taken into consideration, a better qualitative agreement between theory and experiment is obtained. This analysis was done by Bjorkholm [46] under the assumption of pulsed pumping of a plane-plane resonator such that the resonator transverse modes were not established during the pump pulse. By integrating radially over the beam, the pump power transmitted can be calculated by setting the output power equal to threshold where the input pump intensity is greater than threshold, and leaving the output power equal to the input power in the regions where the intensity is insufficient to overcome threshold. In this way the maximum efficiency of a DRO without power dependent reflections is 82 % for N=4, and for a SRO the maximum efficiency is 71 % for pumping 6.5 times threshold. These efficiencies are power conversion efficiencies.

Despite the fact that Bjorkholm's work applied to pulsed pumping the above power efficiencies only apply once steady state has been reached. In chapter 5 we show how energy conversion efficiencies can be calculated, again for steady state, and also derive an empirical relation between conversion efficiency and the number of times the device is pumped above the pulsed threshold. The conversion efficiencies under pulsed pumping are seen to approach the steady state case for pumping sufficiently above threshold.

2.10 Summary

In this chapter we have considered some of the general theory which describes the parametric interaction, and tried to give more detail about the particular theory which is applicable here. The non-linear susceptibility convention adopted was presented leading to the coupled amplitude equations describing transfer of power between waves of different frequency. This lead to the concept of parametric amplification and the effect that momentum or phase mismatch had on this. The plane wave theory was extended to allow for focused gaussian beams. The factors affecting parametric oscillation threshold both in steady state and for pulsed pumping were discussed, including single and double resonance, leading to the development of a model for calculating pulsed thresholds for SROs. This theory forms the foundation for the rest of the work, allowing choice of a non-linear material (ch. 3), requirements for a pump laser (ch. 4), and design and operation of an all-solid-state OPO (ch. 5).

2.11 References

[1] P.A.Franken, A.E.Hill, C.W.Peters and G.Weinreich, 'Generation of optical harmonics' Phys. Rev. Lett. **7** (1961) 118

[2] S.A.Akhmanov and R.V.Khoklov, 'Concerning one possibility of amplification of light waves' Sov. Phys. JETP **16** (1963) 252

[3] R.H.Kingston, 'Parametric amplification and oscillation at optical frequencies' Proc. IRE **50** (1962) 472

[4] N.M.Kroll, 'Parametric amplification in spatially extended media and applications to the design of tuneable oscillators' Phys. Rev. **127** (1962) 1207

[5] J.A.Armstrong, N.Bloembergen, J.Ducuing and P.S.Pershan 'Interactions between light waves in a non-linear dielectric' Phys. Rev. **127** (1962) 1918

[6] W.H.Louisell, *Coupled Mode and Parametric electronics*, John Wiley and Sons Inc. New York 1960

[7] C.C.Wang and G.W.Racette, 'Measurement of parametric gain accompanying optical difference generation' Appl. Phys. Lett. **6** (1965) 169

[8] J.A.Giordmaine and R.C.Miller, 'Tunable coherent parametric oscillation in $LiNbO_3$ at optical frequencies' Phys. Rev. Lett. **14** (1965) 973

[9] S.E.Harris, 'Tunable optical parametric oscillators' Proc. IEEE **57** (1969) 2096

[10] R.G.Smith, 'Optical Parametric Oscillators', in *Lasers : A series of advances*, A.K.Levine and A.J.DeMaria, Eds, Marcel Dekker, New York 1976

[11] R.L.Byer, 'Optical parametric oscillators', in *Quantum Electronics : A treatise vol1 part B*, H.Rabin and C.L.Tang, Eds, Academic Press 1973

[12] R.Fischer and L.A.Kulevskii, 'Optical parametric oscillators (review)' Sov. J. Qu. Elec. **7** (1977) 135

[13] S.J.Brosnan and R.L.Byer, " Optical parametric oscillator threshold and linewidth studies" , IEEE J. Qu. Elec. **QE-15** (1979) 415

[14] S.Guha, F-J. Wu and J Falk, " The effects of focusing on parametric oscillation" , IEEE J. Qu. Elec. **QE-18**, (1982) 907

[15] G.D.Boyd and D.A.Kleinman, 'Parametric interaction of focused gaussian light beams' J. Appl. Phys. **39** (1968) 3597

[16] J.F.Nye, *Physical properties of crystals*, Oxford University Press, 1976

[17] D.A.Kleinman 'Non-linear dielectric polarisation in optical media' Phys. Rev. **126** (1962) 1977

[18] R.C.Miller, 'Optical second harmonic generation in piezoelectric crystals', Appl. Phys. Lett. **5** (1964) 17

[19] D.A.Roberts, 'Simplified characterization of uniaxial and biaxial non-linear optical crystals : A plea for standardization of nomenclature and conventions', IEEE J. Qu. Elec. **28** (1992) 2057

[20] F.Zernike and J.E.Midwinter, *Applied Non-linear Optics* , Wiley Series in Pure and Applied Optics, ed S.S.Ballard, John Wiley, New York, 1973

[21] A.Yariv, *Quantum Electronics*, 3rd edn, John Wiley, Singapore, 1989 ;
A.Yariv, *Introduction to Optical Electronics*, 3rd edn, Holt-Saunders, Japan, 1985

[22] R.G.Smith, 'Effects of momentum mismatch on parametric gain', J. Appl. Phys. **41** (1970) 4121

[23] M. Zahler and Y. Ben-Aryeh, " Loss effects in classical non-degenerate parametric amplifier" , Opt. Comm. 79, 361-365 (1990)

[24] J.M.Manley and H.E.Rowe, 'General energy in non-linear reactances', Proc. IRE **47** (1959) 2115

[25] M.Born and E.Wolf, *Principles of Optics*, 6th (corrected) edn, Pergammon, 1989 GB

[26] B.Wynche and F.Brehat, 'Calculation of the effective second-order non-linear coefficients along the phase matching directions in accentric orthorhombic biaxial crystals', J. Phys. B: At. Mol. Opt. Phys. **22** (1989) 363

[27] W.Koechner, *Solid-State Laser Engineering*, 2nd edn, Springer-Verlag, Germany, 1988

[28] N.P.Barnes and V.J.Corcoran, 'Parametric generation processes : spectral bandwidth and acceptance angles', Appl. Opt. **15** (1976) 696

[29] A.Guy, 'Synchronously pumped optical parametric oscillation in barium borate and potassium titanyl phosphate', Ph.D. thesis, U. Southampton, 1990

[30] G.D.Boyd and A.Ashkin, 'Theory of parametric oscillator threshold with single mode optical masers and observation of amplification in $LiNbO_3$', Phys. Rev. **146** (1966) 187

[31] H.Kogelnik, 'Coupling and conversion coefficients for optical modes', Proc. Symp. Quasi-Optics **14** Brooklyn Polytechnic, New York 1964, 333

[32] R.Asby, "Theory of optical parametric amplification from a focused gaussian beam" , Phys. Rev. B **2** (1970) 4273

[33] D.A.Kleinman, A.Ashkin and G.D.Boyd, " Second harmonic generation of light by focused laser beams" , Phys. Rev. **145** (1966) 338

[34] D.A.Kleinman 'Theory of optical parametric noise' Phys. Rev. **174** (1968) 1027

[35] T.G.Giallorenzi and C.L.Tang 'Quantum theory of spontaneous parametric scattering of intense light' Phys. Rev. **166** (1968) 225

[36] R.L.Byer and S.E.Harris 'Power and bandwidth of spontaneous parametric emission' Phys. Rev. **168** (1968) 1064

[37] Technical digest of IQEC '90, session on novel laser concepts, in particular papers QTHE3-6; also S.E.Harris, J.E.Field and A.Imamoglu 'Non-linear optical processes using electromagnetically induced transparency' Phys. Rev. Lett. **64** (1990) 1107

[38] C.D.Nabors, S.T.Tang, T.Day and R.L.Byer, 'Coherence properties of a doubly resonant monolithic optical parametric oscillator', J. Opt. Soc. Am. B **7** (1990) 815

[39] R.G.Smith, J.E.Geusic, H.J.Levinstein, J.J.Rubin, S.Singh and L.G. van Uitert, 'Continuous optical parametric oscillation in $Ba_2NaNb_5O_{15}$', App. Phy. Lett. **12** (1968) 308

[40] S.T.Yang, R.C.Eckardt and R.L.Byer, 'Continuous-wave singly-resonant KTP optical parametric oscillator', presented at *Conference on Lasers and Electro-optics 1993*, vol 13, OSA Technical Digest Series (Optical Society of America, Washington, DC 1993) p 132

[41] J.A.Giordmaine and R.C.Miller, 'Optical parametric oscillation in $LiNbO_3$', *in Physics of Quantum Electronics*, P.L.Kelley, B.Lax and P.E.Tannewald, eds, M^{c}Graw-Hill, New York 1966

[42] R.C.Eckardt, C.D.Nabors, W.J.Kozlovsky and R.L.Byer, 'Optical parametric oscillator frequency tuning and control', J. Opt. Soc. Am. B **8** (1991) 646

[43] J.Falk, 'Instabilities in the doubly resonant parametric oscillator : A theoretical analysis', IEEE J. Qu. Elec. **QE-7** (1971) 230

[44] J.E.Pearson, U.Ganiel and A.Yariv, 'Rise time of pulsed parametric oscillators', IEEE J. Qu. Elec. **QE-8** (1972) 433

[45] A.E.Siegman 'Non-linear optical effects : An optical power limiter' Appl. Opt. **1** (1962) 739

[46] J.E.Bjorkholm 'Some effects of spatially nonuniform pumping in pulsed optical parametric oscillators' IEEE J. Qu. Elec. **QE-7** (1971) 109

CHAPTER 3

Non-linear Optical Materials

3.1 Introduction

The most important part of an optical parametric oscillator (OPO) is the non-linear optical material on which the system is based, as it is the exceptional properties of the non-linear gain media that allows transfer of energy between waves of different frequency. This is one of the reasons why the development of new non-linear optical materials (e.g. MgO:$LiNbO_3$, $AgGaSe_2$, Ba_2BO_4 and LiB_3O_5 [1-5]) and the advances in crystal growth technology have been accompanied by a resurgence in the popularity of OPOs as sources of tunable, coherent radiation. The other major factor in OPO advances has been the development of new pump sources, such as excimer [6] and diode-pumped solid-state lasers [7].

In order to be useful as a gain medium in an OPO, a non-linear crystal must satisfy a number of criteria, and it is the purpose of this chapter to introduce and discuss these criteria with respect to the material choices that were made. A brief overview of suitable materials for an OPO operating in the near IR will be presented, followed by a more detailed examination of the properties of the material selected for use, potassium titanyl phosphate (KTP).

3.2 Considerations for material selection

The main aspects of a crystal's performance to be considered in the selection process are [8]

high non-linear coefficient
wide phase-match and transparency range
high damage threshold
angular and spectral acceptance properties
obtainable in a large size with good optical homogeneity
low cost and easy fabrication
chemically and mechanically stable

The criteria listed above are not necessarily listed in order of importance but it is convenient to discuss them in that order in a little more detail.

3.2.1 Crystal symmetry and non-linear coefficients

First, and foremost, in considering a material as suitable for use in a non-linear optical application concerning the mixing of three waves, the material must possess a non-zero second order susceptibility, $\chi^{(2)}$, as previously mentioned in chapter 2. Note that from here on we will refer to the non-linear 'd' coefficients, which are related to the non-linear susceptibility by a factor of 2, as discussed in chapter 2. Additionally, the non-linear coefficients are dispersive, and Miller's delta has to be applied to calculate the magnitude of the non-linear coefficient with respect to the wavelengths involved, as also previously discussed in chapter 2. Thus the values of the non-linear coefficients cited for each material are as quoted in the literature, usually defined for SHG of 1 μm light, and their dispersion still has to be accounted for.

Only crystals which are non-centrosymmetric, i.e. do *not* possess inversion symmetry, can exhibit a second order non-linearity. This requirement of acentricity means that the non-linear susceptibility is a tensor property, and therefore to describe the magnitude of any non-linear response we must choose a suitable coordinate frame to refer to. Unfortunately there does not seem to be a universally accepted convention with respect to crystal axes despite institute proposed standards [9] and those in the literature [10].

In order to avoid ambiguity, we adopted the convention of relating both the non-linear coefficients *and* the refractive indices to the crystallographic axes a,b,c. The crystallographic axes a,b,c transform directly to the piezoelectric axes X,Y,Z [11], respectively (for the crystal classes of interest here), and they therefore adopt the same symmetry relations as the piezoelectric axes. For phase matching calculations, the principal dielectric axes, xyz, are used, and are then related to the crystallographic axes, abc.

Other symmetry relations also apply. The non-linear susceptibility is the same regardless of the three wave mixing process due to permutation symmetry [12], and if all three frequencies involved lie within the transparency band of the crystal, then the non-linear coefficient is real, independent of frequency and invariant to any permutation of the indices ijk [13], which relate to the axes abc. This allows the third-order tensor to be reduced to a 6 x 3 matrix where symmetry arguments relate the coefficients, depending on the point group of the crystal. By considering the vector components of the fields involved in the mixing process, and relating those to the non-linear coefficient matrix, an effective non-linear coefficient, d_{eff} ,which is a scalar, can be calculated which encompasses the tensor nature of the interaction and facilitates simpler calculation of the strength of the interaction. An example of this calculation will be given later in section 3.2.3 for the non-linear crystal $KNbO_3$, which has point group symmetry mm2.

3.2.2 Tuning range

Even if a material has a large non-linearity it may not be of use unless the crystal is optically transparent in the wavelength region of interest and there is sufficient birefringence available to facilitate phase matching*. As mentioned previously in chapter 2, phase matching requires the three interacting waves to satisfy the vector relation given in eqn 2.4.8 This can be achieved by all three beams having parallel wavevectors, collinear phase matching, or their being small angles between the wavevectors, non-collinear phase matching. Non-collinear phase matching has the experimental advantage of eliminating feedback on the resonator axis for one or both of the generated waves [14,15], but it does so at the expense of a beam walk-off effect analogous to Poynting vector walk-off.

Phase matching calculations

To simplify calculation of tuning curves it was decided to limit the operation of the OPO to tuning in the principal dielectric planes. This *may* result in a small reduction in the maximum non-linear coefficient available for two of the materials considered, but does so in favour of simplified calculations and experimental operation.

When the wavevectors of the interacting beams are restricted to operation in one of the principal dielectric planes, then biaxial crystals may be treated with the same, and much simpler, formalism which can be applied to uniaxial crystals. That is, beams which have their polarisation vector in the chosen principal dielectric plane produce elliptical wavefronts and have a refractive index which depends on the angle of propagation to the dielectric axes. These beams are termed extra-ordinary waves, or e-waves. If the polarisation vector is normal to the plane, then the refractive index is independent of the angle of propagation in the plane. These beams are termed ordinary waves, or o-waves.

Crystals can be classified by their birefringence, $n_e - n_o$, where n_e and n_o are the refractive indices of the e and o waves respectively. Thus, a crystal which has n_e less than n_o is termed negative, and the case n_e larger than n_o is termed positive. This gives rise to four types of phase matching. In a negative crystal, the possible phase matching interactions are, type I - two o waves produce (or are produced by) an e wave, and type II - one o wave and one e wave produce (or are produced by) an e-wave. The corresponding cases for positive crystals are, type I - ee $\leftrightarrow$ o, and type II - oe $\leftrightarrow$ o.

The phase matching conditions for second harmonic generation in uniaxial crystals [16]

---

* *Note here that although phase matching is usually achieved by use of the birefringence of the material, natural or induced, quasi-phase matching, as originally proposed by Bloembergen et al [12],where the sign of the phase mismatch or non-linear coefficient is periodically reversed is now proving to be a viable alternative [14]. This technique also allows use of non-linear coefficients which are not accessible via standard phase matching.*

and biaxial crystals [17,18,19] have already been published in the literature. However these results are cumbersome and not simple to apply. By restricting our approach to consideration of propagation in the principal planes, each plane can be treated in an analogous way to a uniaxial crystal, as previously discussed.

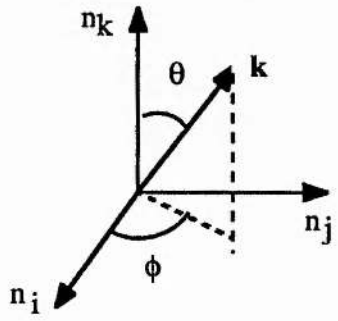

fig. 3.1 - axial convention for phase match calculations

If we consider the coordinate system shown in fig. 3.1, then the two refractive indices of interest for the case $\theta = 90^o$ (i.e. propagation in the ij plane) will be

$$n_o = n_k \tag{3.2.2.1}$$

$$n_e = \left(\frac{n_i^2 n_j^2}{n_j^2 \sin^2 \phi + n_i^2 \cos^2 \phi} \right)^{\frac{1}{2}} \tag{3.2.2.2}$$

These equation apply to any of the three principal planes of the xyz dielectric axial system if the following index relations are applied

$$\text{xy plane} : n_i = n_x, n_j = n_y, n_k = n_z \tag{3.2.2.3a}$$
$$\text{xz plane} : n_i = n_z, n_j = n_x, n_k = n_y \tag{3.2.2.3b}$$
$$\text{yz plane} : n_i = n_z, n_j = n_y, n_k = n_x \tag{3.2.2.3c}$$

The way in which the equations for phase matching have been derived makes it only necessary to refer to one angle. The angle of interest is ϕ for the xy plane, and θ for the xz and yz planes. The general equations for phase matching in the principal planes were obtained by inserting the refractive index equations (3.2.2.1 and 2) into the phase match equation 2.5.1.1 to obtain the following

$$\text{e-oo} \quad \cos^2 \theta = \left(\frac{1}{n_i^2(\lambda_s) - n_j^2(\lambda_s)} \right) \left\{ \left(\frac{n_i(\lambda_p) n_j(\lambda_p)}{\left(\lambda_p / \lambda_s\right) n_k(\lambda_s) + \left(\lambda_p / \lambda_i\right) n_k(\lambda_i)} \right)^2 - n_j^2(\lambda_p) \right\} \tag{3.2.2.4a}$$

$$\text{o-ee } f(\theta)=\left(\frac{\lambda_p}{\lambda_s}\right)\left(\frac{n_i(\lambda_s)n_j(\lambda_s)}{\left(n_j(\lambda_s)\sin\theta\right)^2+\left(n_i(\lambda_s)\cos\theta\right)^2}\right)^{1/2}$$

$$+\left(\frac{\lambda_p}{\lambda_s}\right)\left(\frac{n_i(\lambda_i)n_j(\lambda_i)}{\left(n_j(\lambda_i)\sin\theta\right)^2+\left(n_i(\lambda_i)\cos\theta\right)^2}\right)^{1/2}-n_k(\lambda_p)=0 \qquad (3.2.2.4b)$$

$$\text{o-oe } \cos^2\theta=\left(\frac{1}{n_i^2(\lambda_s)-n_j^2(\lambda_s)}\right)\left\{\left(\frac{\left(\lambda_p/\lambda_s\right)n_i(\lambda_s)n_j(\lambda s)}{n_k(\lambda_p)-\left(\lambda_p/\lambda_i\right)n_k(\lambda_i)}\right)^2-n_j^2(\lambda_s)\right\} \qquad (3.2.2.4c)$$

$$\text{e-eo } f(\theta)=\left(\frac{n_i(\lambda_p)n_j(\lambda_p)}{\left(n_j(\lambda_p)\sin\theta\right)^2+\left(n_i(\lambda_p)\cos\theta\right)^2}\right)^{1/2}$$

$$-\left(\frac{\lambda_p}{\lambda_i}\right)\left(\frac{n_i(\lambda_i)n_j(\lambda_i)}{\left(n_j(\lambda_i)\sin\theta\right)^2+\left(n_i(\lambda_i)\cos\theta\right)^2}\right)^{1/2}-\left(\frac{\lambda_p}{\lambda_s}\right)n_k(\lambda_s)=0 \qquad (3.2.2.4d)$$

The appropriate equations for the uniaxial case require only the additional relation $n_j = n_k$ which gives

$$n_e = n_i \text{ and } n_o = n_j = n_k \qquad (3.2.2.5)$$

Equations (3.2.2.4b and d) are written in the form $f(\theta) = 0$. This is because they are not analytically solvable but can be solved easily by numerical iterative techniques. The method of solution chosen was 'the method of false position'. Despite the fact that some other methods converge faster, this method was chosen as the initial estimates are not required to be accurate and no derivatives are involved.

It is appropriate to also present, for the case of propagation within a principal dielectric plane, the equation for the Poynting vector walk-off angle ρ, which in this formalism is [20]

$$\rho=\tan^{-1}\left(\frac{\left(n_i^2-n_j^2\right)\sin 2\theta}{2\left(n_j^2\sin^2\theta+n_i^2\cos^2\theta\right)}\right) \qquad (3.2.2.6)$$

The walk off angle in the case of uniaxial crystals is defined in terms of n_e and n_o. As it is not solely uniaxial crystals being considered here, the walk off equation has been defined to apply to any principal plane with indices n_i and n_j, where θ is the angle measured from the i-axis. The relations between ijk and xyz defined previously in

(3.2.2.3) still apply.

Equations (3.2.2.4) were used to investigate a number of materials which looked promising for use in an OPO. Some of the phase match curves so generated will be presented later when individual materials are discussed with respect to their potential for construction of an OPO.

The tuning range of an OPO is ultimately limited by the region of the spectrum over which the material is transparent, assuming that the gain is sufficient and the process can be phase matched over the region of transparency. However what must also be borne in mind is that the transparency range quoted in the literature for a crystal is likely to be between the two wavelengths at which the transmission goes to zero. This does not allow for transmission roll-offs where the transmission gradually falls to zero, which then acts as an additional loss mechanism for the OPO and will eventually prevent oscillation. Transmission roll-offs are particularly relevant at the infrared end of the transparency, as is the case in KTP [21,22].

3.2.3 Calculation of d_{eff} for the principal planes

As briefly discussed in section 3.2.1, the non-linear coefficient tensor is determined by the symmetry of the crystal. This can be described, in the reduced notation [23], by a 6 x 3 matrix which relates the vector components of the induced non-linear polarisation to those of the electric fields which generate them. In the previous section, the use of different electric field polarisation vectors to obtain birefringent phase matching was discussed. It is therefore desirable to be able to calculate the magnitude of the non-linearity that will be available for different phase matching geometries. In this section we will discuss the calculation of an effective non-linear coefficient, d_{eff}, which may be applied to individual phase match geometries. We will also see that although certain wavelength combinations can be phase matched, the phase match geometry required can result in a d_{eff} of zero, which results in the exchange of energy between waves being disallowed.

The effective non-linear coefficient can be defined for each crystal point group as [18]

$$d_{eff} = U_1 : d : U_2 U_3 \qquad (3.2.3.1)$$

where U_i (i =1,2,3) are the unit vectors of the three interacting fields, d is the non-linear coefficient tensor, and summation over indices is assumed. The unit vectors can be expressed in terms of the direction cosines, which in turn are expressed in terms of the polar coordinates θ and ϕ [18,19]. This approach gives general results applicable to propagation in an arbitrary direction through the crystal. However, the results so produced are complicated expressions which do not give any immediate insight and are often solved numerically.

The adoption of operation in the principal planes explained earlier with respect to phase match calculations also allows a simplified derivation of d_{eff} which gives a more immediate insight into the behaviour of the non-linear coefficient with propagation direction.

The second order polarisation vector components induced by the interaction of two applied electric fields E_1 and E_2 can be expressed as

$$P_i = d_{ijk} a_j^1 a_k^2 E_1 E_2 \qquad (3.2.3.2)$$

where i = x,y,z are the components along the dielectric axes, $a_{i,j,k}$ are direction cosines, d_{ijk} is the non-linear coefficient tensor, and summation over the indices jk is implied. The easiest way to demonstrate this with respect to its simple application to operation in the principal planes is with an example, e-oo phase matching in the yz-plane of $KNbO_3$, a crystal with mm2 symmetry.

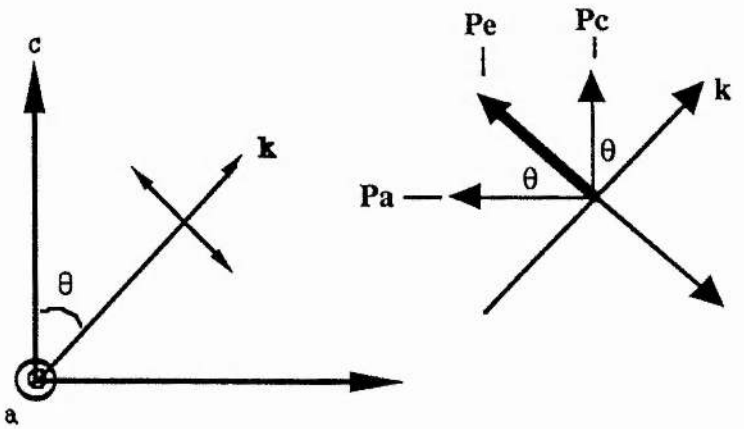

fig. 3.2 - calculation of d_{eff} for e-oo phase matching in the yz plane of an mm2 crystal.

For an interaction in the yz plane, the effective o-wave will be polarised in the x direction. Thus, the components of two waves E_1 and E_2, magnitude E_0, will be

$$a_x^1 = 1 \qquad (3.2.3.3a) \qquad\qquad a_x^2 = 1 \qquad (3.2.3.4a)$$
$$a_y^1 = 0 \qquad (3.2.3.3b) \qquad\qquad a_y^2 = 0 \qquad (3.2.3.4b)$$
$$a_z^1 = 0 \qquad (3.2.3.3c) \qquad\qquad a_z^2 = 0 \qquad (3.2.3.4c)$$

For mm2 symmetry the only nonzero coefficients are d_{31}, d_{32}, d_{33}, d_{24}, and d_{15}, where the specific relations for this crystal class between the dielectric and crystallographic axes have been applied. The induced non-linear polarisation components are then

$$P_x = d_{xxz} a_x^1 E_0 a_z^2 E_0 + d_{xzx} a_z^1 E_0 a_x^2 E_0 = 0 \qquad (3.2.3.5a)$$
$$P_y = d_{yyz} a_y^1 E_0 a_z^2 E_0 + d_{yzy} a_z^1 E_0 a_y^2 E_0 = 0 \qquad (3.2.3.5b)$$
$$P_z = d_{zxx} a_x^1 E_0 a_x^2 E_0 + d_{zyy} a_y^1 E_0 a_y^2 E_0 + d_{zzz} a_z^1 E_0 a_z^2 E_0 = d_{zxx} (E_0)^2 \qquad (3.2.3.5c)$$

Phase matching requires an e-wave from the induced polarisation of the two o-waves. P_y and P_z both contribute to P_e, the e-wave driving polarisation. From fig.3.2 and with $P_y = 0$, the effective polarisation producing the e-wave is

$$P_e = P_z \sin\theta \tag{3.2.3.6}$$

Thus the effective non-linear coefficient is

$$d_{eff} = d_{31} \sin\theta \tag{3.2.3.7}$$

Note that in the example calculation above the formalism is of two o-waves creating an e-wave. In parametric oscillation the case of interest is of one high frequency component splitting into two lower frequency components. However these processes are physically identical as they have been shown to satisfy permutation symmetry [12].

3.2.4 General considerations

In attempting to pump an OPO with a diode-pumped laser it was always known that there would be a limited amount of power available. The prime concern from the start was therefore to select a material that would give the largest gain. As we have already seen in chapter 2, the maximum parametric gain available from a non-linear material depends on its effective non-linear coefficient, the available, or maximum usable, length, and the intensity of pump beam which is incident on it.

The non-linear coefficient has been previously discussed in a general form and will be presented in more detail shortly with respect to each material that was considered for use.

As the technology of crystal growth is more advanced for some materials than for others, the length, aperture, and optical quality to which they can be grown varies greatly. For example, $LiNbO_3$ which was the cornerstone for early experiments in non-linear optics can be grown to lengths exceeding 50 mm, whereas some of the new materials such as some of the organics can only be grown to 0.1 mm. The optical quality also affects the usable length. For example refractive index variations are detrimental to phase matching and materials which are susceptible to domain structure (e.g. $KNbO_3$) do not always support the non-linear conversion that would be expected for a single domain sample. The usable length of the material is also affected by experimental parameters. If a crystal has a high birefringence and a correspondingly high Poynting vector walk-off and low angular acceptance, then the length of crystal that can be used with respect to a required spot size or degree of focusing will be restricted to prevent a loss of conversion efficiency. Equally, as the spectral acceptance varies as the inverse of the length, then the crystal length is restricted, otherwise the whole pump bandwidth will not be usable and the conversion efficiency will be limited.

The susceptibility of the material to optical damage is a major factor which reduces the maximum gain available. The damage thresholds for different non-linear materials can vary over 3 or 4 orders of magnitude. Equally the damage threshold for individual materials is known to vary, and can be reduced by imperfect growth, e.g. inclusions, or poor handling and polishing. Other factors which can tip the scales between one material and another include low loss operation, e.g. low scattering and absorption loss and suitability for AR- coating.

There is no clear formula for selecting an optimum material as no material possess the most favourable aspects of all the properties required. A lot of the factors for consideration are interlinked, for example it may not be possible to focus the pump to a level close to the damage threshold due to the restriction on angular acceptance. The best material must be a compromise of all of the factors already mentioned, and as such it is not a simple task to select a material for use. In the next section some of the steps that were undergone in an attempt to find the best compromise will be presented.

3.2.5 Figures of Merit

As mentioned in the previous paragraph, the choice of a non-linear material is a complex task as there is no single parameter which can isolate any one material to be more suitable than any of the others. However, in order to be able to compare materials it is usual to define a 'figure of merit' for a material which is related to the small signal gain coefficient [24]. A commonly used expression for the figure of merit is d^2/n^3 [8,25,26], but this is rather ambiguous as it does not take into account the material optical damage threshold, nor the acceptance bandwidths (angular, spectral and temperature). It is more appropriate to define a set of figures of merit, each one of which applies to a specific limiting case. The appropriate figure of merit for the case of interest can then be compared for each of the possible materials.

As already discussed, the gain coefficient depends on the non-linear coefficient, the pump intensity and the length of the crystal. If sufficient power is available from the pump laser to reach the damage threshold of the material without the requirement of focusing, then in this instance we can neglect the restriction on the length of the crystal caused by angular acceptance and walk-off. If we assume also that the pump bandwidth is within the spectral acceptance of the interaction, then we can define the 'damage limited' figure of merit as

$$FoM_D = \frac{d_{eff}^2}{n^3} l_c^{\,2} I_D \qquad (3.2.5.1)$$

where d_{eff} is the non-linear coefficient (in pm/V), n is the refractive index (pump, signal and idler refractive indices being similar enough for this calculation), l_c (in cm) the

crystal length, and I_D (in $GWcm^{-2}$) the crystal damage threshold. The maximum gain that is available from the material is proportional to FoM_D, and as such it is also referred to as the intrinsic value [27].

If the pump source is not of sufficient power that the damage threshold is reached with an unfocused beam, then higher gain can be reached by focusing the pump down. There are two limiting cases of interest here, those of non-critically and critically phase matched interactions.

For the case of non-critical phase matching (NCPM) there is no walk-off to be allowed for, and it is the angular acceptance which limits the gain available. A number of authors have considered this problem [28-30] and it can be shown by numerical analysis that there is an optimum degree of focusing for the case of NCPM which is ξ (= l/b) = 2.84, where ξ is the focusing parameter of the pump which is the ratio of the crystal length to the pump confocal parameter b. This then allows a figure of merit to be defined as

$$FoM_{NC} = 11.36 \frac{d^2}{n^2} \frac{l_c}{\lambda_p} \qquad (3.2.5.2)$$

where λ_p (in cm) is the pump wavelength. The factor 11.36 comes from equating the pump spot size to $w_p = \sqrt{(l_c \lambda_p)/(5.68 \pi n_p)}$. Note that if the focusing of the pump reaches damage before the optimised focusing is achieved then the figure of merit will lie between FoM_D and FoM_{NC}, and could be estimated by using the appropriate expression for the pump spot area.

For the case of critical phase matching, using the criterion illustrated in fig 2.2 of $w \approx \rho l$ for a minimum spot size, the appropriate figure of merit can be defined as

$$FoM_C = \frac{d^2}{n^3} \frac{2}{\pi \rho^2} \qquad (3.2.5.3)$$

where ρ is the walk-off angle (in rad). The gain available here is independent of length provided that the spot size is varied proportionally with length. Note that here we have assumed that the walk-off is sufficiently large as to preclude tight focusing. This is a more complex case than can be considered merely by the use of a figure of merit, and has been considered in detail by others [28-30].

Values for the figures of merit will be compared for different materials in a later section.

3.3 Materials suitable for use in the near infrared

The continuing progress in crystal growth technology and in understanding the origin of intrinsic non-linearities has resulted in the improvement in the optical quality of some established non-linear materials and the development of some new ones, e.g. BBO and LBO [5,31]. As well as possessing a second order non-linearity, for a material to be suitable it must also possess excellent linear optical properties, as refractive index variations will degrade phase matching, and multi-domain crystals will degrade the conversion between waves. These restrictions reduce the number of possible materials.

It is the purpose of this section to briefly introduce the materials which were considered for use. In the section following, comparisons will be made between materials by using their figures of merit, and this will be followed by a section on KTP, the material chosen for use, in more detail.

The original group of materials considered for use was selected from an article by Lin and Chen [8] which listed non-linear materials transparent from 0.2 - 5 μm. Despite their successful use as OPO materials in the visible and near infrared [32,33] the transparency ranges of BBO (0.19 - 3.28 μm) [34] and LBO (0.16 - 2.6 μm) [5] did not extend far enough into the infrared for our purposes. The recent interest in organic materials has produced materials which have a large non-linear coefficient due to their strong electron delocalisation and charge transfer characteristics e.g. DAN [35], MBANP [36], d-LAP [37]. Again, however, these materials did not possess the transparency depth into the infrared that was required. The following materials were examined more closely in terms of their non-linear coefficients and phase matching possibilities. These materials are discussed in more detail in appendix A.

Lithium Niobate ($LiNbO_3$) is a negative uniaxial crystal of point group 3m. It has a large birefringence and is transparent in the range 0.4 - 5 μm [38]. Its large non-linearity ($d_{15} \approx 5.95$ pm/V) [39] and the fact that it can be grown in large homogeneous samples has made it a mainstay of non-linear optics, including the first demonstration of an OPO [40]. It supports temperature tuned NCPM for an OPO when pumped at 532 nm. It has a relatively high damage threshold 350 $MWcm^{-2}$ (at 1.064 μm, 25 ns pulses)[41] but is susceptible to photorefractive damage. Periodically poled $LiNbO_3$ has also been developed to utilise the large d_{33} coefficient for second harmonic generation of Nd:YAG lasers and for direct doubling of diode lasers [42].Work to improve the resistance to photorefractive damage resulted in the development of MgO:$LiNbO_3$ [43]. This material has also been successfully used in the demonstration of parametric oscillation [44]. Further discussion of the properties of congruent and doped $LiNbO_3$ is presented in appendix A.

Barium Sodium Niobate ($Ba_2NaNb_5O_{15}$) is a negative biaxial crystal with the orthorhombic point group mm2 at room temperature [45]. It is optically transparent in the range 370 nm to 5 μm and possesses a large non-linearity ($d_{31} = d_{32} = 20$ pm/V) [45]. It is not susceptible to photorefractive damage but does not possess a large surface damage threshold (3 $MWcm^{-2}$ for 10 ns pulses) [46]. Large crystals up to 50 mm have been grown but are susceptible to striae and require poling and processing to remove microtwinning. The refractive indices are described by the single term Sellmeier eqns of Singh et al [45], and are found to be heavily temperature dependent. This temperature dependence, like $LiNbO_3$, allows temperature tuned NCPM when pumped at 532 nm [47], and allowed tuning over the range 0.65 - 3 μm when pumped at 535 nm [48]. The large non-linear coefficients allowed demonstration of a cw threshold of 3 mW when pumped with the 514 nm line of an argon laser [49].

Potassium Niobate ($KNbO_3$, or KN) is again a biaxial crystal with the orthorhombic point group mm2 at room temperature [50]. Its transparency range extends from 400 nm to 5 μm, with absorption loss < 1 % at 1.064 μm [51]. It has a large non-linearity with the (averaged) non-linear coefficients $d_{31} = 15.8$ and $d_{32} = 17.6$ pm/V. This is particularly attractive for direct doubling of diode lasers which can be non-critically phase matched [52]. Its surface damage threshold has been reported to be as high as 1.3 $GWcm^{-2}$ for 7 ns pulses at 1.064 μm [53], and it does not appear to suffer from photorefractive damage. Relatively large crystals up to 30 mm have been grown [54] but the material can be susceptible to depoling when operated at elevated temperatures. The recently published Sellmeier eqns extended into the infrared [50] allow accurate predictions of phase matching angles and temperatures. KN supports temperature tuned NCPM for pumping at 532 nm for a temperature ~ 190 °C [54,55], and has been tuned over the region 1.1 - 5 μm when operated as an OPA pumped at 1.064 μm [53].

Lithium Iodate ($LiIO_3$) is a negative uniaxial crystal which possesses point group symmetry 6 at room temperature [56]. It has a large non-linearity which is characterised by the coefficient d_{31}, where the value taken here is 4.4 pm/V [10]. It is not known to be affected adversely by photorefractive damage and has a reported pulsed optical damage threshold of 250 $MWcm^{-2}$ [57]. It is type I phase matchable throughout its entire transparency range of 0.3 - 5 μm [58], and the phase match angle appears to be temperature insensitive [56]. The absorption is low in the infrared, but is substantial (0.3 cm^{-1} at 347 nm [58]) in the near UV and visible. It can be grown in large high quality single crystals (15 mm aperture, 60 mm length), which have proven efficient for doubling of Nd:YAG and ruby [59], and in providing widely tunable sources (0.63 - 3.4 μm, for a 532 nm pump [60]) when pumped in the green or at 1 μm and operated as an OPO.

Proustite (Ag_3AsS_3) is a negative uniaxial non-linear material of point group 3m. It is transparent over the range 0.6 - 13 μm and is phase matchable over this range due to its large birefringence, ~ 0.2 [61]. It has a large non-linearity, with d_{31} = 11.7 pm/V and d_{22} = 19.5 pm/V. Due to a low damage threshold observed in early experiments, Hanna et al [62] carried out a study of damage to materials for the infrared and found the damage threshold for proustite to be 28 $MWcm^{-2}$ for 18 ns pulses at 2 pps at 1.064 μm. It is particularly useful for upconverting infrared sources, e.g. the CO_2 laser [63], into the wavelength region for which photomultipliers are sensitive. It has also been used to demonstrate probably the widest tunability, in the near to mid-IR from a parametric oscillator, 1.2 - 8.5 μm [15] when pumped at 1 μm with a Nd:$CaWO_4$ laser. The dimensions of crystals reported in the literature seems to be limited to 1 cm, but this has not prevented its successful use as a non-linear material.

Potassium Titanyl Phosphate (KTP) is an orthorhombic biaxial material with point group mm2 [64]. It has a large non-linearity, despite recent measurements that show the non-linear coefficients to be approx. half the original measurements. The magnitudes adopted here, d_{32} = 3.7 pm/V and d_{31} = 2.2 pm/V, are an average of the recent measurements [22,65,66]. KTP has a high surface damage threshold, reported as high as 30 GW cm^{-2} for 30 ps pulses at 526 nm [72], but can be susceptible to bulk darkening, or 'grey tracks', when used for SHG of 1 μm light. Its large birefringence allows type II phase matching throughout the transparency of 0.35 to 4.5 μm, but the presence of an overtone of the fundamental phosphate vibration limits its use as a generator of light beyond 3.3 μm. It has only a small temperature dependence which removes the possibility of temperature tuning, but has the advantage that temperature control is not required. Its main use has been as a doubler of 1 μm light [76], and it has also been used to generate blue light by sum frequency mixing of diode light with Nd:YAG [77]. More recently OPO operation has been demonstrated with KTP when pumped at 532 nm [78] and at 1064 nm [22].

3.4 Selection of material for OPO

The first part of this chapter discusses some of the important attributes that a non-linear material must possess to be suitable for constructing an OPO. In the previous section summaries of the materials considered for use was presented. In this section a comparison is made between the materials and a material is selected for use.

Table 3.1 summarises the properties of the materials considered. However these figures only assist in making a qualitative comparison between materials as there is no one parameter that shows one material to be better than the others. A point to bear in mind is that although $LiNbO_3$ has a higher FoM_D than most of the other materials, in the low energy situation that is the case here, damage will not be reached without focusing of the beam, and so FoM_D cannot be applied directly. Further, although a direct

between these figures and FoM_D. The main comparisons made should be between the same parameter for each material, i.e. values on the same row.

The most promising combination of properties suggest $LiNbO_3$, $KNbO_3$ and KTP.

Material	$LiNbO_3$	BSN	$KNbO_3$	$LiIO_3$	Proustite	KTP
type I/II	I	I	I	I	I	II
I_d / GW cm^{-2}	0.35	0.003	0.2	0.25	0.028	1
d_{eff} / pm/V	5.9	7.9	8.9	1.05	18.6	3.2
$\Delta n/n$ %	3.6	3.9	6.1	7.6	8.4	4.6
l/mm	50	50	20	60	10	20
ρ/mrad	36	34.6	62.3	53	74.9	0
θ/deg	45.2	29.3	48	18.2	27.7	90
$\Delta\lambda_p$/nm	1.5	1.8	0.66	2.85	0.69	1.2
$\Delta\theta_c$/mradcm	1.35	1.4	0.8	1.17	0.5	N/A
$\Delta\theta_{nc}$/mradcm$^{1/2}$	inf	29	21.3	inf	inf	50,178
ΔT/^{o}Ccm	2.75	3.9	80*	N/A	N/A	19
FoM_D	29.7	0.42	6.17	1.6	0.46	7.1
FoM_{NC}	N/A	N/A	N/A	N/A	N/A	7.2×10^5
FoM_C	1677	2806	1278	40.2	1870	N/A

Notes
1) Acceptances and angles are for the case of a 1.6 and 3.2 μm signal/idler pair
2) A conservative value for the damage threshold of KN was used here. Although a damage threshold of 1.3 GWcm^{-2} has been reported, a crystal that we obtained for preliminary experiments was found to damage at intensities as low as 40 MWcm^{-2}.
3) Data on the temperature dependence of refractive indices was not available for $LiIO_3$ and Proustite
4) KTP is NCPM in both ac and ab planes. The values are in the order ac,ab.

table 3.1 Summary table of properties of non-linear materials considered

Bearing in mind that the damage threshold quoted for KTP is a conservative figure, and

* see Appendix A

Bearing in mind that the damage threshold quoted for KTP is a conservative figure, and also the fact that at the time of choosing a material the non-linearity of KTP was thought to be twice the recently measured values, giving a factor of 4 increase to its figures of merit, the material chosen was KTP. The advantage of its NCPM operation would allow tighter focusing than the other materials, and at the wavelengths of operation there would not be a problem with photo-refractive damage. The properties of KTP are therefore discussed in a little more detail in the following section, while further details of the other materials have been included in an appendix.

3.5 Potassium Titanyl Phosphate (KTP)

This section presents in a little more detail the properties of KTP which are relevant to its use in an OPO. Despite the fact that recent measurements have shown the non-linear coefficients to be lower than first measured [64], as will be discussed shortly, it still possesses a high non-linearity and many other properties which make it an excellent material for use as the gain medium in an OPO. KTP can be grown by two different methods, referred to as 'hydrothermal' or 'flux' growth. The method of growth can affect some of the properties of the resulting crystal, and these are mentioned where differences arise.

3.5.1 Crystal symmetry and non-linearity

KTP is an orthorhombic biaxial material with point group mm2 [64]. The non-linear coefficients allowed by this symmetry are d_{15}, d_{24}, d_{31}, d_{32} and d_{33}. Assuming that all the wavelengths involved are within the transparency range, then Kleinman symmetry [13] dictates that the following equalities hold : $d_{15} = d_{31}$, $d_{24} = d_{32}$. The magnitudes of the non-linear coefficients were first measured by Zumsteg et al [64], and these are shown in table 3.2.

d_{15}(pm/V)	d_{24}(pm/V)	d_{31}(pm/V)	d_{32}(pm/V)	d_{33}(pm/V)
6.1	7.6	6.5	5.0	13.7

table 3.2 Original measurement of non-linear coefficients of KTP [64]

Due to lower than expected efficiencies for SHG the non-linear coefficients have been remeasured recently [22,65,66] and found to be approximately half those originally reported. Eckardt et al [65] measured the coefficients of a number of crystals, including KTP and found $d_{eff} = 3.18$ pm/V for type II SHG of 1.064 μm. Assuming the ratio $d_{24}/d_{15} = 1.25$, as measured by Zumsteg et al, gives $d_{24} = 3.3$ and $d_{15} = 2.6$ pm/V. Kato [22] measured the d_{32}/d_{31} ratio as 1.8 and so gives the coefficients as $d_{31} = 1.93$ and $d_{32} = 3.47$ pm/V. The coefficients have also been remeasured by Vanherzeele and Bierlein [66] who found similar results. The values used for calculations in this thesis are an

The values assumed are therefore as given in table 3.3.

$d_{31} = d_{15}$ (pm/V)	$d_{32} = d_{24}$ (pm/V)
2.2	3.7

table 3.3 Values of non-linear coefficients of KTP adopted for use

As all calculations of phasematching considered in this work concern tuning in the principal planes the form of the expression is simply derived in a manner similar to the example given in section 3.2.3. For the e-eo interaction in the ab plane the expression is

$$d_{eff} = d_{31}\sin(\phi+\rho_p)\sin(\phi+\rho_i) + d_{32}\cos(\phi+\rho_p)\cos(\phi+\rho_i) \qquad (3.5.1.1)$$

where the assumption is made that the generated e-wave is labelled the idler, and $\rho_{p,i}$ are the pump and idler walk-off respectively. The other interaction of interest is o-oe phasematching in the ac plane, the equation for d_{eff} being

$$d_{eff} = d_{32}\sin(\theta+\rho_p) \qquad (3.5.1.2)$$

The variation of d_{eff} with wavelength for the latter case is shown, along with the walk-off, in fig. 3.8.

3.5.2 Transmission

The optical transparency of hydrothermally grown KTP was first measured by Zumsteg

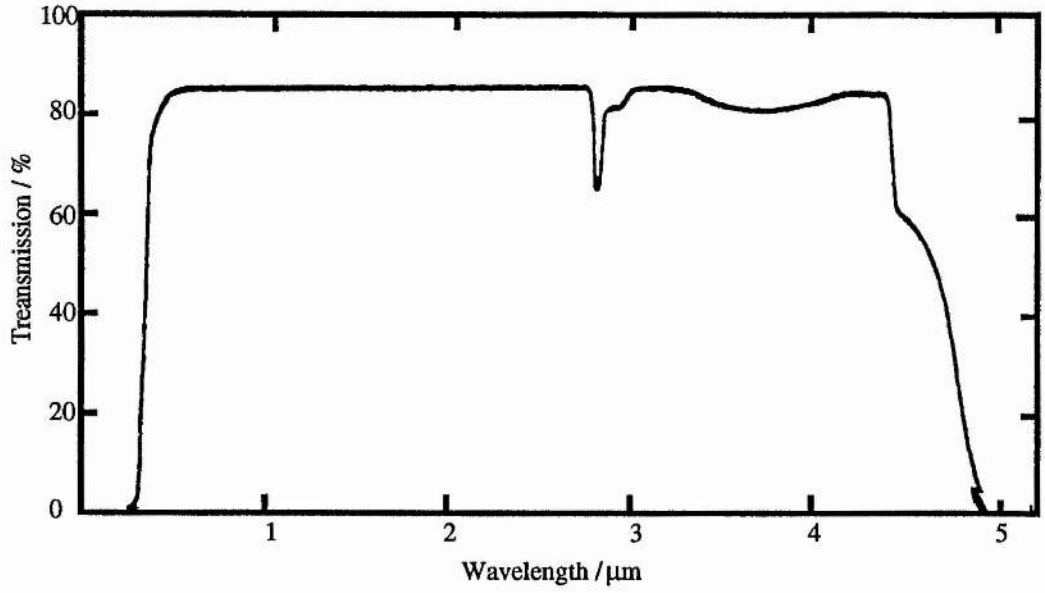

fig. 3.3 Transmission of KTP, from Zumsteg et al [64]

et al [64], and was seen to extend from 350 nm in the near UV to approximately 4.5 μm

et al [64], and was seen to extend from 350 nm in the near UV to approximately 4.5 μm in the mid IR. Their transmission curve is reproduced in fig. 3.3. The absorption feature at 2.8 μm was thought to be due to inclusion of H^+, and has been shown to be due to OH^- [21] (this feature is generally absent in flux grown material [67]), and the broader absorption at 3.8 μm was thought to be due to H_2O. However, more recent measurements of the IR band edge shows that the transmission does not in fact extend as far as 4.5 μm. In particular an absorption at 3.3 μm has been shown [21] to be due to the second overtone of the phosphate fundamental vibration. These features in the transmission properties severely limit the effectiveness of KTP as a generator of radiation beyond 3.3 μm. This is shown clearly in fig.3..4, which shows the transmission beyond 2.5 μm, after Kato [22], for a 15 mm sample of flux grown material.

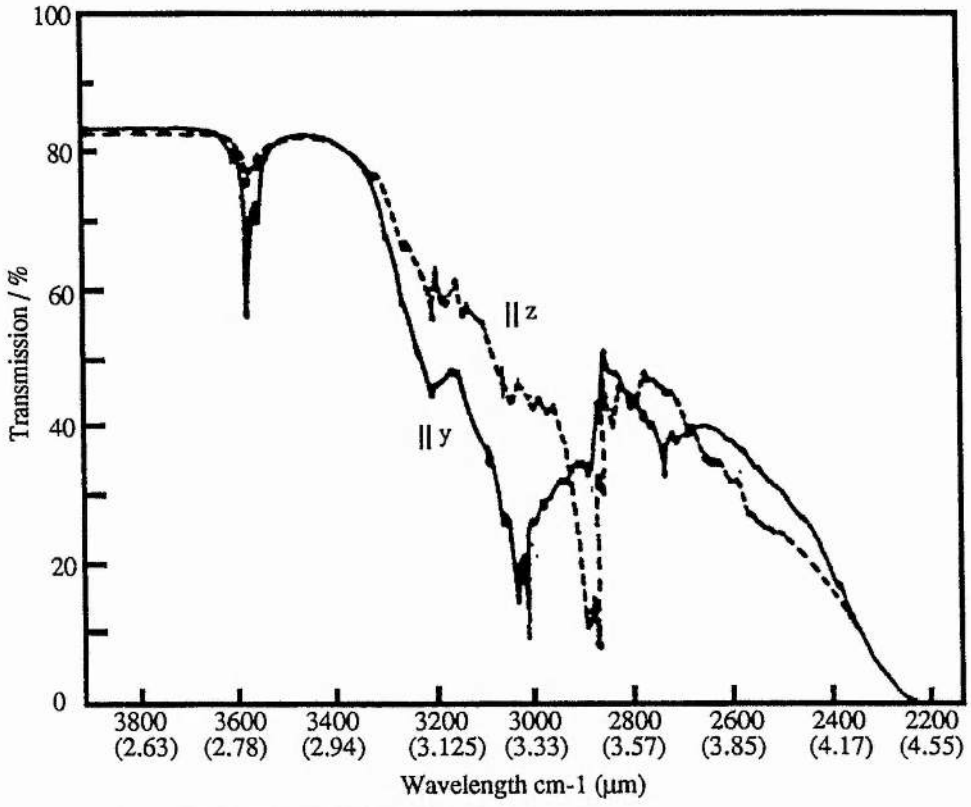

fig. 3.4 Infrared transmission of KTP, from Kato [22]

The absorption in the visible and near infrared (0.514 - 1.32 μm) has been measured by Gettemy et al [68] and found to be low (< 1%/cm for > 660 nm) but was also found to vary for samples from different manufacturers.

3.5.3 Birefringence and Dispersion

The large birefringence and large dispersion in KTP allows phase matching to be achieved over the entire transparency range. The birefringence between the a and b axes is small, ~ 0.5 %, compared to the birefringence between the a(b) and c axes, ~ 5 %.

Thus phasematching is more dependent on θ and a wider tuning range is obtained in the ac and bc planes than in the ab plane.

In order to be able to accurately predict phasematch angles and so obtain the correct cut of crystal it is necessary to know the dependence of the refractive indices on wavelength to a fair degree of accuracy. This is usually achieved with the use of the appropriate Sellmeier eqns which depend on the crystal bonds. A number of Sellmeier eqns have been proposed for KTP, so it is appropriate here to give a short review and comparison to explain the adopted choice.

Comparison of proposed Sellmeier equations

Here we consider 5 sets of proposed Sellmeier eqns, those of Anthon and Crowder (AC) [69], Kato (K) [22,70], Fan and Byer (FB)[67], Dyakov (D) [71], and Vanherzeele and Bierlein (VB) [72], with respect to their formulation and applicability to the case considered here.

Anthon and Crowder used previously published refractive index data and Sellmeier eqns (Weber [73]) and adjusted the coefficients to optimise the fit to their measured phasematch angles. This included adjustment of the refractive index data to fit their phasematch data. They found that angles for flux and hydrothermally grown material differed slightly, and they also found that the published Sellmeier eqn of FB did not accurately predict their measurements at 1.3 μm.

Fan and Byer's Sellmeier eqns were based on refractive index measurements up to 1064 nm made with flux grown material. They point out that their eqns don't accurately predict phase matching past 1 μm, but also point out that this could be attributed to sample variations.

Kato has published two sets of Sellmeier eqns. The first [22] was obtained from extracting refractive index data from the graph of Zumsteg et al [64] and fitting to his observed phasematch angles. The second, which are of more interest here, again involve fitting of phasematch data to published Sellmeier eqns (VB[72]). However this time the wavelengths involved stretch to 3.2 μm, and are therefore more likely to be accurate in the infrared.

Dyakov also produces a fit to phasematch angles from the graphical data of Zumsteg et al, and claims to produce more satisfactory results than FB. In particular they claim their eqn is 'only' 3° out at 2.94 μm compared to 19° for the FB eqn.

Vanherzeele and Bierlein based their Sellmeier eqns on measured refractive index data, using hydrothermal material, in the range 350 nm to 2.4 μm. They also find a good fit between their predictions and measurements with an optical parametric generator

(OPG) tuned over the range 0.6 - 4.3 μm.

At the time of choosing a material, the eqns of VB were deemed most suitable as they were formulated from data that went the furthest into the infrared. Despite the fact that their measurements were based on hydrothermal material and the crystal that was obtained for this project was grown by the flux technique, as shall be discussed in chapter 5, the wavelengths measured experimentally are accurately predicted by the Sellmeier eqns of VB. As a comparison of Sellmeier eqns, table 3.4 shows the predicted wavelengths for collinear o-oe phasematching when pumped at 1.064 and 1.047 μm, and propagating along the a-axis with the pump polarised along the b-axis. It can clearly be seen that the different equations predict very different wavelength combinations.

	1.064 μm		1.047 μm	
Vanherzeele / Bierlein	1.571	3.297	1.539	3.276
Fan / Byer	1.657	2.974	1.621	2.958
Dyakov	1.528	3.506	1.497	3.482
Kato	1.579	3.261	1.547	3.240
Anthon / Crowder	1.492	3.712	1.462	3.688

table 3.4 Comparison of predicted signal/idler pairs for pump wavelengths of 1.064 and 1.047 μm.

The dispersion of the refractive indices using the Sellmeier eqns of Vanherzeele and Bierlein [72] is shown in fig. 3.5.

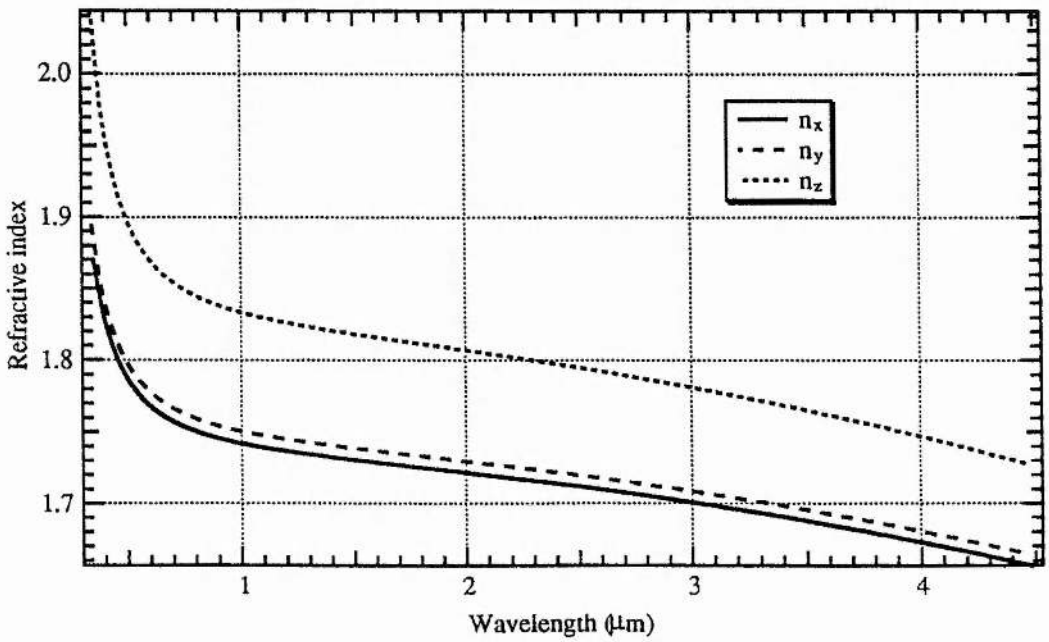

fig. 3.5 The dispersion of the refractive indices using the Sellmeier eqns of VB

The form of their Sellmeier eqn is

$$n^2 = A + \frac{B}{1-(C/\lambda)^2} - D\lambda^2 \qquad (3.5.3.1)$$

with the coefficients listed in table 3.5.

	A	B	C	D
n_a	2.1146	0.89188	0.20861	0.01320
n_b	2.1518	0.87862	0.21801	0.01327
n_c	2.3136	1.00012	0.23831	0.01679

table 3.5 Sellmeier equations for KTP, from VB

3.5.4 Thermal behaviour

The thermal dependence of the refractive indices is small. A temperature acceptance product of 24 ^oC cm^{-1} was measured by Fan and Byer [67] for type II SHG of 1.064 μm. The dependence of the refractive indices on temperature was measured by Gettemy et al [68], at a range of wavelengths up to 1.32 μm and at 35 ^oC. The values for 1.064 μm are given in table 3.6

x 10^{-6} $^oC^{-1}$	a	b	c
dn/dT(1.064)	19	25	37

table 3.6 Temperature coefficients of refractive indices, from Gettemy et al [68]

As they tend to decrease with wavelength, a rough estimate for 1.6 and 3.2 μm from the data of Gettemy et al might be a = 19, b = 14, c = 31 (x10^{-6} $^oC^{-1}$). For propagation at 90^o to the c-axis with a 1.6 and 3.2 μm pair, these estimated temperature dependencies give a temperature acceptance of 19 ^oC cm.

3.5.5 Tuning

As the temperature dependence of the refractive indices is small, only angular tuning has to be considered. It was previously mentioned that the birefringence in the ab plane is small compared to that in the ac or bc planes. This results in a small tuning range and rate, but has the advantage of small walk-off (< 5 mrad) and a reasonable d_{eff} (~ 3.3 for $\phi = 0$, to ~ 1.9 pm/V for $\phi = 90$). The tuning range for a 1.064 μm pump is shown in fig. 3.6.

Due to the larger birefringence in the ac and bc planes a much larger tuning range can be accessed. The ac plane is the preferred choice as it has a larger d_{eff}. The tuning curve

for o-oe phasematching in the ac-plane is shown in fig. 3.7, and the variation of walk-off and d_{eff} with wavelength is shown in fig. 3.8.

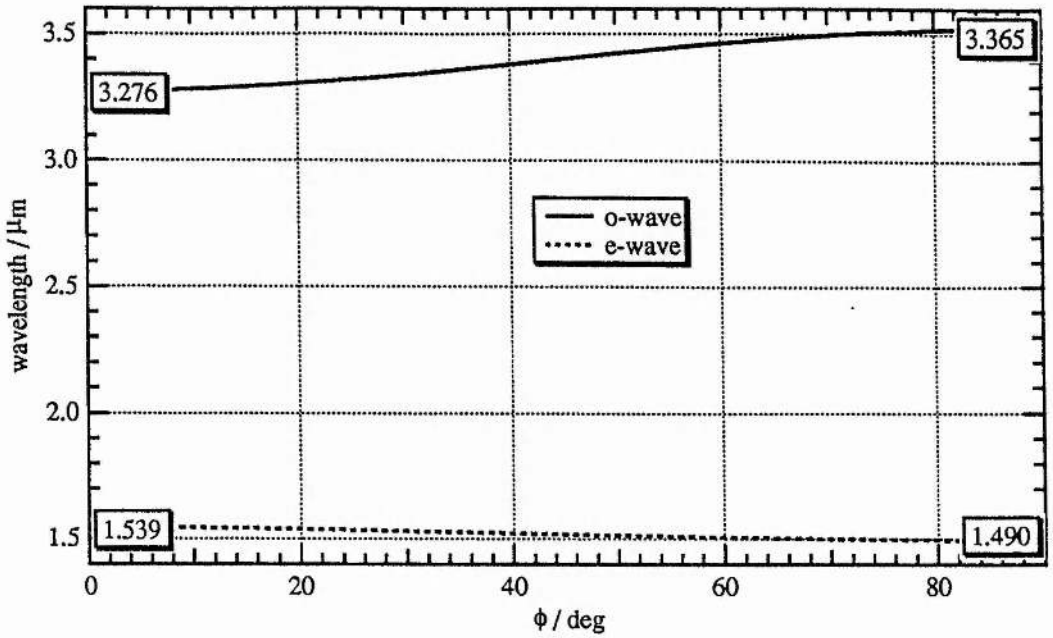

fig. 3.6 Tuning curve for e-oe phasematching in the ab plane, from Sellmeier eqns of VB.

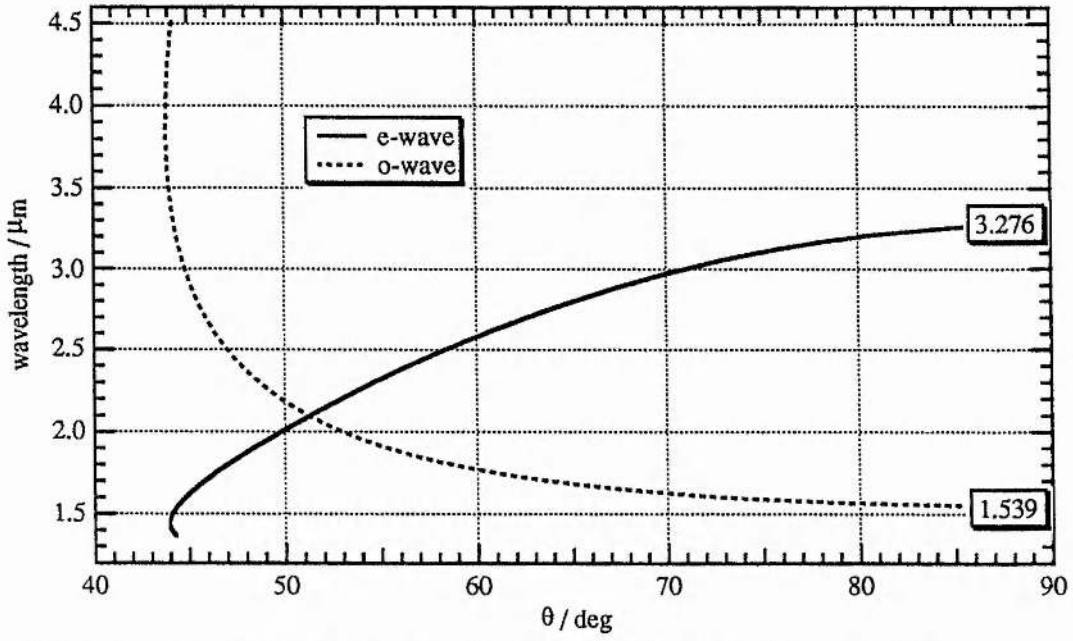

fig. 3.7 Tuning curve for o-oe phasematching in the ac plane, from Sellmeier eqns of VB

As can be seen from fig. 3.8, d_{eff} goes to a maximum and the walk-off tends to zero as θ approaches 90°. At 90° NCPM is achieved and this results in a large angular acceptance and narrow linewidth operation. To obtain a large tuning range the best crystal cut would be one for which the normal to the input and output faces corresponds to operation close to degeneracy, i.e. $\theta \sim 48°$. However due to the increase in walk-off and decrease in d_{eff} this cut would result in a considerable increase in threshold

compared to the case for NCPM. In the early stages of this project, the pulse energies available from the diode pumped lasers that were built at that time were sub-mJ, and so it was decided that a crystal cut that minimised threshold was required, i.e. a crystal cut for propagation along the a-axis, with tuning in the ac-plane. The resultant NCPM geometry results in a large angular acceptance, ~ 50 mrad $cm^{1/2}$ in the ac plane and 178 mrad $cm^{1/2}$ in the ab plane, and a relatively narrow pump spectral acceptance of 1.2 nm cm.

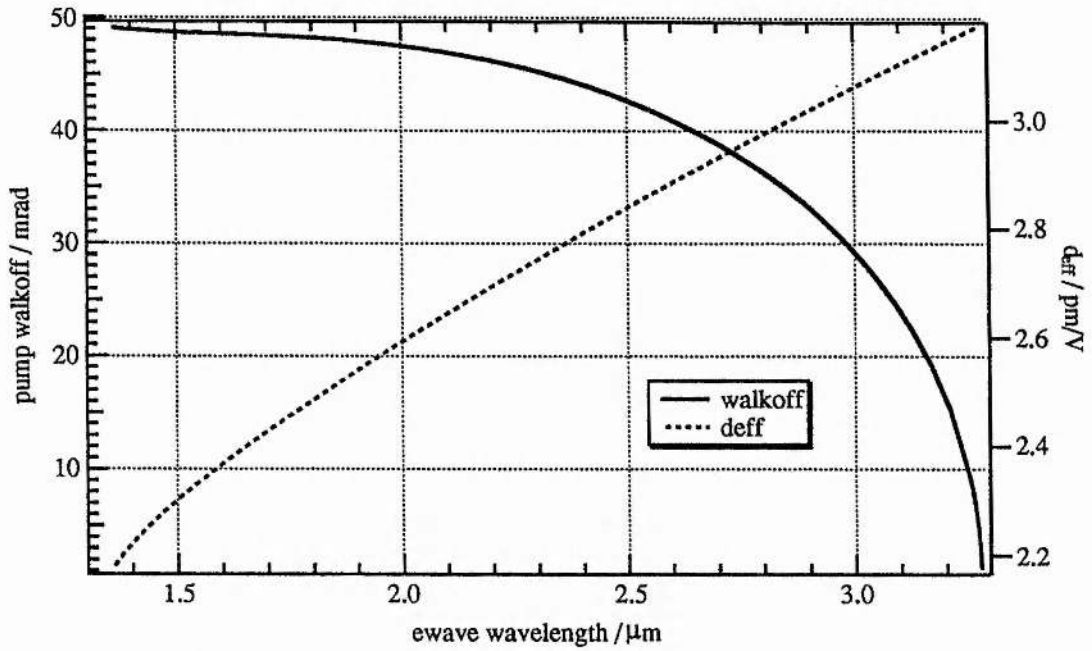

fig. 3.8 Variation of walk-off and d_{eff} with wavelength

3.5.6 Optical damage threshold

The gain that is available from any non-linear material is ultimately limited by the maximum intensity which the crystal can withstand without damaging. KTP has a high surface damage threshold, and it is found that hydrothermally grown material can usually withstand higher intensities than flux grown material, around a factor of 3 difference. The reported damage thresholds are also found to be pulse duration dependent. 30 GW cm^{-2} was reported for hydrothermally grown material (factor of three less for flux) subjected to 30 ps pulses at 10 Hz and 526 nm [72], while an earlier report for 10 ns pulses at 1.064 μm reported possible damage at 400 $MWcm^{-2}$ [74]. This was an early report and manufacturers will normally specify damage at over 1 $GWcm^{-2}$.

As well as surface damage KTP is susceptible to the problem of 'grey tracks' or bulk darkening. Bulk darkening has the effect of reducing the transmission and efficiency of the crystal. A study by Jacco et al [75] concluded that there is a high probability of catastrophic damage at 15 Jcm^{-2}, and that irreversible darkening occurred for 60,000

shots at 8.8 Jcm^{-2}. However they also found that the effect required the presence of 532 nm light, and so may not be a problem in this situation.

3.6 Summary

This chapter summarises the considerations that were made in the decision on a material for the OPO. Firstly the material parameters of interest were introduced, followed by any limitations of applicabilty and the methods of calculation. Summaries of these parameters as they related to a number of suitable materials were then presented. Following this a comparison was made between materials and KTP was deemed to have the best compromise of properties. Finally a more detailed presentation was made of the attributes of KTP.

3.7 References

[1] N.P.Barnes, K.E.Murray, J.R.Heitenen and R.A.Ianinni, 'Low threshold, stable, $AgGaSe_2$ optical parametric oscillator', CLEO 90, paper CWE5

[2] S.T.Amimoto, R.W.F.Gross, M.Jupina, J.Machan and L.Garman-Duvalle, 'A $AgGaSe_2$ optical parametric oscillator pumped by a Raman shifted YAG laser', CLEO 90, postdeadline paper CPD34

[3] W.J.Kozlovsky, C.D.Nabors and R.L.Byer, 'Efficient second harmonic generation of a diode laser pumped cw Nd:YAG laser using monolithic $MgO:LiNbO_3$ external resonant cavities', IEEE J. Qu. Elec. **24** (1988) 913

[4] D.Eimerl, L.Davis, S.Velsko, E.K.Graham and A.Zalkin, 'Optical, mechanical and thermal properties of barium borate', J. Appl. Phys. **62** (1987) 1968

[5] C.Chen, Y.Wu, A.Jiang, B.Wu, G.You, R.Li and S.Liu, 'New nonlinear -optical crystal : LiB_3O_5', J. Opt. Soc. Am. B **6** (1989) 616

[6] M. Ebrahimzadeh & M.H.Dunn, 'Optical parametric fluorescence and oscillation in urea using an excimer laser', Opt. Comm. **69** (1988) 161 ;

[7] C.D.Nabors, R.C.Eckardt, W.J.Kozlovsky and R.L.Byer, 'Monolithic $MgO:LiNbO_3$ optical parametric oscillator pumped by a frequency doubled diode laser pumped Nd:YAG laser', CLEO 88, paper FK2 ;

[8] J.T.Lin and C.Chen, 'Choosing a nonlinear crystal', Lasers and Optronics, Nov 1987, 59

[9] 'IEEE Standards on Piezoelectricty', IEEE/ANSI Std 176-1987

[10] D.A.Roberts, 'Simplified characterization of uniaxial and biaxial nonlinear optical crystals : A plea for standardization of nomenclature and conventions', IEEE J. Qu. Elec. **28** (1992) 2057

[11] J.F.Nye, *Physical Properties of Crystals*, Oxford University Press, 1976

[12] J.A.Armstrong, N.Bloembergen, J.Ducing and P.S.Pershan, 'Interactions between light waves in a nonlinear dielectric', Phys. Rev. **127** (1962) 1918

[13] D.A.Kleinman, 'Nonlinear dielectric polarization in optical media', Phys. Rev. **126** (1962) 1977

[14] J.Falk and J.E.Murray, 'Single cavity noncollinear optical parametric oscillation', Appl. Phys. Lett. **14** (1969) 245

[15] D.C.Hanna, B. Luther-Davies and R.C.Smith, 'Singly resonant proustite parametric oscillator tuned from 1.22 to 8.5 μm', Appl. Phys. Lett. **22** (1973) 440

[16] J.E.Midwinter and J.Warner, 'The effects of phase matching method and of uniaxial crystal symmetry on the polar distribution of second-order non-linear optical polarization', Brit. J. Appl. Phys. **16** (1965) 1135

[17] M.V.Hobden, 'Phase-matched second-harmonic generation in biaxial crystals', J. Appl. Phys. **38** (1967) 4365

[18] B.Wyncke and F.Brehat, 'Calculation of the effective second-order non-linear coefficients along the phase matching directions in acentric orthorhombic biaxial crystals', J. Phys. B: At. Mol. Opt. Phys. **22** (1989) 363

[19] J.Yao, W.Sheng and W.Shi, 'Accurate calculation of the optimum phase matching parameters in three wave interactions with biaxial nonlinear optical crystals', J. Opt. Soc. Am. B **9** (1992) 891

[20] M.Born and E.Wolf, Principles *of Optics*, 6th (corrected) edn, Pergammon, 1989 UK

[21] J.C.Jacco and G.M.Loiacono, 'Nature of the infrared spectrum in band-edge region of $KTiOPO_4$', Appl. Phys. Lett. **58** (1991) 560

[22] K.Kato, 'Parametric oscillation at 3.2 μm in KTP pumped at 1.064 μm', IEEE J. Qu. Elec. **QE-27** (1991) 1137

[23] K.F.Hulme, 'Nonlinear optical crystals and their applications', Rep. Prog. Phys. **36** (1973) 497

[24] R.L.Byer, 'Optical parametric oscillators', Ch.9, *Quantum Electronics : A Treatise*, vol. 1 part B,

Eds H.Rabin and C.L.Tang, Academic Press, 1973

[25] G.C.Catella, J.H.Bohn, D.A.Roberts and W.R.Cook,Jr, 'Application analysis of new nonlinear materials', Proc. SPIE vol. 1104, 1989

[26] J.T.Lin, 'Non-linear crystals for tunable coherent sources', Opt. and Qu. Elec. **22** (1990) S283

[27] A.Guy, 'Synchronously pumped optical parametric oscillation in barium borate and potassium titanyl phosphate', Ph.D. thesis, U. Southampton, 1990

[28] G.D.Boyd and D.A.Kleinman, 'Parametric interaction of focussed gaussian light beams', J. Appl. Phys. **39** (1968) 3597

[29] R.Asby, 'Theory of optical parametric amplification from a focussed gaussian beam', Phys. Rev. B**2** (1970) 4273

[30] S.Guha, F-J.Wu and J.Falk, 'The effects of focussing on parametric oscillation', IEEE J. Qu. Elec. **QE-18** (1982) 907

[31] C.Chen, B.Wu, A.Jiang and G.You, 'A new type ultraviolet SHG crystal β - BaB_2O_4', Sci. Sin. Ser. B **28** (1985) 235

[32] M.Ebrahimzadeh, A.J.Henderson and M.H.Dunn, 'An excimer pumped β-BaB_2O_4 optical parametric oscillator tunable form 354 nm to 2.37 μm', IEEE J. Qu. Elec. **QE-26** (1990) 1241

[33] Y.Cui, M.H.Dunn, C.J.Norrie, W.Sibbett, B.D.Sinclair, Y.Tang and J.A.C.Terry, 'All solid state optical parametric oscillator for the visible', Opt. Lett. **17** (1992) 646

[34] L.K.Cheng, W.Bosenberg and C.L.Tang, 'Growth and characterization of low temperature phase barium metaborate crystals', J. Crystal Growth **89** (1988) 553

[35] P.V.Kolinsky, R.J.Chad, R.J.Jones, S.R.Hall, P.A.Norman, D.Bloor and J.S.Obhi, 'Second harmonic generation in single crystals of 2-(N,N-dimethylamino)-5-nitroacetanilide (DAN) at 1.3 μm', Elec. Lett. **23** (1987) 791

[36] R.T.Bailey et al, 'The quality and performance of the organic nonlinear optical material (-)2-(α-methylbenzylamino)-5-nitropyridine (MBA-NP)', Opt. Comm. **65** (1988) 229

[37] D.Eimerl, S.Velsko, L.Davis, F.Wang, G.Loiacono and G.Kennedy, 'Deuterated L-Argenine phosphate : A new efficient nonlinear crystal', IEEE J. Qu. Elec. **QE-25** (1989) 179

[38] G.D.Boyd, R.C.Miller, K.Nassau, W.L.Bond and A.Savage, '$LiNbO_3$: An efficient phase matchable nonlinear optical material', Appl. Phys. Lett. **5** (1964) 234

[39] S.K.Kurtz, J.Jerphagnon and M.M.Choy, 'Nonlinear dielectric susceptibilities', in *Landolt-Börnstein Numerical data and functional relationships in science and technology, group III : Crystals and solid state physics* , vol 11, K-H.Hellwege and A.M.Hellwege, eds, Springer-Verlag, Berlin, 1979, pp671-743

[40] J.A.Giordmaine and R.C.Miller, 'Tunable coherent parametric oscillation in $LiNbO_3$ at optical frequencies', Phys. Rev. Lett. **14** (1965) 973

[41] technical spec. sheets for Lasermetrics series 3900 $LiNbO_3$ Q-switches

[42] G.A.Magel, E.J.Lim, M.M.Fejer and R.L.Byer, 'Second harmonic generation in periodically poled $LiNbO_3$', Opt. News, Dec 89, 21

[43] D.A.Bryan, R.Gerson and H.E.Tomaschke, 'Increased optical damage resistance in lithium niobate', Appl. Phys. Lett. **44** (1984) 847

[44] C.D.Nabors, R.C.Eckardt, W.J.Kozlovsky and R.L.Byer, 'Efficient, single axial mode operation of a monolithic MgO:$LiNbO_3$ optical parametric oscillator', Opt. Lett. **14** (1989) 1134

[45] S.Singh, D.A.Draegert and J.E.Geusic, 'Optical and ferroelectric properties of barium sodium niobate', Phys. Rev. B**2** (1970) 2709

[46] R.Webb, 'Catastrophic surface damage produced in $Ba_2NaNb_5O_{15}$ crystals during intracavity frequency doubling', Proc. Symposium on Damage in Laser Materials, Boulder, Colorado, 1971, eds J.Glass and A.H.Guenther, NBS spec. publ. 356 (1971) 98

[47] J.E.Geusic, H.J.Levinstein, S.Singh, R.G.Smith and L.G.Van Uitert, 'Continuous 0.532 μ solid

state source using $Ba_2NaNb_5O_{15}$', Appl. Phys. Lett. **12** (1968) 306;
R.G.Smith, J.E.Geusic, H.J.Levinstein, J.J.Rubin, S.Singh and L.G.Van Uitert, 'Continuous optical parametric oscillation in $Ba_2NaNb_5O_{15}$', Appl. Phys. Lett. **12** (1968) 308

[48] G.Ionushauskas, A.Piskarkas, V.Sirutkaitis and A.Yuozopavichyus, 'Optical parametric oscillation in $LiNbO_3$, CsH_2AsO_4 and $Ba_2NaNb_5O_{15}$ crystals pumped synchronously by a picosecond $La_2Be_2O_5$:Nd laser', Sov. J. Qu. Elec. **17** (1987) 1303

[49] R.G.Smith, 'A study of factors affecting the performance of a continuously pumped doubly resonant optical parametric oscillator', IEEE J. Qu. Elec. **QE-9** (1973) 530

[50] B. Zysset, I.Biaggio and P.Gunter, 'Refractive indices of orthorhombic $KNbO_3$. I. Dispersion and temperature dependence', J. Opt. Soc. Am. **B 9** (1992) 380

[51] manufacturers information sheet, Sandoz Ltd / Virgo optics

[52] W.P.Risk, 'Compact blue laser devices', Opt. and Phot. News, May 1990, 10

[53] D.R.Guyer, W.R.Bosenberg and F.D.Braun, 'High efficiency, tunable mid-infrared generation in $KNbO_3$', Proc. SPIE **1409** (Nonlinear optics 1991) 14

[54] V.A.D'yakov, V.I.Pralkin and A.I.Kholodnykh, 'Pottasium niobate optical parametric oscillator pumped by the second harmonic of a garnet laser', Sov. J. Qu. Elec. **11** (1981) 433

[55] I.Biaggio, P.Kerkoc, L.-S.Wu and P.Gunter, 'Refractive indices of orthorhombic $KNbO_3$. II. Phase matching configurations for nonlinear-optical applications', J. Opt. Soc. Am. B **9** (1992) 507

[56] F.R.Nash, J.G.Bergman, G.D.Boyd and E.H.Turner, 'Optical nonlinearities in $LiIO_3$', J. Appl. Phys. **40** (1969) 5201

[57] A.A.Babin, Yu.N.Belyaev, V.N.Petryakov, M.M.Sushchik and G.I.Freidman, 'Parametric oscillator utilizing an $LiIO_3$ crystal pumped by neodymium laser radiation', Sov. J. Qu. Elec. 6 (1976) 613

[58] G.Nath, H.Mehmanesch and M.Gsanger, 'Efficient conversion of a ruby laser to 0.347 μm in low loss lithium iodate', Appl. Phys. Lett. 17 (1970) 286

[59] G.Nath and S.Haussuhl, 'Large nonlinear optical coefficient and phase matched second harmonic generation in $LiIO_3$', Appl. Phys. Lett. **14** (1969) 154

[60] S.A.Akhmanov, B.V.Zhdanov, A.I.Kovrigin, V.I.Kuznetsov, S.M.Pershin and A.I.Kholodnykh, 'Pulse-periodic tunable (0.63 - 3.4 μ) optical parametric oscillator for nonlinear spectroscopy', Sov. J.Qu. Elec. **7** (1977) 1271

[61] K.F.Hulme, O.Jones, P.H.Davies and M.V.Hobden, 'Synthetic proustite (Ag_3AsS_3) : A new crystal for optical mixing', Appl. Phys. Lett. **10** (1967) 133

[62] D.C.Hanna, B.Luther-Davies, H.N.Rutt, R.C.Smith and C.R.Stanley, 'Q-switched laser damage of infrared nonlinear materials', IEEE J. Qu. Elec. **QE-8** (1972) 317

[63] J.Warner, 'Photomultiplier detection of 10.6 μm radiation using optical upconversion in proustite', Appl. Phys. Lett. **12** (1968) 222

[64] F.C.Zumsteg, J.D.Bierlein and T.E.Gier, '$K_xRb_{1-x}TiOPO_4$: A new nonlinear optical material', J. Appl. Phys. **47** (1976) 4980

[65] R.C.Eckardt, H.Masuda, Y.X.Fan and R.L.Byer, 'Absolute and relative nonlinear optical coefficients of KDP, KD^*P, BaB_2O_4, $LiIO_3$, MgO:$LiNbO_3$ and KTP measured by phase-matched second-harmonic generation', IEEE J. Qu. Elec. **26** (1990) 922

[66] H.Vanherzeele and J.D.Bierlein, 'Magnitude of the nonlinear-optical coefficients of $KTiOPO_4$', Opt. Lett. **17** (1992) 982

[67] T.Y.Fan, C.E.Huang, B.Q.Hu, R.C.Eckardt, Y.X.Fan, R.L.Byer and R.S.Feigelson, 'Second harmonic generation and accurate index of refraction measurements in flux-grown $KTiOPO_4$', Appl. Opt. **26** (1987) 2390

[68] D.J.Gettemy, W.C.Harker, G.Lindholm and N.P.Barnes, 'Some optical properties of KTP, $LiIO_3$

and $LiNbO_3$', IEEE J. Qu. Elec. **24** (1988) 2231

[69] D.W.Anthon and C.D.Crowder, 'Wavelength dependent phase matching in KTP', Appl. Opt. **27** (1988) 2650

[70] K.Kato, 'Second-harmonic and sum frequency generation to 4950 and 4589 Å in KTP', IEEE J. Qu. Elec. **QE-24** (1988);

[71] V.A.Dyakov, V.V.Krasnikov, V.I.Pryalkin, M.S.Pshenichnikov, T.B.Razumikhina, V.S.Solomatin and A.I.Kholodnykh, 'Sellmeier equation and tuning characteristics of KTP crystal frequency converters in the 0.4 - 4.0 μm range', Sov. J. Qu. Elec. **18** (1988) 1059

[72] H.Vanherzeele, J.D.Bierlein and F.C.Zumsteg, 'Index of refraction measurements and parametric generation in hydrothermally grown $KTiOPO_4$', Appl. Opt. **27** (1988) 3314;
J.D.Bierlein and H.Vanherzeele, 'Potassium titanyl phosphate : properties and new applications', J. Opt. Soc. Am. B **6** (1989) 622

[73] M.J.Weber, ed, *CRC Handbook of Laser Science and Technology vol. III* (CRC Press 1985) p152

[74] News, Laser Focus **14** (7) (1978) 18

[75] J.C.Jacco, D.R.Rockafellow and E.A.Teppo, 'Bulk-darkening threshold of flux-grown $KTiOPO_4$', Opt. Lett. **16** (1991) 1307

[76] A.J.W.Brown, M.S.Bowers, K.W.Kangas and C.H.Fisher, 'High-energy, high-efficiency second harmonic generation of 1064 nm radiation in KTP', Opt. Lett. **17** (1992) 109

[77] W.P.Risk and W.Lenth, 'Diode laser pumped blue-light source based on intracavity sum frequency generation', Appl. Phys. Lett. **54** (1989) 789

[78] L.J.Bromley, A.Guy and D.C.Hanna, 'Synchronously pumped optical parametric oscillation in KTP', Opt. Comm. **70** (1989) 350

CHAPTER 4

The Pump Laser

4.1 Introduction

The previous two chapters discussed the requirements imposed on a pump laser for constructing an OPO. In this chapter we will discuss how diode-pumped solid-state lasers (DPSSLs) can fulfil these criteria. Firstly the properties of laser diodes which have facilitated their use as pump sources for solid-state lasers will be discussed, followed by a brief review of some of the large amount of work that has been done on diode pumped lasers, particularly in the last decade. The construction of, and comparison amongst, several diode pumped lasers built during the course of this work will be discussed. This will include comparisons between side- and end-pumping, and the use of YAG (yttrium aluminium garnet) and YLF (yttrium lithium fluoride) as host crystals for the Neodymium (Nd) ion.

As the main part of this project centred on design of the OPO and evaluation of the properties and requirements of it, the construction of a pump laser was almost a secondary consideration. In other words, the work described here on the construction of a pump laser does not involve any detailed analysis of the properties of diode pumped lasers, but mainly leans on published work in the field and the experience of colleagues. However, the investigation of different pump geometries and host crystals has provided some insight to the design of lasers for particular applications.

4.2 Laser diode pump sources

A laser diode is in essence a p-n junction where a population inversion is created by current injection across the junction. Electrons in the conduction band combine radiatively with holes in the valence band and the light emitted is reflected at the semiconductor/air interface (which may or may not be coated), providing the feedback necessary for laser action. Lasing takes place at the junction in a region termed the active region. Early devices used homo-junctions [1,2], that is the p and n regions were doped versions of the same semiconductor, which gave no carrier or optical confinement (the active region being determined by carrier diffusion) and the resulting very high threshold current densities required early devices to be operated at cryogenic temperatures. Advances in growth technology, e.g. chemical vapour deposition (CVD) and molecular beam epitaxy (MBE), led to the development of hetero-junction lasers where by growing structures with different atomic compositions the band gap and

refractive index of the material surrounding the active region could be tailored leading to carrier and flux confinement resulting in reduced thresholds [3]. The notion of carrier confinement with the associated enhancement of radiative recombination progressed to the growth of quantum well [4] and super-lattice structures where the layers grown (~ 100 Å) result in quantum effects and reduced threshold current densities even further.

However, the power that can be obtained from these single stripe lasers is limited by catastrophic facet damage due to the absorption of photons at the facet by surface-states and the resulting heat generation and thermal run-away. The use of larger area diodes does not solve this problem as lasing then tends to occur in small filamentary strips which again cause facet damage at high powers. The way towards higher power was found to be the growth of arrays of coupled, multiple stripe lasers as pioneered by Scrifes et al [5] at Xerox, and then Spectra Diode Labs (SDL). The structure of a typical diode laser array is shown in fig. 4.1.

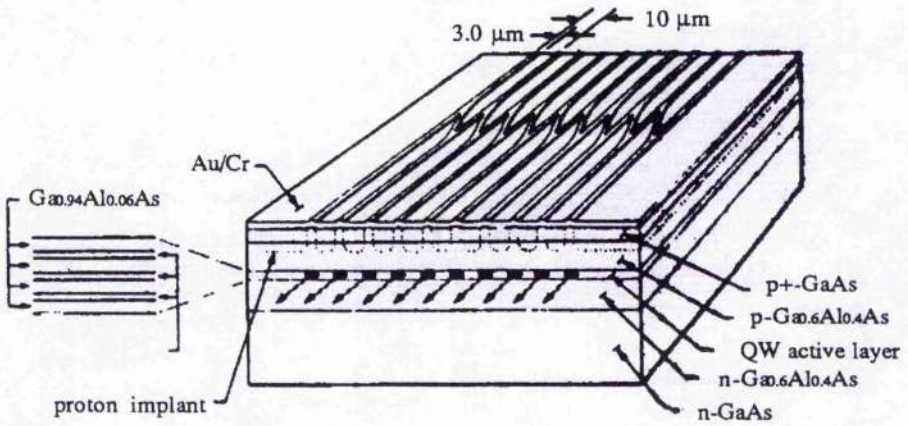

fig. 4.1 Schematic of a coupled multiple stripe quantum well laser, from [5]

These devices form coherent phased arrays in which the evanescent coupling between one stripe and its two neighbours defines a transverse 'supermode'. The coupling together of individual stripes to form arrays is limited to approximately 20 (a transverse distance of ~ 200 μm) due to amplified spontaneous emission in the lateral direction. However, higher powers are obtained by fabricating these devices into bars (typically 1 cm length) which contain 40-50 of the multiple stripe lasers in each bar. Higher powers still, exceeding 1 kW in pulsed mode, are available by stacking the bars, with the limits on power being caused by the problem of removing the heat that is produced when large currents are driven through these devices.

An alternative way of obtaining high powers per unit area from laser diodes is the fast developing field of surface-emitting laser diodes [6]. As opposed to the previously described 'end-emitting' lasers, surface emitting lasers emit perpendicularly to the substrate. This allows the fabrication of monolithic 2-D arrays with high packing

densities and correspondingly high output powers with narrow beam divergences. They are also providing applications as individually addressable optical interconnects in integrated optical chips.

4.3 Laser diode pumped solid-state lasers

Narrow linewidth emission can be obtained from lasers which consist of some form of host material, doped with a rare earth ion [8], such as Neodymium (Nd) and Holmium (Ho). The rare earth ions have the outer electron configuration $5s^2 5p^6 4f^n 5d^1 6s^2$ where n varies through the fifth period of the periodic table from n=1 at caesium to n=13 at ytterbium. When these elements are used as dopants, they can form triply charged ions where the outer 5d and 6s electrons are removed in the bonding process. The electrons of interest are those in the unfilled 4f level which give rise to the excited states. Because the $5s^2 5p^6$ shell is filled and resides outside the 4f shell, the 4f electrons are shielded from the effects of crystal field fluctuations and remain relatively sharp transitions. It is this spectroscopic fact that leads to one of the main advantages of using laser diodes as pump sources as opposed to the previously more conventional flashlamps.

Flashlamp pumped solid-state lasers are prone to instabilities and broad linewidths, mainly due to the 'technical noise' incurred by the necessity for water cooling. Additionally, a large amount of heat is often deposited in the rod due to the quantum defect involved between the absorbed broadband pump radiation and the laser transition, and also direct heating of the crystal by absorption of short wavelength light. This results in thermal focusing and birefringence caused by thermal stresses in the rod. This either increases losses or reduces the level of power at which the laser can be operated. These problems are substantially reduced, or even removed, by the use of laser diodes as the pump source. Laser diodes emit either a single longitudinal mode (index guided) or multiple longitudinal modes (gain guided) when well above threshold. However, even the multi-longitudinal mode output of laser diodes, with an effective linewidth of a few nanometres, is considerably narrower than the broadband emission of flashlamps. The narrow output emission of laser diodes allows selective excitation of the laser ions with a substantially reduced amount of heat being absorbed by the rod. This vastly reduces the cooling requirements and the associated technical noise. The problems of thermal focusing and birefringence are also greatly reduced. These advantages were recognised early on in the field of recombination radiation from semiconductors.

Possibly the first use of semiconductors for pumping a laser was an LED pumped Nd:$CaWO_4$ laser by Newman in 1963 [8]. The first use of a laser diode for pumping was in 1964, not long after the first laser diodes were demonstrated [1,2], using a $CaF_2:U^{3+}$ laser [9], where a side pumping set up was used and both rod and pump source were immersed in a liquid helium filled dewar. Interest soon moved towards

neodymium doped materials as the absorption bands around 800 nm were well situated for pumping with GaAlAs lasers. However, until recently the laser diodes available were inadequate in terms of reliability, ease of handling, operational lifetime and output power. The ever advancing improvements in laser diodes have begun to allow the early optimism placed in laser diode pumped solid-state lasers to be realised.

Developments in laser diode pumped solid-state lasers, in particular miniature Nd lasers, have been the subject of a number of reviews [10]. Interest has concentrated on Nd doped materials because the major advances in high power diode lasers have been with GaAlAs alloys. A lot of work has dealt with Nd:YAG [11,12] as it was an established material with excellent material and spectroscopic properties, but a number of other Nd doped hosts have been made to lase with laser diode pumping, e.g. YLF [13], YAlO [14], glass [15], YVO_4 [16], $MgO:LiNbO_3$ [17]. In doped materials, concentration quenching of the upper state lifetime limits the doping density and absorption. Higher absorption can be obtained in stochiometric Nd materials, where it is part of the chemical composition rather than a dopant [18]. Although Nd is the most commonly used dopant ion, it has not been the only one, e.g. Holmium[19], Thulium[20] and Erbium[21] have also been used.

End pumping of the lasers is more efficient as the pumped mode and lasing mode are collinear and exhibit a greater degree of mode overlap. However a limited amount of power can be coupled in this way. To use higher pumping powers side pumping with laser bars and stacks has been the usual approach [22]. Recently, new approaches are showing that a substantial amount of power can in fact be coupled in using the more efficient end pumping techniques [23]. For higher peak powers the diode pumped lasers can be gain switched [24], Q-switched [25], and mode-locked [26]. Higher average powers can be obtained by using slabs, as opposed to laser rods, where heat removal is easier [27].

Diode pumped lasers have other advantages over lamp pumped lasers, e.g. compact size, higher efficiency, better beam quality and frequency stability, the latter two of which can be important for non-linear optical applications. The intrinsic frequency stability due to the reduced technical noise of diode pumped lasers is particularly evident in monolithic lasers, in particular the MISER developed by Byer's group at Stanford where a unidirectional ring cavity is achieved by using the Faraday rotation in the YAG itself [28]. The Schalow-Townes limit, which applies to a free running laser, was surpassed by Shoemaker et al [29] by using Pound-Drever (or Drever-Hall) locking which uses phase stabilisation techniques. The stability obtained of ~1mHz is less than the shot noise limit. This sort of stability is required for gravity wave experiments.

Laser diode pumped lasers can have frequency versatility by harmonic generation in non-linear crystals [30], sum frequency mixing [31], and as demonstrated here and

elsewhere, optical parametric oscillation. Applications of diode pumped lasers include lidar, space communications and injection seeding of high power systems.

4.4 Laser ions and solid-state hosts

This section briefly introduces the properties of the transition metals and lanthanides (rare earths) which make them suitable active laser ions when doped into solid-state laser hosts. The first section describes the spectroscopic properties of solid-state laser materials in general followed by more details on the Nd ion when doped in the hosts YAG and YLF.

4.4.1 Solid-state laser ions

As mentioned previously, the elements in the fifth period of the periodic table after the element lanthanum produce triply charged ions with sharp transitions when doped in a host due to the shielding of the 4f electrons by the outer 5s and 5p electrons. These sharp features lend themselves to diode pumping where the emission spectrum of the diode is considerably narrower than that of lamp pumped sources. This makes diodes more efficient pumps of laser ions. However, diode lasers can only be used if the emission wavelength of the diode matches an absorption of a laser ion. The fortunate overlap between the absorption feature of Nd doped materials and the emission from AlGaAs lasers at 809 nm has been the reason why so much of the work on diode pumped lasers has involved the Nd ion.

With work progressing on diode lasers for attainment of wavelengths from the far infrared to possibly the blue region of the spectrum, the possibility of pumping other ions is increasing. Erbium has been made to lase at 1.5 and 2.9 μm when diode pumped at around 970-980 nm with InGaAs diodes [32], though this requires the use of Ytterbium as a sensitiser for the 1.5 μm transition due to the three level nature of the transition. Other laser ions which have been diode pumped are Thulium and Holmium [33], where these ions have absorptions close to 800 nm and can be pumped by high power AlGaAs lasers. They are not as efficient as Nd as they do not possess a four level laser structure.

The transition metal elements are also candidates for diode pumping. These elements occur in the fourth period of the periodic table, and lose the outer 4s and possibly some 3d electrons in bonding to give the outer electron configuration $1s^2 2s^2 2p^6 3s^2 3p^6 3d^n$ where n<10. As the 3d electrons reside outside the ion core they interact strongly with the crystal field and can therefore result in broad transitions. These transition metal ions are then capable of producing 'vibronic' or tunable lasers. Of particular note are the Ti:Al_2O_3 and Cr:$LiCaAlF_6$ and Cr:$LiSrAlF_6$ lasers. The trivalent titanium ion consists of a single 3d electron outside the core and is one of the most useful and widely tunable

lasers to date. With its main absorptions in the green it has yet to be pumped directly by a diode laser but has been pumped by frequency doubled diode pumped Nd lasers. The Cr lasers are of current interest for diode pumping as the pump absorption peak at around 630-650 nm is rapidly becoming accessible for direct diode pumping. Diodes are available at these wavelengths but at the moment the power available is small, a few tens of mW.

We now turn our attention to the Nd ion, and in particular the hosts YAG and YLF, which were of interest in this work.

4.4.2 Nd:YAG

The material neodymium doped yttrium aluminium garnet has been the mainstay of solid-state lasers for 3 decades. As such the technology of its growth and fabrication is well established and large, high optical quality samples are readily available. Being a rare earth ion, Nd doping of YAG produces a narrow spectral linewidth and the lasing transitions therefore benefit from a high stimulated cross-section (~ 6.5×10^{-19} cm^2 for 1 % atomic doping [34]). The doping density is constrained to be < 1.5 % (atomic) due to strain and concentration quenching. The pump absorption around 800 nm is shown in fig. 4.2. The peak at 809 nm (width ~1 nm) is amenable to AlGaAs laser diodes which transfers the ions from the $^4I_{9/2}$ ground state to the $^4F_{5/2}$ and $^2H_{9/2}$ manifolds. Rapid non-radiative decay to the metastable $^4F_{3/2}$ (lifetime ~230 μs) results in the 1.064 μm transition to the short lived $^4I_{11/2}$ lower state behaving as a four level laser transition. The upper state lifetime is of sufficient length that efficient energy storage can be obtained with the currently available diode laser pulse lengths of 200-400 μs.

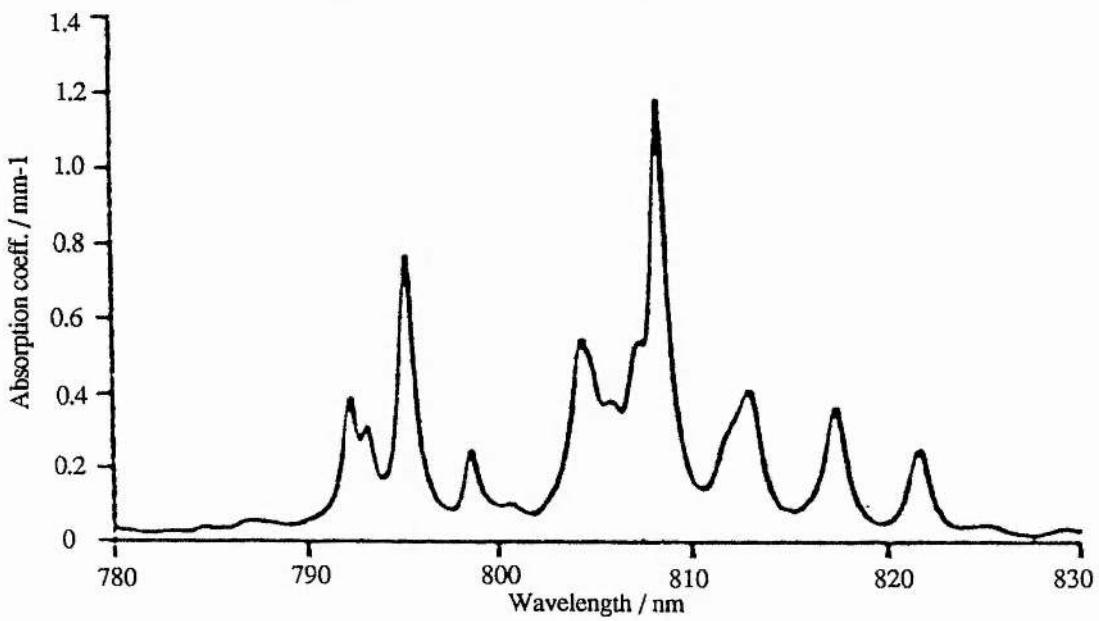

fig. 4.2 Absorption spectrum of 1 % doped Nd:YAG near 800 nm.

The YAG host is robust and has a high thermal conductivity. At high average pump

powers, however, it is susceptible to thermal lensing and thermally-induced birefringence. Both of these can be partially compensated for by proper cavity design but are sources of loss and aberration. The birefringence is particularly a problem when any intracavity polarisation selection is required, such as for electro-optic Q-switching. The high thermal fracture limit means that these lasers can be, and are, used for high average power applications

4.4.3 Nd:YLF

The material Ytrrium Lithium Fluoride is anisotropic with the scheelite structure. This anisotropy results in the emission and absorption properties being polarisation dependent. The emission at 1 μm then consists of two lines, 1.047 μm in the π polarisation being stronger than the orthogonal σ polarisation at 1.053 μm. The 1.053 μm radiation matches the line centre of Nd:glass and Nd:YLF lasers are often used as seeders for high power glass amplifier systems [34].

The absorption near 800 nm for Nd:YLF is polarisation dependent but is wider and stronger than in YAG which, as is found in this work, is beneficial in end pumping as a tighter confined gain mode can be produced. The emission cross section has been measured to be about 75 % that of Nd:YAG [35], but combined with a longer upper state lifetime (~480 μs) the cross-section lifetime product is higher for YLF implying lower thresholds and a greater energy storage capacity. It can therefore be pumped with pump pulses of twice the duration as in YAG while retaining the same storage efficiency.

The natural birefringence dominates over thermally induced birefringence reducing depolarisation losses, and the thermal lensing is much less than in YAG due to partial cancellation between the negative dn/dT and the stress induced index change. A disadvantage it has compared with YAG is a less advanced growth technology resulting in large, high quality samples not being as readily available. Additionally, the thermal fracture limit is less and so YLF cannot be operated at as high average powers as can YAG material. However, as is demonstrated in this work, for lower average powers, particularly Q-switched operation, the spectroscopic and material properties of YLF are superior to YAG.

4.5 Electro-optic Q-switching

A brief account of the theory of Q-switching is presented at this juncture in order that some of the later results can be seen in proper perspective and also to explain the approach taken to overcome a problem in electro-optic Q-switches sometimes referred to as 'ringing'.

4.5.1 General theory of Q-switching

In order for a gain medium to become a laser oscillator it must be placed in a resonator which produces feedback. The 'Q' (for quality) of a resonator can be defined as the ratio of the energy stored in the resonator field to the rate of energy loss from the resonator in an optical cycle. We therefore refer to resonators with low losses as being of high 'Q', and high loss resonators as being of low Q. If in some way the Q of a laser resonator is held at a low value during the pump pulse such that the laser is always below threshold, then no stimulated emission build-up will occur and a large population inversion may be created. It the cavity is suddenly 'switched' to become a high Q cavity then the population inversion that was stored will be many times the high Q threshold and a large gain will be present in the cavity. This results in the fast build-up of a 'giant-pulse' which strips out the energy stored in the population inversion resulting in a high energy, high peak power pulse of nanosecond duration. This pulse is naturally referred to as a giant or Q-switched pulse.

4.5.2 Electro-optic Q-switching

In electro-optic Q-switching the switch between high and low Q is achieved by controlling the polarisation properties of the laser cavity. One way this can be achieved, which is referred to as the quarter-wave configuration is shown schematically in fig. 4.3.

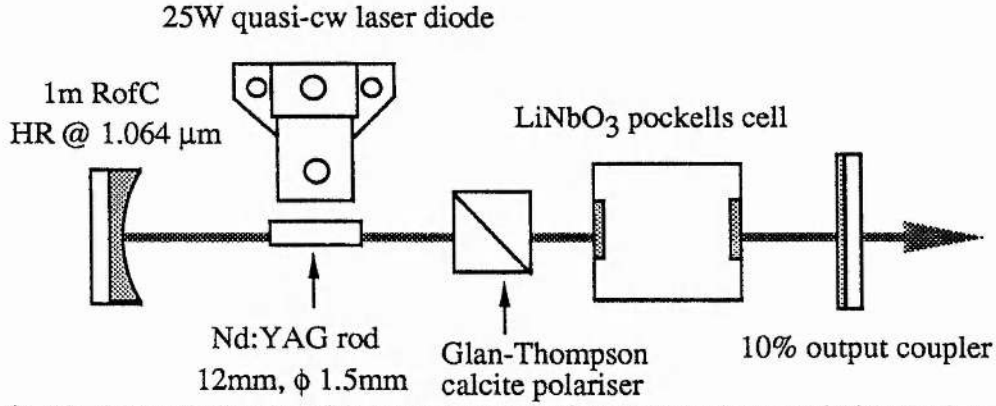

fig. 4.3 Schematic diagram of the quarter-wave configuration for electro-optic Q-switching

An electro-optic crystal can be made to act as a variable retardation plate by application of an (large) electric field. Light emitted from the gain medium travelling to the right in fig. 4.3 is only transmitted by the polariser if it has the correct polarisation. Subsequently it passes through the electro-optic crystal where a quarter-wave retardation transforms it from linear polarisation to circular. After reflection from the mirror it receives another quarter-wave retardation and is now again linearly polarised, but orthogonal to its original polarisation and is therefore rejected from the cavity. In this state the cavity is therefore in a high loss or low Q state. By suddenly removing the applied voltage from the electro-optic crystal the retardation is removed (in approx. <

10 ns) and the cavity is now of high Q and a giant pulse can build-up. In the experiments to be described later, the Q-switched energies obtained were often much less than was expected. This has been attributed to the elasto-optic effect.

When an electric field is applied to an electro-optic crystal the refractive indices are changed due to the electro-optic effect. In addition, as all electro-optic crystals also exhibit piezo-electricity, the applied field additionally compresses the crystal. This crystal compression therefore also contributes to the retardation via a strain-birefringence. Although the electric field is removed in a short time, approx. 10 ns or less, the cavity loss due to induced birefringence does not drop immediately to zero. Instead it drops to some intermediate value (to approx. 30 % loss for $LiNbO_3$) in the time for the voltage to be removed, which is the electro-optic component, followed by a slow (~100s of ns to 1 μs) decay to zero loss. This additional loss may be termed elasto-optic as it results from the residual mechanical compression of the crystal after removal of the applied voltage [36]. When the build-up time of the Q-switched pulse is long compared to the relaxation time of this residual loss then the effect on output energy is small. However when the build-up time is short, the remaining loss during the pulse build-up can substantially reduce the Q-switch efficiency.

The Pockels cell used in this work was a Lasermetrics 3904 $LiNbO_3$ Q-switch. The transient response of the birefringence to removal of the applied field was investigated using the set up shown in fig. 4.4.

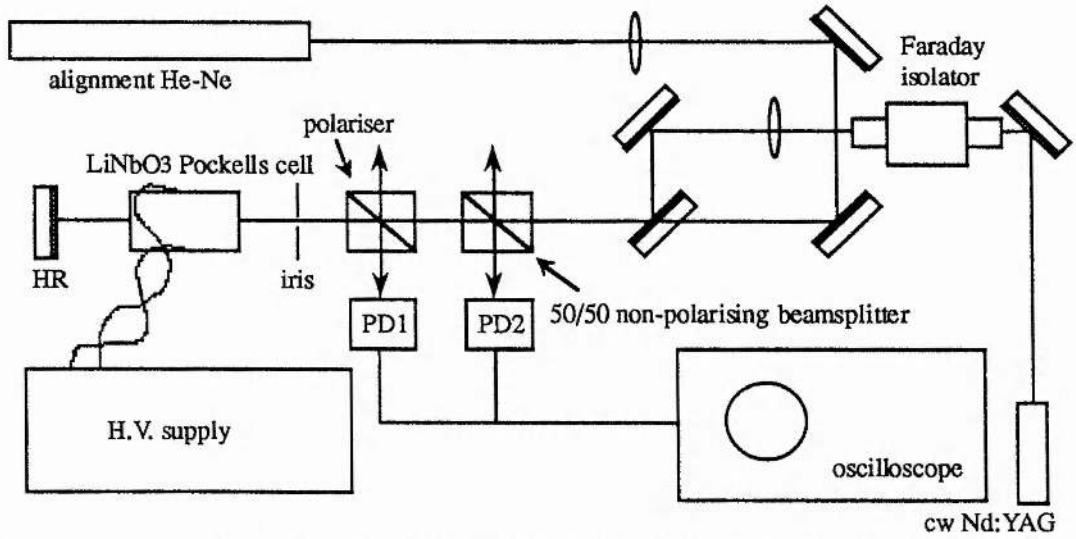

fig. 4.4 Experimental set up for investigation of the transient birefringence in the Pockels cell.

The birefringence in the crystal was mirrored by the signal at photodiode PD1. The transient response of this to removal of the applied field is shown in two time scales in figs. 4.5 and 4.6. The spikes on the traces are electrical noise given off by the Q-switch driver (avalanche transistor chain), and unfortunately obscure some of the information.

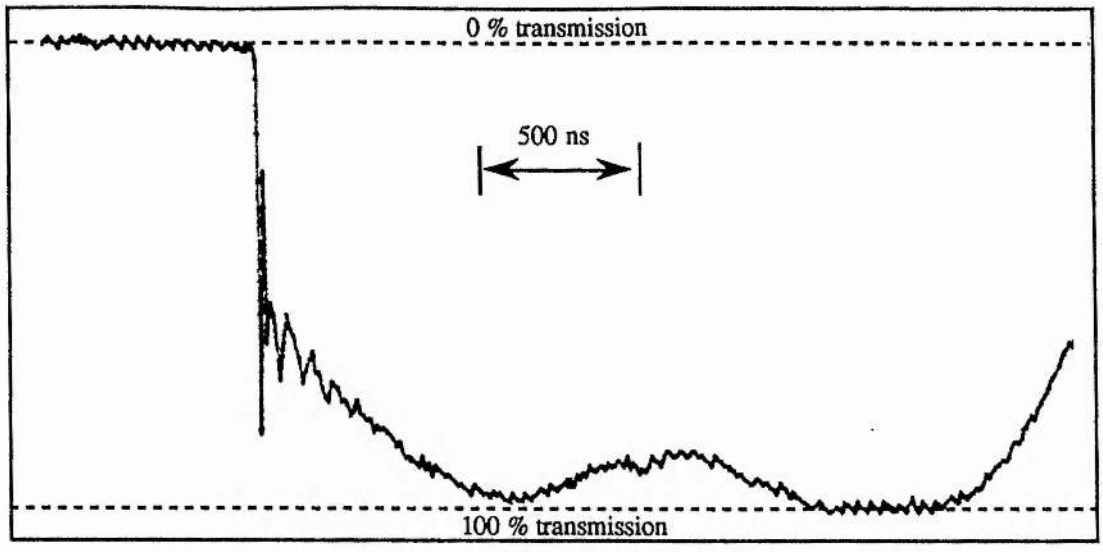

fig. 4.5 Short term transient relaxation of birefringence

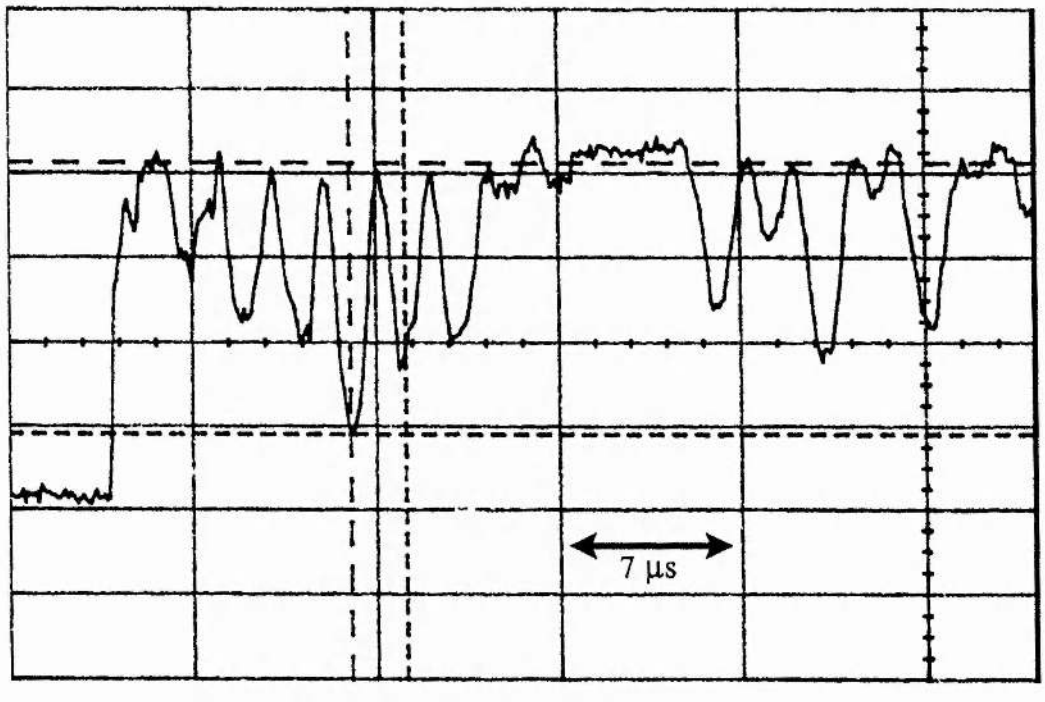

fig. 4.6 Birefringence relaxation on a longer time scale, showing ringing behaviour

On a longer time scale oscillation of the birefringence is observed, fig. 4.6, which is due to the acoustic wave which is caused by the fast expansion of the crystal as the field is removed, propagating back and forth in the crystal. This is not a problem in this work as the build-up time of the laser pulses is short compared to the time for the acoustic wave to cross the crystal.

The birefringence which is still present as the laser pulse builds up can be compensated for by applying a dc field to the opposite electrode of the Pockels cell. In this way the retardation imposed by the dc field is adjusted to reduce the net birefringence at the time of pulse emission to zero. This is demonstrated in fig. 4.7 which shows how the

time taken for the birefringence to reach zero is reduced to less than 300 ns by the application of a 600 V dc bias to the -ve electrode.

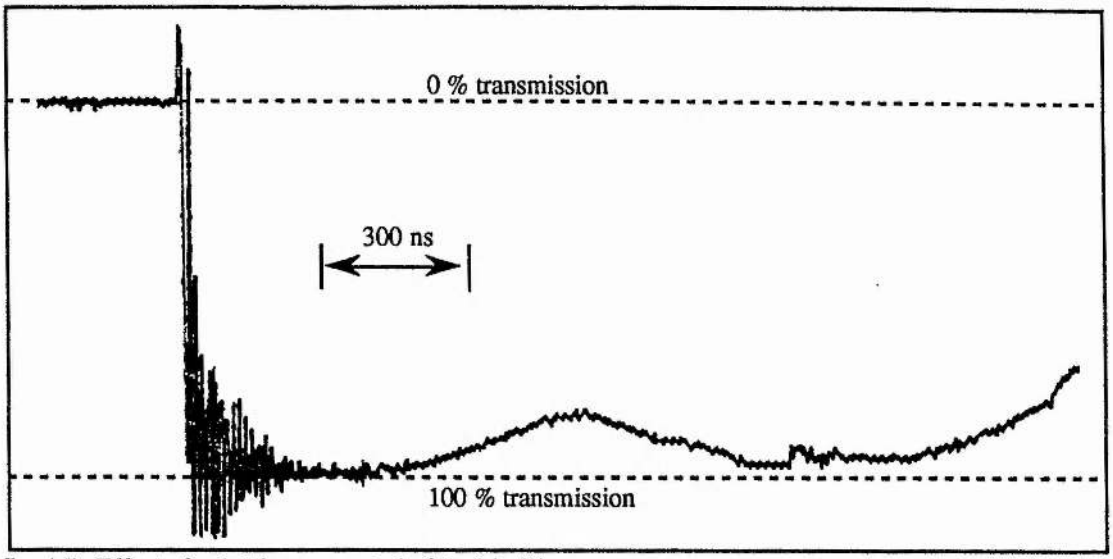

fig. 4.7 Effect of a dc bias on control of the birefringence

This technique helped to increase the output energies from the lasers built here, as will be presented later.

4.6 Side-pumped Nd:YAG lasers

As already mentioned, the general approach taken to increasing the amount of power available from laser diodes is the production of diode laser bars, and further the stacking of these bars. Each bar consists of as many as 1000 individual laser stripes and therefore this linear array endears itself to the side-pumping of laser rods, i.e. the array is situated parallel to the axis of the laser rod, with the diode light either focused into the rod with some form of lens, or merely close-coupled to the rod. As will be discussed later, suitable design of collection optics also allows the diode light to be input along the axis of the rod, referred at as end- or longitudinal-pumping, which can result in a higher value of gain due to the smaller pump mode size. Side-pumping is a simpler technique for pumping with laser diode arrays and was therefore the first one used here. In this work two lasers were built which relied on side-pumping, and these are described in this section.

4.6.1 Nd:YAG laser side pumped by a single diode laser array

At the start of this work, the most powerful diode laser array that was available commercially was the SDL-3220-J, from Spectra Diode Labs, which was capable of a peak power of 25W in a 200 μs pulse producing 5 mJ. These 'quasi-cw' devices could be operated up to a maximum rate of 100 Hz due to heating considerations. This laser was used to side-pump a 1.3 % (atomic) Nd:YAG rod of 1.5 mm diameter and 12 mm

length. Nd:YAG was chosen as it was an established material which was readily available and would allow a good match between the emission wavelength of the diode and the absorption peak at ~ 809 nm. The work that is described in this subsection was performed in collaboration with Callum Norrie, and can also be found in the final section of his thesis [37].

The laser diode array had to be characterised so that its use as a pump laser could be optimised. As mentioned above, the diode could be operated with up to a 200 μs pump pulse, which allows good energy storage due to the 230 μs upper state lifetime. The limit on this pump pulse length was the ability to remove heat from the device. If the temperature of the diode changes, then so does its wavelength, which must be matched to the 1 nm absorption bandwidth of the Nd:YAG. The emission wavelength of the diode array was found to vary both across the array length and also with time due to the dynamic heating of the array by the driving current pulse [38]. This gave a time averaged linewidth from the array of approx. 5 nm. To achieve the best possible match between the emission and absorption requires control of the temperature of the diode array, or at least of its heatsink. Temperature control was obtained by inserting the laser diode inside an insulated copper block, and removing heat using two peltier coolers. The current to the peltier coolers was controlled with a Photon Control 290 Peltier Driver, with temperature sensing using a thermistor. The heat was then removed from the hot sides of the peltier coolers by finned heat sinks and passive air cooling.

The emitting dimension perpendicular to the plane of the laser array is only 1 μm which results in a large divergence angle of the emitted light in this dimension, ~40° (FWHM), while in plane of the array the divergence is ~ 10°. The close coupled scheme adopted here allowed the use of the rod surface as a lensing element to control the divergence in the vertical plane. The diode facet can be aligned to be parallel to a reference axis which will contain the laser rod, by observing the diffraction pattern produced when a He-Ne is directed at the diode facet. The gain region which is produced by this arrangement was observed by detecting the 1 μm fluorescence that is produced with a Si CCD camera (EEV photon). Use of a small aperture at the camera lens allows the whole length of the rod to be imaged. The fluorescence profile was sampled with an in-house video frame grabber controlled by a BBC Archimedes micro-computer, and is shown in fig.4.8. The fluorescence, and hence gain, profile consisted of a stripe opposite the diode with the peak close to the diode side of the rod where the pump intensity is highest. The rod was held in a polished brass holder which would reflect unabsorbed pump light back into the rod.

Using a short cavity, ~ 12 cm, with a 1m highly reflecting (HR) mirror and a 10 % plano output coupler (o/c) and with the rod roughly centred, a best free running energy of 0.9 mJ in a single transverse mode was obtained for 5 mJ pump. Energy

fig. 4.8 Fluorescence profile viewed through one end of the rod

measurements were made with a Molectron J50 pyroelectric detector and J1000 energy meter. Normally the laser mode size is kept as small as possible to obtain a low threshold provided that the pump mode can be confined to be within this size. However, when the pump mode is spatially extended, as is the case here, the mode size is a trade off between low threshold, good overlap between pump and lasing mode, and the requirement that only the TEM_{00} mode is allowed to oscillate. Single transverse mode is obtained here by aligning the cavity such that the TEM_{00} mode uses the peak gain close to one side of the rod, and the rod itself acts as an aperture to prevent higher order modes. The gaussian output profile and measured spot sizes agreed with those expected from cavity mode calculations and was therefore taken to be diffraction limited, although no direct measurement of the closeness to diffraction limited (i.e. number of times diffraction limit or the 'M^2' parameter) was made with this laser. The temporal properties were measured with a BPX65 Si photodiode and seen to give the expected shape of relaxation oscillations tending to a steady state output.

For non-linear optical applications a high peak power is required and so the next step was to Q-switch the laser. This was achieved with the set-up shown in fig. 4.3. Firstly the laser cavity had to be extended in length to allow insertion of the polariser and electro-optic Q-switch. The change in mode size due to extension of the cavity (from 310 μm to 380 μm at the rod) reduced the free-running energy to ~0.7 mJ. With the polariser and Q-switch in the cavity the energy was reduced further to ~0.5 mJ. Using the Findlay-Clay technique [39] (which looks at the way threshold varies with output coupling) the intracavity losses were estimated to be ~9 %. Most of these losses were found to be due to the polariser.

Q-switching of the laser produced a best output of 0.41 mJ in a 38 ns (FWHM) pulse giving a peak power of over 10 kW, though a more typical output was 0.33 mJ in 40 ns. The drop in output energy compared to free running is attributed to the relatively large losses which reduced the number of times above threshold to which the laser could be pumped which affects the extraction efficiency. The loss due to the elasto-optic effect, as mentioned earlier, was not too serious for this laser as the long pulse build up time meant that the Q-switch was almost fully opened when the pulse had built up. The pulse to pulse stability was good, as can be seen in fig. 4.9 which shows a persistence trace over 100 pulses indicating a stability of approx. ± 5 %.

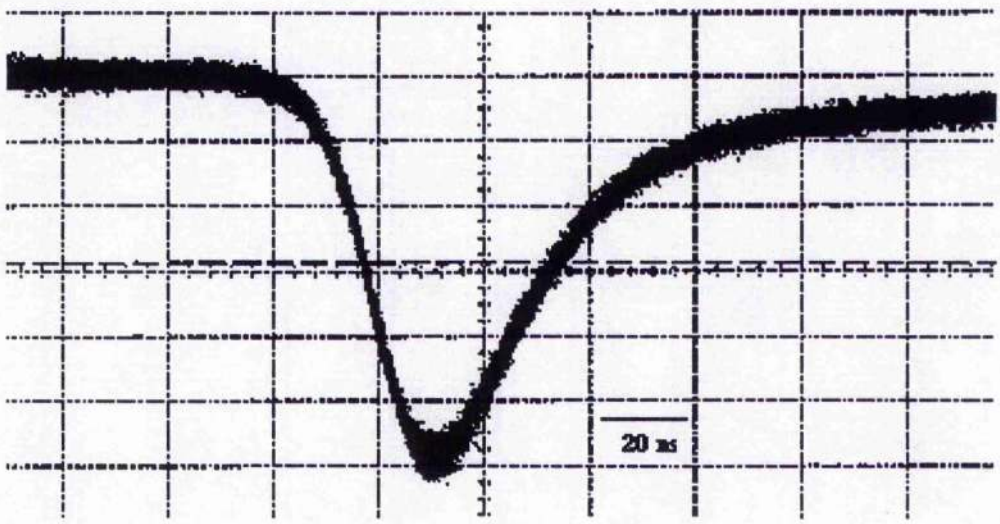

fig. 4.9 100 pulse persistence trace of Q-switched pulses

The characterisation of the Q-switched output agrees well with standard Q-switch theory, as found in advanced textbooks, e.g. Siegman [40], giving a slope efficiency of 17 %, as shown in fig. 4.10.

Lack of success at this point with the OPO lead to the requirement of a laser which was capable of producing higher output powers. The logical step to achieve this was to use more diodes for pumping, and also to use the higher powered diode arrays which were available by this time.

4.6.2 Double side-pumped Nd:YAG laser

With the technology of the growth of semiconductor structures advancing all the time, the power available from laser diode arrays was also increasing. We obtained two SDL-3230-T diode lasers from Spectra Diode Labs which were each specified to give 12 mJ output in a 200 μs pulse (60 W peak power). To obtain this power requires a power supply capable of current pulses of 80 Amps. The power supply was the same as the one used to drive the single device of the previous section, that is a SDL 922, where the

diodes were connected in series and driven by a single power supply. The wavelength

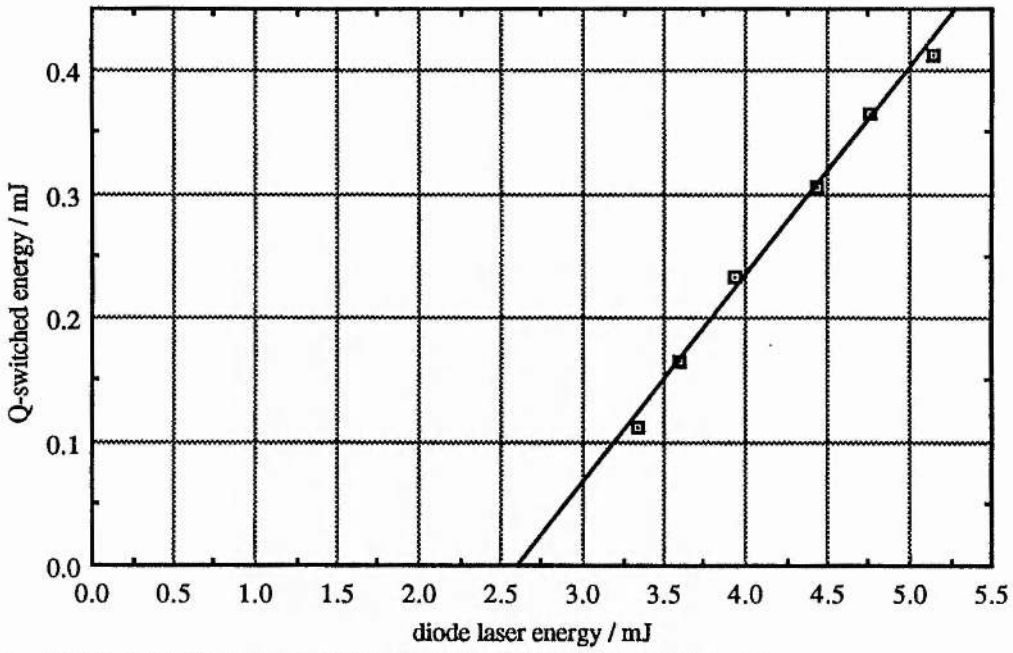

fig. 4.10 Q-switched laser energy as a function of laser diode pump energy

specification that comes with the diodes is only ± 2 nm, and it was found that to get a good spectral match to the Nd:YAG absorption the diodes had to be run at close to 40 °C. This has the advantage that there is no chance of condensation on the diode facet which can be a problem if the diodes have to be cooled substantially, but has the major disadvantage that operation at an elevated temperature is likely to reduce the lifetime. Therefore, the diode heatsinks which were similar to as described in the previous section and were designed for cooling of the diodes in fact had to be used to heat the diodes.

The output from the diode lasers was again close coupled into the rod, this time with the two diodes pumping opposite sides of the rod, as shown in fig. 4.11. Three different rods in all were investigated with this configuration, as it was found that the quality of rods could vary and affect the output. These consisted of the 1.3 % doped 1.5 mm ϕ 12 mm length rod as used in the previous section, a 1.1 % doped 2 mm ϕ 16 mm length (both of these plano-plano with AR coatings), and a 1.3 % doped 2 mm ϕ 12 mm length Brewster angled rod. Use of Brewster angled surfaces should give low loss and also expand the mode inside the rod to give a better spatial match to the linear gain stripe.

With the two diodes opposite each other, the gain profile is again a stripe with peaks at either side where the diode light enters, as shown in fig. 4.12. The reason for the slight asymmetry is that due to their mounts, one diode facet can be brought closer to the rod than the other.

fig. 4.11 Photo of initial pumping arrangement for double side-pumped laser.

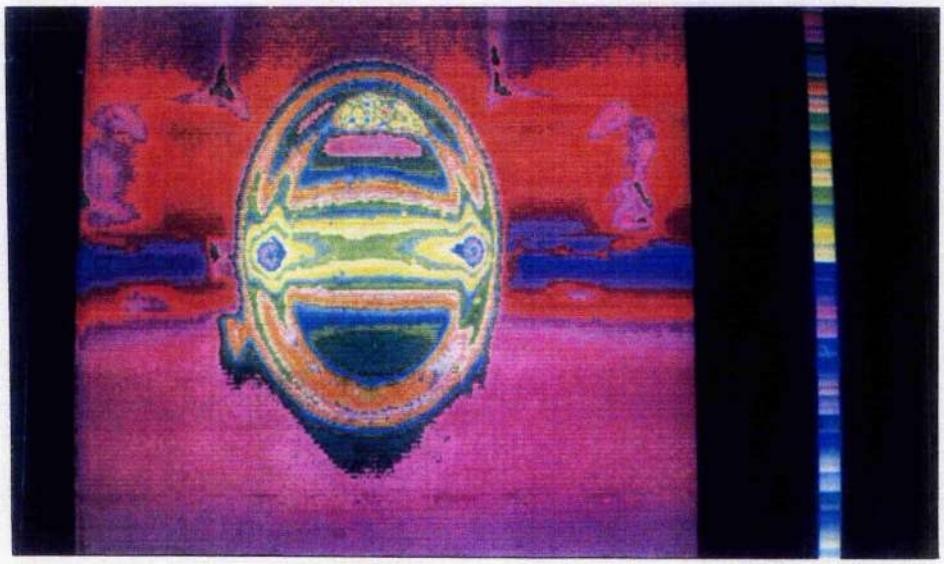

fig. 4.12 Fluorescence for double pumped laser, when diodes are opposite each other horizontally

The Brewster rod was used in the same cavity as previously described, i.e. a 1m HR and 10 % plane o/c separated by ~ 11 cm. Due to mode expansion on entering at Brewster's angle, the mode dimensions at the rod were approx. 330 x 580 μm. This larger mode size and the fact that the gain profile doesn't peak in the centre are attributed to the relatively poor long pulse efficiency of 2.5 mJ output, with a slope efficiency of 14 % and a high threshold of 7.5 mJ. Unlike pumping with a single diode laser where the lasing mode could be aligned to the peak of the gain at one side of the rode, with the double pumped case there is a peak at either side of the rod and the gain at the centre, which is used, is slightly lower. A larger overlap between gain mode and lasing mode can be achieved by expanding the laser mode at the expense of threshold, with the

restriction that too large a mode will experience clipping losses due to the rod.

When Q-switching this laser, the build up time of around 400 ns meant that the Q-switch was not fully open when the pulse was emitted resulting in poor efficiency. The best output was 2.1 mJ in a 50 ns pulse where the output coupler was replaced with a HR and the loss of the Q-switch was used to polarisation output couple.

As the quality of rods was found to vary, this pump geometry was also used with the 1.5 mm plano rod that was used in the single diode pump experiments. With the same short cavity and 10 % output coupling as used for the free-running work above, 4 mJ was obtained with only the rod in the cavity. Lengthening of the cavity and inclusion of the polariser and Pockels cell reduced this to 2.9 mJ. However, again the Q-switch performance was disappointing with only 1 mJ obtained with a 10 % output coupler. Even though the cancellation of the residual Q-switch retardation as described in section 4.4 was being applied, the build up time and associated loss is attributed to the poor performance. Not only does the loss reduce the efficiency of the output coupling, but it also reduces the number of times threshold to which the laser can be pumped, and so reduces the extraction efficiency.

In order to try and increase the efficiency due to overlap between the pump mode and laser mode, a 1.1 % 2 mm ϕ 16 mm length plano rod was used in a concave-convex cavity. Chesler and Maydan [41] showed that cavities consisting of one concave and one convex mirror could be used to obtain large mode sizes while still maintaining stable cavities which were relatively insensitive to misalignment. They also found experimentally, for the case of flashlamp pumping, the optimum ratio of lasing mode size to rod radius as 2. Using a cavity consisting of 75 cm concave and 100 cm convex mirrors separated by 20 cm the mode size at the rod was ~ 500 μm. A $\lambda/4$ plate was used to provide polarisation output coupling as both these mirrors were HR. With the polariser and Q-switch inserted, this configuration gave 3 mJ long pulse, however it was necessary to lengthen the physical length of the cavity to 30 cm to ensure TEM_{00} operation. Again, despite the improved long pulse output energy, the Q-switching performance was disappointing with only 0.75 mJ.

To try and understand why the efficiency was low the gain and losses of the system were measured. By inserting a Brewster plate into the cavity and rotating until oscillation is only just obtainable this gives the maximum loss which the system can withstand. This is then equal to the gain that the rod provides, which was $gl = 0.215$ with the round trip gain as $G = \exp(2gl) = 1.54$. Using a cw Nd:YAG the passive losses of the other cavity components, i.e. $\lambda/4$ plate, polariser and Q-switch, were measured giving a round trip loss of ~ 8 %. It must then be that the residual retardation loss of the Q-switch even with a 600 V dc cancellation bias applied was killing the system. Other work in the department had shown that an end-pumped Nd:YLF laser exhibited higher

gain and Q-switched efficiently [42]. It seemed to be that the low gain available from the double side-pumped system was unable to cope with the residual loss of the Q-switch.

To try and improve the side pumped system by obtaining a gain profile with a central maximum an 'angled pump' scheme was attempted in contrast to the previous linear arrangement. It was hoped to angle the diode lasers at 45 ^{o} to the horizontal and in this way the rod could be mounted in a polished brass mount which would reflect back some of the diode light which was not absorbed (58 % was absorbed in a single pass). Unfortunately, the facet of the diode (particularly for one diode) sits back slightly from its mount and it was not possible to angle the diodes at 45 ^{o}. In fact, as is shown in fig. 4.13, the best that could be obtained was approximately half this. Although a gain profile with a central peak was obtained, as the diodes could not be brought as close to the rod due to mount restrictions, the system showed no improvement over the linear pumping scheme.

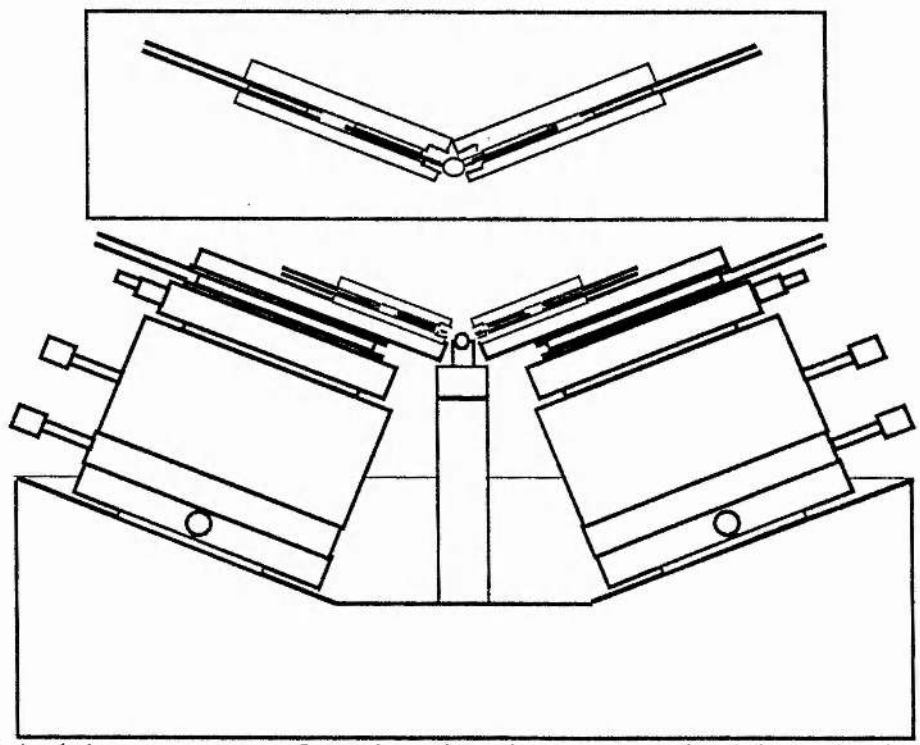

fig. 4.13 Angled pump geometry. Inset shows how the mounts restricted the angles that could be employed.

The success of the end-pumped Nd:YLF system just mentioned encouraged us to build an end-pumped system with Nd:YAG.

4.7 End-pumped Nd lasers

4.7.1 Introduction

When designing a laser cavity for a particular application it is usually borne in mind

that the lowest threshold occurs for the smallest lasing mode size. However, if the pump mode size cannot be confined to be within the lasing mode size, then not all of the pump will contribute and therefore the coupling efficiency will be reduced as described by an overlap integral between pump and lasing modes. In essence, the problem is therefore to confine as much of the pump in as small a volume as possible, with final restrictions placed by host properties such as thermal fracture. It is for this reason that lower thresholds and higher efficiencies are normally obtained by end-pumping of laser rods as opposed to side-pumping. However, as mentioned previously, the highest powers available from laser diodes come in the form of laser array bars and stacks, implying side-pumping techniques for high power operation of solid-state lasers. However, spurred by the greater efficiency and lower thresholds that are obtainable with end-pumping, a variety of schemes have been demonstrated that show that it is in fact possible to couple in a large amount of power using end-pumping geometries. These include angular and polarisation multiplexing of single diodes and laser bars such that the thermal limits of the material, as mentioned above, can be approached [23]. The work here utilised a geometry originally proposed by Shannon and Wallace [43] for collimation and focusing the output from a single laser bar.

4.7.2 End-pumped Nd:YAG laser

To try and achieve enough gain to overcome the losses that were being imposed by the Q-switch it was decided to try end-pumping Nd:YAG as this pump geometry had already proved successful in Nd:YLF [42]. The collection optics which collimated and focused the diode light are shown in fig. 4.14.

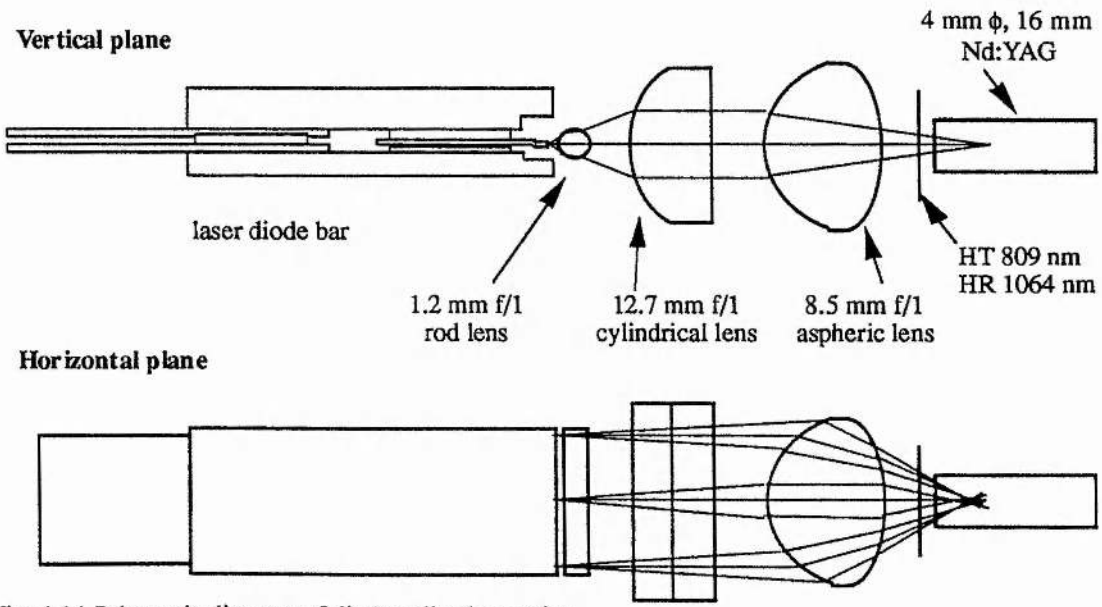

fig. 4.14 Schematic diagram of diode collection optics

This scheme has the advantage that in using bulk refractive optics, as opposed to lenslet arrays or diffractive methods, it is independent of the number of emitters in the laser bar

and does not have to be aligned to micron tolerances. The rod lens and cylindrical lens collimate the light in the vertical dimension, the combination being used as opposed to a single rod lens to reduce spherical aberration. The aspheric condenser lens then focuses the light in both planes through the rear cavity mirror, which is a thin mica sheet coated to be highly transmitting at the pump wavelength and highly reflecting at the lasing wavelength, into the rod. The transmission of the optics, despite AR coatings, was only 75 %, probably due to the high angles of incidence at the interfaces and aperturing in the horizontal plane at the aspheric condenser.

The fluorescence profile, and hence gain distribution, obtained is shown for the two planes in figs. 4.15 and 4.16.

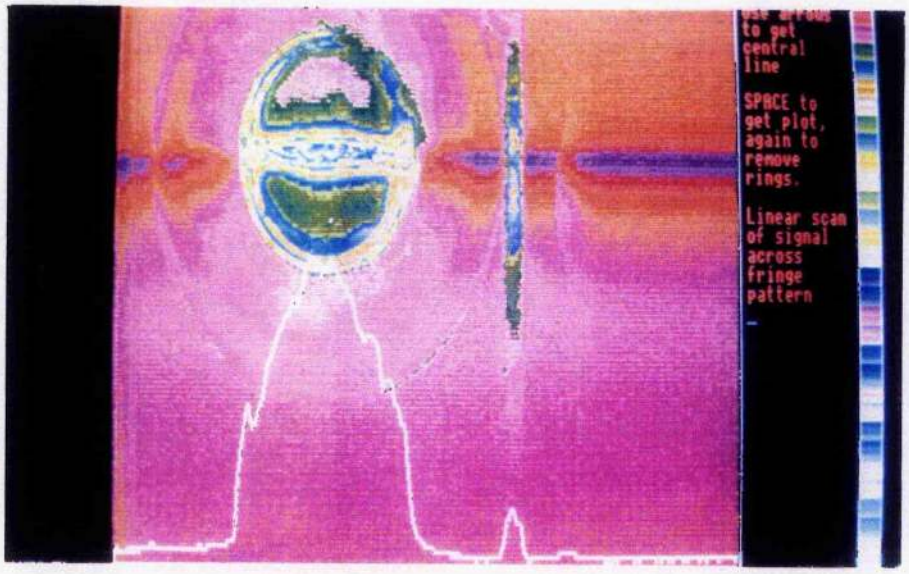

fig. 4.15 Fluorescence profile in the horizontal plane for the end-pumped Nd:YAG laser

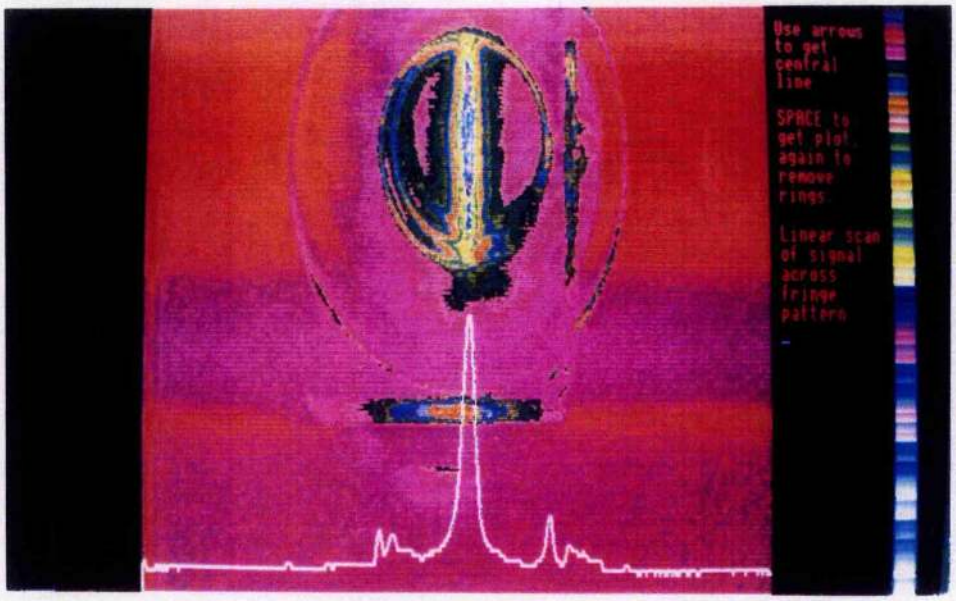

fig. 4.16 Fluorescence profile in the vertical plane for the end-pumped Nd:YAG laser

Although the focused spot size of the pump light was measured to be approx. 30 x 640 μm (measured after adjusting the collimating optics for maximum laser output and then removing the rod) it is clearly seen that the profile in the horizontal plane has a central maximum but still fills the entire rod. The profile in the vertical plane is considerably narrower, with a FW1/e^2 of approx. 700 μm. Both of these are considerably larger than the focused spot of the pump light due to the spreading of the beam as it propagates through the absorption depth of the crystal. It was seen during the experiments that the important thing was to minimise this fluorescence profile rather than just minimising the pump spot because of the finite absorption depth required, and it will be shown later that tighter gain profiles were obtained when using Nd:YLF due to its larger absorption coefficient.

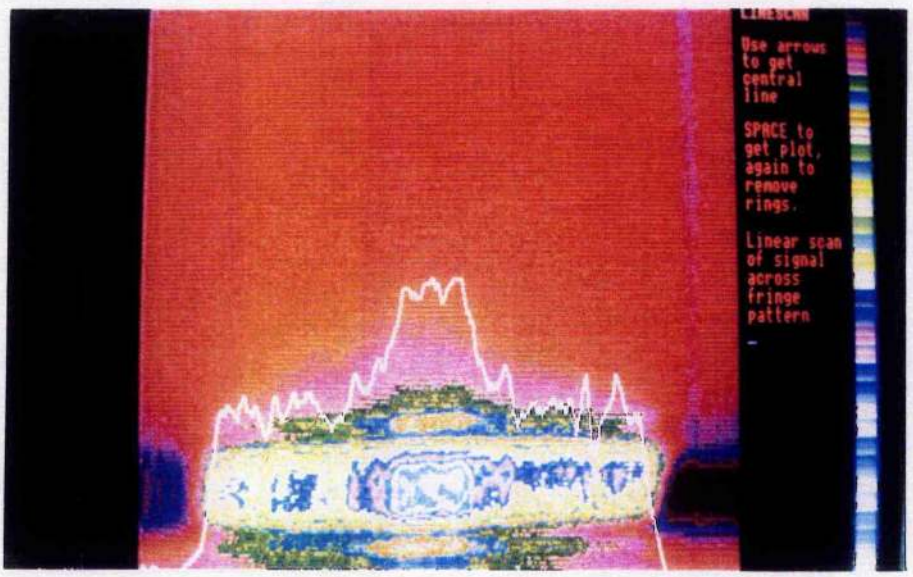

fig. 4.17 Horizontal profile of end-pumped Nd:YAG multi-mode output

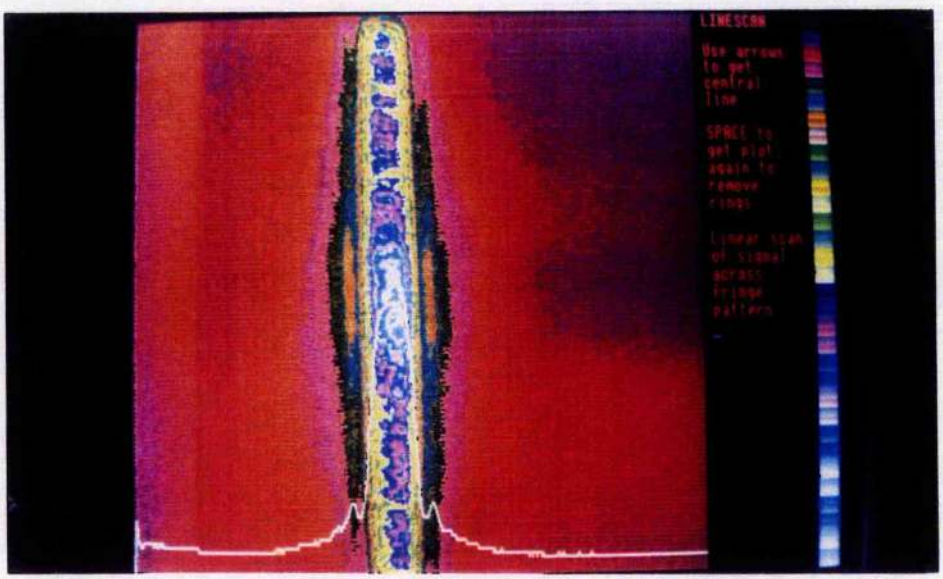

fig. 4.18 Vertical profile of end-pumped Nd:YAG multi-mode output

With the Nd:YAG at one end of a 25 cm cavity consisting of the thin mica HR and a 50 cm 10 % output coupler, the elliptical gain mode results in a multi-transverse lasing mode. The transverse mode profiles for the horizontal and vertical planes are shown in figs. 4.17 and 4.18 respectively.

The horizontal profile consists of a central peak due to the TEM_0 mode superimposed on top of what appears to be TEM_5. The vertical profile is almost single transverse mode, but due to the elliptical gain being slightly larger than the lasing mode, which from cold cavity calculations is approx. 290 μm, there are additional small ripples due to higher order modes. The energy that was obtained in this multi-transverse free running output was 2.4 mJ, which was achieved with a 4.1 mJ threshold and 25.7 % slope efficiency. This corresponds to a round trip gain on centre, calculated by measuring the loss at which oscillation is just achieved, of G = 2.1, which is an improvement on the side pumped scheme where two diodes were used. This demonstrates how end-pumping is more efficient at these pump levels where the diode light can be efficiently collected and focused into the laser rod.

For non-linear optical applications a TEM_{00} output is desired. This can be achieved with an elliptical gain by anamorphic expansion of the lasing mode in the horizontal plane to provide a better match to the elliptical gain. In the work here an anamorphic prism pair consisting of two Brewster angled prisms fabricated from SF4 glass are used to provide x3 expansion in the horizontal plane. An alternative method is the use of a telescope consisting of two cylindrical lenses, which was the approach adopted in the Nd:YLF work mentioned above. Three times anamorphic expansion produces a cold cavity waist of approx. 825 x 290 μm. However, because of the large spatial extent of the gain due to the small absorption of the Nd:YAG, the use of x3 expansion was insufficient to produce single transverse mode output, with the horizontal profile still showing higher order modes and with the small ripples still evident in the vertical plane. Due to the insufficient anamorphic expansion, the coupling to TEM_{00} was therefore not complete and the resulting low output energy, 1.2 mJ, is attributed to this and also to the high losses that were measured for the prisms. Despite the fact that one face of the prism was entered at Brewster's angle and the other was AR coated, the loss was measured with a cw Nd:YAG laser to be approx. 2 % single pass per prism, which gives an additional round trip cavity loss of nearly 8 %. This was disappointing as one of the main reasons why the prism pair was chosen in preference to the cylindrical telescope was that the losses were expected to be lower. The other reason was that the cylindrical telescope had proven difficult to align, a fact that was borne out when an attempt was made to use a x4 cylindrical telescope (formed from a -6.5 mm and a 25.4 cm lens) in the Nd:YAG cavity without success.

It was possible to obtain TEM_{00} output from the cavity by insertion of an iris of approx.

5 mm aperture approx. 5 cm from the plane mirror, however at a low output energy. To obtain a laser that was capable of producing 2 mJ in a Q-switched pulse and in a single mode output it was decided to build another Nd:YLF laser based on the success already obtained with this material [42].

4.7.3 End-pumped Nd:YLF laser

The low efficiency obtained in this work with Nd:YAG, both side- and end-pumped, was mainly attributed to the large spatial extent of the gain in the laser rod. It was hoped that this could be improved upon by using the host material Yttrium Lithium Fluoride (YLF) which has better absorption properties than YAG. As well as the peak of the absorption being larger in YLF than in YAG material, the width of the absorption is also greater which is a benefit due to the large (~ 5 nm) time-averaged emission of the diode lasers, as mentioned previously. The absorption spectrum of Nd:YLF near 800 nm is shown in fig. 4.19.

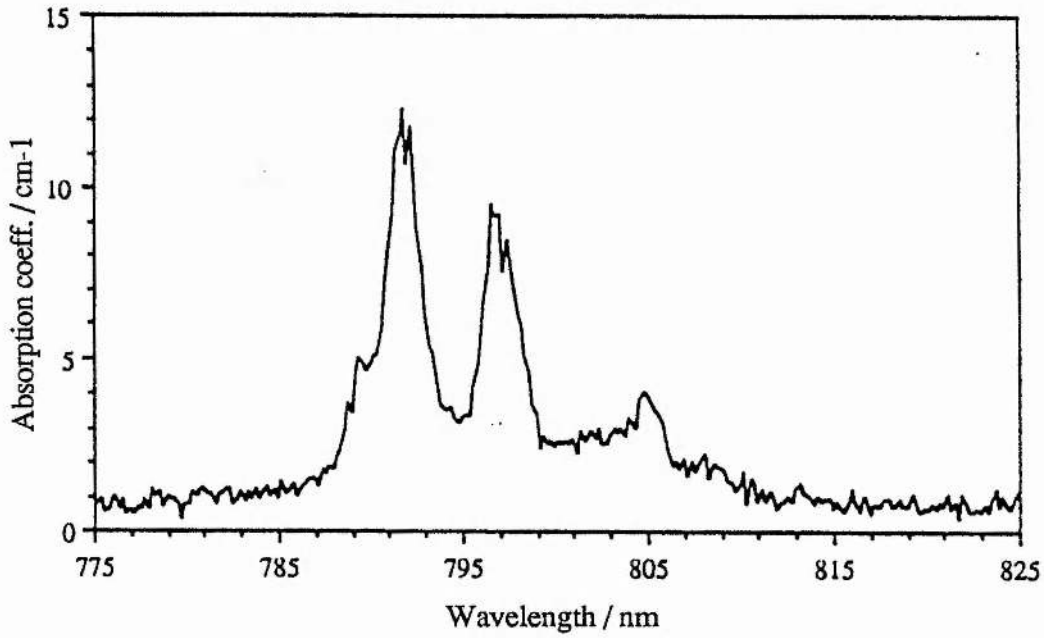

fig. 4.19 Measured absorption spectrum of 1.5 % Nd:YLF, E⊥c.

The uniaxial structure of Nd:YLF results in anisotropic absorption and emission spectra, with the strongest absorption for light polarised along the c-axis. The emission near 1 μm is in two orthogonally polarised lines, 1.047 μm, which is the strongest, being polarised along the c-axis and 1.053 μm in the orthogonal plane (a and b axes having identical properties). The absorption spectrum shows three peaks at 792, 797 and 806 nm. The AlGaAs lasers that are available at present are only just recently becoming capable of pumping the strongest peak at 792, with the 797 line being the usual choice. The laser diodes that were immediately available were those that had been used to pump the Nd:YAG rods, and these could not be practically cooled to pump the 797 absorption. A brief investigation using one of these diodes to pump the 806 nm

absorption of a 1.5 % doped 4 mm ϕ by 10 mm length Nd:YLF rod was only capable of 1.9 mJ free-running with the same cavity and pump optics as described previously for the end-pumped YAG experiments. This low efficiency was due to the weak absorption available at 806 nm and the resulting large gain profile filling the rod.

Good efficiency was obtained by using an alternative laser diode, the same model as the diodes used for the YAG work but with the room temperature wavelength specified as 797 nm. First of all, the transmission of the light emitted from this diode through the coupling optics was measured as 83 %, which is thought to be due to smaller divergence in the horizontal plane reducing aperturing at the aspheric condenser.

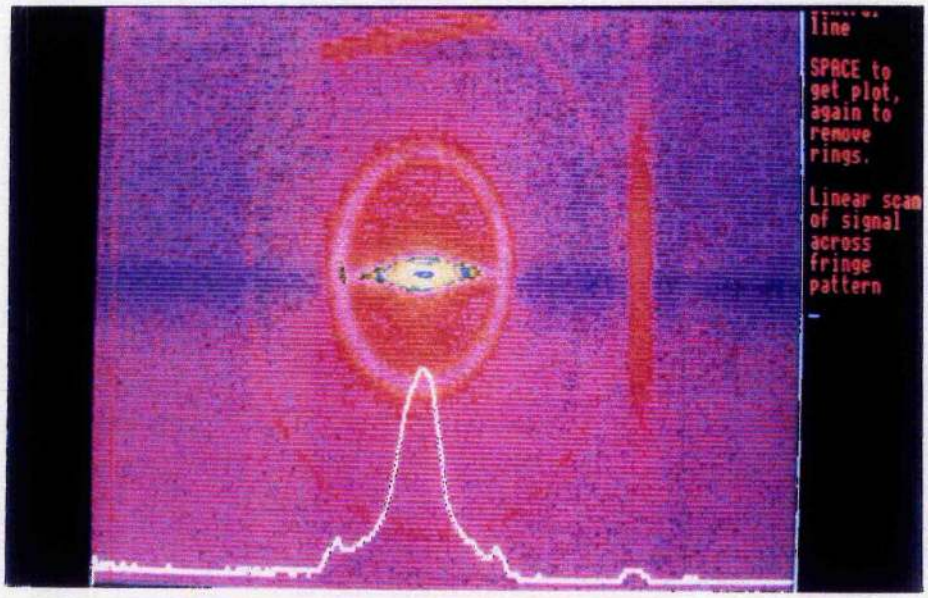

fig. 4.20 Fluorescence profile from horizontal plane for Nd:YLF

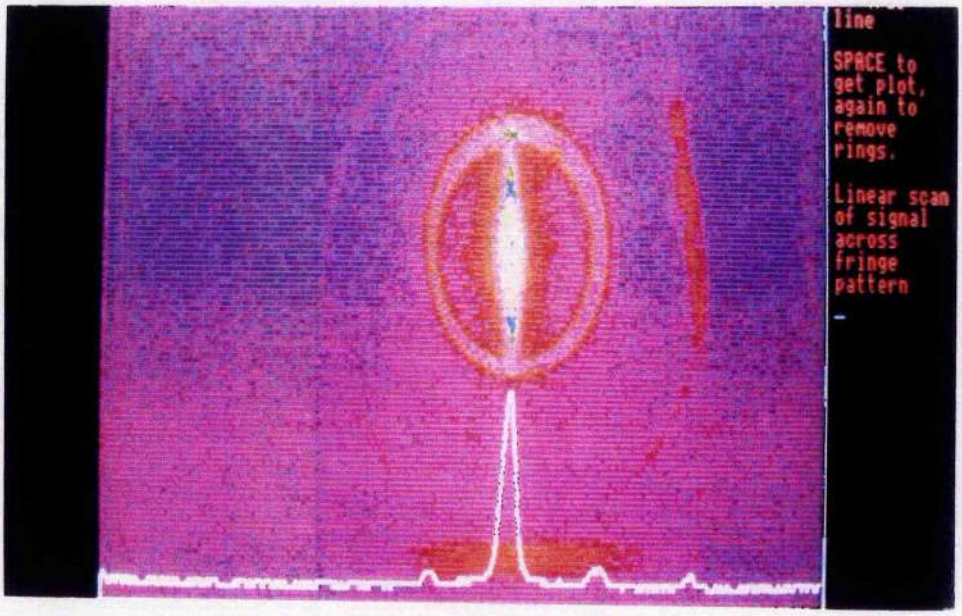

fig. 4.21 Fluorescence profile from vertical plane for Nd:YLF

The fluorescence profiles obtained for the horizontal and vertical planes are shown in

figs. 4.20 and 4.21 respectively.

It is seen that the fluorescence, and hence gain, that filled the rod in the case of the end-pumped Nd:YAG, is confined closer to the axis for Nd:YLF with FWHM widths of approx. 1.3 mm and 380 μm for the horizontal and vertical planes respectively. With a 23 cm cavity, multi-transverse output with a 10 % (20 %) 50 cm RofC output coupler was 3.5 (4.1) mJ with a slope efficiency of 38 (40 %). Insertion of the prism pair for achievement of single transverse mode output resulted in an output of 2.5 mJ, for either output coupler, with the slope efficiency reduced to 30 %. The intracavity losses were measured as 10 % using the Findlay-Clay technique which verified that the major passive loss in the cavity was the 8 % round trip loss of the prism pair. Again by measuring the maximum loss sustainable the gain was estimated as G = 4.7, which is much superior to the side-pumped Nd:YAG geometry even though only one diode is used to pump the Nd:YLF.

Electro-optic Q-switching was obtained with the polarisation selection of the prism pair and the anisotropy of the gain providing sufficient hold-off at these pump powers (12 mJ in 200 μs). The short cavity used and the high gain resulted in an output of 1.8 mJ in a 14 ns (FWHM) pulse. However, it was noticed that the slope efficiency increased close to the peak pump power which turned out to be indicative of a higher order transverse mode coming above threshold. By lenthening the cavity to 28 cm this was prevented giving 1.8 mJ in an 18 ns pulse. These results were obtained with 2.1 kV to the +ve electrode of the $LiNbO_3$ Pockels cell and 600 V as the dc bias on the -ve electrode. With no polariser in the cavity, the net voltage had to be finely adjusted to provide the hold-off until the Q-switch was triggered.

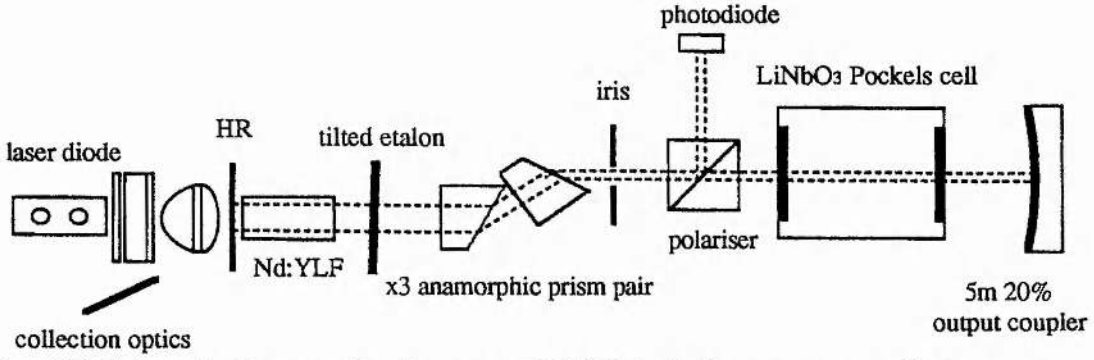

fig. 4.22 Schematic diagram of end-pumped Nd:YLF, including components for transverse and longitudinal mode control.

As other experiments had shown that the isolator which was to be used in the OPO experiments had a high insertion loss (~ 20 % due to poor quality polarisers) it was decided to increase the pump energy deposited in the rod. This was done by increasing the pump pulse duration to 230 μs (limited by the diode driver) to take advantage of the long upper state lifetime (~ 480 μs) and also increasing the drive current slightly, to

give an estimated 14 mJ input pump energy. With the higher gain this provided, it was necessary to use a Glan-laser polariser to achieve hold-off. The output at the higher pump power was 2.2 mJ in a 16 ns pulse with 16 % slope efficiency. However, measurement of the beam profile showed an asymmetry in the vertical plane due to a higher order mode. Insertion of an iris gave TEM_{00} output of 2 mJ with a measured M^2 ~ 1.1 in both planes, with the profiles obtained with a pinholed photodiode showing a near perfect fit to a gaussian. A schematic diagram of the laser is shown in fig. 4.22.

Measurements of the output profiles and focal positions after a lens indicated that the output from the laser was both slightly elliptical and astigmatic. These are both a direct result of the use of the prism pair as the source of the anamorphic expansion in the cavity. The large mode at the rod in the horizontal plane (~ 840 μm) diverges initially less than that of the vertical plane which results in the output spot sizes at the output coupler being approx. 330 (horiz.) and 370 μm (vert.). Calculating an effective waist for the horizontal plane which would allow for the prism pair gives an effective waist slightly behind the prism pair, and therefore displaced from the vertical waist at the plane mirror by approx. 10 cm. The effective waists for the two planes allowing for the diverging effect of the plano-concave output coupler are 225 and 235 μm with an astigmatism of 5.5 cm. Spot size measurements indicated a slightly larger ellipticity than the calculations but agree roughly for the astigmatism. Both the ellipticity and astigmatism had to be taken into account when mode matching the output from the laser into the OPO cavity, or for any other application.

Use of a cylindrical lens telescope may be a preferred option to that of the prism pair. The losses obtained with the lenses were less than the prism pair, but that may have been due to poor quality coatings on the prism pair. In addition, slight adjustment of the telescope allows a small focal power to be incorporated into the telescope which can be used to obtain a circular, non-astigmatic output. The alignment sensitivity of the cylindrical telescope, which was its disadvantage over the prism pair, could be improved by using longer focal length lenses (the x3 telescope used in other experiments, as mentioned earlier, used - 6.5 mm and 19.1 mm focal length lenses).

For some of the experiments where the laser was used as a pump source for the OPO, it was desired to have a single frequency output. A technique which is often used to achieve this with Q-switched lasers is referred to as 'slow Q-switching' [44] or sometimes self-injection seeding. By controlling the retardation induced by the Pockels cell the loss can be set to allow a single relaxation spike to occur at the end of the pump pulse. Normally the Q-switched pulse will grow from noise and so a large number of modes will have developed before the saturation of the gain exerts any control on the magnitudes of the modes. However, if a single relaxation oscillation is allowed to build up with the gain only just above threshold, then the large number of round trips that this

pulse experiences will saturate the gain and results in either a single or double longitudinal mode output depending on the position and separation of the modes with respect to the peak and width of the gain linewidth respectively [45].

Fine adjustment of the net bias to the Pockels cell in these experiments allowed the emission of a relaxation oscillation pulse at the end of the pump pulse. By monitoring this build up with a photodiode looking at the leakage field from the polariser, the Q-switch was fully opened at the peak of the relaxation oscillation. Unfortunately, the high gain of the laser resulted in a short relaxation oscillation (~ 600 ns) and the slow Q-switched output therefore consisted of one or two main modes, with some weaker modes evident approx. 5 axial mode spacings from the main modes. It was possible to eliminate these additional modes by insertion of a 2 mm tilted etalon with a low finesse. By passing the laser output through a 10 GHz FSR 1 cm etalon and monitoring the FP fringes with a CCD camera the output was then seen to be single longitudinal mode on some of the pulses, as shown in fig. 4.23.

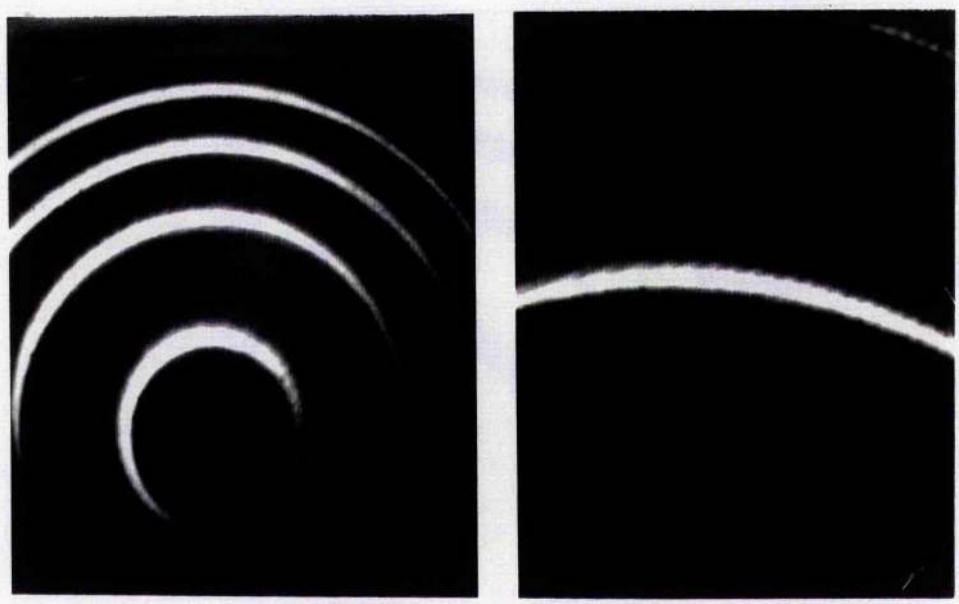

fig. 4.23 Photograph of FP fringes indicating SLM operation, with blow up for clarity.

The output energy of the SLM output was only 1.4 mJ due to the effects of spatial hole burning and etalon losses.

4.8 Comparison of side and end-pumping and Nd:YAG and Nd:YLF

The construction of lasers involving both side and end pumping geometries and also using both the materials Nd:YAG and Nd:YLF allow a direct comparison between pump geometries and materials for pumping at the power levels involved here. Insight into performance differences at higher pumping levels can also be postulated.

Using a single 1 cm laser bar, suitably designed collection optics show that end-pumping is a superior technique to side-pumping. This is due to the ability to concentrate the gain into a smaller volume which lowers threshold and by choice of a suitable lasing mode size the overlap efficiency can also be maximised. With slightly different optics two individual diode bars could be polarisation coupled into one end of a rod. Stacking of diode bars also increases the pump power by replacement of the rod lens by a larger aperture cylindrical lens to collect light from each of the bars [46]. Angular multiplexing of sufficient diode bars in an end-pumped geometry approaches the thermal fracture of laser materials [23] disproving the myth that only a limited amount of power can be coupled in using end-pumping techniques.

At powers below its thermal fracture limit, Nd:YLF appears to be a superior material to Nd:YAG. As was demonstrated in this work, the higher absorption coefficient allows for the generation of a tighter gain profile with the resulting improvement in threshold and efficiency. The wider absorption also requires less stringent control on diode wavelength. Although there still seems to be uncertainty over the exact ratio between the stimulated emission cross-sections of Nd:YAG and Nd:YLF, it is generally accepted that the upper state lifetime is at least twice as long in YLF. This alone allows higher energy storage where ASE is not a problem. Two recent measurements of the spectroscopic properties of the materials both give the product of cross-section and lifetime to be larger in YLF, resulting in a lower threshold, despite the fact that one finds the cross section to be larger in YAG [47] while the other finds the converse [48]. The negative dn/dT partially compensates for the stress-optic coefficients resulting in a much reduced thermal lensing in YLF compared to YAG, and in addition, the natural birefringence of Nd:YLF swamps the thermally induced birefringence. Nd:YAG would only seem to be superior in very high average power cases due to its higher thermal fracture limit.

4.9 Summary

This chapter describes the experimental approach taken to construction of a suitable pump laser for the OPO experiments. Both side- and end-pumping techniques were examined, and both the materials Nd:YAG and Nd:YLF were used, with a comparison made between the two pump geometries and the two materials.

Side pumping with either one or two diodes was investigated for Nd:YAG, but it was found that the low gain and low efficiency due to the resulting large spatial extent of the gain distribution in the rod resulted in poor Q-switched operation. The dynamic loss of an electro-optic Pockels cell was examined and it was found that the remaining loss after Q-switching due to the elasto-optic effect could be reduced by application of an additional bias to the normally grounded electrode, but that due to the fast build up of the pulses in the short cavities used here the Q-switch loss during pulse emission was still substantial and was responsible for the poor Q-switching performance.

End-pumping techniques with single laser-diode bars have been shown to be more efficient than side-pumping due to the better confinement of the gain on axis, reducing threshold and increasing the slope efficiency. Nd:YLF proved superior to Nd:YAG due to its stronger and wider absorption at the diode wavelength. The high gain available with the Nd:YLF rod produced near diffraction limited output pulses of 2 mJ and less than 20 ns duration for an input pulse energy of ~ 14 mJ. Slow Q-switching of this laser produced a source of single frequency output.

4.10 References

[1] N.G.Basov, O.N.Krokhin and Y.M.Popov 'Production of negative temperature states in p-n junctions of degenerate semiconductors' J.E.T.P. **40** (1961) 1320

[2] R.N.Hall, G.E.Fenner, J.D.Kingsley, T.J.Soltys and R.O.Carlson 'Coherent light emission from GaAs junctions' Phys. Rev. Lett. **9** (1962) 366

[3] T.Tsukada 'GaAs - $Ga_{1-x}Al_xAs$ buried heterostructure injection lasers' J. Appl. Phys. **45** (1974) 4899

[4] N.Holonyak, R.M.Kolbas, R.D.Dupuis and P.D.Dapkus 'Quantum-well heterostructure lasers' IEEE J. Qu. Elec. **QE-16** (1980) 170

[5] D.R.Scrifes, W.Streifer and R.D.Burnham 'Experimental and analytical studies of coupled multiple stripe diode lasers' IEEE J. Qu. Elec. **QE-15** (1979) 917
D.R.Scrifes, R.D.Burnham and W.Streifer 'High power coupled multiple stripe quantum well injection lasers' Appl. Phys. Lett. **41** (1982) 118

[6] D.F.Welch, R.Parke, A.Hardy, R.Waarts, W.Streifer and D.R.Scrifes, 'High power, 16 W, grating surface emitting laser with a superlattice substrate reflector', Elec. Lett **26** (1990) 757

[7] B.Henderson and G.F.Imbusch, *Optical Spectroscopy of Inorganic Solids*, Oxford University Press, 1989 London

[8] R.Newman 'Excitation of the Nd^{3+} fluorescence in $CaWO_4$ by recombination radiation in GaAs' J. Appl. Phys. **34** (1963) 437

[9] R.J.Keyes and T.M.Quist 'Injection luminescent pumping of $CaF_2:U^{3+}$ with GaAs diode lasers' Appl. Phys. Lett. **4** (1974) 50

[10] for example
J.P.Budin, M.Neubauer and M.Rondot 'On the design of neodymium miniature lasers' IEEE J. Qu. Elec. **QE-14** (1978) 831
G.Huber 'Miniature neodymium lasers', *in Current Topics in Materials Science, vol4*, ed E.Kaldis, North-Holland, 1980 Amsterdam
I.I.Kuratev 'Solid state lasers with semiconductor pumping' Bull. Acad. Sci. U.S.S.R. Phys. Ser. **48** (1984) 104

[11] L.C.Conant and C.W.Reno 'GaAs diode pumped Nd:YAG laser' Appl. Opt. **13** (1974) 2457

[12] C.J.Norrie, B.D.Sinclair, N.Gallaher, M.H.Dunn and W.Sibbett 'Single frequency operation of diode laser array transverse pumped Q-switched Nd:YAG laser' Elec. Lett. **25** (1989) 1115

[13] G.T.Maker and A.I.Ferguson 'Ti:sapphire pumped by a frequency doubled diode pumped Nd:YLF laser' Opt. Lett. **15** (1990) 375

[14] F.Hanson 'Laser diode side pumped Nd:$YAlO_3$ laser at 1.08 and 1.34 μm' Opt. Lett. **14** (1989) 674

[15] W.J.Kozlovsky, T.Y.Fan and R.L.Byer 'Diode pumped continuos wave Nd:glass laser' Opt. Lett. **11** (1986) 788

[16] R.A.Fields, M.Birnbaum and C.L.Fincher 'Highly efficient Nd:YVO_4 diode laser end pumped laser' App. Phys. Lett. **51** (1987) 1885

[17] T.Y.Fan, A.Cordova-Plaza, M.J.F.Digonnet, R.L.Byer and H.J.Shaw 'Nd:MgO:$LiNbO_3$ spectroscopy and laser devices' J. Opt. Soc. Am. B **3** (1986) 140

[18] K.Kobodera and K.Otsuka 'Single transverse mode $LiNdP_4O_{12}$ slab waveguide laser' J.Appl. Phys. **50** (1979) 653

[19] H.Hemmati 'Diode laser pumped Ho:YLF laser' CLEO '87, paper WI4

[20] S.W.Henderson and C.P.Hale 'Tunable single longitudinal mode diode laser pumped Tm:Ho:YAG laser' Appl. Opt. **29** (1990) 1716

[21] G.J.Kintz, R.Allen and L.Esterowitz 'Diode pumped 2.8 μm laser emission from Er^{3+}:YLF at room temperature' CLEO '87, paper FL2

[22] R.Burnham and A.D.Hays 'High power diode array pumped frequency doubled cw Nd:YAG laser' Opt. Lett. **14** (1989) 27

[23] S.C.Tidwell, J.F.Seamans and M.S.Bowers , 'Highly efficient 60-W TEM_{00} cw diode-end-pumped Nd:YAG laser', Opt. Lett. **18** (1993) 116

[24] A.Owyoung, G.R.Hadley, R.Esherick, R.L.Schmitt and L.A.Rahn ' Gain switching of a monolithic single frequency laser diode excited Nd:YAG laser' Opt. Lett. **10** (1985) 484

[25] K.Chan 'Generation of high power nanosecond pulses from laser diode pumped Nd:YAG lasers' Appl. Opt. **27** (1988) 1227

[26] T.E.Dimmick 'Semiconductor laser pumped, mode locked, and frequency doubled Nd:YAG laser' Opt. Lett. **14** (1989) 677

[27] M.K.Reed, W.J.Kozlovsky, R.L.Byer, G.L.Harnagel and P.S.Cross 'Diode laser array pumped neodymium slab oscillators' Opt. Lett. **13** (1988) 204

[28] T.J.Kane and R.L.Byer 'Monolithic, unidirectional single mode Nd:YAG ring laser' Opt. Lett. **10** (1985) 65

[29] D.Shoemaker, A.Brillet, C.N.Man, O.Crégut and G.Kerr 'Frequency stabilized laser diode pumped Nd:YAG laser' Opt. Lett. **14** (1989) 609

[30] W.J.Kozlovsky, C.D.Nabors and R.L.Byer 'Efficient second harmonic generation of a diode laser pumped cw Nd:YAG laser using monolithic MgO:$LiNbO_3$ external resonant cavities' IEEE J. Qu. Elec. **QE-24** (1988) 913

[31] W.P.Risk and W.Lenth 'Diode laser pumped blue light source based on intracavity sum frequency generation' Appl. Phys. Lett. **54** (1989) 789

[32] J.A.Hutchison, T.H.Allik, 'Diode array-pumped Er, Yb:Phosphate glass laser', Appl Phys. Lett. **60** (1992) 1424

[33] R.C.Stoneman and L.Esterowitz, 'Diode-pumped mid-infrared solid-state lasers', Opt. and Phot. News, Aug 1990, p10-15

[34] W.Koechner, *Solid State Laser Engineering*, 2nd edn, Springer Series in Optical Sciences, vol. 1, Springer-Verlag, Berlin, 1988, chapter 2

[35] T.M.Pollack, W.F.Wing, R.J.Grasso, E.P.Chicklis and H.P.Jenssen, 'CW laser operation of Nd:YLF', IEEE J. Qu. Elec. **QE-18** (1992) 159

[36] R.P.Hilberg and W.R.Hook, 'Transient elastooptic effects and Q-switching performance in lithium niobate and KD*P Pockels cells', Appl. Opt. **9** (1970) 1939

[37] C.J.Norrie, 'Holosteric Nd:YAG lasers', Ph.D. thesis, U. St. Andrews, 1990

[38] C.J.Norrie, B.D.Sinclair, N.Gallaher, W.Sibbett and M.H.Dunn 'Measurement of frequency sweep in a quasi-c.w. diode laser array, and its implication for pumping solid state lasers' J. Mod. Opt. **36** (1989) 1

[39] D.Findlay and R.A.Clay, 'The measurement of internal losses in 4-level systems', Phys. Lett. **20** (1966) 277

[40] A.E.Siegman, *Lasers*, University Science books, 1986 U.S.A.

[41] R.B.Chesler and D.Maydan, 'Convex-concave resonators for TEM_{00} operation of solid state ion lasers', J. Appl. Phys. **43** (1972) 2254

[42] C.F.Rae, J.A.C.Terry, B.D.Sinclair, M.H.Dunn and W.Sibbett, 'Single frequency, end-pumped Nd:YLF laser excited by a 12 mJ diode laser array', Opt. Lett. **17** (1992) 1673

[43] D.C.Shannon and R.W.Wallace, 'High power Nd:YAG laser end pumped by a cw, 10 mm x 1

μm aperture, 10 W laser diode bar', Opt. Lett. **16** (1991) 318

[44] D.C.Hanna, B.Luther-Davies and R.C.Smith, 'Single longitudinal mode selection of high power actively Q-switched lasers', Opto-Elec. **4** (1972) 249

[45] W.R.Sooy, 'The natural selection of modes in a passive Q-switched laser', Appl. Phys. Lett. **7** (1965) 36

[46] H.R.Verdun and T.Chuang, 'Efficient TEM_{00}-mode operation of a Nd:YAG laser end pumped by a three-bar high-power diode-laser array', Opt. Lett. **17** (1992) 1000

[47] N.Mermilliod, R.Romero, I.Chartier, C.Garapon and R.Moncorgé, 'Performance of various diode-pumped Nd:laser materials: Influence of inhomogeneous broadening', IEEE J. Qu. Elec. **28** (1992) 1179

[48] N.P.Barnes, M.E.Storm, P.L.Cross and M.W.Skolaut, 'Efficiency of Nd laser materials with laser diode pumping', IEEE J. Qu. Elec. **26** (1990) 558

CHAPTER 5
KTP OPO

5.1 Introduction

This thesis describes the successful operation of an all solid state optical parametric oscillator based on the non-linear material potassium titanyl phosphate (KTP). It is the purpose of this chapter to describe the steps towards the achievement of this goal. Firstly, the design considerations which were undertaken will be discussed, with particular reference to early experiments. The early attempts will then be described, with discussion of the lessons learned. The decision to adopt 'zero-power' mirrors had a large impact on the success of this work, and so the properties of these mirror substrates are described. Results are then presented for the operation of the OPO, describing the threshold, efficiency and spectral characteristics. Where appropriate these are compared with theoretical calculations.

In the following sections, in order to ease notation, the term "signal" is used to refer to the higher frequency, or shorter wavelength, of the two generated waves, and the term "idler" is used for the corresponding lower frequency, or longer wavelength, wave. Although this convention seems to have been adopted in general, it is not a universally adopted approach and it is therefore sensible to spell out the notation that has been adopted.

5.2 Design considerations

As the gain available from a non-linear process critically depends on the intensity in the interacting beams, when trying to design a system when the pump power available is limited it is important to optimise the parameters which maximise gain and minimise losses. This is why a lot of consideration was given to the choice of non-linear material, and why the material properties were examined in detail in chapter 3.

5.2.1 Gain

Both the theory presented in chapter 2 and the general considerations of chapter 3 introduced how the gain that could be obtained from a non-linear material basically depends on the non-linear coefficient, the maximum usable crystal length and the intensity of the pump beam.

The non-linear coefficient is a property of the material alone, emphasising again why

the material choice is important. This is also reiterated by the fact that the major advances in OPO technology of late have been influenced heavily by the development of new materials. In addition, if possible for the interaction of interest, it is desired to choose a phasematch geometry which maximises the value of d_{eff}.

The available crystal length depends not only on the physical length of the crystal, but on the geometry in which it is used. In critical phase matching, if there is substantial walk-off then after a certain distance the interacting beams will no longer overlap, and will therefore no longer interact. In non-critical phase-matching (NCPM) there is no walk-off and so the whole crystal length is used. However, unless temperature tuning is available, the benefit of NCPM is countered by a likely reduction in tunability from the device.

Even with only a small amount of power available from the laser, a large intensity can be obtained by focusing. There is an optimum degree of focusing for each geometry, as discussed in chapter 2, beyond which the available gain drops of due to phase mismatch, despite the increase in intensity. However, for pulsed lasers, focusing of the laser will usually damage the material before the optimum focusing is obtained. The damage of the non-linear material, and sometimes more importantly any coating on the material, is then usually found to be the limiting factor to how much gain can be obtained from a system. What must also be considered though is that although the crystal is at the focus of the pump beam and will therefore receive the highest energy fluence, any other optical elements through which the beams pass, such as lenses and especially cavity mirrors, will also be subjected to high optical intensities. The intensities at these elements also have to be kept below their optical damage thresholds.

These are the main factors which must be considered when trying to obtain as high a gain as possible from a non-linear crystal. However, as well as compromising between these variables in order to achieve an optimum, other factors affect these choices, such as cavity losses, and also, something which is not always given adequate consideration, the practicality of any optimised design.

Bearing these considerations in mind, and because of the limited power available from the pump laser that was currently available in our lab, it was decided to sacrifice the tuning from the device in favour of the higher gain that could be achieved with a NCPM geometry. This geometry maximises the non-linear coefficient as well as eliminating the deleterious effect of walk-off.

5.2.2 Loss

Obviously in any system it is desired to keep the losses as low as possible. In the case of OPOs, and lasers, losses have a double effect. Firstly they increase the threshold of

the device, and so a higher pump power is required simply to achieve operation. Secondly, to couple out the generated waves a discrete amount of useful loss must be included in the form of the output coupler. However, when there are additional losses in the system, the fraction of the generated waves that contributes to useful output depends on the ratio of useful loss, or output coupling, to that of the unwanted, or parasitic loss. A compromise has to be reached, as increasing the output coupling excessively so as to have most of the output as useful, will also have increased the threshold due to the increase in total loss. Thus it is desirable to keep the cavity losses as low as possible, which for a pulsed OPO basically means using AR coatings on the crystal faces. As has been discussed in chapter 2, the build-up time required to reach oscillation threshold can also be regarded as an effective loss. To minimise this loss, a short cavity is required.

In an OPO, waves are generated at two frequencies and so there are the losses of two separate cavities, signal and idler, to be considered. As discussed in chapter 2, a lower threshold can be obtained for an OPO if both the signal and idler waves are resonated, i.e. a doubly resonant oscillator (DRO), compared to the case where only one wave is resonated, i.e. a singly resonant oscillator (SRO). However, this lower threshold comes at the expense of strict requirements on pump linewidth and stability, and also on the OPO cavity length stability. Instability of the output occurs unless the pump laser and OPO cavity are maintained within the requirements mentioned above. To achieve a stable output would require a large exercise in laser and OPO cavity stabilisation and would not necessarily give a large benefit in the situation considered here due to the considerable absorption at the idler frequency, as mentioned in chapter 3. This would result in a low Q cavity at the idler wave and therefore resonating this wave would not decrease the threshold by more than a factor of 2 or so. However, the arguments above with respect to required stabilities are expected to apply more strictly to cw and long pulse set ups. It was thought that the cavities would be stable during the short duration of a Q-switched pulse, and so the requirements on stability might not be so harsh. It was therefore decided to adopt a DRO design in the first instance for the reason just mentioned, and also with the wish to achieve a working device as soon as possible and with the lowest possible threshold due to the limited energy available at the time (~0.3 mJ in 40 ns). This device would likely have an unstable output in terms of both amplitude and frequency but would give us a reference point on which to base improvements.

5.3 Early experiments

The first crystal that we obtained was a 10x4x4 mm (axbxc) flux grown KTP crystal from Photox Optical Systems, of Oxford, UK. This was an uncoated crystal as the Chinese suppliers of the crystal to Photox preferred not to coat the crystal. Despite it

being desirable to have the faces AR coated to minimise loss, it was decided to proceed with no coating on the crystal as we could then afford to focus quite tightly into the crystal and so hopefully achieve sufficient gain as to offset these losses. KTP, even flux grown material, is quoted in the literature [1] to have a damage threshold greater than 1 $GWcm^{-2}$. This is however for ps pulses, and the damage threshold is expected to be less for the pulses of interest here, which have durations of 10s of ns. The damage quoted by the crystal supplier was 500 $MWcm^{-2}$, which would allow reasonably tight focusing in the crystal without damage.

As well as tight focusing of the pump, a resonator was required which could produce a small signal confocal parameter. In wanting to keep the cavity length to a minimum we obtained mirrors for the signal with the smallest radius of curvature that was available commercially. These plano-concave mirrors were supplied by Laseroptik of Garbsen, Germany, and had a radius of curvature of 10 mm polished from fused silica substrates. They were coated to be 95 % reflecting centred on 1.6 and 3.2 μm and AR coated at 1.064 μm, i.e. coated for double resonance, with 10 % output coupling at both waves. Adoption of a confocal cavity would result in only a small drop in gain from the optimum focusing for no walk-off, i.e. $\xi = 1 / b = 2.84$, but would provide a cavity which was less sensitive to misalignment. The plano-concave nature of the mirror substrate acts as a highly diverging lens, resulting in the requirement of a short focal length positive lens close behind the substrate to mode match the pump beam to the OPO cavity mode. A schematic of this design is shown in fig. 5.1.

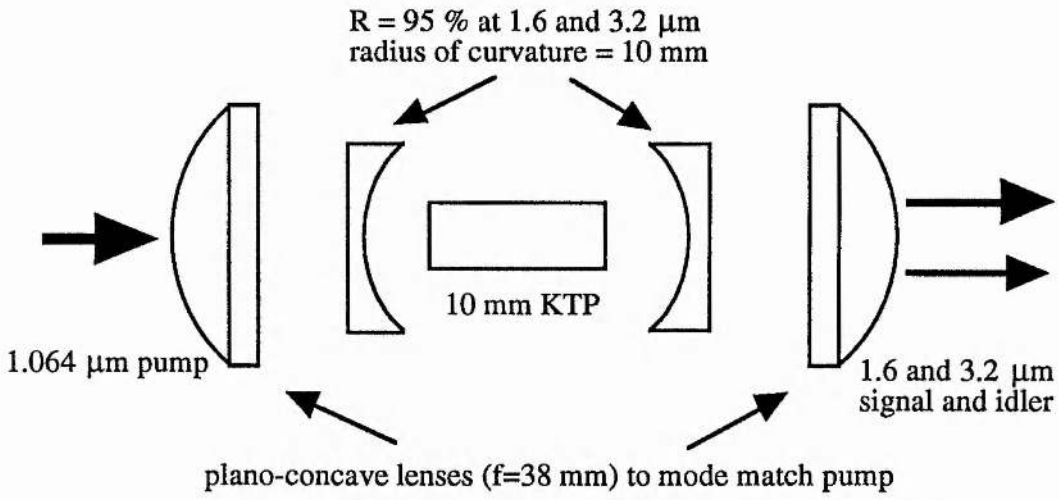

fig. 5.1 - Schematic diagram of OPO design for 10 mm crystal using plano-concave mirrors

The crystal itself was held in a perspex mount which had a spring loaded plunger to hold the crystal in place. This mount was attached to a 4-axis mount (Micro-Controlle, 'mount with four degrees of freedom') which allowed the crystal to be rotated in the ac and ab planes and allowed the crystal to be translated perpendicularly to the pump. Due to the short focal lengths of the optics used, alignment of this system proved difficult. The input lens and mirror substrate were mounted in separate 5-axis gimbal mounts

(Newport LP-1B) for individual adjustment, with the output mirror and collimating lens mounted together in a third mount. To aid alignment, a low power He-Ne laser was made to be coaxial with the output from the diode pumped Nd:YAG laser by coupling in through a side face of the intra-cavity polariser and adjusting the He-Ne beam steering mirrors until the beam passed through two irises which were set up for the YAG beam. Alignment of lens and mirrors was achieved by observing both the reflection and transmission of the reference He-Ne, in particular the FP ring patterns that they produced.

Unfortunately, all attempts to achieve operation of an OPO with this set up were unsuccessful. Some surface damage of the crystal was observed during alignment when the pump focus coincided with the crystal output face. This damage occurred at ~ 500 $MWcm^{-2}$ when the pump was focused to an estimated spot size of 25 μm, which is the damage threshold specified by the supplier. The main reason for the failure of the experiment was attributed to the problems of alignment which required the input lens and mirror to be both coaxial and parallel, and also required their separation to be accurate to fractions of a mm.

To determine if the lack of success so far was due to insufficient pump power, as an intermediate step it was decided to pump the OPO with a flashlamp pumped Nd:YAG laser (Quantel YG481) that was available in the department and could provide substantially more power than the diode pumped laser. As the Quantel laser could supply 12 mJ in a 20 ns pulse, the focusing employed would not have to be so tight, and this should make alignment easier. When using a 0.6 mm spot from the flashlamp pumped laser, catastrophic bulk damage occurred at an intensity of ~ 190 $MWcm^{-1}$. It was thought that the damage occurring at this relatively low intensity must have been caused by an inclusion in the crystal absorbing the pump and causing intense localised heating of the crystal. The crystal actually broke into a few pieces when removed from its holder.

With the main cause for the failure to achieve operation of the OPO thought to be alignment, as detailed above, a new design was required which would drastically reduce the alignment problems. The problem was the effect that the OPO mirrors had on the pump beam. The answer was therefore to have mirrors which didn't have such a large effect on the pump beam. The design of these mirrors which can be called 'zero-power mirrors' is described in the next section.

5.4 Zero-power mirrors

5.4.1 Mirror design

The majority of OPOs pumped by pulsed lasers use plane mirrors in which the effect on

the pump beam is only that of displacing the focus slightly due to the optical thickness of the substrate. In the experiments described here, because of the low power available from the pump laser, it is necessary to focus the pump into the resonator and also to have an OPO resonator which confines the resonant wave with a small confocal parameter. This requires the inner surface of the mirror to have a curved surface, which will always cause a beam passing through it to diverge. What was therefore required was something which would cancel out this divergence, yet do it in a way which was insensitive to misalignment. The most logical way to do this is to have the correcting focusing element as part of the mirror. This is done by polishing the outer surface of the mirror such that the two surfaces are nearly concentric. This is shown in fig. 5.2.

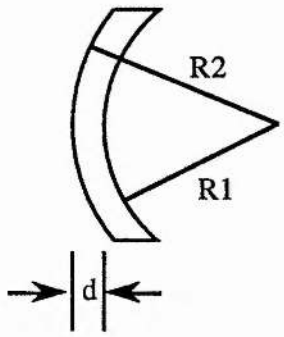

fig. 5.2 Schematic diagram of design of zero-power mirror

With these mirrors the diverging effect is almost cancelled by the outer surface, it is in any case substantially reduced. The improved properties of this design over plano-concave mirrors is shown in figs. 5.3(a) and (b) which display the variation of pump focus position and size when the position of the mirror is altered, for mirrors with radii of curvature (inner and outer) of 100 and 500 mm, and substrate thickness 5 mm.

Fig. 5.3(a) shows that for a movement of the mirror substrate of 10 cm, the position of the pump focus changes by only ~ 5 mm. This is a substantial improvement over the effect of plano-concave mirror substrate, even when a short focal length lens is placed close behind the mirror to counteract its divergence. The small effect of the zero-power mirror also means that mode matching can be accomplished with a single lens, reducing complexity and losses. The waist size that is produced differs only slightly from that expected when the mirror is not present, and is not affected strongly by the mirror position. The size and position without the mirrors is shown by the horizontal line in each graph. Although a slight improvement in approaching "zero-power" behaviour of the substrate would ensue by using a slightly thicker substrate than that corresponding to concentric surfaces, the concentric design was retained because of its additional benefit in not displaying a unique optical axis. Hence, the tilting of the mirror to align the OPO cavity does not affect the eventual focus of the pump beam.

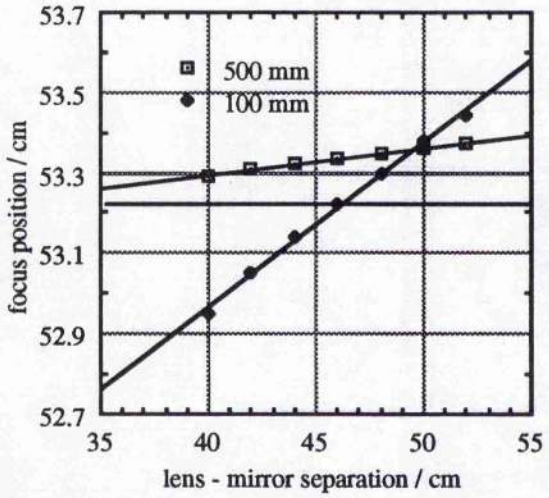

fig.5.3(a) Effect of mirror position on focus position for 100 and 500 mm radii mirrors

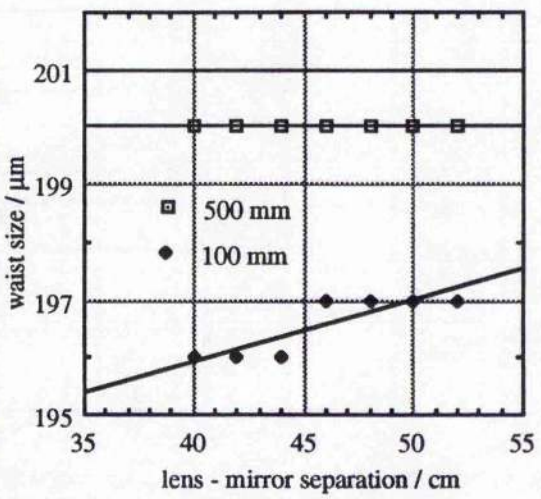

fig.5.3(b) Effect of mirror position on waist size for 100 and 500 mm mirrors

5.4.2 Mirrors obtained

The zero-power mirrors used in these experiments were obtained from two different sources.

Another member of the group was also using zero-power mirrors for an OPO application and had some uncoated substrates which were made available to me. These substrates were supplied by IC Optical Systems Ltd, of Kent, UK., and were fashioned from quartz glass. One set had an inner radius of curvature of 96.7 mm, and an outer radius of 100.3 mm. The on-axis substrate thickness calculated from measurement of the off-axis thickness is 3.65 mm. A second set had inner radius 495 mm and outer radius 500.2 mm, with a thickness of 5.2 mm. The coating of these substrates will be discussed when their use is discussed later.

A second series of mirror substrates were obtained from PMS-Optik, of Frankfurt, Germany. The substrates were manufactured from infrasil (synthetic fused silica). Three different radii of curvature were obtained, with the inner radii being 20, 100 and 500 mm and the outer radii being 25, 100 and 500 mm respectively. The substrate thickness on axis was 5 mm. By a simple thick lens calculation, the focal lengths for the 100 and 500 mm mirrors with equal inner and outer radii are 14 and 345 m respectively. With these large focal lengths it was thought the mirrors would be adequate without having to have the outer radii concentric with the inner, incurring the additional cost due to tooling requirements of the manufacturer. Figs. 5.3(a) and (b) are calculated with the assumption of equal inner and outer radii. For the 20 mm case, there is a reasonable improvement obtained by going to a concentric outer, justifying the difference in this case. However, there is still a reasonable effect on the pump focusing produced by the 20 mm mirrors as shown in fig. 5.4.

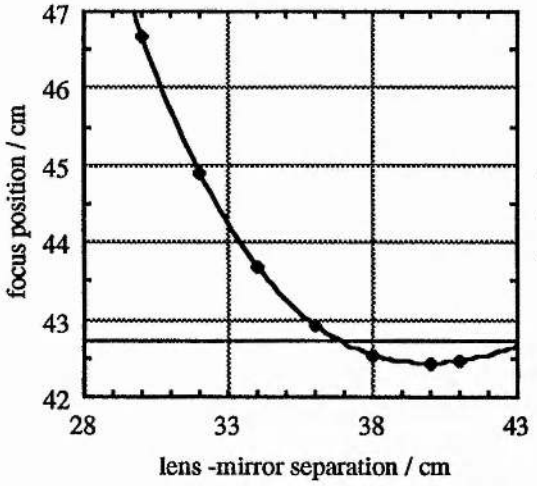

fig.5.4(a) Effect of mirror position on focus position for 20 mm radii mirrors

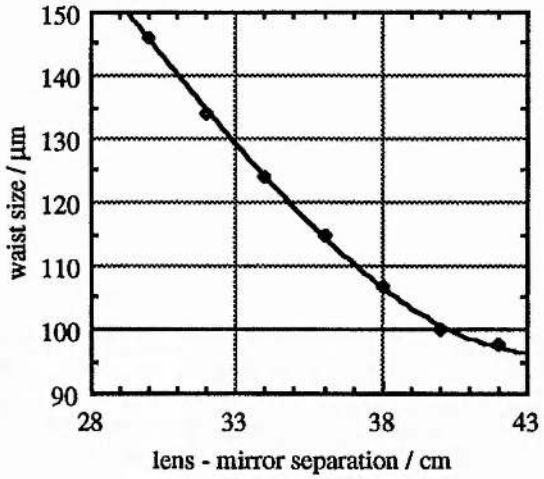

fig.5.4(b) Effect of mirror position on waist size for 20 mm mirrors

The graphs are calculated for a pump focused to a 100 µm spot without the mirror present. For pump spots of 200 µm and greater, if the mirror were positioned near the focus as would be required for the OPO cavity, a waist is prevented from being formed by the divergence of the mirror. The size and position of the focus that would occur without the mirror present are shown by the horizontal lines. It can be seen clearly that despite the concave-convex design the size and position of the pump focus is still strongly dependent on the mirror position. The fact that the 20 mm mirrors still show strong sensitivity of placement is thought to be the main reason why operation with these mirrors was not obtained successfully, as will be discussed later.

5.5 KTP crystals

As mentioned above, the first crystal obtained was a 10x4x4 mm flux grown crystal, purchased from Photox Optical systems. This crystal was damaged at an intensity less than the damage threshold specified by the manufacturer. A replacement crystal was therefore required. The threshold modelling described in chapter 2 indicated that with the 2 mJ expected from a new laser that was to be constructed, a singly resonant device could be pumped above threshold if a longer crystal was obtained. A singly resonant device, as discussed previously, would have superior amplitude and frequency properties as compared to a doubly resonant device. If it was found that the singly resonant threshold was too high, then doubly resonant operation would be obtainable as a back up. However, we were confident that a SRO could be constructed with the zero-power mirrors and longer crystal. A 20x4x4 mm (axbxc) flux grown KTP crystal was obtained from Philips Components of Saugerties, NY. The faces of the crystal were dual-band AR coated at the centre wavelengths of 1.6 and 3.2 µm. Again a flux grown crystal was obtained in preference to the higher damage threshold hydrothermally grown material due to the considerable price difference between the two.

Early experiments with this crystal showed a considerable pump reflection from the crystal faces. This was measured to be approximately 34 % per face. This reflection arose due to the coating being only specified as AR for 1.6 and 3.2 μm. This coating was specified in order to keep the OPO cavity losses to a minimum for both singly resonant operation, signal or idler resonated, or doubly resonant. Philips offered to re-coat the crystal, for free, with a triple-band AR coating. However, as well as the time delay that would have been incurred, the additional layers in the coating would probably reduce the damage threshold of the coating. As will be discussed shortly, damage to the AR coating was the limiting factor on how much power could be input. At this point operation of the OPO had already been achieved and it was therefore decided to proceed with the present coating and withstand the pump loss. With hindsight the optimum coating would be one which was AR at pump and signal, loss at the idler being less important as it was the non-resonant wave. Use of only a dual-band coating would keep the damage threshold as high as possible.

5.6 Experimental set-up and measurements

This section describes the experimental set up that was used to successfully obtain parametric oscillation with the 20 mm KTP crystal. Firstly the pump lasers used, which were described in detail in chapter 4, are described, followed by the OPO configuration. Next the experimental method and a description of the measurements made. The results obtained with respect to threshold, efficiency, output profile and spectral properties are given and discussed in the following sections.

5.6.1 Pump lasers

In all, three different pump lasers were used in the experiments described here. The two variations of the end pumped Nd:YLF laser described in chapter 4 were both used, as was a diode-pumped, side-pumped Nd:YAG laser which was available in the laboratory. The higher powered YAG laser was used to see if the power levels could be immediately scaled.

The side-pumped Nd:YAG laser that was used was based on a 20 mm long by 3 mm diameter Nd:YAG rod (1.1 % doping) which was pumped by six diode laser bars (SDL 3230-TA) which were arranged symmetrically around the rod in three pairs. An earlier version of this laser that was pumped by only three diodes was described in detail elsewhere [2]. The use of six pump diodes resulted in a pump energy of 144 mJ in a 200 μs pulse. This gain medium was situated in a concave-convex resonator (100 cm convex, 75 cm concave) which used HR mirrors and polarisation output coupling. Electro-optic Q-switching of this laser is achieved with a KD*P Pockels cell, producing 10 mJ in around 8 ns (FWHM). The output from this laser is a circular TEM_{00} beam.

For ease of notation, from here on the Nd:YLF laser which had its anamorphic expansion provided by the cylindrical telescope, and therefore produced a circular output beam, will be referred to as YLF 1. Correspondingly, the laser in which a prism pair was used for the expansion will be referred to as YLF 2.

Different pump spot sizes were used to see the effect this had on threshold and conversion efficiency. These were measured in the case of the circular pump beam of YLF 1, by measuring the fractional transmission through a 200 μm pinhole. For the elliptical, astigmatic beam from YLF 2, spot sizes were obtained by a quadratic fit to 5 or 6 spot sizes measured with a pinholed (12 μm) photodiode. This allowed determination of pump waist size, position and M^2. With YLF 1, pump spot sizes of 230 and 210 μm were used with the 100 mm and 500 mm mirrors respectively. YLF 2 was focused to a spot size of 160 μm in one plane and 180 μm in the other, with small (~ 5 mm) astigmatism. Both 100 and 500 mm mirror OPO cavities were used with this pump focusing. In addition the beam from YLF 2 was also focused to the effect that one plane had a waist of 225 μm and the other had 185 μm, again with only small astigmatism . The effect that these different pump spot sizes and astigmatism had on the threshold and efficiency will be discussed in conjunction with the experimental results.

5.6.2 OPO configuration

In these experiments, the OPO consisted of the 20 mm KTP crystal previously described positioned centrally within a cavity formed by two of the concave-convex zero-power mirrors. Different radii of curvature mirrors were used in order to investigate the effect of signal confocal parameter on the interaction. The mirrors were held in brass holders which were inserted in the gimbal mounts with xyz translation, as mentioned in section 5.3. Unlike the plano-concave mirrors, in the case of the zero-power mirrors it was no longer necessary for the pump beam to go through the centre of the mirror on account of their near concentric design. This meant that the xyz translation of the mount was no longer strictly required. Future work would benefit from replacing these mounts with precision gimbal mounts with differential screws to allow for more accurate cavity alignment. Again the crystal was held in the perspex mount by the spring-loaded plunger.

The mirrors were positioned approximately 1-2 mm from the crystal faces in order to keep the cavity length down, and so maximise the number of round trips that the signal would experience during the pump pulse. For the 100 mm mirrors this results in a signal cold cavity waist of ~ 110 μm, with the equivalent waist for the 500 mm mirrors ~ 170 μm. This assumes that with NCPM the mode will be circular, and the crystal refractive index at signal is taken as 1.74.

Allowing for the gain guiding effect of a gaussian profile non-linear gain, as described

in chapter 2, the signal waists expected for 100 mm mirrors and pump spots of 230 and 170 μm were 97 and 87 μm, respectively, and for 500 mm mirrors and pump spots of 210 and 170 μm were 108 and 94 μm, respectively. Note that for an elliptical pump waist, an average of the two dimensions is taken as this is seen to be non-critical.

As the original intention was to use a Nd:YAG laser as the pump source most of the mirror coatings were specified with respect to a pump wavelength of 1.064 μm. The difference between this wavelength and the 1.047 μm output from the YLF lasers is negligible as far as the coatings employed here are concerned. The rear surfaces of the mirrors were therefore AR coated at the pump wavelengths and high transmitting at both signal and idler wavelengths. Inner surfaces were coated to be highly transmitting at pump and idler wavelengths with a variety of reflectivities at the signal. In all, signal reflectivities available were 98, 91 and 82 %, allowing the use of signal output couplings varying from 4 to 27 %. Although the coatings for these mirrors were specified to be high transmitting at the idler wavelengths so that true single resonance could be obtained, the requirement on the coating to perform at three different wavelengths is a difficult task and resulted in non-zero idler reflectivities. These were always small enough that threshold would not be noticeably affected, but were large enough in that the spectral properties of the oscillator were affected. This will be discussed in detail later with regard to the spectral properties.

In addition, mirrors were coated with high reflectivities at the idler wavelength, i.e. centred at 3.2 μm, where one set would allow construction of a DRO, and another would allow a SRO with resonant idler and non-resonant signal. With the success of the SRO with resonant signal, time restrictions meant that these other options were untried. In any case, it was expected that the high idler absorption and resultant low Q of any idler cavities would not be conducive to favourable experimental conditions.

5.6.3 Experiments

The basic experimental set-up that was used in this work is shown schematically in fig. 5.5. Isolation between the pump laser and the OPO was provided by a Faraday rotator (OFR IO-5-YAG) positioned between two calcite polarisers. Isolation was provided for two reasons. Firstly, the work of Smith [3] showed that feedback into the laser can cause instability of the laser output, and hence instability of the OPO. This is perhaps of more relevance to doubly resonant oscillators where a single frequency pump is required. It was found that isolation was required in any case to prevent damage to the pump laser due to on-axis reflections from the OPO. When operating without isolation, the laser polariser was seen to damage due to a reflection from extra-cavity optics. No damage occurred when isolation was employed. The zero-order λ/2 plate combined with the first polariser additionally acted as a variable attenuator. A zero-order wave-plate was required to provide sufficient bandwidth for operation at both 1.047 and

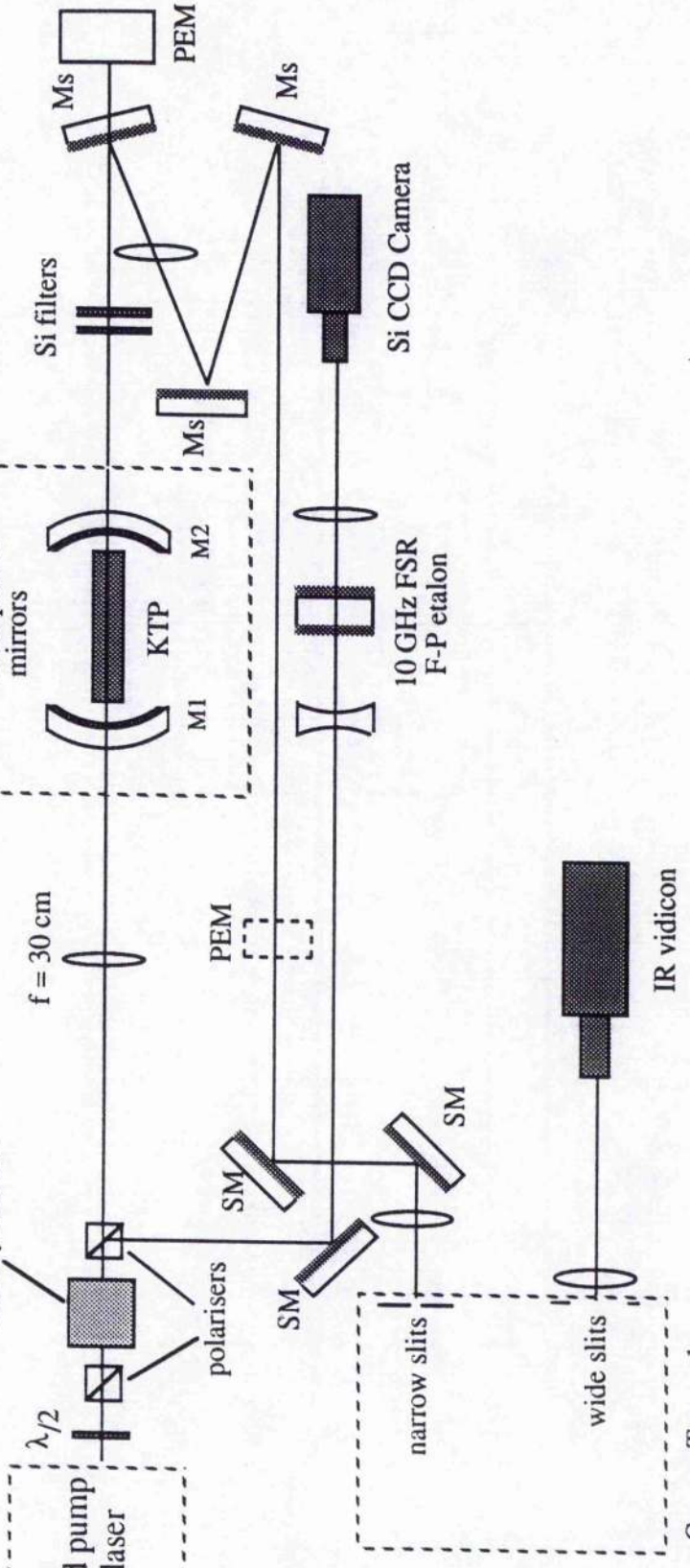

Fig. 5.5 Schematic diagram of basic experimental set-up

1.064 μm.

With the zero-power mirrors, mode matching was achieved with a single 30 cm fused silica lens, AR coated for the pump. A fortunate coincidence was the fact that for the pump spot sizes of interest, this spherical lens produced pump focal spots which, although they were elliptical in the case of the YLF 2 laser, possessed little astigmatism. This is despite the fairly large (~10 cm) astigmatism present in the laser.

All measurements of the OPO output were based on the signal wave. Although the pyroelectric detectors (Molectron J25 and J3 probes) which were used to measure the signal and pump beams were capable of measuring the idler output at 3.3 μm, most of the idler was absorbed in the crystal, the mirror substrates and signal steering mirrors. In addition, no detectors were available for temporal or spatial measurements of the idler.

For signal wave measurements the pump was blocked with two silicon filters, and the signal was tapped off from the remaining beam with signal steering mirrors, Ms. These mirrors were highly reflecting (98 %) at the signal wavelength, and highly transmitting at pump and idler wavelengths. The signal energy was measured directly with the J3 probe. The measurements were then corrected for the measured signal transmission of the pump blocking filters and the collimating lens, and also for the small losses at the signal steering mirrors. The output profile of the signal was measured with a pinholed germanium photodiode in the focal plane of the signal collimating lens. Temporal profiles were measured with a fast germanium photodiode (Germanium Power Devices GM3) which had a bandwidth > 1 GHz. The active area was only 100 μm diameter, therefore tight focusing into the photodiode had to be employed to obtain the fast time response.

The internal conversion to both signal and idler was measured via pump depletion. The pump depletion measurement was made by removing the pump filters and detecting the beam with signal removed from behind the first signal mirror. The transmission of the idler to the detector for these measurements was measured to be only ~ 2 % of the pump due to mirror substrate and crystal absorption, and was therefore not expected to affect the pump depletion measurements significantly.

The output spectrum at signal wavelengths was observed by using a Czerny-Turner 1 m monochromator (Monospec 1000) in conjunction with an IR vidicon (Hamamatsu Beam Finder II, C3283). The wavelength of the monochromator was calibrated with the 780.02 and 794.76 nm lines of Rb in second order. To monitor the pulse to pulse spectral variation the output slits were opened up (~ 4 mm) and imaged onto the IR vidicon with a 2.5 cm lens. The dispersion of the Czerny-Turner monochromator can be expressed as

$$\frac{dx}{d\lambda} = \frac{nF\cos(\phi/2)}{d\cos(\phi-\theta)} \qquad (5.6.3.1)$$

where x is the spatial co-ordinate at the output slit, n is the diffraction order, F is the focal length (1 m), ϕ is the blaze angle (18.43° for a 600 lines/mm grating blazed for 1 μm), d is the grating spacing, and θ is the rotation angle of the grating. This gives the dispersion at the output slit. To get the magnification of this dispersion at the vidicon, the separation of the Na D-lines was measured in first and second order. This measurement allowed the vidicon output to be calibrated in terms of the dispersion for 1.54 μm. Thus the spectrum of the OPO signal could be monitored, while accurately knowing the width of any features in the spectrum. The output from the vidicon was input to an in-house frame grabber, with the images stored in a BBC Archimedes computer. Thus the output spectrum, in terms of the time averaged spectrum throughout an entire pulse, could be examined on a pulse to pulse basis. No information, however, was obtained from this about the dynamics of any mode jumps of the signal throughout an individual pulse.

The spectral content of the pump laser was monitored by passing part of the beam through a 10 GHz etalon and monitoring the fringes with a Si CCD camera (EEV photon). This allowed for any correlation between the pump mode spectrum and the signal spectrum to be identified.

5.7 Results for threshold, efficiency and transverse modes

Due to its non-linear nature, an OPO has a large number of interesting properties. To describe the operation properly requires characterisation of all these properties. This section attempts to do this, with discussions of the results and comparison with theory where applicable. A brief note on the cause of some damage to the crystal coatings is presented prior to the results. The threshold and efficiency properties of the device are then presented. The output profiles are discussed along with some proposals for the origins of an annular ring structure that was also observed.

5.7.1 Optical damage

Early attempts to achieve operation with zero-power mirror pairs with 98 % reflection at the signal (singly resonant for signal), either 100 or 500 mm radii of curvature, did produce above threshold operation. However, these high Q cavities resulted in damage to the crystal coatings. Damage was generally noticed while adjusting the cavity such that shortly after signal output started, a small, but audible, click would be heard accompanied by a decrease or cessation of signal output. This, accompanied by the fact that no damage was evidenced with only the pump incident, showed that the damage to the coating was being caused by the resonant signal. Even with moderate Q values the

signal intracavity flux can exceed that of the pump when pumping above threshold [4]. At the expense of a small increase in threshold it was therefore necessary to move to higher output couplings and lower cavity Qs for the resonant signal.

After the isolator was inserted, the pump energy that was available was ~ 1.8 mJ. With the exception of operation with 11 % output coupling, it was possible to use all of this available pump power without damage to the crystal coating once the OPO was aligned. Damage occurred occasionally during alignment. At no point was any bulk damage observed, and it was noted that damage to the crystal coating was the limiting factor to the maximum pump power that could be used. This reinforces the point made earlier that triple-band AR coating of the crystal may not have been of benefit if it substantially reduced the coating damage threshold.

5.7.2 OPO threshold

As the pump lasers used in this work were of low power, it was necessary throughout to try and minimise thresholds. The designs employed were therefore inspired by the threshold modelling that was described in chapter 2. That work is responsible for the success to be described here of obtaining low threshold operation of the KTP OPO.

The measured signal output energies v pump energies are shown graphically in figs. 5.6 and 5.7, and the results are summarised in table 5.1. Note that the parasitic loss, as estimated from a comparison between measured signal energy and pump depletion, was found to vary for different sets of measurements. More is said on this with regard to thresholds and slope efficiencies.

The measurements displayed in these graphs were all taken under NCPM with operation normal to the crystal faces. The graphs demonstrate the effect that the choice of pump spot size, resonated wave spot size and output coupling have on threshold and efficiency. A point of immediate note is that the configuration which exhibits the lowest threshold doesn't necessarily result in the highest output energy. This is due to the way in which the pump overlaps with the generated signal and idler waves, and will be explored in detail in the next section which discusses efficiency, both absolute and slope efficiency.

Thresholds for pump light incident on the crystal at the 0.5 mJ level have been achieved, which, allowing for the 34 % pump reflection from the input crystal face, can be considered sub 0.5 mJ. The measured thresholds for 20 % output coupling are compared with the calculated values from the BB model and the Guha model for mirrors with radii of curvature of 100 and 500 mm in figs.5.8 and 5.9 respectively.

The measured threshold is deemed to be the pump energy which gave 20 μJ output at signal. This is the same criterion that was used in the modelling. This value was chosen

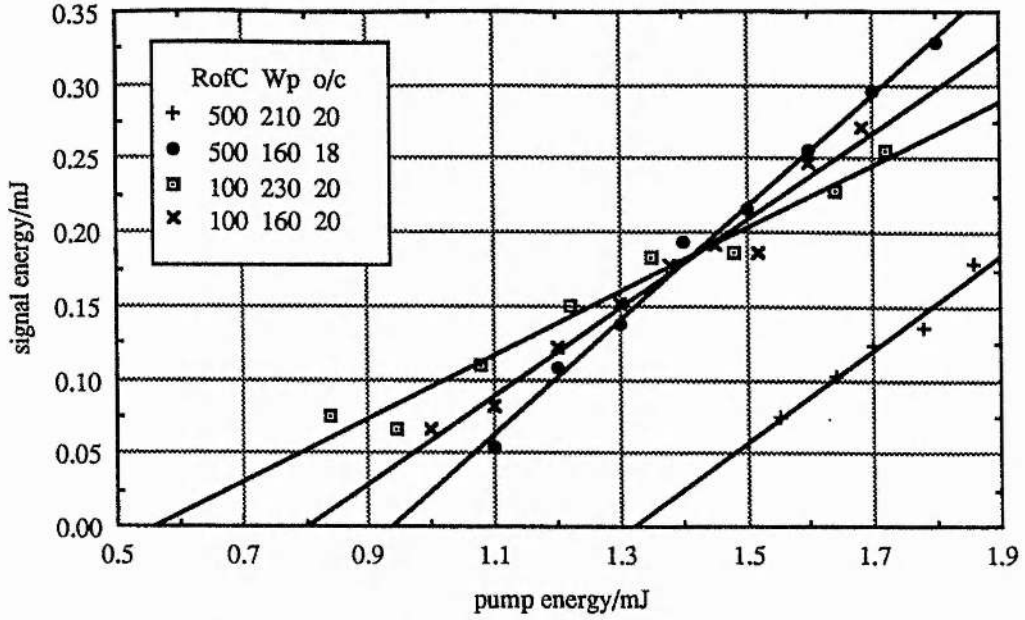

fig. 5.6 Signal output energy v pump energy for different pump spot sizes and 18-20 % output coupling. Units are mm for RofC, μm for Wp and percentage for output coupling

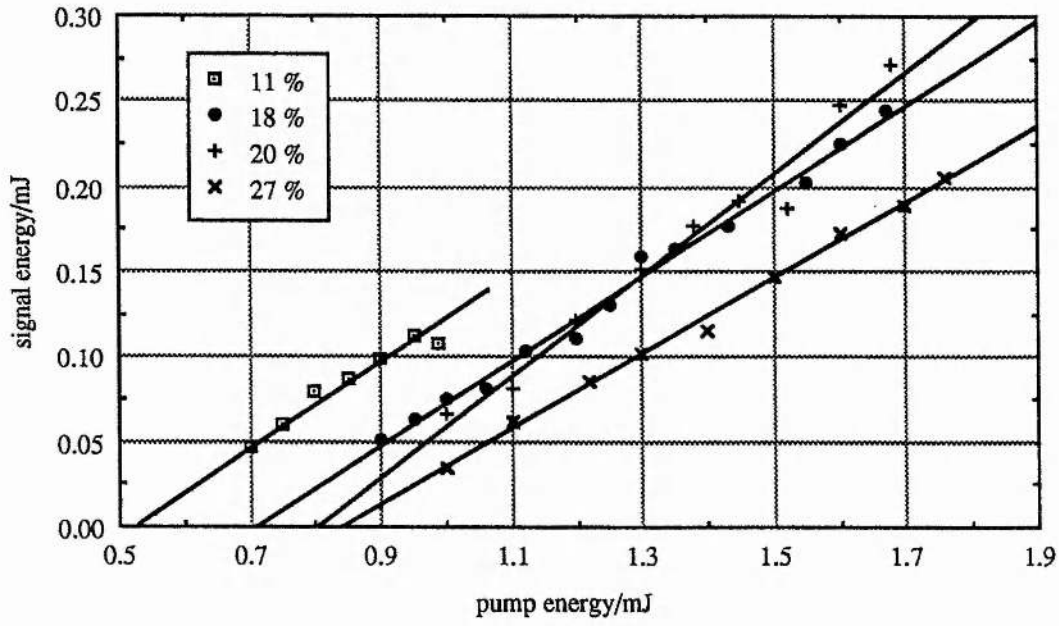

fig. 5.7 Signal output energy v pump energy for a pump focus of 160/180 μm, 100 mm RofC mirrors and different output couplings

as the output of the OPO is unstable when just above threshold, and an output of 20 μJ roughly corresponded to the level at which an output at the signal would be observed for every pump pulse. Fig. 5.10 shows the variation of threshold with output coupling for the case of 100 mm mirrors and an elliptical pump spot of dimensions 160 and 180 μm. It is seen that the calculated thresholds show reasonable agreement with the measured thresholds, and that the values predicted by the BB model are lower than those predicted by the Guha model.

pump laser	mirror radius of curvature / mm	pump spot size / μm	output coupling / %	threshold energy / mJ	slope efficiency / %	maximum pump depletion / %	maximum pump energy / mJ	maximum signal energy / mJ
Nd:YLF	100	160/180	11(2+9)	0.58	31	45	1.0	0.14
"	"	160/180	20 (2+18)	0.87	30	40	1.68	0.27
"	"	160/180	18 (2x9)	0.79	25	43	1.67	0.25
"	"	160/180	27(9+18)	0.93	22	35	1.76	0.21
"	"	185/225	20(2+18)	0.87	17.7	26	1.79	0.18
"	"	230	20(2+18)	0.7	22.8	31	1.72	0.26
"	500	160/180	18(2x9)	0.88	39	49	1.76	0.35
"	"	210	20(2+18)	1.38	32	18	1.86	0.18
Nd:YAG	100	240	27(9+18)				2.65	0.7

Table 5.1 Summary of measured thresholds, slope efficiencies and maximum conversion efficiencies

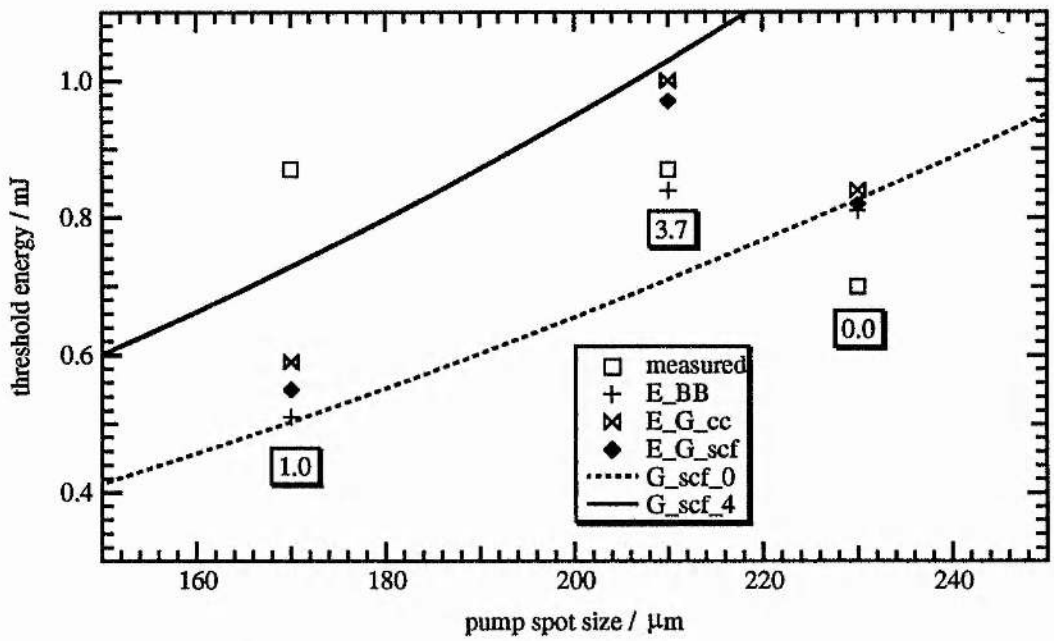

fig. 5.8 Measured and calculated threshold energies for the case of 100 mm mirrors and 20 % output coupling. In this graph, and also the two following graphs, E_BB is the value calculated using the BB theory, E_G_cc and E_G_scf are the values obtained using the Guha model with the cold cavity and self-consistent-field spot sizes respectively. The two curves are calculated from the Guha model, assuming a scf spot, with a parasitic loss of either 0 or 4 % per crystal face. It should also be noted in the following graphs that the parasitic loss (per crystal face) varies from point to point as indicated.

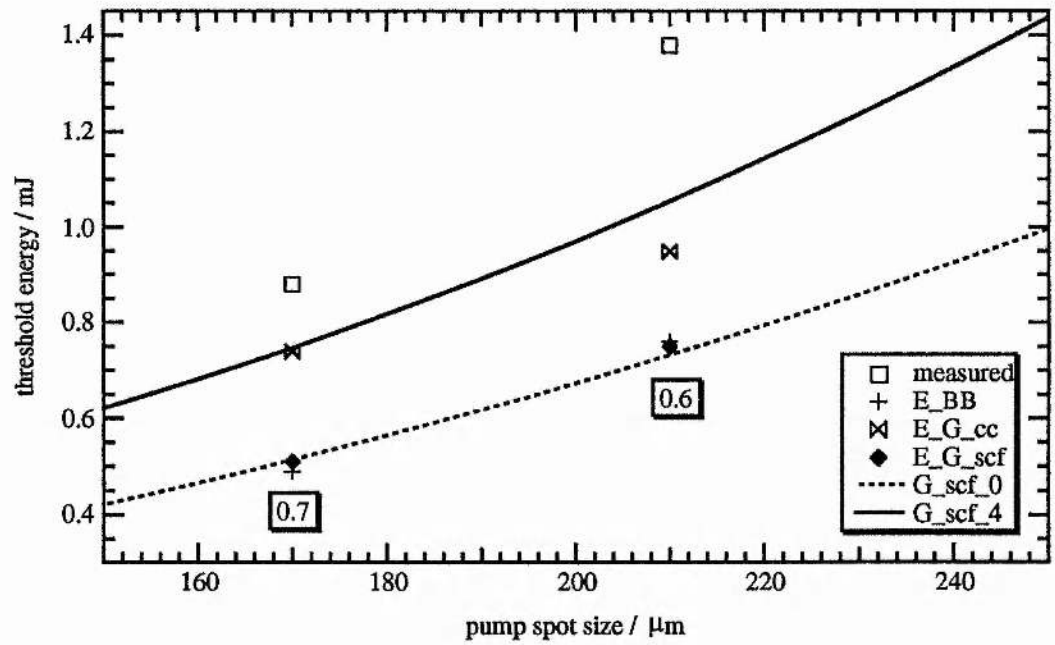

fig. 5.9 Measured and calculated threshold energies for the case of 500 mm mirrors and 18 (w_p = 160/180 µm) or 20 (w_p = 210 µm) % output coupling

The points which refer to elliptical pump spots have been plotted at the spot size which corresponds to the average of the two orthogonal dimensions. We find that for the spot sizes considered here, the difference between the expected threshold for an elliptical

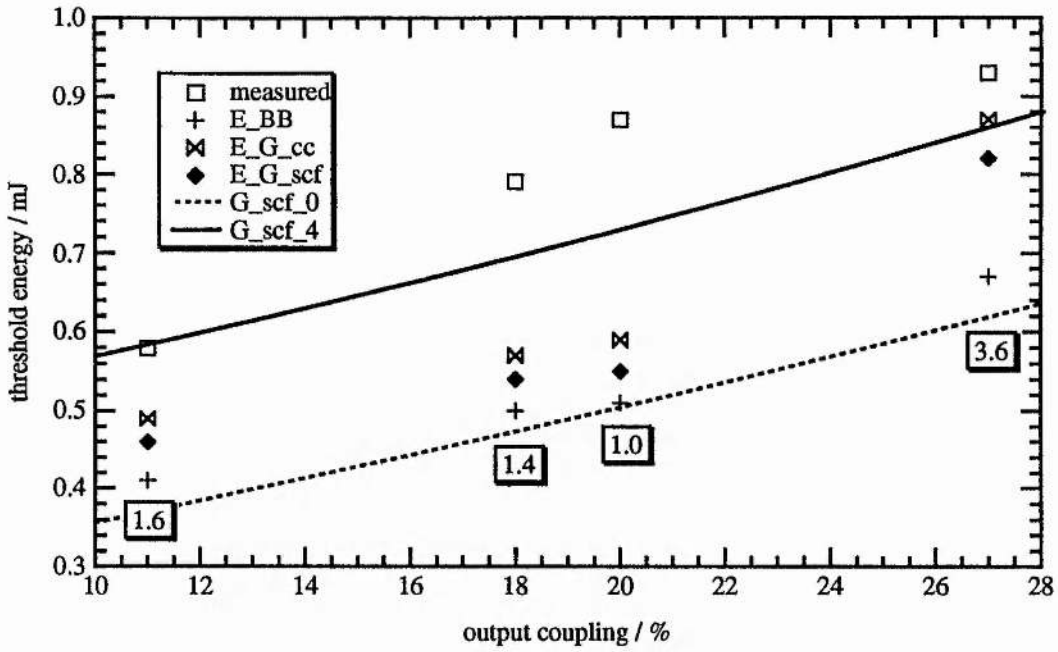

fig. 5.10 Measured and calculated threshold energies as a function of output coupling for the case of 100 mm mirrors and160/180 μm pump spot

beam and that for a circular beam with the average spot size is less than 1 %. This has not been proven rigorously, but comes from multiplying the gains that would be obtained for a circular beam with a spot size corresponding to each orthogonal dimension of the elliptical beam, and then taking the square root. The effects of astigmatism are shown by the model to be insignificant in relation to the measurement accuracy of these spot sizes. The ellipticity is expected to have more of an effect that the astigmatism as the threshold was seen in chapter 2 to be fairly dependent on spot sizes. However, the ellipticity in these measurements was never more than 10 % and hence would only be expected to have a minor effect.

For most cases, the measured threshold is higher than that expected from the calculations. This may be partly attributable to the choice of d_{32}= 3.7 pm/V rather than the value proposed by Eckardt et al [5] of 3.3 pm/V. This would give closer agreement for the smaller pump spot sizes. On the other hand, the fact that the thresholds calculated with the BB model are smaller than measured is not surprising. As mentioned previously, that model assumes that the pump is collimated and therefore the curvature of the wavefronts exhibited here for tight focusing of the waves will reduce the gain from that expected for a plane wave. In the case of the Guha analysis, it is assumed that the resonated wave can be represented by the cold cavity mode, and this may not be completely valid due to gain guiding effects. In addition both the above models assume signal and idler wave amplitudes which are approximately constant in a single pass. There will not be substantial pump depletion at threshold, but if the cavity losses are significant, including build up times, then the gain required may make the low gain assumption of constant signal and idler not strictly valid. The two cases where

the measured threshold is less than that calculated, i.e. 100 mm radius of curvature mirrors and either a 230 or 185/225 μm pump spot, may be attributable to a small double passing of the pump due to the 34 % pump reflection from the back face. This reflection would only interact if the pump was completely normal to the crystal faces, which may not have been the case in the other measurements.

The measured points do not show up the trends that were predicted in chapter 2 for the variation of individual parameters, the parameters investigated here being pump and signal spot size, and output coupling. This is mainly attributed to the fact that the intracavity losses, as estimated by a comparison between measured signal output energy and that expected from measured pump depletions, are seen to vary for different sets of measurements. This is attributed to damage to the crystal coating caused by the resonant signal, and explains why the losses were found to be higher for measurements that were carried out later. The calculated losses are included in the calculations of thresholds at the individual points and the curves show the effect that would be expected for different losses.

Due to a number of experimental uncertainties, e.g. the effect of the pump back reflection from the rear crystal face, the loss per face at the signal, the differences between measured and calculated thresholds do not allow a direct comparison between the BB model and the model developed here. In addition, uncertainties in the choice of non-linear coefficients including whether or not to apply Miller's delta can have an effect on threshold almost as large as the difference between observed and calculated thresholds. What can be said though, is that the model developed here based on adding time dependence to the Guha analysis is expected to be more accurate than the BB model as it makes less simplifying assumptions. In particular, the BB model is not expected to give accurate predictions when the pump and/or signal is focused tightly as this model assumes plane, gaussian wavefronts.

Despite the differences between the measured and calculated threshold energies, it is seen that low threshold operation, sub 0.5 mJ, has been achieved. The predicted threshold values agree within 50 % of those measured, and it is seen that the values predicted by the model developed here, which introduces time dependence to the Guha analysis, are higher and therefore closer to the experimental values than those of the established Brosnan and Byer model.

5.7.3 Efficiency

Despite the dependence of gain on pump intensity, high conversion efficiencies have been demonstrated here with relatively low powers due to the optimisation of the interaction geometry. Referring to table 5.1 it is seen that internal conversion efficiencies (pump depletion measurements) approached 50 %, and slope efficiencies of

signal output to pump input approached 40 %. Allowing for the pump reflection of 34 % would result in a best slope efficiency for signal output only of nearly 60 %, which is close to the theoretical maximum of 68 % determined by the Manley-Rowe relation [6]. The maximum conversion to signal for the case of 500 mm radius of curvature mirrors, 18 % output coupling and an elliptical pump spot size of dimensions 160/180 μm was 20 %, which, again allowing for the pump reflection loss rises to 30 %.

Internal conversion efficiencies

Expected pump depletions for pumping with gaussian beams was investigated by Bjorkholm [7]. Despite the fact that that work was specifically intended for the case of pulsed operation, no time integration was performed. The resulting calculations predict the expected pump power depletions in steady state and do not allow for build-up time effects. In addition, the analysis was restricted to the case where a plane-plane OPO cavity was used, with the pump beam not mode matched to a cavity mode, and with the expectation that steady state modes would not have been established. With these restrictions, it would not be expected that the theoretical results are directly applicable here. However, what can be seen is that the measured pump energy depletions approach the calculations (energy depletions can be obtained from the results for power by multiplying by the ratio of signal to pump pulse widths, which is approximately 1-1/N [8]) if allowance is made for both the *pulsed* threshold and the effect of mode coupling. This is seen in fig. 5.11 for the case of 500 mm RofC mirrors, 18 % output coupling and a 160/180 μm pump spot size.

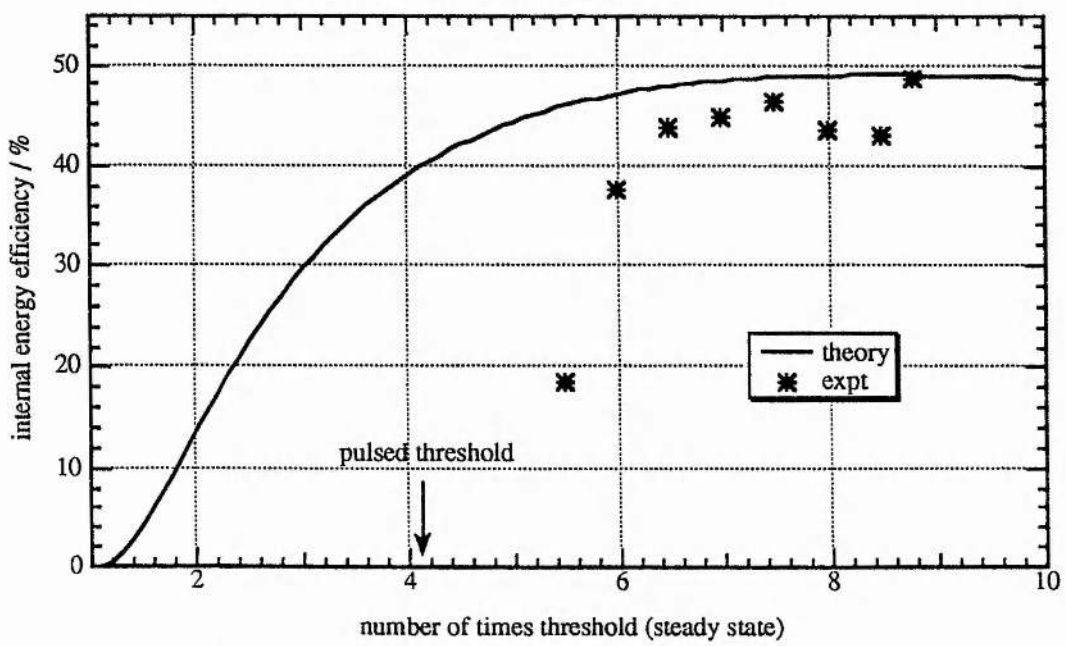

fig. 5.11 The experimental pump depletions for the case of 500m RofC mirrors, 18 % output coupling and a 160/180 μm pump spot size are compared with theoretical pump energy conversion efficiency. The theoretical values have been scaled by 0.8, which is approximately the mode coupling coefficient, and the scaling of pulsed to steady state threshold is calculated as 4.1.

The theoretical curve is calculated from Bjorkholm's analysis, with energy conversion obtained by multiplying by 1-1/N, as mentioned above. The calculated curve has then been scaled by the factor 0.8, which is approximately the value expected for the mode coupling coefficient, on which more will be said shortly. The measured pump depletions have been plotted against number of times steady state threshold, despite the fact that they are measured as number of times pulsed threshold, so a comparison can be made with the theory. (The scaling factor used here of 4.1 is the calculated ratio of pulsed to steady state thresholds, where both were calculated using the Guha analysis, with time dependence included in the pulsed calculation.)

In this way, it is clearly seen that when pumping sufficiently above the pulsed threshold, the pump depletions predicted for steady state operation are approached. It can also be seen that it is important to keep the ratio of pulsed threshold to steady state threshold to a minimum. The reason why pump depletion isn't obtained until pumping many times the steady state threshold is due to the build-up time required before oscillation occurs. If the ratio of pulsed to steady state thresholds is very high, then the build-up time will be so long that pump depletion will not begin until after the peak of the efficiency curve and so no matter what pump power is available the maximum pump depletion will not be achieved. To get a quantitative comparison between theory and experiment would require temporal and spatial integration of the exact equations of parametric oscillation [4], which due to time restrictions is beyond the scope of this work.

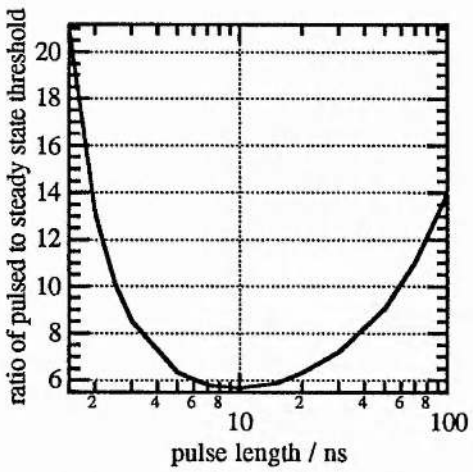

fig. 5.12 Effect of pulse duration on ratio of pulsed to steady state thresholds, with the same parameters assumed as in ch.2, section 2.8

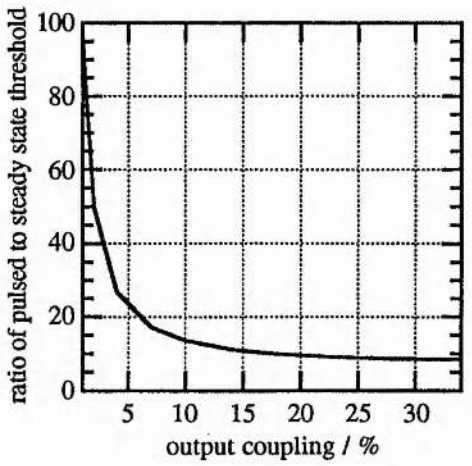

fig. 5.13 Effect of output coupling on ratio of pulsed to steady state thresholds, again with same parameters as in section 2.8

The two main parameters that would be expected to affect the ratio of pulsed to steady state thresholds, and hence the attainable maximum pump depletion, are pulse duration and output coupling. The effect of pulse duration on the ratio of pulsed to steady state thresholds is shown in fig. 5.12, where the other parameters are as given in section 2.8

with regard to threshold modelling. The dependence here follows the dependence of the pulsed threshold on pulse duration. Fig. 5.13 shows that the ratio can be minimised at high output coupling. This dependence comes about by the raising of the steady state threshold with output coupling, and would therefore require a large pump power to pump many times threshold.

The pump depletion can be observed in a meaningful way by monitoring the temporal profile of the pump when depleted, and comparing it to the undepleted pump. This is shown in fig.5.14, which exhibits 30 % pump depletion. The resolution of the pulse measurements was not sufficient to allow investigation of the duration of the signal pulses for different levels of pumping. However the build-up time before threshold is reached can be clearly seen, as can the fact that the generated signal pulse is shorter in duration than the pump. When pumping far enough above threshold, the build-up time will be reduced and the duration of the signal (and idler) pulse(s) will approach that of the pump.

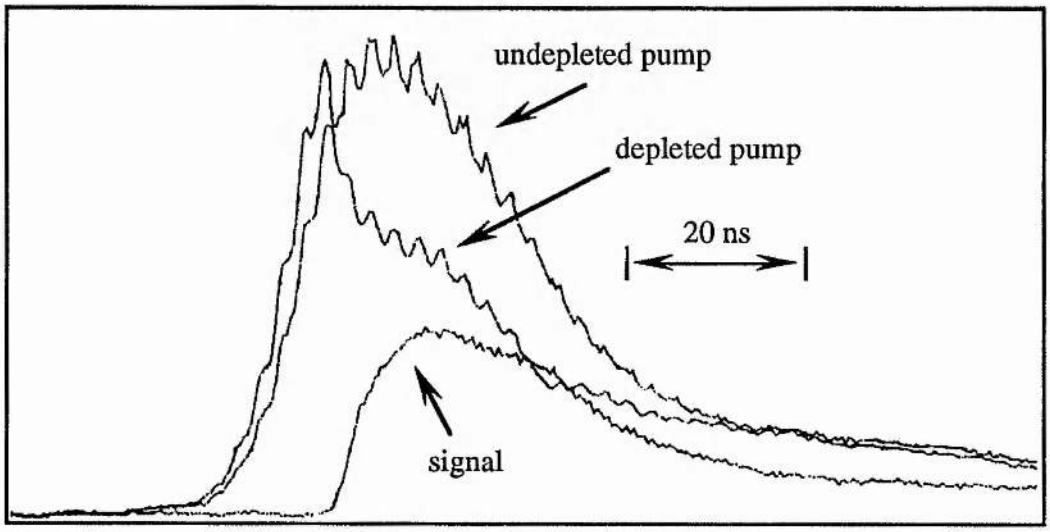

fig. 5.14 Temporal profile for 30 % pump depletion

Slope efficiency

It is clearly seen from figs. 5.6 and 5.7 that the signal output increases linearly with pump energy. This is perhaps not intuitive considering the non-linear relation of pump depletion with pump power [7]. However, as is shown here, a linear relation between signal energy and pump energy is consistent with observed pump depletions. This relationship can be written as

$$E_s = \eta\left(E_p - E_{pt}\right) \qquad (5.7.3.1)$$

where E_s is the signal energy, η is the slope efficiency, E_p is the pump energy and E_{pt} is the threshold pump energy. In practice, above a certain energy back-conversion will cause the behaviour to deviate from linear, but this was not observed in the present

experiments.

The magnitude of slope efficiency is due to a number of factors, namely the mode coupling coefficient, the fraction of the total energy produced at the signal wavelength (0.68), the pump transmission (0.66), and the internal losses. The mode coupling coefficient is similar to the factor g_s calculated in the BB threshold analysis, but for efficiency calculations an overlap integral between the pump and signal must also be performed. The internal losses are calculated by comparing the measured output, adjusted for losses external to the cavity, with that expected from the pump depletion measurements. Losses are seen to be larger for experiments that were carried out later, the losses being attributable to coating damage. The measured and calculated slope efficiencies are given in table 5.2.

pump spot size / μm	mirror radii of curv./ mm	calculated internal loss / %	output coupling / %	measured slope eff.	calculated cold cavity slope eff.	calculated s.c.f. slope efficiency
230	100	0	20	22.8	26.5	22.4
210	500	2.5	20	32	32.1	25.3
225/185	100	13.9	20	17.7	17.5	14.8
160/180	500	2.9	18	39	28.6	26.9
160/180	100	6.2	11	31	22.2	18.6
160/180	100	5.3	18	25	26.9	22.5
160/180	100	4.1	20	30	28.9	24.2
160/180	100	13.5	27	22	23.2	19.4

table 5.2 Comparison of measured and calculated slope efficiencies, where s.c.f stands for self-consistent field, as this is the spot size calculated allowing for gain guiding.

Reasonable agreement is seen, with differences accountable to actual signal spot sizes being between those calculated for cold cavity and gain guided modes, and estimates of intracavity losses from pump depletion measurements being affected slightly by the remaining idler field, as mentioned previously.

The slope efficiency, η, can therefore be written as

$$\eta = g_s T_p \left(\frac{T}{T+L}\right)\left(\frac{\omega_s}{\omega_p}\right) \qquad (5.7.3.2)$$

where g_s is the mode coupling coefficient, Tp is the pump transmission at the input crystal face, T is the output coupling, L is the parasitic loss and $\omega_{s,p}$ are the signal and pump frequencies. We can write the output signal energy in terms of the pump

pump frequencies. We can write the output signal energy in terms of the pump depletion δE_p as

$$E_s = \left(\frac{T}{T+L}\right)\left(\frac{\omega_s}{\omega_p}\right)\delta E_p \qquad (5.7.3.3)$$

Using the form of E_s from (5.7.3.1) allows the fractional pump depletion to be written as

$$\frac{\delta E_p}{E_p} = g_s\left(1-\frac{1}{N}\right) \qquad (5.7.3.4)$$

where N is the number of times above threshold of the pumping energy. It can be seen from this that the maximum pump energy depletion is equivalent to the mode coupling coefficient. The factor $(1-1/N)$ is simply the ratio of signal to pump pulsewidths, as mentioned earlier.

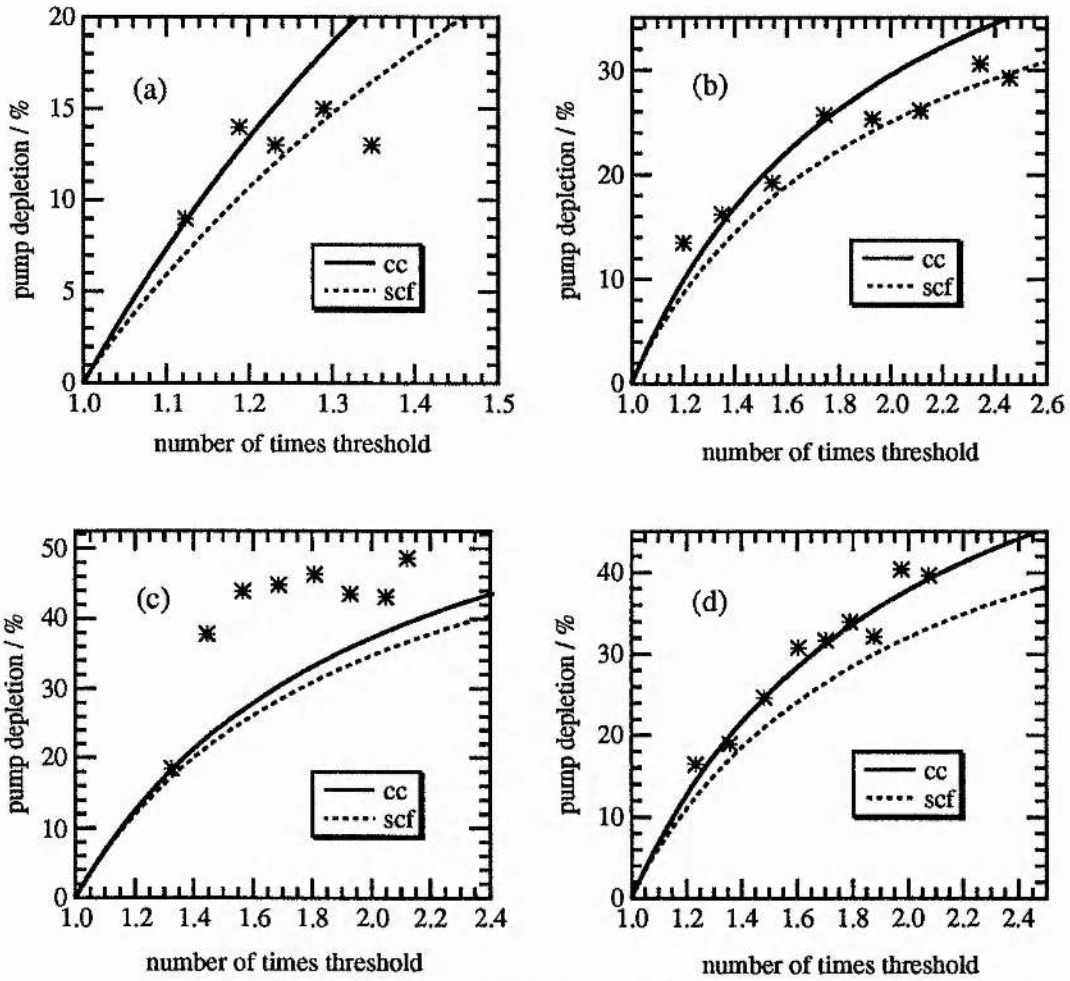

figs. 5.15(a)-(d) Comparison of measured pump depletions with the curves calculated using (5.7.3.4) and either the cold cavity (upper curve) or gain guided (lower curve) spot sizes. (a) 210 μm pump spot size, 500 mm RofC mirrors, (b) 230 μm pump spot size, 100 mm RofC mirrors, (c) 160/180 μm pump spot size, 500 mm RofC mirrors, (d) 160/180 μm pump spot size, 100 mm RofC mirrors.

The agreement between this empirically derived relation and the measured pump depletions is shown in figs. 5.15(a)-(d). The disparity in the case of 500 mm RofC mirrors and a 160/180 μm pump spot can be attributed to the fact that the maximum mode coupling coefficient occurs for a signal waist between those of the cold cavity and gain guided cases.

5.7.4 Transverse mode

For each case of mirror radius of curvature and pump spot size, the signal beam was profiled with a pinholed (12 μm) photodiode. This measurement was taken in the back focal plane of a 30 or 40 cm lens so that the far field profile of the beam was being sampled. In all cases a single lobed transverse output was obtained. However, as only a far field measurement was taken, no quantitative information can be obtained about how close to diffraction limited the output was. Generally, however, the profiles obtained give a reasonable fit to a gaussian for the larger pump spot sizes, and an excellent fit to gaussian for the smaller pump spot sizes.

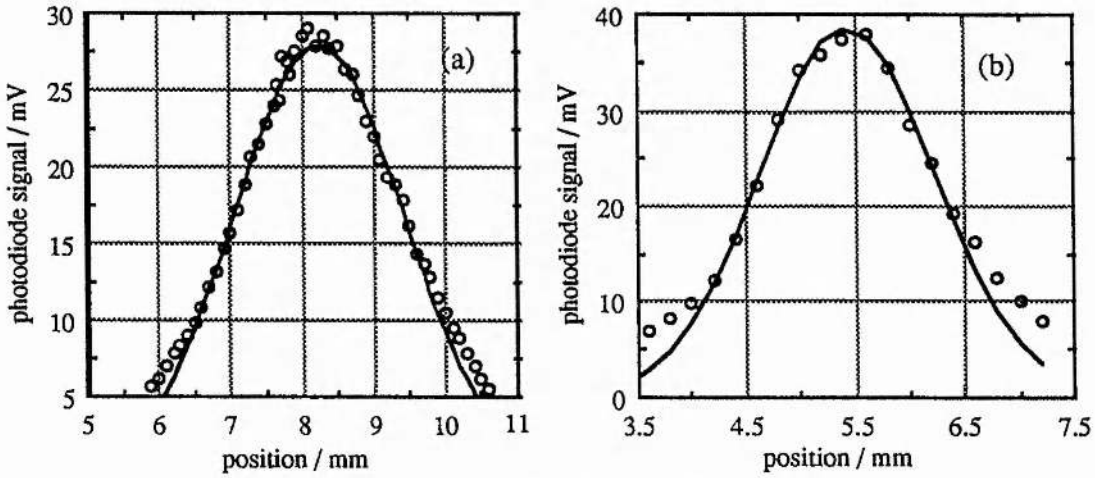

fig. 5.16 (a) horizontal and (b) vertical profiles of signal beam in far field for the case of a 230 μm pump spot and 100 mm radius of curvature mirrors

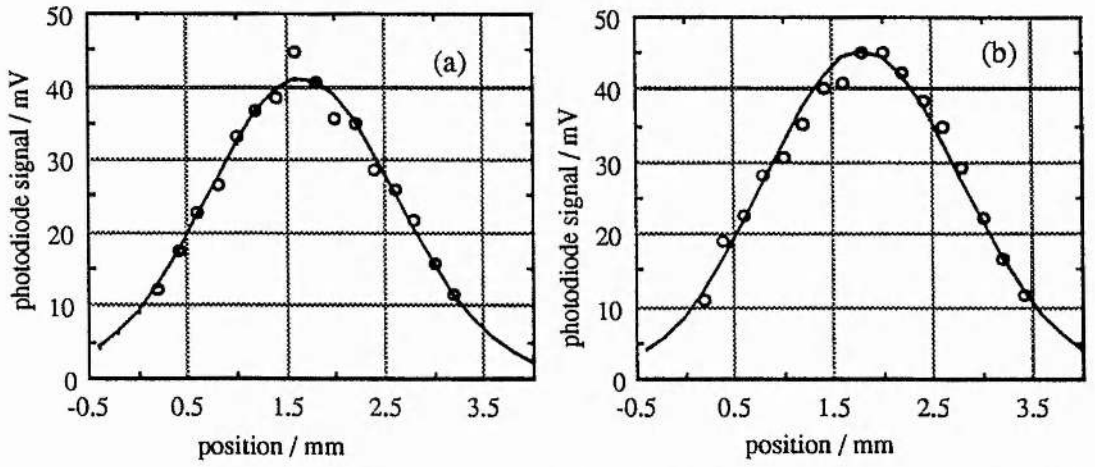

fig. 5.17 (a) horizontal and (b) vertical profiles of signal beam in far filed for the case of a 160/180 μm pump spot size and 100 mm radius of curvature mirrors.

Examples of profiles are shown in figs. 5.16(a) and (b), and 5.17(a) and (b). The small wings observed for the case of 100 mm radius of curvature mirrors and a 230 μm pump spot indicate that the output is not quite diffraction limited. This is likely due to a small amount of higher order mode which can oscillate in this case as the TEM_{00} mode radius of the signal is less than half that of the pump The fit to gaussian in the case of 160/180 μm pump spot indicate that the output is likely diffraction limited. Estimates of cavity spot sizes from these measurements produce signal waists which are between those calculated for the cold cavity and gain guided cases, as would be expected.

Annular ring

The above profiles were obtained despite the appearance, on occasion, of an annular ring structure. That is, under certain conditions, which were not identified, the signal output seemed to contain what could only be described as an angular 'exclusion zone', within which no output would be obtained. The appearance of this ring structure in the output was not completely random, but seemed to occur during some set-ups but not others. In addition, the ring structure appeared one evening despite the fact that it was not evident in the afternoon and no adjustments had been made. This ring resembles what might be expected under non-collinear phase matching, but no reason could be found which would explain why non-collinear phase matching would be favoured over collinear phase matching. There may be some connection between the observed phenomenon here and the prediction of a similar ring structure for difference frequency mixing in gases [9], which is due to the phasing of the waves involved. At this point in time, the cause of the ring structure observed in these experiments is unexplained.

If the cavity mode were aligned collinear to the pump beam then the output would be a ring. However, TEM_{00} operation could still be achieved by tilting the OPO resonator axis such that the resonant mode occurred outside the 'exclusion zone'. This is demonstrated by figs. 5.18 (a) - (c) which show the profile obtained as this operation is carried out. It is seen clearly that a circular spot is in fact obtained despite starting with the ring structure. Further investigation of this phenomenon is required. There was insufficient time for a full investigation in this work.

5.8 Spectral properties

In this section the observed spectral properties are described. The tuning and gain bandwidth are mainly dependent on the geometry of the non-linear crystal, and the way in which the waves interact. These properties are described in the next section. The detailed spectral structure within the gain bandwidth is determined by the optical cavity, and this will be discussed in a following section.

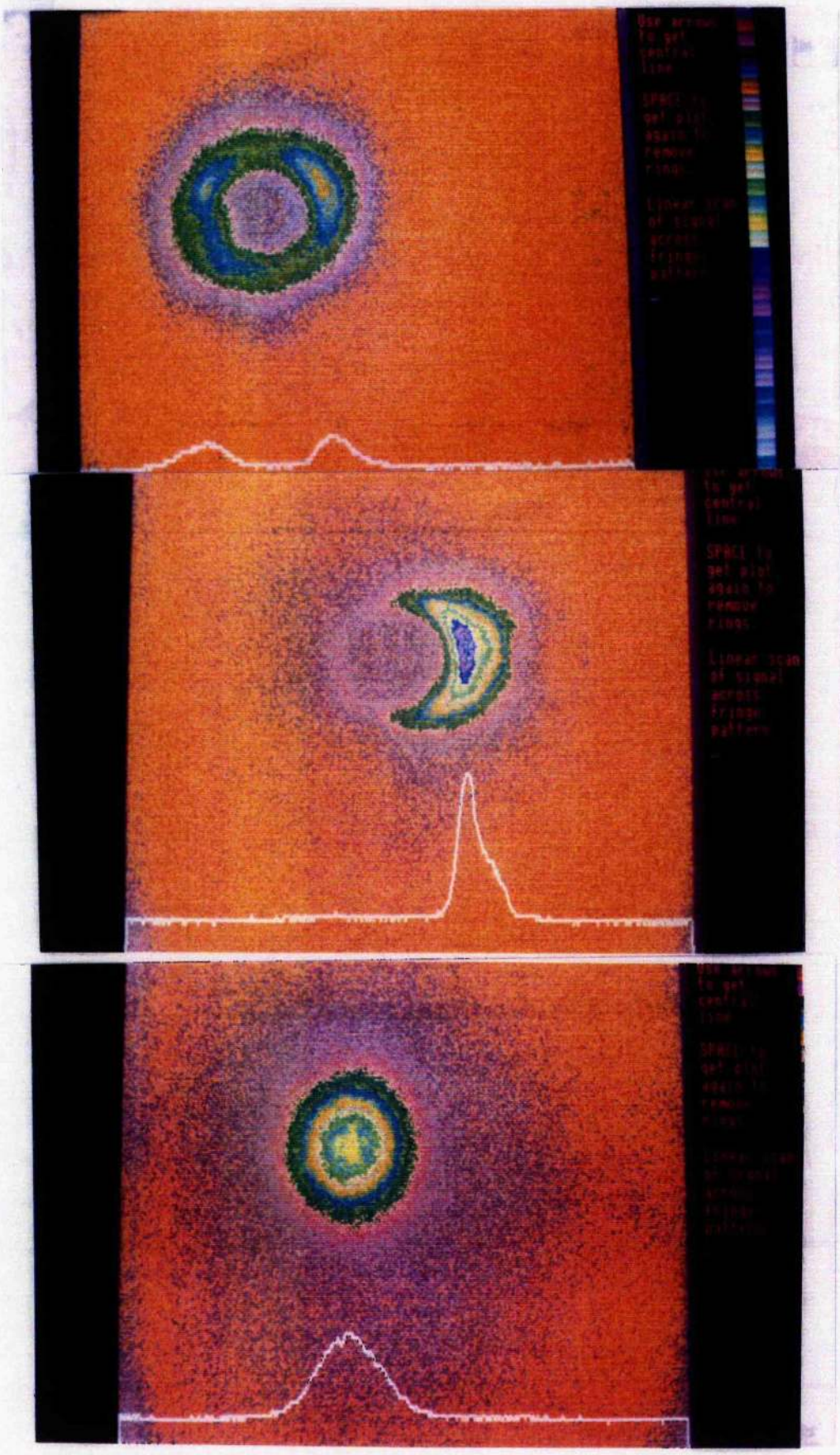

fig. 5.18 (a) -(c) Here the output profile is seen to change from the annular ring structure to a circular TEM_{00} mode as the OPO cavity is tilted at an angle to the pump beam, allowing the resonant mode to be outside the angular 'exclusion zone'.

5.8.1 Output wavelength

The output signal wavelength for the NCPM geometry used here, which is shown schematically in fig. 5.19, with a pump wavelength of 1.047 μm was measured to be 1.539 μm. The corresponding idler wavelength, from energy conservation, is therefore 3.276 μm. The accuracy of this measurement is estimated to be ± 0.5 nm due to the calibration of the monochromator with a Rb lamp. These are exactly the wavelengths predicted by the Sellmeier equations of Vanherzeele et al [11], validating the choice of this set of Sellmeier equations in chapter 3. It was also found that the signal wavelength for NCPM when pumping with 1.064 μm from the Nd:YAG laser was 1.571 μm, again in agreement with these Sellmeier equations. The NCPM geometry results in a more efficient way of generating nanosecond pulses at the eye-safe wavelength of 1.54 μm than has been achieved with the Er:glass laser. High energy pulses of 1 J have been achieved for flashlamp pumping of the Er lasers, but at an efficiency of less than 0.5 % [12]. Although the efficiency for diode pumping is improved by using Yb as a sensitiser, the low gain obtained results in a poor Q-switched performance (0.3 mJ for 240 mJ pump [13]).

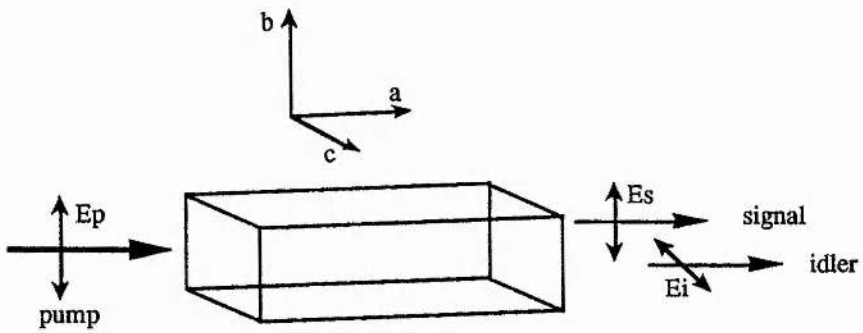

fig. 5.19 Schematic diagram of NCPM geometry and polarisations

Angle tuning brought about by tilting the crystal was found to be small, approximately 1 nm deviation from the value for propagation along the a-axis. A similar level of tuning could be obtained by tilting the cavity while keeping the crystal and beam alignment fixed. This corresponds to the limits of non-collinear phase matching.

The large birefringence of KTP accompanied by the NCPM operation both result in a narrow (for OPOs) bandwidth. The bandwidth is determined by restrictions on the maximum value of Δk which the system will tolerate. The expression for the signal bandwidth for the type II o-oe geometry can be obtained from the more general equation presented in chapter 2. By assuming, for calculation purposes, single frequency pump and idler, the expression for the signal bandwidth is

$$\Delta\lambda_s = \frac{\lambda^2}{l_c}\left\{(n_s - n_i) + \lambda_i \frac{\partial n_i}{\partial \lambda_i} + \lambda_s \frac{\partial n_s}{\partial \lambda_s}\right\}^{-1} \qquad (5.8.1.1)$$

For the case considered here this is $\Delta\lambda_s$~1.1 nm (FWHM). The finite linewidth of the pump, ~ few GHz, will widen this slightly but not noticeably so. This pump linewidth is well within the calculated pump spectral acceptance of ~ 0.28 nm, which is calculated in a similar fashion to the signal bandwidth above by assuming single frequency signal and idler. As mentioned above, the tuning corresponded effectively to tuning within this signal bandwidth. More will be said about this in the following section which discusses the detailed spectral properties of the output.

It is thought that the main reason that larger tuning was not achieved is probably due to the cavity misalignment when the crystal is rotated. Readjustment of the mirrors was unable to compensate for this, mainly due to the curvature of the mirrors which is itself responsible for the attainment of low thresholds. Although the walk-off angle increases dramatically as the crystal is rotated away from the a-axis, the threshold modelling presented in chapter 2 showed that for the values of angle and walk-off concerned the increase in threshold was not sufficient to explain why operation could not be obtained away from NCPM.

This points towards potential coarse tunability from this device, while maintaining low thresholds, by using a tunable pump laser, with fine tuning within the gain bandwidth controlled by cavity adjustments. This scheme has already been demonstrated by Kato and Masutani [11] who achieved tuning over the ranges 1.04-1.38 and 2.15-3.09 μm when pumping with several dye lasers. Tuning could be achieved over a much larger range, 1-3.3 μm, with an all solid state device if the pump source was a Ti:sapphire laser. Ti:sapphire lasers can produce nanosecond pulses in all-solid-state configuration

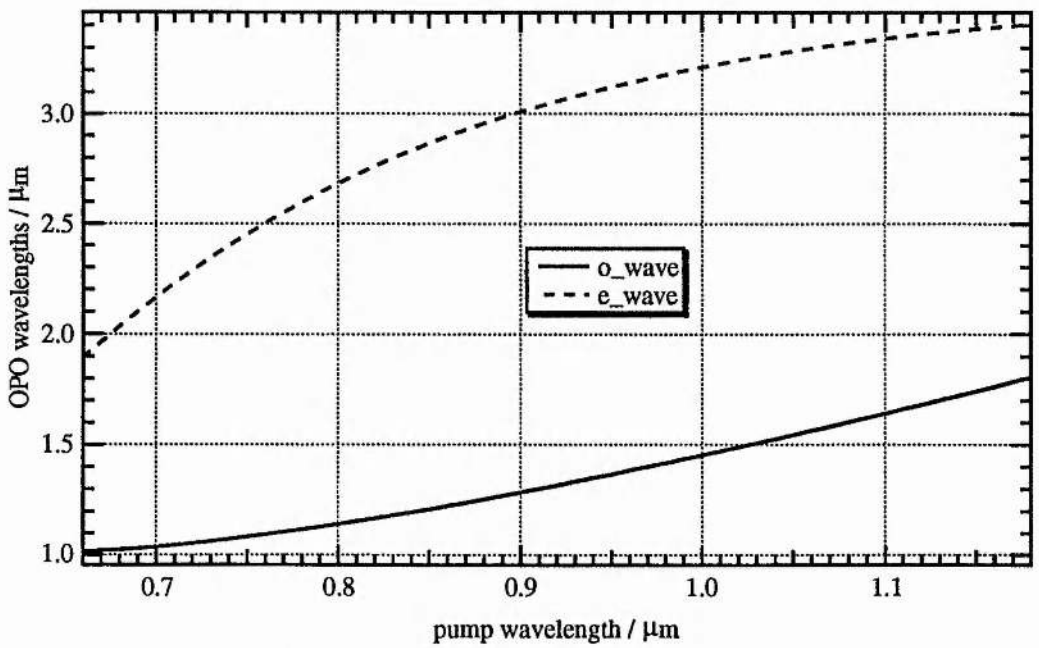

fig. 5.20 Potential tuning when using a Ti:sapphire laser to pump the low threshold NCPM KTP OPO

when pumped by a doubled diode-pumped Nd:YAG or YLF laser [14]. Fig. 5.20 shows the potential tuning that could be obtained with this scheme.

5.8.2 Spectral structure

One of the disadvantages of OPOs as sources of tunable radiation is the broad linewidth that is generally emitted. Normally there will be a large number of signal and idler axial modes that fall under this wide gain bandwidth. An early theoretical study by Kreuzer [15] showed that under steady state conditions, a singly resonant oscillator pumped at up to ~ 4.8 times threshold will operate on a single axial mode due to the gain saturation which is a result of pump depletion. In pulsed operation these steady state conditions are rarely reached and therefore a line narrowing element of some description is required to achieve the narrow linewidths that are required for some applications. Methods of achieving single axial mode operation usually consist of insertion of intra-cavity elements such as etalons [16] or diffraction gratings [17]. The insertion of any additional elements into the cavity increases the threshold due to losses of the line narrowing element itself, and also the increased build-up time losses with the required increase in cavity length. An alternative is to injection seed the OPO which requires an additional tunable source of narrow linewidth. An elegant way to achieve this is to use one laser to pump two OPOs, one of which is a narrow linewidth master oscillator which seeds the other, a high power slave oscillator or amplifier [18]. The spectral properties exhibited in this work suggest a possible way of achieving narrow linewidth without the insertion of additional cavity elements, or the requirement of an additional source for a seeder.

The spectral properties observed here of the nominally singly resonant design are partly complicated by a small amount of double resonance. The idler feedback is small, a few percent per round trip, and is due to the strict requirements on the coatings for the three wavelengths being partially unfulfilled. As the feedback at idler is small, but non-zero, the effect on threshold is small. However, as we will discuss shortly, even weak double resonance effects can perturb the output spectrum. However, in practice we found another mechanism to be the dominant one in this respect.

As was mentioned in section 5, the spectral content of the OPO output was examined by opening the output slits of the monochromator, and then imaging onto an IR vidicon. The signal from the vidicon went to a monitor via a frame grabber. The use of the frame grabber allowed the pulse to pulse spectral variations to be observed. However, no information was obtained in these experiments about mode competition within an individual pulse. An example of a spectrum that was 'grabbed' is shown in fig. 5.21. Wavelength is displayed horizontally. It can be seen that the spectrum consists of equally spaced 'clusters' of modes, with more than 5 clusters under the gain bandwidth. The appearance of such a large number of clusters is partly due to the integration time

of the vidicon tube. When the repetition rate of the laser was reduced to less than 1 pps, it could be seen that operation was sometimes on a single mode, as can be seen in fig. 5.22. Rotation of the crystal tuned the operating wavelength within the gain bandwidth in hops between these 'clusters'.

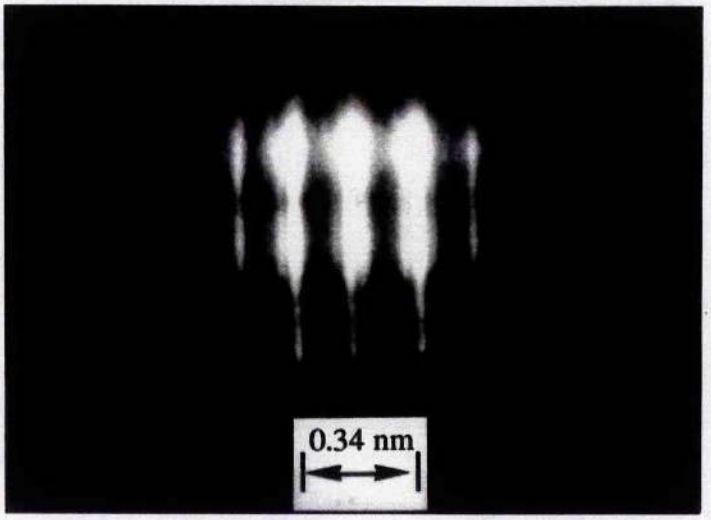

fig. 5.21 Example of a spectrum obtained for 10 Hz operation and the 5 mm substrates

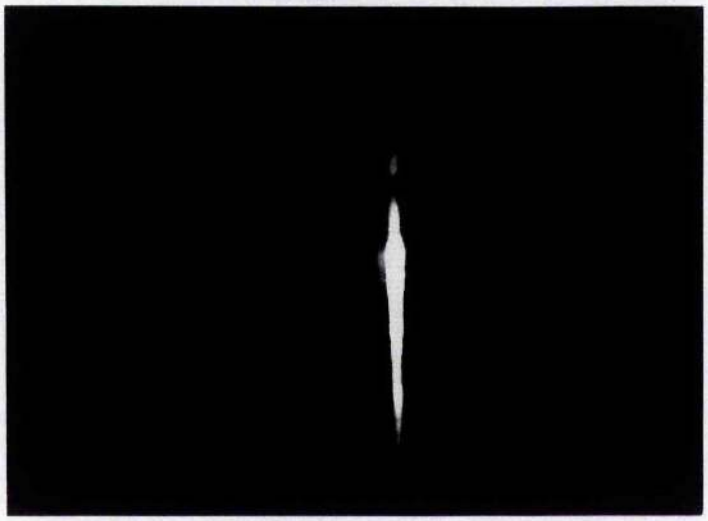

fig. 5.22 Near single mode operation

In these spectra the separation between each 'cluster' is ~ 0.17 nm, and the individual signal axial modes are resolvable with a separation of ~ 0.032 nm. The separation between signal axial modes is exactly that expected from the optical length of the cavity allowing for the dispersion of the KTP crystal. However, the 'cluster' separation, which was assumed to be double resonance clusters, did not agree with that expected from the difference in dispersion at signal and idler frequencies (~0.55 nm). In addition, it was observed that despite the fact that the pump laser was multi-longitudinal mode, the

position of the clusters did not jump about in frequency despite the quasi-random nature of the pump frequency and phase. To investigate this the pump was operated in slow Q-switch mode [19] which would give single frequency from the pump for sufficient periods that the effect this had on the OPO spectrum could be observed. Two things were noticed. Firstly, the position of the signal resonances was seen to not move when the pump laser hopped modes, and secondly, the efficiency of the OPO didn't increase in the case of the single frequency pump. These results pointed to the fact that double resonance was not the (main) cause of the observed spectrum.

Due to the fixed nature of the signal 'clusters' it was thought that there may be an accidental etalon effect in the cavity. This was traced to the zero-power mirrors. Due to the fact that the mirrors were obtained from two suppliers and had different substrate thicknesses, when using the different mirror substrates it was seen that the 'cluster' separations were different, depending on the mirrors used. The measured 'cluster' separations were found to correspond to the c/2nL free spectral ranges calculated for the mirror substrates. (0.17 nm for the 5 mm substrates and 0.225 nm for the 3.6 mm substrates). The concave-convex design of the mirrors with the two surfaces nearly concentric seemed to be acting as a resonant reflector despite the fact that the outer surface was specified to be high transmitting at signal and idler frequencies. The effect that a reflection on the outer surface has on the reflective properties is shown in fig. 5.23.

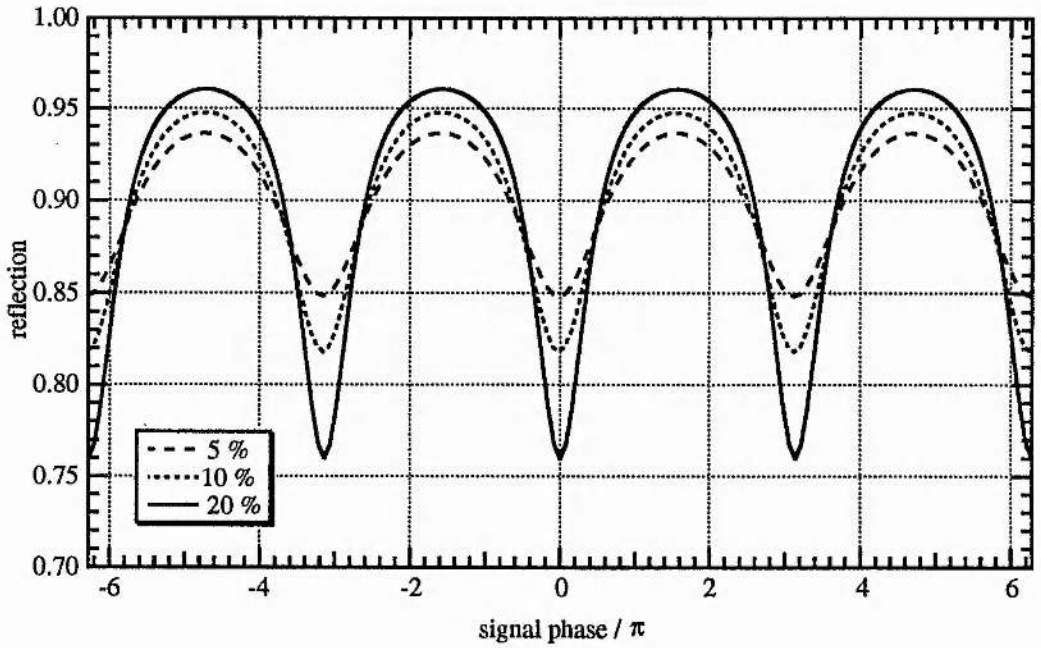

fig. 5.23 The reflectivity profile that would be produced for an inner reflectivity of 90 % and an outer reflectivity in the range 5 - 20 %.

A second reflecting surface with a reflectivity considerably smaller than that of the first produces a ripple on the reflectivity. The 'finesse' of this resonant reflector isn't high as

it can be seen that there are a number of signal axial modes capable of oscillating within each resonance of the reflector. This suggests a method of obtaining narrow linewidth operation of the OPO if a sufficiently thin mirror substrate was used such that only one resonance fell within the gain bandwidth. It may even be possible to use two mirror substrates of different thicknesses and finesses such that the combination of the two selects a single axial mode.

The resonant reflection was not a particularly strong effect and it is thought that the reason why the signal was seen to hop between the resonances was probably attributable to the weak double resonance. The double resonance was seen for one set of mirrors (3.65 mm substrates) to have a comparable effect to that of the resonant reflector, and explains why for this set of mirrors the resonances were not always equally spaced. Figs. 5.24(a), (b) and (c) show a sequence of spectra that were observed as the mount that was holding one of the mirrors was heated and allowed to cool. The centre resonance is seen to be closer to the right resonance in (a), and progresses to be centralised in (b) and then closer to the left resonance in (c). This is attributable to the double resonance being strong enough to 'pull' the resonance to which it is closest. The movement of the centre resonance is then due to the mirror resonances being scanned as the mirror substrate cools and the double resonance moving as cavity length is scanned due to cooling of the mirror mount.

5.9 Summary

In summary, this chapter has described the design steps and early experiments which resulted in demonstration of a low threshold all-solid-state OPO based on the material KTP. Sub 0.5 mJ thresholds were obtained due to the high quality beams from a diode-pumped Nd:YLF laser and optimisation of the confocal parameters of the interacting waves, with high efficiency also attained. Internal conversion efficiencies approaching 50 % were achieved, with an external slope efficiency into the signal wave of nearly 60 % obtained. The measurements of threshold energy are seen to show reasonable agreement with the predictions of the model developed in chapter 2, but the agreement between experiment and theory is not good enough to allow determination of which model is the most accurate. However, it is expected that the model developed here should be more accurate in the case where the interacting waves are focused.

The NCPM geometry produces a signal wavelength of 1.539 μm, an 'eyesafe wavelength', more efficiently than the alternative laser source of the Er:glass laser. Potential tuning in the range 1- 3 μm could be obtained with the use of a tunable pump laser. Narrow linewidth operation is observed, with the concave-convex zero-power mirrors acting as resonant reflectors. This suggests a method of obtaining single frequency output from this device, while maintaining low thresholds and high efficiency.

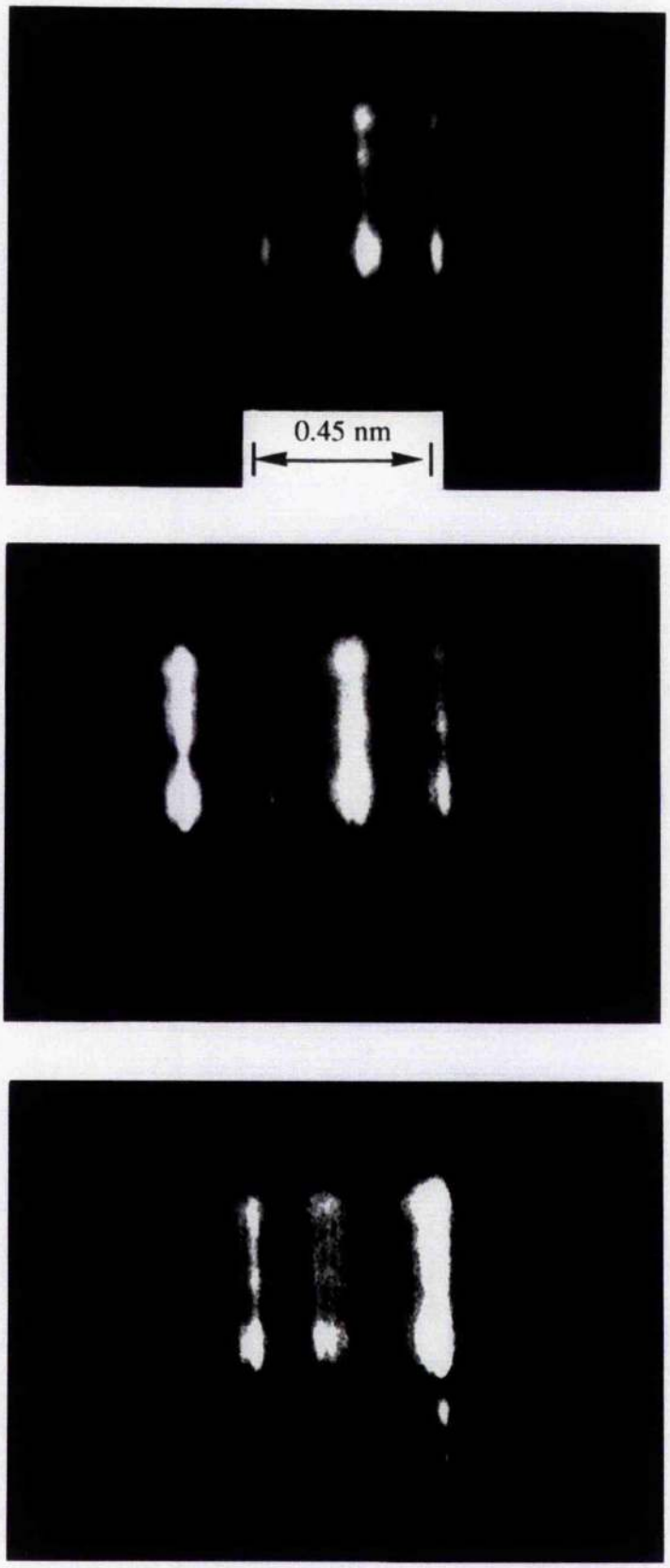

fig. 5.24 Spectra observed when the mount holding one of the 3.65 mm mirrors is heated and allowed to cool. It can be seen that the centre resonance is pulled from right of centre, to central, to left of centre as the double resonance cluster is scanned with the cavity length due to cooling of the mount.

5.10 References

[1] T.Y.Fan, C.E.Huang, B.Q.Hu, R.C.Eckardt, Y.X.Fan, R.L.Byer and R.S.Feigelson, 'Second harmonic generation and accurate index of refraction measurements if flux-grown $KTiOPO_4$', Appl. Opt. **26** (1987) 2390

[2] Y.Cui, M.H.Dunn, C.J.Norrie, W.Sibbett, B.D.Sinclair, Y.Tang and J.A.C.Terry, 'All-solid-state optical parametric oscillator for the visible', Opt. Lett. **17**(1992) 646

[3] R.G.Smith, 'A study of the factors affecting the performance of a continuously pumped doubly resonant optical parametric oscillator', IEEE J. Qu. Elec. **QE-9** (1973) 530

[4] P.P.Bey and C.L.Yang, 'Plane-wave theory of parametric oscillator and coupled oscillator-upconverter', IEEE J. Qu. Elec. **QE-8** (1972) 361

[5] R.C.Eckardt, H.Masuda, Y.X.Fan and R.L.Byer, 'Absolute and relative nonlinear optical coefficients of KDP, KD*P, BaB_2O_4, $LiIO_3$, MgO:$LiNbO_3$ and KTP measured by phase matched second harmonic generation,', IEEE J. Qu. Elec. **26** (1990)922

[6] J.M.Manley and H.E.Rowe, 'General energy relations in nonlinear reactances', Proc. IRE **47** (1959) 2115

[7] J.E.Bjorkholm, 'Some effects of spatially nonuniform pumping in pulsed optical parametric oscillators', IEEE J. Qu. Elec. **QE-7** (1971) 109

[8] S.J.Brosnan and R.L.Byer, 'Optical parametric oscillator threshold and linewidth studies', IEEE J. Qu. Elec. **QE-15** (1979) 415

[9] G.Hilber, D.J.Brink, A.Lago and R.Wallenstein, 'Optical frequency conversion in gases using gaussian laser beams with different confocal parameters', Phys. Rev. A **38** (1988) 6231

[10] H.Vanherzeele, J.D.Bierlein and F.C.Zumsteg, 'Index of refraction measurements and parametric generation in hydrothermally grown $KTiOPO_4$', Appl. Opt. **27** (1988) 3314

[11] K. Kato and M. Masutani, " Widely tunable 90^o phase-matched KTP parametric oscillator" , Opt. Lett. **17** (1992) 178

[12] B. I. Denker, V. V. Osiko, S. E. Sverchkov, Yu. E. Sverchkov, A. P. Fefelov and S. I. Khomenko, " Highly efficient erbium glass lasers with Q-switching based on frustrated total internal reflection" , Sov. J. Qu. Elec. **22**, 500-503 (1992)

[13] J. A. Hutchison and T. H. Allik, " Diode array-pumped Er,Yb:phosphate glass laser" , Appl. Phys. Lett. 60, 1424-1426 (1992)

[14] T. R. Steele, D. C. Gerstenberger, A. Drobshoff and R. W. Wallace, " Broadly tunable high -power operation of an all solid state titanium doped sapphire laser system" , Opt. Lett. **16** (1991) 399

[15] L.B.Kreuzer, 'Single and multimode oscillation of the singly resonant optical parametric oscillator', in *Proc. Joint Conf. Lasers Opto. Electron. U. Southampton, London (1969) 53*

[16] G.Robertson, A.Henderson and M.H.Dunn, 'Efficient, single axial mode operation of a beta barium borate oscillator pumped by an excimer laser', Appl. Phys. Lett. **62** (1993) 123

[17] W.R.Bosenberg and D.R.Guyer, 'Single frequency optical parametric oscillator', Appl. Phys. Lett. **61** (1992) 387

[18] A commercial device is now available using this technology. The MOPO 700 series from Spectra-Physics

[19] C.F.Rae, J.A.C.Terry, B.D.Sinclair, M.H.Dunn and W.Sibbett, 'Single-frequency, end-pumped Nd:YLF laser excited by a 12 mJ diode-laser array', Opt. Lett. **17** (1992) 1673

CHAPTER 6
Conclusions

The main aim of this work was to demonstrate that the high quality output obtainable from a diode pumped solid-state laser could be used to efficiently pump an OPO when the energy available from the laser was limited. The results presented in the previous chapter demonstrate the achievement of that aim. In this chapter, each aspect of the work leading up to the achievement of the above general aim is discussed, as are ways in which improvements and further work could be implemented.

Chapter 4 described the construction of a number of pump lasers, with the end-pumped Nd:YLF laser being of sufficient energy to pump the OPO above threshold. Therefore the work on pump lasers can be considered to have achieved its aim in the sense that a laser was built which allowed operation of the OPO. The important parameters for this laser were the selection of an end pumping geometry and the host material Nd:YLF.

The work with the side pumped lasers using Nd:YAG as the gain medium showed that the large spatial spread of the gain associated with this geometry resulted in higher thresholds and poorer efficiencies than were obtained with end pumping. The coupling scheme adopted here where the output of a single diode bar is focused into a small gain volume showed that diode bars could be used effectively in end pumping geometries. The resulting high single pass gain and good mode overlap obtained showed relative insensitivity to intracavity loss and high energy extraction was achieved, as witnessed by an output of 2 mJ in an 18 ns Q-switched pulse for a pump energy of 12 mJ. Immediate improvement of this efficiency might be obtained by replacing the prism pair with its relatively high insertion loss (4 % per pass, which was likely due to poor quality manufacture) by a cylindrical telescope, where the small astigmatism can also be compensated for by incorporating a small power into the telescope.

In the low average power regime, it was seen in this work that YLF is a superior host to YAG for the Neodymium ion. The main reason for the superior performance of YLF in this work was the stronger absorption of the pump light. The shorter absorption depth therefore meant that the highly diverging pump light was confined to a smaller volume in the YLF material. The higher gain per unit area resulted in a smaller threshold, and the improved confinement of the gain to the axis of the rod allowed more efficient coupling of the laser mode to the gain resulting in more efficient output. YLF would also appear to be a superior material when scaling to higher output power is required. The natural birefringence and superior thermal lensing properties result in considerably

reduced thermal problems in YLF. This argument only holds up to the thermal fracture limit, which is smaller in YLF than in YAG, requiring that YAG, or an alternative host, be used for very high average power operation. However, the low thermal fracture of YLF may be due to the growth technology of this material being less mature than that of YAG as recent work in these labs has shown that cw powers of 18 W can be input to thin slabs of Nd:YLF without causing fracture.

Scaling of these devices to higher energies and average powers appears to be relatively straightforward. A number of schemes have been reported in the literature for coupling the output of more than one diode bar into a single gain element. Thermal fracture considerations dictate the maximum power density that can be input, restricting the focusing of the diode light in the plane perpendicular to the diode junction. However, this has the advantage that a more circular gain region is obtained, and so anamorphic expansion of the laser mode would no longer be required.

The use of multiple gain elements in oscillators and also oscillator/amplifier set ups allows high power and energy outputs to be obtained by using the more efficient geometry of end pumping. With the price of diode laser bars decreasing due to increased demand it will not be long before stable, compact and efficient diode pumped solid-state lasers can effectively replace their lamp pumped equivalents.

The agreement between the thresholds calculated for a pulsed singly resonant OPO with the computer model, based on introducing build-up time effects to the Guha analysis, and the experimentally measured ones was seen to be as good as 50 % under the conditions investigate here. Considering the complexity of the interaction involved this agreement is encouraging. Direct comparison between this model and the established model due to Brosnan and Byer (BB) shows that when the interacting beams are focused to a reasonable degree, the model developed here with less limiting assumptions is expected to give a better prediction of performance than the BB model which is only directly applicable to the weakly focused regime. Measurement of threshold under a wider range of conditions (e.g. pump and signal focusing) and with improved determination of actual experimental parameters (e.g. crystal losses) should give a better vindication of the modelling. In any event, the threshold curves produced from the model provide a basis for optimisation of the OPO parameters.

An empirically derived relation for internal efficiency (pump depletion) allows calculation of expected system efficiencies and optimisation of this. The parameters which need to be optimised are mode overlap (optimisation of pump and signal focusing), pulse duration and output coupling. It would be assumed that AR coating of the crystal faces for pump and signal would allow external efficiencies to match internal ones. From the efficiency and threshold curves with respect to pulse duration it would appear that the optimum pulse length optimises both threshold and efficiency, as might

be expected.

Scaling to higher powers seems feasible, and has been demonstrated by Marshall and co-workers at Fibertek [1]. Optical damage to the crystal coatings (no bulk damage was observed) was seen to be the limiting factor on how much power could be input to the OPO. No damage was observed when only the pump was incident, and the cause of the damage was seen to be the resonant wave (signal in this case). By using a sufficiently high output coupling (27 %), when 2.65 mJ from a Nd:YAG laser was incident on the OPO, 0.7 mJ were produced at the signal, where the reduced Q of the signal cavity avoided damage to the coatings without increasing the threshold dramatically. A high output coupling also has the advantage that when there are intracavity losses present, the external efficiency is greatest with a large output coupling. The limits of scalability of the present device are therefore dominated by the coating damage threshold. Increasing pump and signal spot sizes would allow more input pump power at the expense of threshold, however, pumping sufficiently above threshold would result in an increased output at signal and idler.

The use of the concentric 'zero-power' mirrors was seen to be a central component in the operation of the OPO. The zero-power nature eased considerably the alignment difficulties that had been experienced with plano-concave mirror substrates. The small modes sizes and strong overlap produced by the curved mirrors was responsible for the low thresholds, but also seemed to limit the tuning to within the gain bandwidth as adjustment of the mirrors was unable to compensate for the perturbation of the cavity as the crystal was rotated away from normal incidence. The mirrors also had a pronounced effect on the detailed spectral properties of the oscillator due to their resonant reflector behaviour. It was seen that this characteristic of the mirrors restricted the number of signal axial modes that were above threshold, and was seen to produce single-axial mode operation on occasion. Although this was not the original intention, proper design of the mirror coatings might provide a way of achieving single mode operation without the requirement of additional intracavity mode selection optics, or a seeding source. The use of two mirror substrates of different thicknesses, and hence different free-spectral ranges, might allow controlled selection of a single axial mode. The weak resonant reflection (weak as one side was specified to be highly transmitting) was seen to be sufficient to have some control over the modes, suggesting that any mirror resonances would not have to be very sharp to obtain mode control, which would make overlapping of the resonances easier and less critical.

The NCPM geometry and the cavity geometry resulted in the OPO operating as an efficient down-converter. The 1.54 μm signal wavelength is a particularly useful wavelength as it is described as 'eyesafe' and has many applications including rangefinders and laser radar. The efficient conversion to this wavelength (30 %)

produces it more efficiently than the usual alternative method which relies on an inefficient three level transition in Er^{3+} doped phosphate glass.

Wavelength diversity could be obtained, while retaining the low threshold and high efficiency operation, by the use of a tunable pump source. For example, use of a Ti:sapphire laser as the pump would allow tuning over most of the region 1-3.3 μm. Alternatively, if a higher power Nd:YLF pump laser was constructed, then critical phase matching could be employed where the higher power available from the laser would be required to offset the increase in threshold that would ensue due to the operation away from NCPM. Operation further into the IR could be achieved if other non-linear materials were considered. The material KTA, an isomorph of KTP which is currently under development, has higher non-linear coefficients than KTP and transmits to 5 μm, which would allow access to the technologically important regime of 3-5 μm, which is inaccessible with KTP.

In summary, the work here describes an extension to the theory of pulsed OPOs brought about by a computer model which introduces time dependence to the steady-state theory of Guha et al. Use of the high quality output from an end pumped, Q-switched Nd:YLF laser allowed demonstration of a low threshold, efficient OPO based upon non-critically phase matched KTP. The use of meniscus mirror substrates was a major factor in the attainment of the low threshold operation, and the resonant reflector behaviour of same suggests a way in which single axial mode operation might reliably be obtained. Extension of this work to higher powers and other wavelengths has been discussed.

[1] L.R.Marshall, A.Kaz and R.L.Burnham, 'Eyesafe laser with 2% electrical efficiency', CWQ2 presented at CLEO '92, Anaheim, CA, May 1992

APPENDIX A

Non-linear Optical Materials

A.1 Introduction

An overview of some of the materials suitable for constructing an OPO pumped at 1.064 μm was presented in section 3 of chapter 3. In this appendix a more detailed discussion of the materials is presented. No further discussion of KTP is presented here as it has already been presented in detail in chapter 3.

A.2 Lithium Niobate ($LiNbO_3$) and MgO:$LiNbO_3$

$LiNbO_3$ is a negative uniaxial crystal of point group 3m [2.1]. It possesses a large non-linearity which is often characterised by the coefficient d_{15} (= d_{31}) = 5.95 pm/V [2.2], though the known variation of the non-linearity with composition may explain a recent measurement for 5% MgO:$LiNbO_3$ of d_{31} = 4.7 pm/V [2.3].

It also possesses a relatively high surface damage threshold, given by one manufacturer as 350 MWcm^{-2} for 25 ns pulses at 1.064 μm (no rep rate) [2.4]. An intensive study of damage mechanisms by Brosnan and Byer [2.5] found a surface damage fluence of 2.7 J cm^{-2} for pulses at 1.06 μm in the 10-30 ns range for a bare surface, which increases to 11 J cm^{-2} when the spot size is reduced below the mean defect spacing of 60 -70 μm. The damage threshold was also seen to increase when the crystal was in an O_2 atmosphere or AR coated with SiO_2. The damage fluence pulsewidth scaling was found to be $(\tau)^{0.5}$ for pulses short enough to not completely heat the surface, and τ for longer pulses.

However, early samples were found to suffer photorefractive damage at much lower intensities, < 50 MWcm^{-2} [2.6]. The damage is thought to arise due to the presence of impurities in the crystal (possibly Fe^{3+} [2.7]). As the impurity level is already low, improvement of this would likely add substantially to the cost of fabrication. The most successful improvement technique to date has been that of doping the congruent melt with approx. 5 % MgO which has increased the photorefractive damage level by a factor of a hundred due to an increase in the photoconductivity [2.8]. Another technique involved growth of crystals with an adjusted Li/Nb ratio which raised the SHG temperature for 1.064 μm from 4 to 238 °C, which, being above the annealing temperature, meant that any damage was annealed out [2.9].

$LiNbO_3$ possesses a large negative birefringence which varies from ≈ 0.1 to 0.06 throughout its transparency range of 0.4 to 5 μm [2.1], with a refractive index of ≈ 2.2 at

1.06 μm. The large birefringence facilitates a large tuning range with degeneracy for 1.06 pumping at ≈ 44 °, but also results in a relatively large walk-off 36 mrad. The tuning curve and variation of walk-off and d_{eff} calculated from the Sellmeier eqns of Hobden and Warner [2.10] are shown in figs. a.1 (a) and (b). This critical phase match geometry results in the angular and spectral acceptances for a signal and idler wavelength pair of

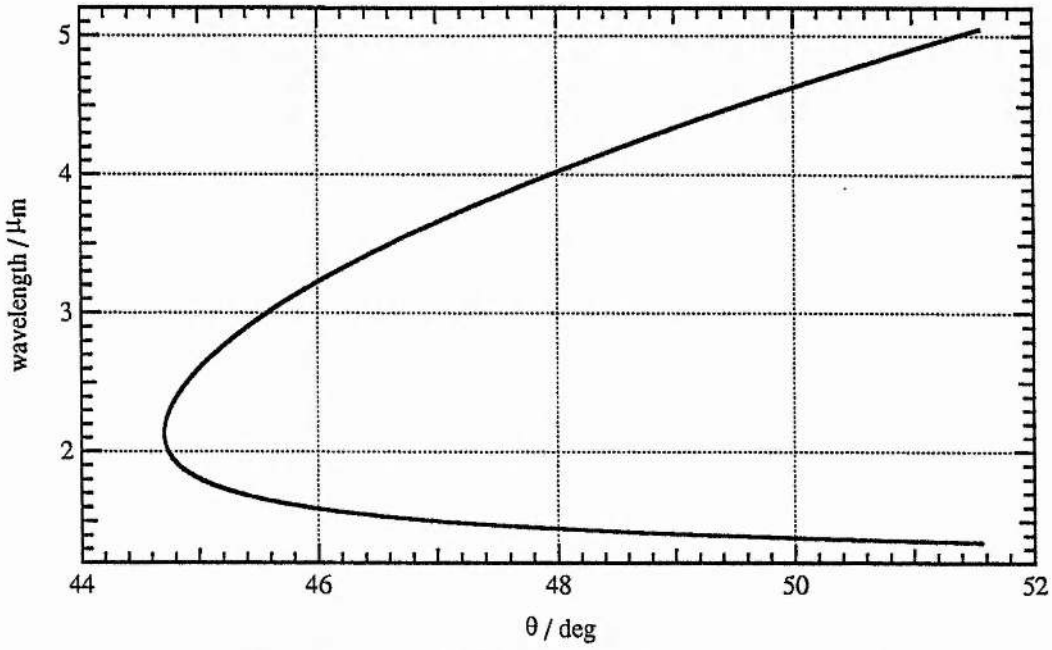

fig.a.1 (a) tuning curve for e-oo phase matching in the ac-plane at 22°C pumped at 1.064 μm (from Sellmeier eqns of [2.8])

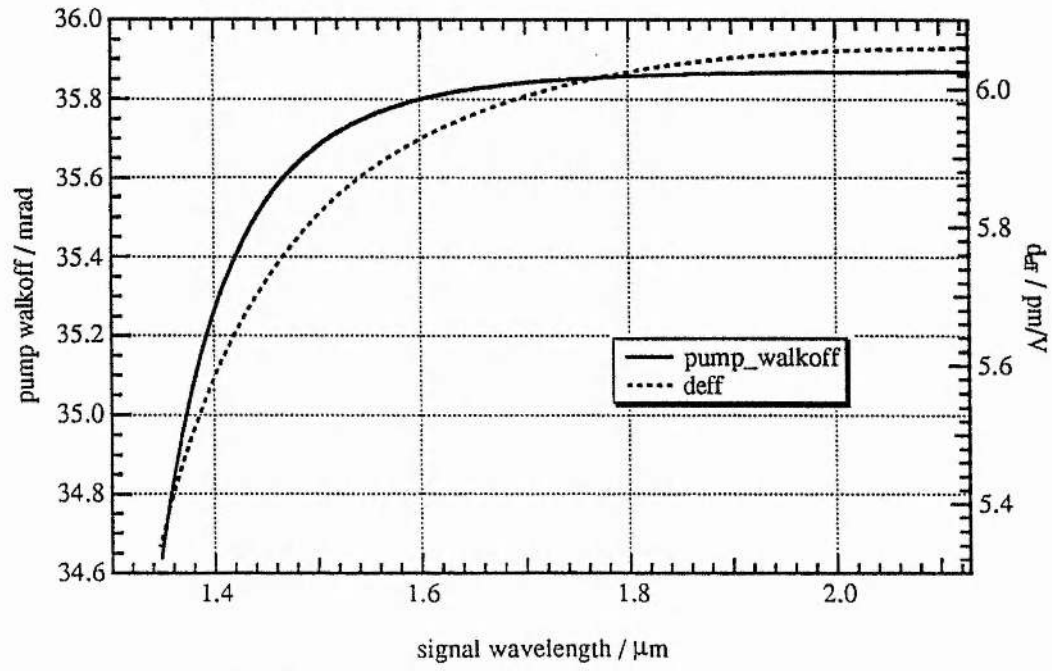

fig. a.1 (b) (b) walk-off and d_{eff} curves for e-oo phase matching in the ac-plane at 22°C pumped at 1.064 μm (from Sellmeier eqns of [2.8])

1.6 and 3.2 μm being ~ 1.4 mrad cm in, and 9.8 mrad $cm^{1/2}$ orthogonal to, the tuning plane and 1.5 nm respectively. Although the calculated temperature for a 1.06 μm pumped OPO with NCPM is an unpractical 552 °C [2.10], NCPM for a 532 nm pump

has been demonstrated in MgO:$LiNbO_3$ at 107 °C [2.11]. The calculated temperature acceptance for a 1.6 and 3.2 μm pair is 2.7 °C. Note that the acceptance parameters quoted here and for all other materials are FWHM, and are as defined in chapter 2.

After much investigation into its growth properties, $LiNbO_3$ can be grown with high optical quality and large dimensions. High optical quality crystals have been grown as large as 50 mm long by 15 mm diameter [2.12], and the loss of high quality MgO:$LiNbO_3$ at 1.064 μm has been measured as less than 0.003 cm^{-1}. These properties along with those already mentioned have ensured its success as a non-linear material.

Parametric oscillation has been demonstrated in $LiNbO_3$ with both pulsed [2.14,15] and cw [2.16] pump lasers, and with both angle [2.15] and temperature tuning [2.14,16]. Although temperature tuning is normally employed with 532 nm pumping for NCPM, $LiNbO_3$ has also been temperature tuned when pumped at 1.064 μm [2.17]. The improved photorefractive properties of MgO:$LiNbO_3$ have been utilised as an excellent material for resonant doubling of 1 μm light [2.18], and for cw [2.11] and Q-switched, mode-locked [2.19] operation of OPOs.

$LiNbO_3$ has also been used in fibre and waveguide geometries. Periodic domain reversal in waveguides facilitates quasi-phase matching which allows use of the large d_{33} coefficient [2.20]. The photorefractive effect in $LiNbO_3$ has actually been productively utilised in an OPO by creating a dynamic diffraction grating in the material for linewidth control [2.21].

A.3 Barium Sodium Niobate ($Ba_2NaNb_5O_{15}$, BSN, BNN)

At room temperature, Barium Sodium Niobate , sometimes abbreviated as BNN or BSN, is a negative orthorhombic crystal, with point group mm2 [3.1]. Above 260 °C it is tetragonal [3.2] and is believed to possess 4mm symmetry. It has a large non-linearity with the non-linear coefficients in the orthorhombic state being $d_{31} = d_{32} = 20$ pm/V, and $d_{33} = 28$ pm/V [3.3]. Crystals have been grown up to 50 mm long and 20 mm in diameter [3.3] but these require processing to eliminate microtwinning and to pole the material [3.2].

As well as possessing higher non-linear coefficients than $LiNbO_3$, it has the added advantage that it is not susceptible to photorefractive damage [3.1]. Unfortunately it doesn't possess a high surface damage threshold. Reported damage thresholds for 1.064 μm radiation include 3 $MWcm^{-2}$ for 10 ns pulses [3.4] and 25 $MWcm^{-2}$ for 80 ps pulses when operated in a clean vacuum environment [3.5].

The transparency of the crystal stretches from 370 nm to 5 μm, though an OH absorption has been observed at approx. 3500 cm^{-1} [3.3]. Low loss operation in the visible and near

infrared is achieved with typical absorptions of 0.04 cm^{-1} at 532 nm and 0.002 cm^{-1} at 1.064 μm [3.6]. The birefringence is negative and varies for 1.064 μm from 0.09 at 0 °C to 0.06 at 300 °C. The difference in refractive indices between x and y axes is small (≈ 0.002) and the wavelength dependencies of the three components are satisfied by the single term Sellmeier eqns of Singh et al [3.3]. The indices are found to be heavily temperature dependent with n_x and n_y both decreasing with increasing temperature in the orthorhombic phase ($dn_x/dT = -2.5 \times 10^{-5}$ °C^{-1}) and n_z increasing ($dn_z/dT = 8 \times 10^{-5}$ °C^{-1}). Crystal to crystal phase match temperature variations are also less than $LiNbO_3$ at less than 10 °C [3.1].

As with $LiNbO_3$, NCPM can be achieved at elevated temperatures for pumping of an OPO at 532 nm [3.7], but 1.064 μm pumping is restricted to angle tuning. A tuning curve using the Sellmeier eqns of Singh et al [3.3], is shown for e-oo phase matching in the bc plane in fig. a.2a and the dependence of d_{eff} and walk-off is shown in fig.a.2b.

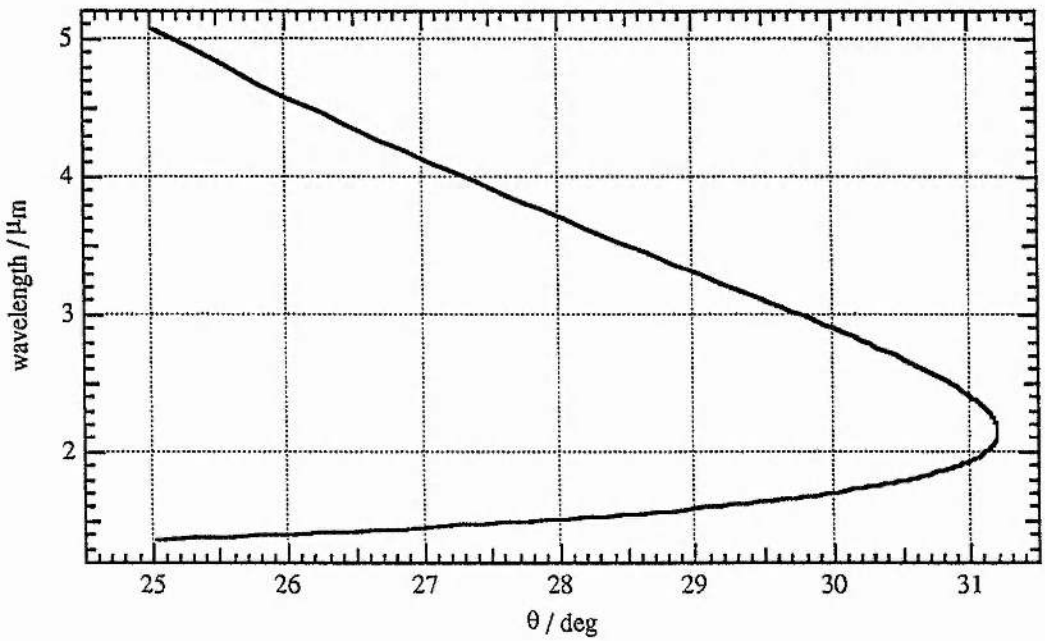

fig. a.2 (a) tuning curve for e-oo phase matching in the bc-plane of $Ba_2NaNb_5O_{15}$ (from Sellmeier eqns of Singh et al [3.3])

The calculated angular, spectral and temperature acceptance parameters for the critical tuning shown above for a signal/idler pair of 1.6 and 3.2 μm are 1.4 mrad cm in, and 29 mrad $cm^{1/2}$ orthogonal to, the tuning plane, 1.8 nm cm and 3.9 °C cm respectively.

Barium sodium niobate has been operated as an OPO for various pumps in the green region of the visible, including the lowest reported threshold for cw operation of 3 mw for pumping at 514 nm with an argon laser [3.8]. Tuning is usually by temperature, and for an OPO pumped by the second harmonic of a mode locked lanthanum beryllate laser at 535 nm produced tunable output over the region 0.65 - 3 μm [3.9].

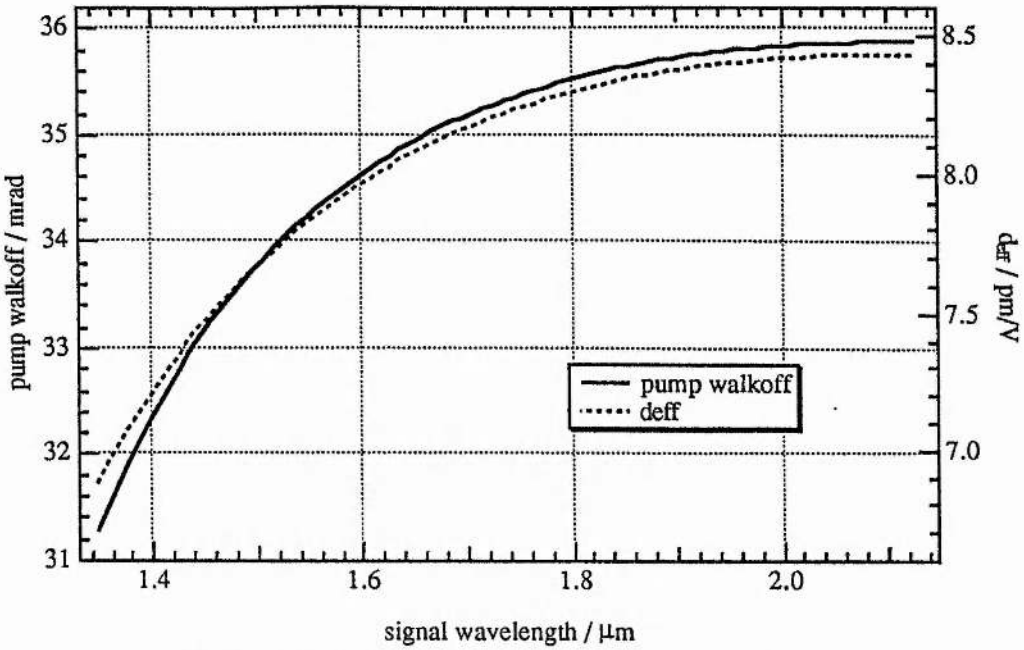

fig. a.2 (b) walk-off and d_{eff} curves for e-oo phase matching in the bc-plane of $Ba_2NaNb_5O_{15}$ (from Sellmeier eqns of Singh et al [3.3])

Other applications of barium sodium niobate include wavefront reversal [3.10] and waveguide structures [3.11].

A.4 Potassium Niobate ($KNbO_3$, KN)

Potassium Niobate (KN) is a biaxial crystal of point group mm2 at room temperature [4.1]. Below -50 °C it is rhombohedral, and above 223 °C it becomes tetragonal [4.2]. It has a large non-linearity close to that of barium sodium niobate and three times that of lithium niobate. The non-linear coefficients which have been used here are d_{31} = 15.8 pm/V and d_{32} = 17.6 pm/V which were arrived at by averaging the values in the literature [4.3,4] and assuming that Kleinman's conjecture [4.5] holds. Both of the references calculate the non-linear coefficients with respect to those of d_{11} for quartz, which in itself varies in the literature. Note that the relation between the piezoelectric axes and the crystallographic axes still holds as XYZ ↔ abc despite the fact that the convention for labelling a and b as a<b has not been upheld [4.1].

The optical damage threshold can be reasonably high, but values in the literature seem to differ considerably. While one author reports damage at 150 - 180 $MWcm^{-2}$ for 10 ns pulses at 1.064 μm [4.6], a more recent report gives 1.3 $GWcm^{-2}$ for 7 ns pulses at 1.064 μm [4.7].

High quality crystals can be grown exhibiting low loss throughout the transparency of 400 nm - 4.5 μm, with a loss of < 1% cm^{-1} at 1.064 μm [4.8]. Until recently, the refractive indices had only been measured out to 1 μm in the infrared [4.3,4], and experimentally obtained phase matching angles were seen to differ by as much as

10° from calculated values [4.7]. The refractive indices have now been measured in the range 400 - 3400 nm and have been fitted to a two oscillator Sellmeier eqn with infrared correction [4.2]. The large birefringence (0.22 at 430 nm and 22 °C in the bc plane to 0.115 at 3 μm) allows phase matching throughout the transparency range.

As in the case of lithium niobate and BSN, potassium niobate supports NCPM at elevated temperatures (~ 190 °C) when pumped at 532 nm. This has been demonstrated recently [4.9]. Pumping at 1.064 μm is again limited to angle tuning. A tuning curve based on the recent Sellmeier eqns of Zysset et al [4.2] and the variation of walk-off and d_{eff} are shown respectively in figs. a.3 (a) and (b). This critical geometry results in an

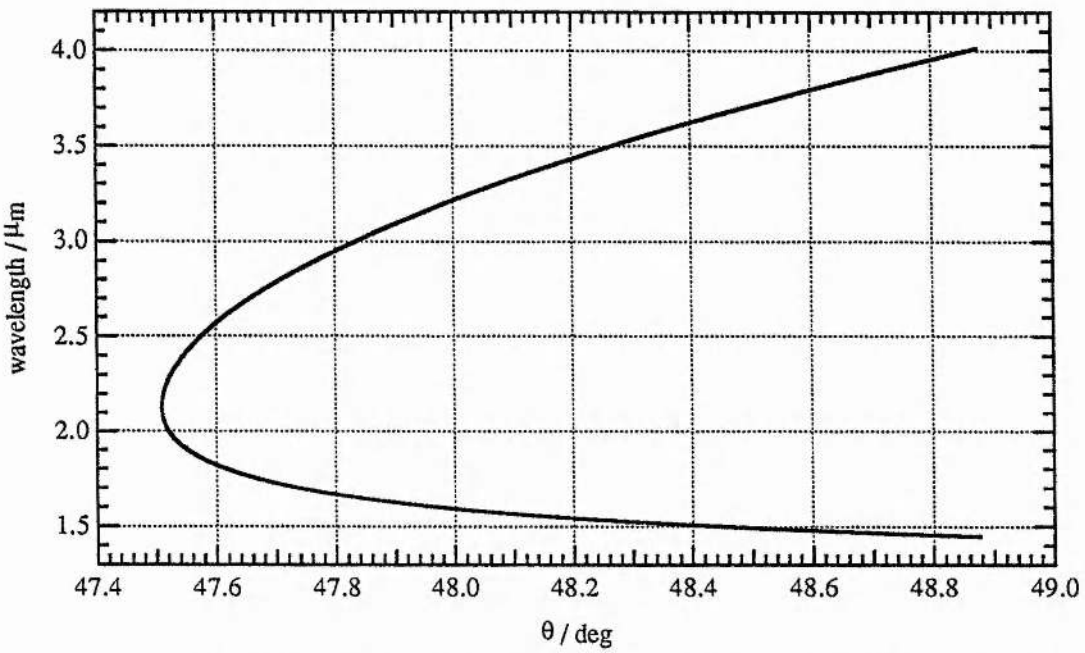

fig. a.3 (a) tuning curves for e-oo phase matching in the bc plane at 22 °C pumped at 1.064 μm (from Sellmeier eqns of Zysset et al [4.2])

angular acceptance in the tuning plane of 0.8 mrad cm and 21.3 mrad $cm^{1/2}$ in the orthogonal plane, for a 1.6 and 3.2 μm pair. The pump spectral acceptance and temperature bandwidth are 0.7 nm cm and 80 °C cm respectively. The value of temperature acceptance is calculated by interpolating the data of [4.2] and therefore the near cancellation of temperature coefficients which results in the large temperature acceptance may not be strictly accurate.

High optical quality crystals of large size have been grown, up to about a 1 cm aperture and 30 mm length [4.6]. However the crystals are susceptible to domain formation and have to be poled. Experience of others in this laboratory showed that to prevent domain formation during temperature cycling, it was necessary to cool the crystal in the presence of a poling field along the c-axis [4.10].

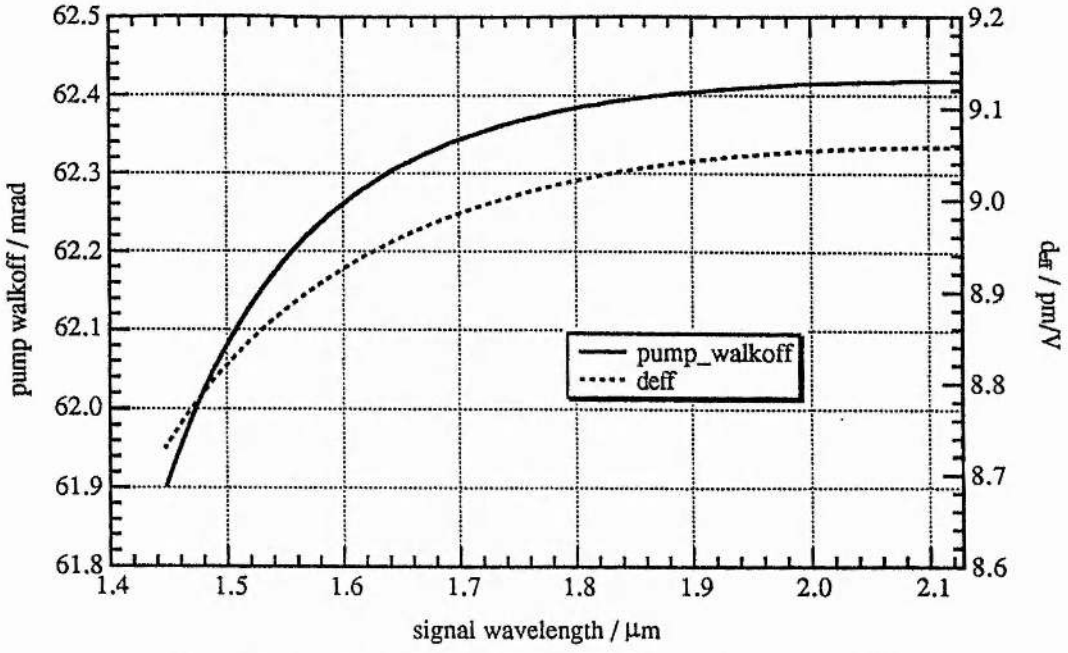

fig. a.3 (b) walk-off and d_{eff} curves for e-oo phase matching in the bc plane at 22 °C pumped at 1.064 μm (from Sellmeier eqns of Zysset et al [4.2])

KN has successfully been used in SHG, SFG, OPA and OPO applications. One of its most promising and technologically important applications is in the use of an external monolithic resonant cavity for the direct doubling of diode lasers [4.11] for the generation of blue light. Intracavity doubling of Nd:YAG lasers has also been demonstrated [4.12,13]. Temperature tuned OPOs have been demonstrated with a 532 nm pump with output in the region 0.86 - 1.4 μm [4.6,9,14]. The only 1.064 μm pumped device to my knowledge is an OPA which generated output over the range 1.1 - 5 μm [4.7].

A.5 Lithium Iodate ($LiIO_3$)

Lithium Iodate is a negative uniaxial crystal which possesses point group 6 at room temperature, and up to 256 °C where it undergoes a phase change [5.1]. The non-linear coefficient d_{31} was measured by the parametric fluorescence technique to have a value 7.1 pm/V [5.2], which was considerably higher than that obtained using SHG [5.3]. The fact that measurements by parametric fluorescence also seem to be erroneously high for other materials led us to adopt the value obtained from the SHG measurements. An average of the SHG measurements for d_{31} published in the literature is 4.4 pm/V [5.4], and it is this value which is adopted here.

Lithium Iodate is not susceptible to optical or photorefractive damage, at least none was observed at an intensity of 2 $kWcm^{-2}$ [5.1]. The only relevant optically induced damage figures for a pulsed source which could be found were 130 $MWcm^{-2}$ for 20 ns pulses at 694 nm [5.5] and 250 $MWcm^{-2}$ for 100 ns pulses at 1.064 μm [5.6]. As damage intensity increases with shorter pulses it is appropriate to assume the higher value of 250

$MWcm^{-2}$ even though the pulse duration of concern here is nearer 20 ns.

The crystal has a wide transparency, from 300 nm in the UV [5.5] to 5 μm in the infrared [5.1], with the birefringence varying from ~ 0.15 - 0.12. The dispersion of the refractive indices is described by the Sellmeier eqns of Herbst [5.7], and these are found to be temperature insensitive, or at least the birefringence is found to be, as the phase matching angle was seen to vary by only 0.3 ° when the temperature was varied over the range 20 ° to 256 °C [5.1]. With no potential for temperature tuning only angle tuning had to be considered. The tuning curve for pumping at 1.064 μm, and the variation of walk off and d_{eff} are shown respectively in figs. a.5 (a) and (b). The absorption is quite high in the

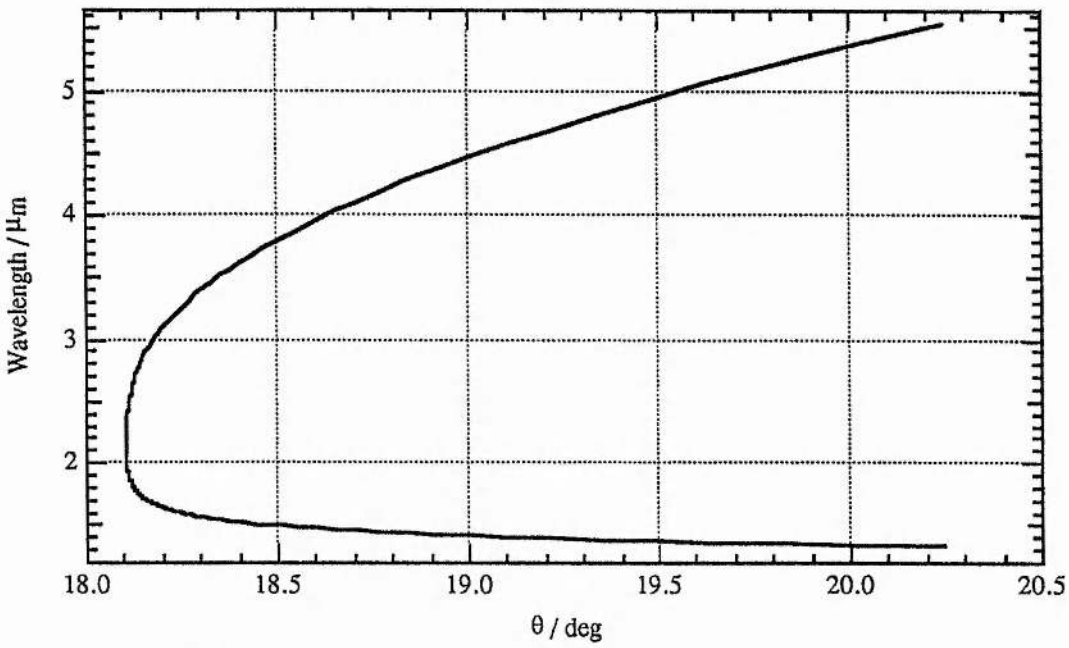

figs. a.5. (a) tuning curve for e-oo phase matching in $LiIO_3$ pumped at 1.064 μm (from Sellmeier eqns of Herbst [5.7])

near UV and visible, 0.3 cm^{-1} at 347 nm [5.5], but falls to a reasonable value in the near IR, 0.06 cm^{-1} at 1.064 μm [5.1]. The calculated spectral and angular acceptances for a 1.6 and 3.2 μm pair are, respectively, 2.85 nm cm and 1.2 mrad cm in, and 10.7 mrad $cm^{1/2}$ orthogonal to, the tuning plane.

Single crystals can be grown without the problem of domain formation to large sizes, up to 15 mm aperture [5.5] and 60 mm length [5.8]. These large single crystals have facilitated their use successfully in non-linear optics. $LiIO_3$ has been used to generate the second harmonic of Nd:YAG [5.9] and ruby [5.5]. Optical parametric oscillation has been demonstrated with second harmonics of Nd:glass [5.10] and Nd:YAG, both Q-switched [5.11] and mode-locked [5.12]. In one case [5.11], tuning was obtained over the range 0.63 - 3.4 μm. Pumping with 1 μm light was demonstrated when a $LiIO_3$ crystal was operated as an intracavity OPO with the pump laser a Q-switched Nd:YAG laser operating at 80 Hz, with tuning obtained in the ranges 1.92 - 2.34 μm, and 3.8 - 4.2

μm [5.13].

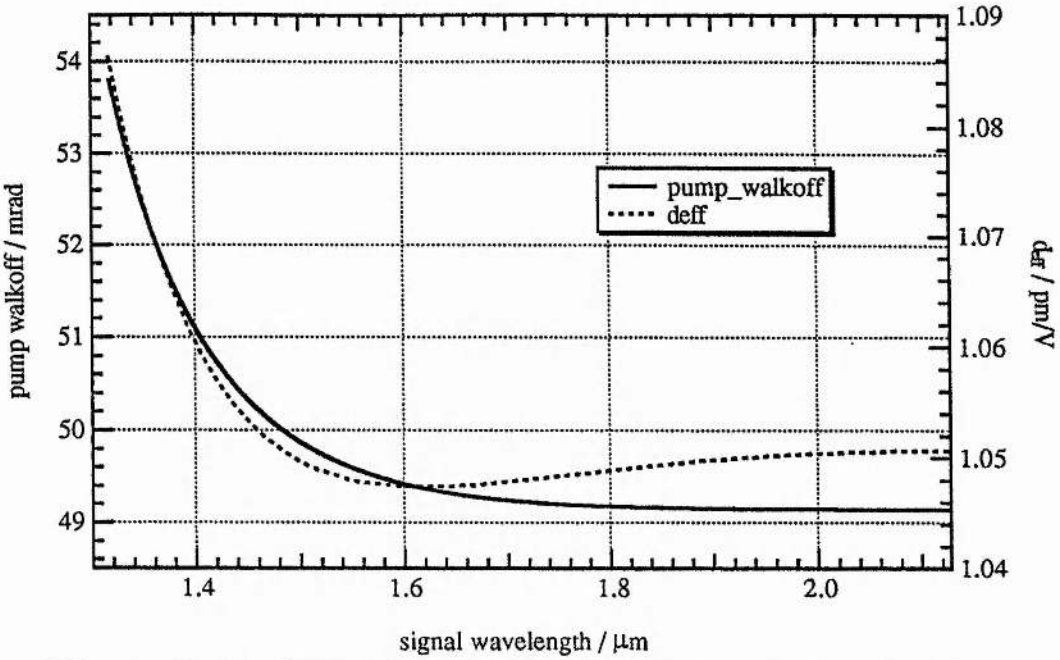

fig. a.5 (b) walk off and d_{eff} for e-oo phase matching in $LiIO_3$ pumped at 1.064 μm (from Sellmeier eqns of Herbst [5.7])

A.6 Proustite (Ag_3AsS_3)

Proustite is a negative uniaxial material, of point group 3m, with the axial assignment as in the IRE standard of 1949 [6.1], i.e. Z = c, X = a_1. It has a very large non-linearity, characterised by the non-linear coefficients d_{31} = 11.7 pm/V and d_{22} = 19.5 pm/V [6.2]*. Care must be taken such that the crystal cut is for the correct quadrant so that the coefficients add [6.4], similarly to the case for $LiNbO_3$.

In the first reported use of proustite as a gain medium for an OPO [6.5] the crystal surface damaged at pulsed intensities as low as 450 $kWcm^{-2}$, when subjected to pulses from a Q-switched Nd:YAG laser at 2 kHz. Following this disappointing result, Hanna et al [6.6] carried out an investigation of damage thresholds and mechanisms for materials suitable for parametric generation in the infrared, with particular emphasis on proustite. No definite conclusions could be drawn on the exact damage mechanism, but it is thought that a damage initiating centre is formed at intensities below the single pulse damage threshold, with a lifetime of 1-2 minutes. It was also noticed that no irreversible bulk damage is created at the level of intensities which cause surface damage. The surface damage threshold found in these experiments for 18 ns pulses at 1.064 μm and 2 pps was 28 $MWcm^{-2}$.

One of the attractions of proustite is its large transparency region, 0.6 - 13 μm, and also

* These values are calculated by assuming that d_{36}(KDP), with reference to which the non-linear coefficients were measured, can be taken as 0.39 pm/V [6.3].

its large birefringence, ~ 0.2, which allows phase matching throughout the transparency region [6.2]. The absorption is less than 0.1 cm^{-1} in the range 0.63 - 9 μm but increases rapidly at the long and short wavelengths ends. It has been reported that there may be a problem with two photon absorption at high intensities [6.7], but elsewhere this was found not to be the case [6.8]. The dispersion is adequately described by the Sellmeier eqns of Hobden [6.9], which were based on measurements of thirty wavelengths between 0.58 and 1 μm , and ten between 1 and 10.6 μm. The temperature variation was found to be small, ~ 1.5 x 10^{-4} for both indices at 650 nm, and less in the infrared. This is corroborated by Amman and Yarborough [6.5] who found that the rate of change is

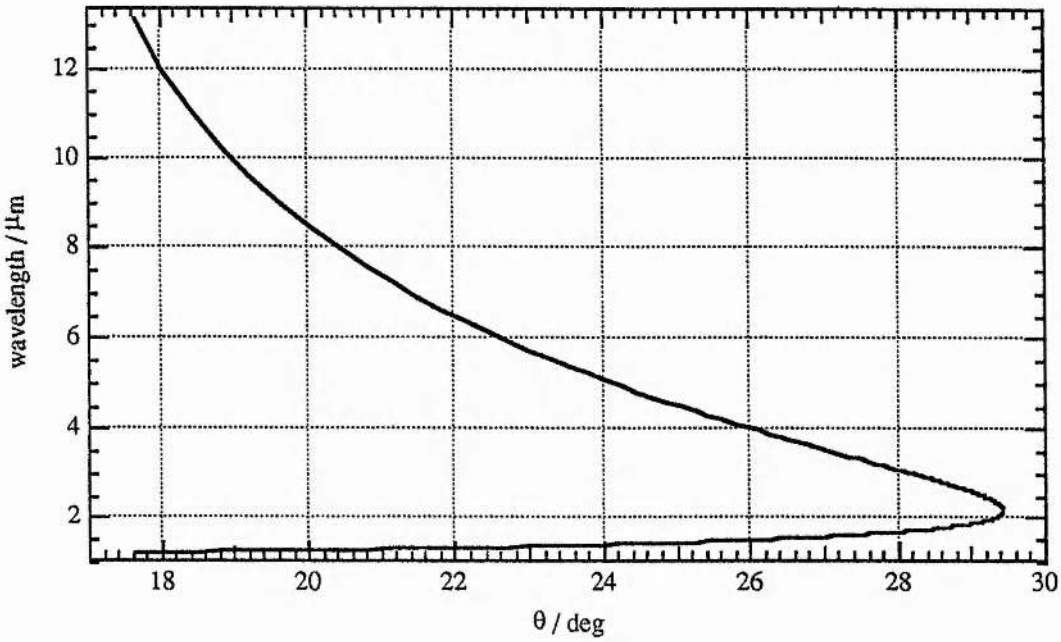

fig. a.6 (a) tuning curve for e-oo phase matching in proustite (from Sellmeier eqns of Hobden [6.9]

several times less than for lithium niobate. Pumping at 1.064 μm allows a large proportion of the transparency to be accessed, as can be seen from fig. a.6 (a). Fig. a.6 (b) shows the corresponding variation of pump walk off and d_{eff} for the case of e-oo phase matching. Type II, e-oe, phase matching is also possible but results in a lower value of d_{eff}. It can be seen that the large birefringence results in a large walk off angle for this critical phase matching. The calculated spectral and angular acceptances are 0.7 nm cm and 0.5 mrad cm in, and 8.7 mrad $cm^{1/2}$ orthogonal to, the tuning plane for the case of a 1.6 and 3.2 μm pair. No temperature acceptance could be calculated due to the lack of published information on the temperature dependence of the birefringence.

The largest size of crystal, to my knowledge, reported in the literature is 10 mm length and aperture, yet this small size has not prevented its use as a non-linear material for a variety of different non-linear processes. SHG of a CO_2 laser at 9.2 μm [6.10], and upconversion of lines from CO_2 with ruby [6.11] and He-Ne [6.12] lasers as the second wavelength source have been achieved. Early attempts for an OPO with proustite used a

DRO configuration [6.5,13], yet tuning in the range 1.22 - 8.5 μm was achieved with a SRO pumped by a Q-switched Nd:$CaWO_4$ laser [6.4] and by parametric generation with a mode locked pump [6.8].

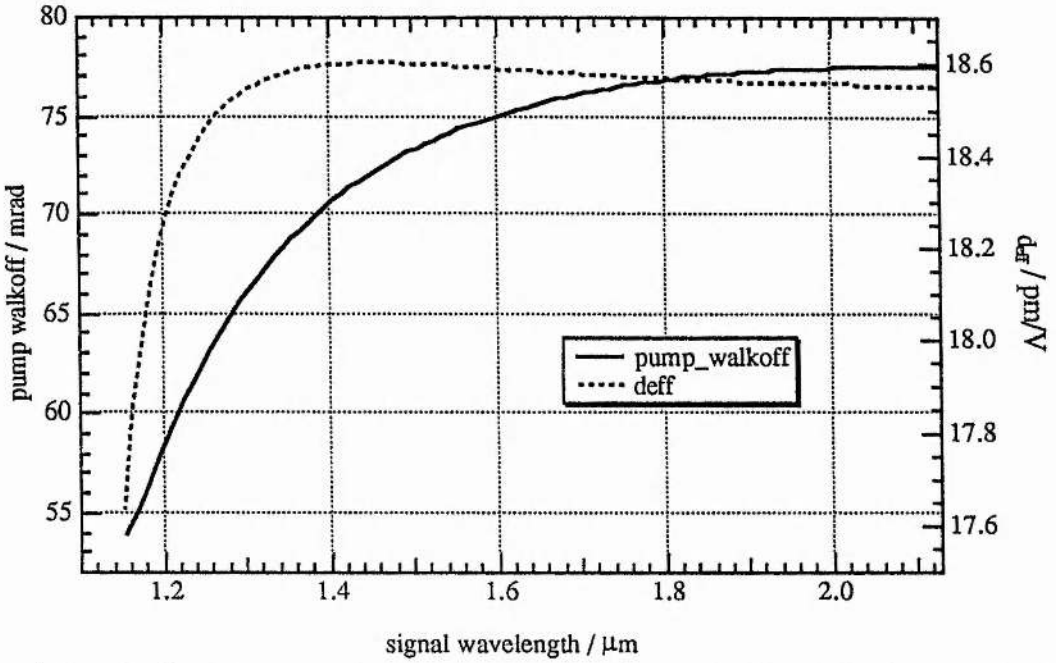

fig. a.6 (b) walk off and d_{eff} curves for e-oo phase matching in proustite (from Sellmeier eqns of Hobden [6.9]

A.7 References

A.7.2 $LiNbO_3$ and MgO:$LiNbO_3$

[2.1] G.D.Boyd, R.C.Miller, K.Nassau, W.L.Bond and A.Savage, '$LiNbO_3$: An efficient phase matchable non-linear optical material', Appl. Phys. Lett. 5 (1964) 234

[2.2] S.K.Kurtz, J.Jerphagnon and M.M.Choy, 'Non-linear dielectric susceptibilities', in *Landolt-Börnstein Numerical data and functional relationships in science and technology, group III : Crystals and solid state physics* , vol 11, K-H.Hellwege and A.M.Hellwege, eds, Springer-Verlag, Berlin, 1979, pp671-743

[2.3] R.C.Eckardt, H.Masuda, Y.X.Fan and R.L.Byer, 'Absolute and relative non-linear coefficients of KDP, KD*P, BaB_2O_4, $LiIO_3$, MgO:$LiNbO_3$, and KTP measured by phase matched second harmonic generation', IEEE J. Qu. Elec. **26** (1990) 922

[2.4] technical spec. sheets for Lasermetrics series 3900 $LiNbO_3$ Q-switches

[2.5] S.J.Brosnan and R.L.Byer, 'Optical parametric oscillator threshold and linewidth studies', IEEE J. Qu. Elec. **QE-15** (1979) 415

[2.6] A.Ashkin, G.D.Boyd, J.M.Dziedzic, R.G.Smith, A.A.Ballman, J.J.Levinstein and K.Nassau, 'Optically induced refractive index inhomogeneities in $LiNbO_3$ and $LiTaO_3$', Appl. Phys. Lett. **9** (1966) 72

[2.7] E.Krätzig, 'Photorefractive effects and photoconductivity in $LiNbO_3$:Fe', Ferroelectrics **21** (1978) 635

[2.8] D.A.Bryan, R.Gerson and H.E.Tomaschke, 'Increased optical damage resistance in lithium niobate', Appl. Phys. Lett. **44** (1984) 847

[2.9] Y.S.Luh, M.M.Fejer, R.L.Byer and R.S.Feigelson, 'Stochiometric $LiNbO_3$ single crystal fibres for non-linear optical applications', J. Cryst. Growth **85** (1987) 264

[2.10] M.V.Hobden and J.Warner, 'The temperature dependence of the refractive indices of pure lithium niobate', Phys. Lett. **22** (1966) 243

[2.11] C.D.Nabors, R.C.Eckardt, W.J.Kozlovsky and R.L.Byer, 'Efficient, single axial mode operation of a monolithic MgO:$LiNbO_3$ optical parametric oscillator', Opt. Lett. **14** (1989) 1134

[2.12] R.L.Byer, J.F.Young and R.S.Feigelson, 'Growth of high quality $LiNbO_3$ crystals from the congruent melt', J. Appl. Phys. **41** (1970) 2320

[2.13] J.L.Nightingale, W.J.Silva, G.E.Reade, W.J.Kozlovsky and R.L.Byer, 'Second harmonic generation in MgO doped lithium niobate', Proc. SPIE, vol 681, Lasers and Non-linear Materials, Bellingham 1987, pp 20-26

[2.14] J.A.Giordmaine and R.C.Miller, 'Tunable coherent parametric oscillation in $LiNbO_3$ at optical frequencies', Phys. Rev. Lett. **14** (1965) 973

[2.15] R.L.Herbst, R.N.Fleming and R.L.Byer, 'A 1.4 - 4 μm high energy angle tuned $LiNbO_3$ parametric oscillator', Appl. Phys. Lett. **25** (1974) 520

[2.16] R.L.Byer, M.K.Oshman, J.F.Young and S.E.Harris, 'Visible cw parametric oscillator', Appl. Phys. Lett. **13** (1968) 109

[2.17] J.E.Pearson, A.Yariv and U.Ganiel, 'Observations of parametric fluorescence and oscillation in the infrared', Appl. Opt. **12** (1973) 1165

[2.18] W.J.Kozlovsky, C.D.Nabors and R.L.Byer, 'Efficient second harmonic generation of a diode laser pumped cw Nd:YAG laser using monolithic MgO:$LiNbO_3$ external resonant cavities', IEEE J. Qu. Elec. **24** (1988) 913

[2.19] G.T.Maker and A.I.Ferguson, 'Doubly resonant optical parametric oscillator synchronously pumped by a frequency doubled, mode-locked and Q-switched diode laser pumped neodymium yttrium lithium fluoride laser', Appl. Phys. Lett. **56** (1990) 1614

[2.20] G.A.Magel, E.J.Lim, M.M.Fejer and R.L.Byer, 'Second harmonic generation in periodically-poled $LiNbO_3$', Opt. News, Dec 89, 20

[2.21] E.Gaizhauskus, A.Piskarskas, V.Smil'gyavichyus and G.Shlekis, 'Optical parametric oscillation in an $LiNbO_3$ crystal in the presence of a photorefractive diffraction grating', Sov. J. Qu. Elec. **21** (1991) 577

A.7.3 Barium Sodium Niobate

[3.1] J.E.Geusic, H.J.Levinstein, J.J.Rubin, S.Singh and L.G.Van Uitert, 'The non-linear optical properties of $Ba_2NaNb_5O_{15}$', Appl. Phys. Lett. **9** (1967) 269

[3.2] L.G.Van Uitert, J.J.Rubin and W.A.Bonner, 'K-1 - Growth of $Ba_2NaNb_5O_{15}$ single crystals for optical applications', IEEE J. Qu. Elec. **QE-4** (1968) 622

[3.3] S.Singh, D.A.Draegert and J.E.Geusic, 'Optical and ferroelectric properties of barium sodium niobate', Phys. Rev. **B2** (1970) 2709

[3.4] R.Webb, 'Catastrophic surface damage produced in $Ba_2NaNb_5O_{15}$ crystals during intracavity frequency doubling', Proc. Symposium on Damage in Laser Materials, Boulder, Colorado, 1971, eds J.Glass and A.H.Guenther, NBS spec. publ. 356 (1971) 98

[3.5] J.E.Murray, R.J.Pressley, J.H.Boyden and R.B.Webb, 'CW mode locked source at 0.532 μm', IEEE J. Qu. Elec. **QE-10** (1974) 263

[3.6] J.D.Barry and C.J.Kennedy, 'Thermooptical effects of intracavity $Ba_2Na(NbO_3)_5$ on a frequency doubled Nd:YAG laser', IEEE J. Qu. Elec. **QE-11** (1975) 575

[3.7] J.E.Geusic, H.J.Levinstein, S.Singh, R.G.Smith and L.G.Van Uitert, 'Continuous 0.532 μ solid state source using $Ba_2NaNb_5O_{15}$', Appl. Phys. Lett. **12** (1968) 306;
R.G.Smith, J.E.Geusic, H.J.Levinstein, J.J.Rubin, S.Singh and L.G.Van Uitert, 'Continuous optical parametric oscillation in $Ba_2NaNb_5O_{15}$', Appl. Phys. Lett. **12** (1968) 308

[3.8] R.G.Smith, 'A study of factors affecting the performance of a continuously pumped doubly resonant optical parametric oscillator', IEEE J. Qu. Elec. **QE-9** (1973) 530

[3.9] G.Ionushauskas, A.Piskarskas, V.Sirutkaitis and A.Yuozopavichyus, 'Optical parametric oscillation in $LiNbO_3$, CsH_2AsO_4 and $Ba_2NaNb_5O_{15}$ crystals pumped synchronously by a picosecond $La_2Be_2O_5$:Nd laser', Sov. J. Qu. Elec. **17** (1987) 1303

[3.10] S.G.Odulov and O.I.Olenik, 'Wavefront reversal in barium sodium niobate crystals', Sov. J. Qu. Elec. **17** (1987) 562

[3.11] L.Zhang, P.J.Chandler and P.D.Townsend, 'Ion-implanted planar waveguides in barium sodium niobate', Appl. Phys. Lett. **53** (1988) 544

A.7.4 Potassium Niobate

[4.1] L.Katz and H.D.Megaw, 'The structure of potassium niobate at room temperature : The solution of a pseudosymmetric structure by fourier methods', Acta. Cryst. **22** (1967) 639

[4.2] B. Zysset, I.Biaggio and P.Gunter, 'Refractive indices of orthorhombic $KNbO_3$. I. Dispersion and temperature dependence', J. Opt. Soc. Am. **B 9** (1992) 380

[4.3] Y.Uematsu, 'Non-linear optical properties of $KNbO_3$ single crystal in the orthorhombic phase', Jpn. J. Appl. Phys. **13** (1974) 1362

[4.4] J.-C.Baumert, J.Hoffnagle and P.Gunter, 'Non-linear optical effects in $KNbO_3$ crystals at

$Al_xGa_{1-x}As$, dye, ruby and Nd:YAG laser wavelengths', Proc. SPIE **492** (ECOOSA '84) 374

[4.5] D.A.Kleinman, 'Non-linear dielectric polarization in optical media', Phys. Rev. **126** (1962) 1977

[4.6] V.A.D'yakov, V.I.Pralkin and A.I.Kholodnykh, 'Pottasium niobate optical parametric oscillator pumped by the second harmonic of a garnet laser', Sov. J. Qu. Elec. **11** (1981) 433

[4.7] D.R.Guyer, W.R.Bosenberg and F.D.Braun, 'High efficiency, tunable mid-infrared generation in $KNbO_3$', Proc. SPIE **1409** (Non-linear optics 1991) 14

[4.8] manufacturers information sheet, Sandoz Ltd / Virgo optics

[4.9] I.Biaggio, P.Kerkoc, L.-S.Wu and P.Gunter, 'Refractive indices of orthorhombic $KNbO_3$. II. Phase matching configurations for non-linear-optical applications', J. Opt. Soc. Am. B **9** (1992) 507

[4.10] J.Hong, personal communication

[4.11] W.P.Risk, 'Compact blue laser devices', Opt. and Phot. News, May 1990, 10

[4.12] G.J.Dixon, Z.M.Zhang, R.S.F.Chang and N.Djeu, 'Efficient blue emission from an intracavity doubled 946 nm Nd:YAG laser', Opt. Lett. **13** (1988) 137

[4.13] I.Biaggio, H.Looser and P.Gunter, 'Intracavity frequency doubling of a diode pumped Nd:YAG laser using a $KNbO_3$ crystal', Ferroelectrics **94** (1989) 157

[4.14] K.Kato, 'High efficiency high power parametric oscillation in $KNbO_3$', IEEE J. Qu. Elec. **QE-18** (1982) 451

A.7.5 Lithium Iodate

[5.1] F.R.Nash, J.G.Bergman, G.D.Boyd and E.H.Turner, 'Optical nonlinearities in $LiIO_3$', J. Appl. Phys. **40** (1969) 5201

[5.2] S.K.Kurtz, J.Jerphagnon and M.M.Choy, 'Non-linear dielectric susceptibilities', in *Landolt-Börnstein Numerical data and functional relationships in science and technology, group III : Crystals and solid state physics* , vol 11, K-H.Hellwege and A.M.Hellwege, eds, Springer-Verlag, Berlin, 1979, pp671-743

[5.3] J.Jerphagnon, 'Optical non-linear susceptibilities of lithium iodate', Appl. Phys. Lett. **16** (1970) 299

[5.4] D.A.Roberts, 'Simplified characterization of uniaxial and biaxial non-linear optical crystals : A plea for standardization of nomenclature and conventions', IEEE J. Qu. Elec. **28** (1992) 2057

[5.5] G.Nath, H.Mehmanesch and M.Gsanger, 'Efficient conversion of a ruby laser to 0.347 μm in low loss lithium iodate', Appl. Phys. Lett. 17 (1970) 286

[5.6] A.A.Babin, Yu.N.Belyaev, V.N.Petryakov, M.M.Sushchik and G.I.Freidman, 'Parametric oscillator utilizing an $LiIO_3$ crystal pumped by neodymium laser radiation', Sov. J. Qu. Elec. **6** (1976) 613

[5.7] M.M.Choy and R.L.Byer, 'Accurate second order susceptibility measurements of visible and infrared non-linear crystals', Phys. Rev. B 14 (1976) 1693

[5.8] I.I.Ashmarin, Yu.A.Bykovskii, V.A.Ukraintsev, A.A.Cgristyakov and L.V.Shishonkov, 'High-power $LiIO_3$ optical parametric oscillator for infrared laser chemistry applications', Sov. J. Qu. Elec. 14 (1984) 1237

[5.9] G.Nath and S.Haussuhl, 'Large non-linear optical coefficient and phase matched second harmonic generation in $LiIO_3$', Appl. Phys. Lett. 14 (1969) 154

[5.10] A.I.Izrailenko, A.I.Kovrigin and P.V.Nikles, 'Parametric generation of light in high efficiency

non-linear $LiIO_3$ and α-HIO_3', JETP Lett. **12** (1970) 331

[5.11] S.A.Akhmanov, B.V.Zhdanov, A.I.Kovrigin, V.I.Kuznetsov, S.M.Pershin and A.I.Kholodnykh, 'Pulse-periodic tunable (0.63 - 3.4 μ) optical parametric oscillator for non-linear spectroscopy', Sov. J.Qu. Elec. **7** (1977) 1271

[5.12] P.G.Kyukov, Yu. A. Matveets, D.N.Nikogosyan, A.V.Sharkov, E.M.Gordeev and S.D.Franchenko, 'Generation of frequency tunable single ultrashort light pulses in an $LiIO_3$ crystal', Sov. J. Qu. Elec. **7** (1977) 127

[5.13] L.S.Goldberg, 'A repetitivley pulsed $LiIO_3$ internal optical parametric oscillator', *Tech. Digest of VII I.Q.E.C., May 1972, Montreal, Canada* in IEEE J. Qu. Elec. **QE-8** (1972) 573

A.7.6 Proustite

[6.1] 49 IRE 14, 'Standards on Piezoelectric crystals, 1949', Proc. IEEE, Dec 1949, 1378

[6.2] K.F.Hulme, O.Jones, P.H.Davies and M.V.Hobden, 'Synthetic proustite (Ag_3AsS_3) : A new crystal for optical mixing', Appl. Phys. Lett. **10** (1967) 133

[6.3] D.A.Roberts, 'Simplified characterization of uniaxial and biaxial non-linear optical crystals : A plea for standardization of nomenclature and conventions', IEEE J. Qu. Elec. 28 (1992) 2057

[6.4] D.C.Hanna, B.Luther-Davies and R.C.Smith, 'Singly resonant proustite parametric oscillator tuned from 1.22 to 8.5 μm', Appl. Phys. Lett. 9 (1973) 440

[6.5] E.O.Amman and J.M.Yarborough, 'Optical parametric oscillation in proustite', Appl. Phys. Lett. **17** (1970) 233

[6.6] D.C.Hanna, B.Luther-Davies, H.N.Rutt, R.C.Smith and C.R.Stanley, 'Q-switched laser damage of infrared non-linear materials', IEEE J. Qu. Elec. **QE-8** (1972) 317

[6.7] V.V.Berezovskii, Yu. A.Bykovskii, S.N.Potanin and I.S.Rez, 'Two photon absorption in proustite', Sov. J. Qu. Elec. **3** (1973) 134

[6.8] T.Elsaesser, A.Seilmeier and W.Kaiser, 'Parametric generation of tunable picosecond pulses in proustite between 1.2 and 8 μm', Opt. Comm. **44** (1983) 293

[6.9] M.V.Hobden, 'The dispersion of the refractive indices of proustite (Ag_3AsS_3)', Opto-Elec. **1** (1969) 159

[6.10] G.J.Ernst and W.J.Witteman, 'Second harmonic generation in proustite with a cw CO_2 laser,' **QE-8** (1972) 382

[6.11] J.Warner, 'Photomultiplier detection of 10.6 μm radiation using optical upconversion in proustite', Appl. Phys. Lett. **12** (1968) 222

[6.12] N.Ito, 'Sum frequency mixing of CO_2 and He-Ne lasers in proustite', Opt. Lett. **7** (1982) 63

[6.13] D.C.Hanna, B.Luther-Davies, H.N.Rutt and R.C.Smith, 'Reliable operation of a proustite parametric oscillator', Appl. Phys. Lett. **20** (1972) 34

APPENDIX B

Computer Programs

B.1 Program to evaluate function h_S from Guha, Wu and Falk

The majority of the code for evaluating h_S was written by Tang Yan.

```
c       guha.f

        program guha

        double precision dz2,e,d,lc,lp,ls,np,ns,xp,xs,bp,bs
        double precision r,f,fo,fe,f1,f2,dk,k,kp,ks,ki,ro,wop,wos
        double precision x5,x6,max,hsm,hs(400),dkL
        double precision fp,ai,v1,v2,v3,v4,v5
        integer m
        common  k,dk,lc,bp,bs,wop,wos,ki,ro,fp,ai,v3,v4,v5,x5,x6

c       open(12,file='KTPex.d',status='unknown')

        m=20
        dz2=1.00d00/dble(2*m)
        lc=20.00d00
        lp=1.047d00
        np=1.748d00
        ls=1.54d00
        ns=1.738d00

        kp=2.00d00*3.141592654d00*np*1000.00d00/lp
        ks=2.00d00*3.141592654d00*ns*1000.00d00/ls
        k=kp/ks

        write(*,'("What is pump spot size, in microns ?")')
        read*,wop
        wop=wop/1.00d03
        bp=wop**2*kp
        xp=lc/bp

        write(*,'("Where is it focussed ?")')
        write(*,'("0 = input face, 0.5 = centre, 1 = output face")')
        read*,fp

        write(*,'("What is signal spot size, in microns ?")')
        read*,wos
        wos=wos/1.00d03
        bs=wos**2*ks
        xs=lc/bs

        write(*,'("What is the walk-off angle, in mrads ?")')
        read*,ro
        ro=ro*1.00d-03

        write(*,'("What is the idler absorption coefficient, in cm-1 ?")')
        read*,ai
        ai=ai/10.00d00

        x5=xp*xs*(k-1.00d00)/(k*xp+xs)
```

```
      x6=(k*xs+xp)/(k-1.00d00)
      v1=(xs-2.00d00*fp*xp)/(xs*xp)

      fo=0.00d00
      max=0.00000001d00

c     Between here and line 40, simpson's rule is employed to solve for
c     the outer integral, which uses the values of the inner integral
c     which are calculted using subroutine sp. This is then iterated 60
c     times for different values of dk, in order to maximimize.

      do 40 jj=1,200

      dk=-4.00d00+dble(jj-1)*0.03d00
      ki=kp-ks-dk

      v2=(kp-2.00d00*fp*ks)/ki
      v3=((1.00d00+2.00d00*fp)/x5+(xs-xp)/(xs*xp)*v2+v1)*xp*xs/x6*0.25d00
      v4=(2.00d00*fp/x5+v1*v2)*xp*xs/x6*0.25d00
      v5=(v2**2-v2*(1.00d00+2.00d00*fp)+2.00d00*fp)*xp*xs/x6*0.25d00

      call sp(1.00d00,f)
      fe=f
      r=0.50d00*(fo-fe)

      do 20 i=1,m
      e=dble(2*i-1)*dz2
      d=dble(2*i)*dz2
      call sp(e,f)
      f1=f
      call sp(d,f)
      f2=f
20    r=r+2.00d00*f1+f2

      r=r/dble(3*m)
      hs(jj)=(1.00d00+k)*0.25d00*r/(xp+xs*k) max=DMAX1(hs(jj),max)

40    continue
      hsm=max

      do 60 jj=1,200
      if(DABS(hs(jj)-hsm).le.0.0000000001)
           then dkL=(-4.00d00+dble(jj-1)*0.03d00)*lc
      end if
60    continue

      write(*,21)hsm,dkL
21    format('hsm = ',f7.5,2x,'dkl = ',f8.4)
      end

c     The subroutine sp evaluates the inner integral by simpson's rule

      subroutine sp(z2,f)

      integer n
      double precision y,z2,dz1,f,yo,ye,a,b

      n=20
      dz1=z2/dble(2*n)
      yo=y(0.00d00,z2)
      ye=y(z2,z2)
      f=0.50d00*(yo-ye)

      do 10 i=1,n
      a=dble(2*i-1)*dz1
      b=dble(2*i)*dz1
```

```
10      f=f+2.00d00*y(a,z2)+y(b,z2)
        f=f*z2/dble(3*n)
        end

c       The complex integrand is contained in this function

        double precision function y(z1,z2)
        double complex cp,cpp,cs,csp,u,v,yo,fw,a3,ib1
        double complex ccp,cc,v0
        double precision wop,wos,lc,bp,bs,ki,dk,ai,v3,v4,v5,x5,x6
        double precision k,z1,z2,z,zp,a,tsp,tpp,ts,tp,b,ro,fp,v1
        common  k,dk,lc,bp,bs,wop,wos,ki,ro,fp,ai,v3,v4,v5,x5,x6

        if (ro.le.0.00000001d00) then
        goto 20
        end if

        zp=z2*lc
        z=z1*lc
        tp=2.00d00*(z-fp*lc)/bp
        ts=2.00d00*(z-lc/2.00d00)/bs
        tpp=2.00d00*(zp-fp*lc)/bp
        tsp=2.00d00*(zp-lc/2.00d00)/bs
        cpp=DCMPLX(1.00d00, tpp)*wop**2
        cp=DCMPLX(1.00d00, tp)*wop**2
        cs=DCMPLX(1.00d00, ts)*wos**2
        csp=DCMPLX(1.00d00, tsp)*wos**2
        ccp=1.00d00/cpp+1.00d00/DCONJG(csp)
        ccp=1.00d00/ccp
        cc=1.00d00/cp+1.00d00/DCONJG(cs)
        cc=1.00d00/cc

        a3=-ki/(ki*ccp+DCMPLX(0.00d00,2.00d00*(z-zp)))
        ib1=1.00d00/cc-DCONJG(a3)
        fw=(z-zp)**2*((DCONJG(a3)**2)/ib1+DCONJG(a3))

20      u=DCMPLX(0.00d00,dk*lc*(z1-z2))+ro**2*fw-(ai*lc/2.00d00)*dabs(z1-z2)
        a=dble(u)
        b=DIMAG(u)

        v1=1.00d00/x5+1.00d00/x6
        v0=dcmplx(0.00d00,-0.25d00)*(z1-z2)*v1+z1*z2+0.25d00/(x5*x6)
        v=v0-(z1+z2)*v3+v4+(z1-z2)*v5/dcmplx(0.00d00,1.00d00)
        yo=DEXP(a)*DCMPLX(DCOS(b),DSIN(b))/v
        y=dble(yo)

        end
```

B.2 Program to evaluate pulsed thresholds using choice of BB or Guha models

program thresholds;

This program calculates the OPO threshold for KTP using either the Brosnan-Byer model, in either of its two forms, or the Guha model, with added time dependence. The choice is whether to use the iterative version for either gaussian pulses or for the actual time dependence of Q-switch pulses, or the simplified version which assumes a top hat shape to the pump pulse

```
const
        c = 3e8;            speed of light in vacuo
        kbb = 1.5e-8;       this is calculated with d=3.7 pm/V, delta = 0.25
        K3 = 1.615e-3;
        pi = 3.14159;
        d = 1e-3;
        lambda = 1.54e-6;
        n = 1.738;

var
        textwindowrect : rect;
        dummy : boolean;
        Rd, Rdd, R1, R2, Rc, Rp, gammaL, gamma, round_trip_time, tm, intensity, cavity_photons,
        emitted_photons, output_coupling, net_gain, Ws, gs, lc, L, Wp, tor, fwhm_m, zi, z1, z2, x, z,
        No, inv_frac, photon_frac, tc, r, initial_actual, hs_1, hs_2, power, cavity_trans, as, ai, a_av,
        delta_a, RofC, dkl, dp : real;
        round_trips, i, j, index, refl : integer;
        data : text;
        filename, ans, ans1 : string;
        pump_frac_array : array[1..250] ofreal;

function cosh (x : real) : real;
begin
        cosh := 0.5 * (exp(x) + exp(-x))
end;

function sinh (x : real) : real;
begin
        sinh := 0.5 * (exp(x) - exp(-x))
end;
```

The procedure iterate finds a solution to nonlinear equations of the form f(x) = 0, by halving the separation between two successive guesses

```
procedure iterate (function f (x : real) : real;
                y1, y2, accuracy : real; var y : real;
                                        var soln : boolean);
var
        oldy, newy, y3, f1, f2, f3 : real;

begin
        f1 := f(y1);
        f2 := f(y2);
        soln := false;
        if f1 * f2 < 0 then
        begin
                soln := true; oldy := y1;
                newy := y2 + (2 * accuracy);
                while abs(oldy - newy) > accuracy do
```

```
                begin
                        y3 := (y1 + y2) / 2; f3 := f(y3);
                        oldy := newy; newy := y3;
                        if f1 * f3 <= 0 then
                        begin
                                y2 := y3;
                                f2 := f3
                        end
                        else
                        begin
                                y1 := y3;
                                f1 := f3
                        end
                end;  {end of while loop}
                y := newy
        end
end;
```

This is the error function solved by simpson's rule

```
function erf (x : real) : real;
const
        n = 10;
var
        i : integer;
        sum, h : real;
begin
        sum := 0;
        h := x / 2 / n;
        for i := 1 to n do
        begin
                sum := sum + 4 * exp(-sqr(h * (2 * i - 1))) + 2 * exp(-sqr(h * 2 * i))
        end;
        erf := 2 / sqrt(pi) * h / 3 * (1 + sum - exp(-sqr(x)))
end;
```

This a formulation of simpson's rule which can accept any function

```
procedure simpson (fucntion f (x : real) : real;
                                        a, b : real;
                                        var ans : real);
const
        n = 20;
var
        i : integer;
        h : real;
begin
        h := (b - a) / (2 * n);
        ans := f(a) - f(b);
        for i := 1 to n do
        begin
                ans := ans + 4 * f(a + ((2 * i) - 1) * h) + 2 * f(a + (2 * i * h))
        end;
        ans := (h / 3) * ans
end;
```

This calculates an effective square pulse gain, and gives an approximate solution for the Brosnan-Byer model

```
function gain (x : real) : real;
var
        torhat, g : real;
begin
        torhat := 2 * tor * sqrt(ln(x / (ln(1 / sqrt(Rd) + sqrt(1 / Rd - 1)))));
        g := 2 / sqrt(pi) * (torhat / 2 / tor / erf(torhat / 2 / tor));
        g := g * (L / c / torhat * 32 + (1 - dp) * as * lc + ln(1 / sqrt(Rdd)) + ln(2)) - x;
```

```
        gain := g
end;
```

This is f(z) which determines the evolution of a Q-switched pulse

```
function f (z : real) : real;
begin
        f := 1 / (exp(-zi) - exp(-z) + zi - z)
end;
```

Normally the evolution of a Q-switched pulse is solved by finding the time required to reach a certain inversion. Function time allows a time to be specified for a Q-switched pulse, and then iteration will find the appropriate value of inversion, and from there, the photon fraction

```
function time (x : real) : real;
var
        t_est : real;
begin
        simpson(f, z1, x, t_est);
        t_est := t_est * tc;
        time := tm - t_est
end;
```

This allocates the appropriate pump fraction depending on time, and assumed time dependence

```
function pump_frac (tm : real) : real;
begin
        if ans = 'g' then
                pump_frac := exp(-sqr(tm / tor))
        else
                pump_frac := pump_frac_array[index]
end;
```

This is the main function which iterates through the pulse to find the number of photonsproduced within the envelope of the pump pulse

```
function iterated_gain (intensity : real) : real;
var
        m : integer;
```

Here the effective gain is calculated, depending on model and intensity/power

```
function nonlinear_gain (x : real) : real;
var
        g, theta, gamma, gam, delta, denom, delta_k, A : real;

function bb_gen_gain (gamma : real) : real;
var
        f : real;
begin
        delta_k := dkl / lc;
        theta := (delta_k * delta_a) / (4 * sqr(gamma) + sqr(delta_a / 2) - sqr(delta_k));
        denom := sqrt(sqr(sqr(2 * gamma) + sqr(delta_a / 2) - sqr(delta_k)) + sqr(delta_k * delta_a));
        gam := sqrt(denom) * cos(0.5 * theta);
        delta := sqrt(denom) * sin(0.5 * theta);
        a := (sqr(delta_a / 2) + sqr(delta_k)) / denom;
        f := (gam * delta_a / 2 + delta * delta_k) * sinh(gam * lc);
        f := f + (delta * delta_a / 2 - gam * delta_k) * sin(delta * lc);
        f := f * 2 / denom;
        f := f + ((1 + a) * cosh(gam * lc) + (1 - a) * cos(delta * lc));
        f := f / 2 * exp(-a_av * lc);
        bb_gen_gain := f
end;

begin
        if refl = 1 then
```

```
                x := x * (1 - Rp);
        if ans1 = 'bb' then
        begin
                gamma := sqrt(x * kbb * gs);
                gammaL := gamma * lc;
                gamma := gamma * pump_frac(tm);
                g := bb_gen_gain(gamma);
                if dp <> 0 then
                begin
                        gamma := sqrt(Rp) * gamma;
                        g := g * bb_gen_gain(gamma);
                end;
                nonlinear_gain := g
        end
        else
        begin
                power := x * (pi / 2) * sqr(Wp);
                power := power * pump_frac(tm);
                g := 1 + K3 * hs_1 * power;
                if dp <> 0 then
                        g := g + K3 * hs_2 * power * Rp;
                nonlinear_gain := g
        end
end;

begin           iterated gain

cavity_photons is the number of photons actually in the cavity at a point in time
emiited photons is the number of signal photons that have exited the cavity

        index := 0;
        cavity_photons := 1;
        emitted_photons := 0;
        if ans = 'g' then
                tm := -2 * tor      this gives 2 % of the peak for the gaussian pulse
        else
                index := 1;

where as is the signal intensity absorption coefficient

        cavity_trans := (R1 * R2 * sqr(sqr(1 - Rc)) * exp(-(1 - dp) * as * lc));
        output_coupling := (1 + R2 * ((1 - R1) * sqr(1 - Rc) * exp(-(1 - dp) * as * lc) - 1));
        output_coupling := output_coupling / (R1 * R2 * (1 - Rc) * sqr(1 - Rc)*exp(-(1 - dp)* as * lc));

        for m := 1 to round_trips do                    this iterates the pump intensity by one round trip
        begin
                net_gain := cavity_trans * nonlinear_gain(intensity);
                cavity_photons := cavity_photons * net_gain;
                if cavity_photons < 1 then
                        cavity_photons := 1;
                if cavity_photons > 1 then
                emitted_photons := emitted_photons + (cavity_photons * output_coupling);
                if cavity_photons > 1e15 then
                        cavity_photons := 1e15;     this line prevents a computer floating point error
                tm := tm + round_trip_time;
                index := index + 1
        end;
        if ans1 = 'bb' then
                writeln(intensity / 1e10 : 18 : 1, gammaL : 9 : 3, (emitted_photons / 1.6e14) : 24 : 2)
        else
                writeln(intensity * (pi / 2) * sqr(Wp) / 1e3 : 7 : 1, (emitted_photons / 1.6e14) : 23 : 2);
        iterated_gain := emitted_photons - 1.6e14;
end;
```

calculates the gain guided signal spot for plane-plane cavity

```
function spot_size (x : real) : real;
begin
        spot_size := sqr(pi / 2 / L / lambda) * sqr(x * sqr(x)) + sqr(x) - sqr(Wp) / 2
end;

function curved (x : real) : real;
var
        A, B, c, leff : real;
begin
        leff := lc / 2 / n + d;
        A := 1 - (8 / RofC) * leff * (1 - (1 / RofC) * leff);
        B := 4 * n * leff * (1 - 3 * leff / RofC + (2 / sqr(RofC)) * sqr(leff));
        c := sqr(x * sqr(x)) + sqr(sqr(x) * Wp) * (1 / sqr(A) - 1) / 2;
        c := c + sqr(B * (lambda / n) * x / A / pi) - sqr(B * (lambda / n) * Wp / A / pi) / 2;
        curved := c
end;
```

This setups all the values and initial conditions required to solve for the time evolution of the Q-switched pulse, depending on r, the number of times threshold

```
procedure initialise;
var
        x, T1, N1, N2, T_peak, T2, N_half, HW1, HW2 : real;
```

Producing the values of time v photon fraction for the Q-switched pulse is the most time consuming part of the program. It is therefore most efficient to do this only once and save the values in an array

```
procedure set_up_array;
var
        ii : integer;
begin
        for ii := 1 to 250 do          this assures that any unused part of the array is zero
        pump_frac_array[ii] := 0;
        tm := initial_actual;
        writeln('preparing time v photon_frac array');
        writeln;
        for ii := 1 to round_trips do
        begin
                iterate(time, z1, z2, 1e-3, z, dummy);
                inv_frac := exp(-z) / r;
                photon_frac := ((1 - inv_frac) + (1 / r) * ln(inv_frac)) / No;
                pump_frac_array[ii] := photon_frac;
                tm := tm + round_trip_time
        end
end;
```

The extraction efficiency is required for the calculations

```
function extraction_efficiency (a : real) : real;
begin
        extraction_efficiency := ln(a) / (a - 1) - r
end;
```

This allows the time for a certain photon fraction to be calculated, ie the halfwidths

```
function halfwidth (x : real) : real;
begin
        halfwidth := x * exp(-r * x) - exp(r * (photon_frac * No - 1))
end;

begin                initialise
        writeln('What value of r ?');
        readln(r);
        writeln;

        iterate(extraction_efficiency, 0.99, 0.005, 1e-3, x, dummy);
```

initialisation and calculation of the values zi, z1, z2, T1, T_peak, T2, and the FWHM

```
zi := -ln(r);
z1 := -ln(r) +      0.01;
z2 := -ln(x * r) - 0.001;
T1 := 0;
N1 := exp(-z1) / r;
N2 := exp(-z2) / r;
No := (1 - 1 / r) + (1 / r) * ln(1 / r);
simpson(f, z1, 0, T_peak);
simpson(f, z1, z2, T2);
```

By finding the points where photon_frac = 0.5, one before and one after the peak, the FWHM is calculated

```
photon_frac :=    0.5;
iterate(halfwidth, N1, 1 / r, 1e-3, N_half, dummy);
N_half := -ln(N_half * r);
simpson(f, z1, N_half, HW1);
iterate(halfwidth, 1 / r, N2, 1e-3, N_half, dummy);
N_half := -ln(N_half * r);
simpson(f, z1, N_half, HW2);
tc := fwhm_m / (HW2 - HW1);
```

calculate time at which photon_frac is 0.05, for the initial time for the round_trips to start

```
photon_frac :=    0.05;
iterate(halfwidth, N1, 1 / r, 1e-3, N_half, dummy);
N_half := -ln(N_half * r);
simpson(f, z1, N_half, HW1);
initial_actual := tc * HW1;
set_up_array;
end;
```

main program

```
begin
        textwindowrect.top := 40;                    this set of instructions opens up the text window on
entering
        textwindowrect.left := 40;          the program to which all write statements, go except those
        textwindowrect.bottom := 330;  which have 'data' as the ouput textfile, where the write
        textwindowrect.right := 460;        statement puts the data into a textfile for use in cricket graph
        settextrect(textwindowrect);
        showtext;
        filename := 'thresholds.data';        this names and then opens the textfile for outputing data
        rewrite(data, filename);

        repeat
        begin
                writeln('Which model for threshold, Brosnan - Byer (bb) or Guha (g)');
                readln(ans1);

                writeln('Allow for pump reflection (y/n)?');
                readln(ans);
                if ans = 'y' then
                begin
                        refl := 1;
                        writeln('What value of reflection % ?');
                        readln(Rp);
                        Rp := Rp / 100;
                        writeln('Allow for double pass (y/n) ?');
                        readln(ans)
                end
                else
                        Rp := 0;
```

```
if ans = 'y' then
begin
        dp := 1;
        if ans1 = 'g' then
        begin
                writeln('What value of hs for the first pass ?');
                readln(hs_1);
                writeln('What value of hs for the second pass ?');
                readln(hs_2)
        end
end
else
begin
        dp := 0;
        if ans1 = 'g' then
        begin
                writeln('What value of hs ?');
                readln(hs_1)
        end
end;

writeln('crystal length (mm) ?');
readln(lc);
lc := lc * 1e-3;
L := lc / n + 2 * d;

writeln('What is the estimated crystal reflection loss per face at signal (%) ?');
readln(Rc);
Rc := Rc / 100;

writeln('What is the estimated crystal absorption at signal (cm-1) ?');
readln(as);
as := as * 100;
if ans1 = 'bb' then
begin
        writeln('What is the estimated crystal absorption at idler (cm-1) ?');
        readln(ai);
        ai := ai * 100;
        a_av := (as + ai) / 2;
        delta_a := (ai - as);

{writeln('What value of dkl, from guha analysis ?');}
{readln(dkl)}

        dkl := 0
end
else
begin
        a_av := 0;
        delta_a := 0
end;

writeln('What value of input miror reflectivity for signal (%) ?');
readln(R1);
R1 := R1 / 100;

writeln('What value of output miror reflectivity for signal(%) ?');
readln(R2);
R2 := R2 / 100;
Rd := R1 * R2 * sqr(sqr(1 - Rc)) * exp(-(1 - dp) * as * lc);
                                                    total cavity round trip transmission
Rdd := R1 * R2 * sqr(sqr(1 - Rc));          cavity transmission without absorption
loss

writeln('What pump spot size (μm) ?');
readln(Wp);
```

```
Wp := Wp * 1e-6;

writeln('What is the pulse width (fwhm, ns) ?');
readln(fwhm_m);
fwhm_m := fwhm_m * 1e-9;
tor := fwhm_m * 0.6;                    this converts the fwhm in ns to hw(1/e) in s

Ws := 0;
gs := 0;

if ans1 = 'bb' then
begin
        writeln('Are the mirrors plane (p) or curved (c) ?');
        readln(ans);
        if ans = 'p' then
        begin
                iterate(spot_size, 20e-6, 800e-6, 2e-6, Ws, dummy)
        end
        else
        begin
                writeln('What radius of curvature, in mm ?');
                readln(RofC);
                RofC := RofC / 1e3;
                Ws := 100e-6;
                iterate(curved, 0, Wp, 1e-7, Ws, dummy)
        end;

        writeln('Which method, top-hat (t) or iterated pulse (i) ?');
        readln(ans);
end;
```

gs is just a mode coupling parameter which comes from the BB model, it is incidently wrong but close enough for our purposes

```
gs := sqr(Wp) / (sqr(Wp) + sqr(Ws));

if ans = 't' then       this is if you want to solve the simplified eqns which assume that
begin                   the pump pulse has a top hat temporal profile
        dummy := false;
        gammaL := 0;
        iterate(gain, 0.1 + ln(1 / sqrt(Rd) +sqrt(1 / Rd - 1)),2,1e-2, gammaL, dummy);
        writeln;
        writeln('gammaL = ', gammaL : 10 : 4);
        intensity := sqr(gammaL) / (kbb * gs * sqr(lc));
        writeln('Threshold = ', intensity / 1e10 : 10 : 1, ' MW/cm^2')
end
else
begin
        writeln('What time dependence, gaussian assumption (g) or actual (a)');
        readln(ans);

        round_trip_time := 2 * (1.75 * lc + 2 * d) / c;    {this is just 2*(n*lc+2*d)/c}
        round_trips := trunc(4 * tor / round_trip_time);
```

The round trips are calculated to iterate between the 5 % points of a gaussian. Although the5 % points are different for the actual profile, it goes between 5% and 7%, this will give both the same number of round trips, as they both have the same FWHM

```
        if ans = 'a' then initialise;
        writeln;
        writeln('round trips = ', round_trips : 5);

        if ans1 = 'bb' then
        begin
                writeln;
                writeln('Ws = ', Ws * 1e6 : 5 : 1, ' µm   ');
```

```
                writeln;
                writeln('Intensity(MW/cm^2)', 'gammaL', 'no. of photons (*1.6e14)');
                writeln
        end
        else
        begin
                writeln;
                writeln('Power(kW)     fraction of threshold photons');
                writeln
        end;
```

The form of this function call is
iterate(function to be iterated,lower limit, upper limit, accuracy, answer, dummy variable)
it changes the value of intensity, starting at 1 MW/cm^2, until two successive estimates differ by the accuracy parameter, which is 1 MW/cm^2

```
        iterate(iterated_gain,1e10,4/(1-Rp)/(kbb*gs*sqr(lc)), 1e10, intensity, dummy);
```

the value for the second limit gives gammaL = 2

```
        writeln;
        writeln('Threshold intensity is ', (intensity * 1e-10) : 4 : 1, 'MW/cm^2');

    end;
    writeln('Threshold energy is ', intensity * 2.78 * sqr(Wp) * tor * 1e3 : 4 : 2, ' mJ');
    writeln('Threshold power is ', intensity * (pi / 2) * sqr(Wp) / 1e3 : 4 : 1, ' kW');
    writeln;
    writeln('The paramaters chosen were := ');
    writeln;
    writeln('Input reflectivity ', R1 * 100 :4:2, ' % Output relectivity ',R2 * 100 :4:2, '%');
    writeln('Crystal length ', lc * 1e3 : 3 : 1, ' mm');
    writeln('Pump spot size ', Wp * 1e6 : 4 : 1, ' µm');
    write('Method of solution was -  ');
    if ans = 't' then
        writeln('top-hat')
    else if ans = 'g' then
        writeln('iterative : gaussian time dependence')
        else
        writeln('iterative : actual time dependence');

    write(data, l * 1e3 : 2, chr(9), Wp * 1e6 : 4 : 1, chr(9), Ws * 1e6 : 4 : 1);
    writeln(data, chr(9), intensity / 1e10 : 4 : 3);
end;
writeln;
writeln('Another ? (y/n)');
readln(ans);
writeln
until ans = 'n';
close(data)        closes the output data textfile which is necessary before it can be read
end.
```